Scaling of clearance by body size and composition

Jaydeep Sinha

A thesis submitted for the degree of

Doctor of Philosophy

at the University of Otago, Dunedin,

New Zealand.

24 May 2019

DEDICATED TO MY PARENTS

ABSTRACT

Dose scaling is a critical component of dose individualisation that helps ensure that the required amount of drug exposure is achieved in each and every patient. This is typically achieved by scaling the pharmacokinetic (PK) parameters by relevant covariates, on the assumption that variability in drug response is linked to PK. Body size is the most important covariate when CL is scaled for differently sized populations, e.g. obese or paediatric patients, in order to calculate the maintenance dose. Conventionally, total body weight (WT) has been used as the size scaler, however, fat-free mass (FFM) is a suitable alternative as it accounts for body composition as well.

Accurate scaling of CL by body size needs an accurate value of the scaling exponent (i.e. the allometric exponent). Since there is no consensus on the true value of the exponent, it is often empirically chosen from the *a priori* recommended values ($2/3$, $3/4$, 1) or estimated. In either situation, the accuracy of the empirical value would depend on the study design, which is assessed in this thesis by modelling and simulation. The finding indicates that sub-optimal study designs risk bias to the allometric exponent, which in turn risks bias to CL prediction.

For sub-optimal study designs, it is recommended to use a biologically plausible *a priori* value for the allometric exponent. While a theoretical value exists for WT, it is currently lacking for FFM. Therefore, the value for FFM was investigated by modelling the relationship between liver size and FFM. Further attempt was made to empirically estimate the exponent from literature data. A literature based meta-analysis revealed a disconnect between the theoretical (expected) and the empirical values; this needs further research.

Given the issue with the choice of the allometric exponent, an alternative 'bottom-up' approach could be used to scale CL by *in vitro-in vivo* extrapolation (IVIVE). Unlike the classical 'top-down' approach above, the accuracy of scaling CL by IVIVE would depend on choosing an accurate descriptor of

'functional' liver size, instead of study design. In this thesis, lean liver volume (LLV) was identified as a more accurate descriptor of 'functional' liver size by comparing its predictive performance with the conventional descriptor, total liver volume (LV).

Another issue is that FFM is not a readily measurable covariate and hence, accuracy of FFM prediction is of utmost importance in dose scaling. Janmahasatian's FFM model, although extensively used, is known to over-estimate FFM in Indian population. Therefore, an extended version of Janmahasatian's FFM model was developed for Indians. The extended FFM model structure includes (estimable) ethnicity specific body composition parameters, which can be further estimated for other relevant populations as well.

ACKNOWLEDGMENTS

I would like to express my special appreciation and gratitude to my PhD supervisors Dr Hesham Al-Sallami and Professor Stephen Duffull. They have been impeccable mentors throughout the past three years of my PhD journey. Their judicious guidance has transformed my ways of thinking and has helped my critical thinking of science.

I would like to acknowledge my collaborator Dr Bruce Green for his generous contribution towards my projects and invaluable inputs, and my PhD facilitator, Professor Sarah Hook, for all the support throughout my PhD.

I am grateful to the School of Pharmacy, University of Otago for providing me the Doctoral Scholarship during my PhD studies. I am also thankful to University of Otago for giving me the opportunity to study and providing me with all the necessary support that immensely helped me carry out my research.

I am grateful to my colleagues and friends at the Otago Pharmacometrics Group for being highly supportive, and for all the friendly discussions, journal club and weekly seminars. Special thanks to the members with whom I've interacted closely including Chihiro, Vijay, Qing Xi, Derek, Shamin, and Sudeep.

The help and support that I have received from my friends in Dunedin cannot be expressed by words. Very special thanks to my friends Aniruddha, Akash, Parul, Radhika, Nilanjan and Ranjan for everything that helped me survive far away from home! Finally, words cannot express how grateful I am to my parents and my sister for standing beside me through this journey and for their continuous motivation.

PUBLICATIONS

THAT HAVE ARISEN FROM WORK ASSOCIATED WITH THIS THESIS

International peer-reviewed journals

Published

Sinha J, Duffull SB, Al-Sallami HS. *Review of the methods and associated mathematical models used in the measurement of fat-free mass.* Clinical Pharmacokinetics. 2018; 57(7): 781–795.

Sinha J, Al-Sallami HS, Duffull SB. *Choosing the allometric exponent in covariate model building*. Clinical Pharmacokinetics. 2019; 58(1): 89-100.

Under review

Sinha J, Duffull SB, Green B, Al-Sallami HS. *Evaluating the relationship between lean liver volume and fat free mass.*

Sinha J, Al-Sallami HS, Duffull SB. *An extension of Janmahasatian's fat-free mass model for universal application across populations of different ethnicities.*

Sinha J, Duffull SB, Green B, Al-Sallami HS. *Lean liver volume as a potential scaler for in vitro-in vivo extrapolation of drug clearance in obesity.*

Oral Presentations

Sinha J, Al-Sallami HS, Duffull SB, Green B. *An extension of Janmahasatian's fat-free mass model to incorporate differences due to ethnicity*. In proc. of the Annual meeting of Population Approach Group in Australia and New Zealand (PAGANZ) 2019, Auckland, New Zealand.

Sinha J, Duffull SB, Green B, Ponnuswamy TK, Devanand B, Ramanathan M, Ramalingam S, Al-Sallami HS. *Development of a predictive model for lean liver volume, a potential scaler for in vitro-in vivo extrapolation (IVIVE) of drug clearance*. In proc. of Annual Scientific Meeting of Australasian Society of Clinical and Experimental Pharmacologists and Toxicologists (ASCEPT) 2018, Queenstown, New Zealand.

Sinha J, Duffull SB, Green B, Al-Sallami HS. *Development and evaluation of a model for predicting lean liver volume*. In proc. of the Annual meeting of Population Approach Group in Australia and New Zealand (PAGANZ) 2018, Melbourne, Australia.

Sinha J, Al-Sallami HS, Duffull SB. *Influence of clinical study design on ensuring accurate scaling of dose to patients*. In proc. of Annual Scientific Meeting of Australasian Society of Clinical and Experimental Pharmacologists and Toxicologists (ASCEPT) 2017, Queenstown, New Zealand.

Sinha J, Al-Sallami HS, Duffull SB. *Influence of study design on choice of the allometric exponent*. In proc. of the Annual meeting of Population Approach Group in Australia and New Zealand (PAGANZ) 2017, Adelaide, Australia.

Poster Presentations

Sinha J, Al-Sallami HS, Duffull SB. *Extension of the Janmahasatian fat-free mass model to account for ethnicity-related bias*. In proc. of the Annual meeting of Annual Meeting of the Population Approach Group in Europe (PAGE) 2019, Stockholm, Sweden.

Sinha J, Duffull SB, Green B, Ponnuswamy TK, Devanand B, Ramanathan M, Ramalingam S, Al-Sallami HS. *Development of a model to predict lean liver volume for use in scaling drug clearance*. In proc. of the American Conference on Pharmacometrics (ACoP) 2018, San Diego, USA.

TABLE OF CONTENTS

LIST OF FIGURES

LIST OF TABLES

LIST OF EQUATIONS

GLOSSARY

ABBREVIATIONS

ABW	Ideal body weight
AC	Alternating current
ADME	Absorption, distribution, metabolism, and excretion
AIC	Akaike Information Criteria
AUC	Area under the concentration-time curve
BFAT	Body fat percentage
BIA	Bio-impedance analysis
BIA	Bio-impedance analysis
BM	Body mass
BMC	Bone mineral content
BMI	Body mass index
BMR	Basal metabolic rate
BOV	Between-occasion variability
BSA	Body surface area
BSV	Between-subject variability
BSVP	Predictable between-subject variability
BSVR	Random between-subject variability
CD4+	Cluster of differentiation 4
CDC	Centres for Disease Control and Prevention
CI	Confidence interval
CL	Elimination clearance
cm	Centimetre
CNS	Central nervous system
CT	Computed tomography
CV	Coefficient of variation
CYP	Cytochrome P450 enzymes
[CYP]	CYP abundance
DC	Direct current
DXA	Dual-energy X-ray absorptiometry
EBE	Empirical Bayes estimates
ECW	Extra-cellular water
Eq	Equation
FFM	Fat-free mass
FFM_{BIA}	Fat-free mass measured by bioimpedance analysis
FFM_{Ext}	Fat-free mass predicted by extended model
$FFM_{Ext(Ind)}$	Fat-free mass predicted by extended model in Indians
FFM_{Jan}	Fat-free mass predicted by Janmahasatian's model
FFM_{Kul}	Fat-free mass predicted by Kulkarni's model
FIC	First-in-children
FIH	First-in-human
FM	Fat mass
FO	First-order approximation
FOCE	First-order conditional estimation
g	Gram
GFR	Glomerular filtration rate

GFR	Glomerular filtration rate
GoF	Goodness-of-fit
h	Hour
Ht	Height
HU	Housenfield units
Hz	Hertz
I/O	Input-output
ICW	Intra-cellular water
IQR	Interquartile range
IV	Intra-venous
IVIVE	In vitro in vivo extrapolation
keV	Kilo electron volt
kg	kilogram
L	Litre
LBW	lean body weight
LC-MS	Liquid chromatography mass spectrometry
LFAT	Liver fat percentage
LLV	lean liver volume
LRT	Log-likelihood ratio test
LV	Total liver volume
MBMA	Model-based meta-analysis
MLE	Maximum likelihood estimation
MPPGL	Microsomal protein per gram of liver
MRI	Magnetic resonance imaging
N	Sample size
NAFLD	Non-alcoholic fatty liver disease
NASH	Non-alcoholic steatohepatitis
NHANES	National Health and Nutrition Examination Survey
NLME	Non-linear mixed effects
PD	Pharmacodynamics
PE	Prediction error
PK	pharmacokinetics
PNWT	Predicted normal weight
PO	Per oral
Pop-PK	Population pharmacokinetics
RF	Radio frequency
RSE	Relative standard error
RSE	Relative standard error
RUV	Residual unexplained variability
SAA	Surface area artefact
SSE	Stochastic simulation estimation
TBK	Total body potassium
TBW	Total body water
TMDD	Target mediated drug disposition
TNFα	Tumor necrosis factor-α
UGT	Uridine glucuronyl transferase
VPC	Visual predictive check
WT	Total body weight

C_p	Drug concentrations of plasma
C_e	Drug concentration in a hypothetical effect compartment
C	Predicted concentration of central compartment
C_{obs}	Observed concentration of central compartment
C_{avg}	Average concentration of central compartment
$C_{p,min}$	Trough concentration
$C_{p,max}$	Peak concentration
$C_{p,ss,min}$	Trough concentration at steady state
$C_{p,ss,max}$	Peak concentration at steady state
$C_{p,ss,avg}$	Average concentration at steady state
CL	Elimination clearance
CL_H	Hepatic elimination clearance
CL_{int,u_H}	Scaled intrinsic hepatic clearance (unbound)
$CL_{int,u}$	*in vitro* intrinsic clearance
Q	Distribution clearance
Q_H	Hepatic blood flow
V_c	Volume of central compartment
V_p	Volume of peripheral compartment
$f_{u,t}$	Free fraction of drug in tissue
$f_{u,p}$	Free fraction of drug in plasma
$f_{u,b}$	Free fraction of drug in blood
τ	Dosing interval
F	Bioavailability
D	Dose
$t_{1/2}$	Elimination half-life
E	Drug effect
E_{max}	Maximum drug effect
C_{50}	Concentration for half-maximal effect
k_{eo}	First order rate constant for disappearance of drug from the effect compartment
R_{in}	Zero order input rate
R_{out}	First order rate constant for output
S	Stimulation
I	Inhibition
p	Number of parameters
f	Mathematical function
$\hat{Y}_{ij}$	Model prediction
$Y_{ij,obs}$	Observation
θ	Fixed effects parameter
$\boldsymbol{\theta}$	Vector of population parameters
η_i	Random error between individuals on a population parameter
ω	Standard deviation of η_i distribution
$\boldsymbol{\Omega}$	Variance-covariance matrix of between-subject variability
η_k	Random error between occasions on an individual parameter
κ	Standard deviation of η_k distribution
$\mathbf{K}$	Variance-covariance matrix of between-occasion variability
ϵ	Residual error

σ	Standard deviation of ϵ
$\boldsymbol{\Sigma}$	Variance-covariance matrix of residual error
$\boldsymbol{\varphi_i}$	Vector of individual parameters
$\boldsymbol{x_{ij}}$	Vector of design variables
$\boldsymbol{Z_i}$	Vector of covariates
$\boldsymbol{\eta_i}$	Vector of random errors on individual parameters
L	Likelihood
OBJ	Objective function
β	Type-II error
Exp	Exponent of allometric scaling
Z	Bioimpedance
R	Electrical Resistance
X_c	Reactance
µA	Micro ampere
φ	Specific resistivity
r	Attenuation ratio
Ψ	Set of body composition parameters extended FFM model
N_{80}	Number of subjects required to achieve 80% power
V_B	Total body volume
V_F	Volumes of fat mass
V_{FF}	Volumes of fat-free mass
ρ_{BM}	Total body density
ρ_{FM}	Fat mass density
ρ_{FFM}	Fat-free mass density
ρ_{AT}	Adipose tissue density
f_{FM}	Fraction of fat mass of body
f_{FFM}	Fraction of fat-free mass of body
f_{AT}	Fraction of fat of adipose tissue
Δ	Difference
V_R	Residual air in lung
P_1	Pressure in first chamber of BOD POD®
P_2	Pressure in second chamber of BOD POD®
V_1	Volume in first chamber of BOD POD®
V_2	Volume in second chamber of BOD POD®
V_L	Lung volume
δ	Instrument specific constant for surface area artefact of BOD POD®
$R_{\mathrm{water/FFM}}$	Ratio of total body water to fat-free mass
$R_{\mathrm{TBK\,/\,FFM}}$	Ratio of total body potassium to fat-free mass

STRUCTURE OF THE THESIS

In this thesis covariate based scaling of drug doses from standard body size to differently sized individuals has been assessed. Under *Part I*, *Chapter 1* covers an introduction of the current state of knowledge about scaling of maintenance doses and the importance of accurate scaling of pharmacokinetic (PK) parameters. In particular, the influence of body size and composition on between-subject variability of drug clearance and identification of the right covariate to quantify are discussed.

Chapters 2 to *7* cover the assessment of key covariates, i.e. total body weight (WT) and fat-free mass (FFM) for the purpose of quantifying the influence of body size and composition on clearance. Broadly, these chapters are divided into three parts: *Part II* covers body size-based scaling, *Part III* covers body composition-based scaling, and *Part IV* covers scaling of clearance by lean liver volume (LLV).

Under *Part II*, *Chapter 2* covers a stochastic simulation-estimation based assessment of the current methodologies of *allometric* scaling of clearance by WT, which has been the conventionally used descriptor of body size.

Under *Part III*, methodologies associated with FFM based scaling are discussed. FFM has emerged as an alternative scaler of clearance since it accounts for body composition. However, FFM is not a readily measurable characteristic and several experimental methods are available for its measurement. The applicability and validity of the methods in a particular population depend on some key assumptions. Therefore, an extensive review of these FFM measuring methods is provided in *Chapter 3* that would help rationalise the use of these methods.

In practice, FFM is estimated by predictive models since the FFM measuring methods are quite resource intensive. The Janmahasatian model is mostly used for this purpose in clinical pharmacology. However, there is evidence that this model does not perform well in some population, e.g.

Indians, which can be attributed to ethnicity-related differences in body composition. Therefore, in *Chapter 4*, an extension of the Janmahasatian model has been developed that can extend the model's application to other populations. This extended model has been evaluated in a cohort of Indian patients.

Although FFM has been validated in a number of studies and recommended as the choice of scaler of clearance, the scaling relationship (i.e. exponent) varies across studies, and it is mostly empirical. In this context, a model based meta-analysis has been conducted and reported in *Chapter 5* in order to determine the average observed value of the exponent for scaling clearance by FFM.

Under *Part IV*, a new physiological variable, lean liver volume (LLV) is introduced for use as a universal descriptor of functional liver size. The key role of LLV in describing the variation in clearance is highlighted, especially in obese. Therefore, a predictive model of LLV has been developed in *Chapter 6*, where FFM is considered as the covariate. The relationship (i.e. exponent) between LLV and FFM can serve as the theoretical basis for clearance vs. FFM scaling exponent.

Additionally, further use of the LLV model, which has been developed in *Chapter 6*, is explored in *Chapter 7* by evaluating its potential use as a scaler in *in vitro-in vivo* extrapolation (IVIVE) of clearance.

Under *Part V, Chapter 8* concludes the thesis with a discussion of the findings and an outline for future research. This is followed by appendices which contain additional material such as NONMEM control files, MATLAB code files, and the References section.

PART I

INTRODUCTION TO THESIS

Chapter 1: Introduction

1.1. Quantitative clinical pharmacology

The goal of quantitative clinical pharmacology is to predict the right dose and regimen for every patient which, helps ensure a safe and effective drug treatment. The required (safe and effective) dose in a patient is influenced by the underlying pharmacology of the administered drug. From a quantitative point of view, the pharmacology of a drug is defined by two distinct set of properties known as pharmacokinetics (PK) and pharmacodynamics (PD) [1].

PK refers to the time course of drug concentration in a body fluids as a result of an administered dose of drug, whereas PD refers to the magnitude of drug effect in relation to its concentration in a body fluid [2]. Ideally, the effect of a drug is related to the concentration at the site of action [3] which is often impossible to measure. Therefore, it is common practice to use plasma concentration as the surrogate measurement, assuming the drug is in equilibrium between the water spaces of plasma and the tissue of interest where drug action takes place. In a broader framework [4], PK describes drug "exposure" over time $\pm$ summary measures such as the area under the concentration-time curve (AUC) and PD describes drug "effect" which can be a change in a pharmacological marker (e.g. TNFα/CD4+ count), an efficacy index (e.g. pain score), or a measure of safety (e.g. QT prolongation). The biological processes that govern the PK such as drug absorption, distribution, metabolism, and excretion (ADME) involve almost all parts of the body. On the other hand, the biological processes that govern the PD such as drug-target binding, target abundance, and turn-over primarily occur at the pharmacological target level. In either case, whether PK or PD, these associated biological processes vary widely in the population which makes the PK and the PD properties of a drug variable between individuals.

1.1.1. Pharmacokinetics (PK)

The time course of drug in the body after an intravenous (IV) administration is primarily defined by two PK parameters clearance (CL) and volume of distribution (V). Biologically, these two parameters are independent from each other within an individual. This means, if the CL values of two different drugs were similar, their V values would not necessarily be similar in an individual. However, individual values of CL and V of a drug are often correlated in the population, since they often share common biological factors (e.g. body size) which causes the individual parameter values to deviate from the population estimate.

1.1.1.1. Volume of distribution

Volume of distribution (V) is a measure of the distribution volume of a drug inside the body water [5]. If a drug freely distributes into the body water by passive diffusion, its V will be equal to the volume of total body water. For example, the reported mean V (CV%) of antipyrine in normally hydrated adults is 31 L (17%) [6]. Similarly, highly polar drugs like aminoglycosides that can only distribute into the extra-cellular water demonstrate a V of about 0.16 L/kg [7]. Some drugs exist in ionic form and thus cannot permeate beyond the plasma water of vascular space, so their V is nearly equal to the plasma volume, e.g. heparin [8]. The range of V across drugs varies hugely from a lower limit of about 0.04 L/kg (i.e. plasma volume) to several thousands of litres (e.g. chloroquine [9]). A higher value of V than total body water volume indicates substantial binding of the drug inside tissue(s) leaving the tissue free fraction ($f_{u,t}$) to be lower than plasma free fraction ($f_{u,p}$). The higher the volume of distribution of a drug the lower will be the total concentration of the drug in plasma at a given time point.

Volume of distribution depends on the drug's physico-chemical properties as well as the (patho)physiological status of the patient. Theoretically, a more lipophilic drug (e.g. general anaesthetics) will distribute more into adipose tissue than a less lipophilic drug. Therefore, from PK point

of view, it is expected that an obese individual has a higher (absolute) V than a lean individual for the former (more lipophilic) drug, e.g. phenytoin, diazepam, lorazepam whereas both individuals will have similar (absolute) V for the case of latter (less lipophilic) drug, e.g. digoxin, antipyrine [10]. However, within the high lipophilic category, it is difficult to predict the magnitude of change in V during obesity, i.e. whether the change is proportional (e.g. lorazepam) or less than proportional (e.g. digoxin) or more than proportional (e.g. diazepam) to WT [11, 12]. Even, a highly lipophilic drug's V can remain unaffected in obesity as seen in the case of propofol [13]. Similarly, V can increase during critical illness (e.g. sepsis [14]) most commonly due to altered protein binding, fluid shifts, and changes in pH [15]. Clinically significant alteration in V due to critical illness can be expected for hydrophilic drugs that have limited intra-cellular penetration and have low volume of distribution [15]. Therefore, variation in the physiological status (e.g. obesity, critical illness) between individuals in the population potentially causes variation in V, and thereby variation in the time course of the drug concentration.

1.1.1.2. Clearance

Clearance is a quantitative measure that quantifies the capacity of the body to eliminate xenobiotics (i.e. drugs). Primarily, the liver and kidneys are the two main organs that eliminate drugs from the body. Thus clearance of a drug often refers to the summation of hepatic and renal clearance where their individual contributions to the overall clearance vary across drugs.

1.1.1.2.1. Hepatic clearance

The majority of drug elimination in the liver is caused by bio-transformation (i.e. metabolism) by intra-cellular enzymes. Bio-transformation leads to (chemical) conversion of drug molecules to metabolites that are physico-chemically different (i.e. more polar) than the parent drug molecule, which facilitate their excretion through the kidney and/or bile. The majority of the hepatic bio-transformation happens by a set of oxidative enzymes known as cytochrome P450 enzymes (CYPs). CYPs are membrane bound enzymes that

are located within the microsomes of the hepatocytes and present in several isoforms, e.g. CYP3A4, CYP2D6, CYP2C9. CYP mediated bio-transformation is commonly referred as Phase-1 metabolism. The rest of the hepatic bio-transformation is caused by Phase-2 enzymes that are located within the cytosol of the hepatocytes, e.g. uridine glucuronyl transferase isoforms (UGTs).

The hepatic (systemic) CL of a drug depends on its intrinsic clearance and physiological variables. These physiological variables typically include CYP abundance (defined as pmol of CYP enzymes per mg of microsomal protein), functional liver size, hepatic blood flow, and drug free-fraction in the blood. The intrinsic clearance of a drug is very much specific to the drug and the metabolising enzymes (i.e. a drug specific property). However, physiological variables can vary widely across individuals, based on characteristics such as age, body size, health status, etc. For example, individuals with different body sizes likely have different liver sizes, which may influence drug CL differently. This implies, an obese patient (with normal organ function) may have a higher CL, and a child may have a lower CL, than an adult with normal body weight.

1.1.1.2.2. Renal clearance

Many drugs are eliminated from the body by the kidneys. Renal drug elimination primarily occurs through glomerular filtration and/or active secretion process from the distal tubular region. Similar to hepatic clearance, renal CL also depends on drug specific properties such as molecular weight, polarity, and also physiological variables such as glomerular filtration rate (GFR), plasma protein concentration, etc. Therefore, renal CL also varies with individual characteristics, due to the variation in physiological variables. For example, renal failure patients demonstrate lower CL than healthy patients due to a reduction in GFR.

1.1.2. PK model

The time course of drug concentration in the body (at a given dose) can be quantitatively described by a PK model where the PK parameters (e.g. CL) are

used as constants. A simple one compartmental PK model has been shown in Eq 1.1 where the drug is administered by an intra-venous (IV) bolus dose. Here, the basic assumption is that the distribution equilibrium between plasma water and tissue water is achieved instantaneously following drug administration, and the drug follows a first order elimination kinetics. Under this assumption, the (total) drug concentrations of plasma (C_p) and tissue(s) are not necessarily be the same, but tissue drug concentration proportionally changes with plasma concentration.

$$\frac{dC_p}{dt} = -\frac{CL}{V} \times C_p \qquad where,\ \ C_p(0) = \frac{Dose}{V}$$

Eq 1.1 One compartment PK model with intra-venous bolus dose

In reality, the distribution kinetics of drugs across different tissues can vary largely depending upon the physico-chemical properties of the drug and/or the perfusion to the respective tissues. Typically, when distribution is perfusion rate limited (i.e. no active process is involved), highly perfused tissues such as the liver, lungs, and kidneys achieve equilibrium much faster than the poorly perfused tissues such as muscles and adipose tissues. In such situation, it is common to assume two different pools (i.e. compartments) of tissues in which the drug resides throughout its time course in the body. The former pool which instantaneously reaches equilibrium with plasma is considered as the central compartment, and the latter pool is considered as the peripheral compartment. This means (total) drug concentration of plasma (C_p) proportionally changes with concentration of drug in the tissues of the central compartment (similar to one compartment). It is also assumed that the drug elimination occurs from the central compartment.

The schematics of one compartment and two compartment PK models [16] have been shown in Figure 1.1 (a, b). The two compartment model has two clearance parameters, i.e. elimination (CL) and distribution (Q) clearance, and also two volume parameters, i.e. central (V_c) and peripheral (V_p) volume of

distribution. A one compartmental model would produce a straight line (Figure 1.1c) when concentration-time profile is plotted on a semi-logarithmic scale, whereas a two compartment model would produce a bi-phasic profile (Figure 1.1d) due to initial distributional delay in the peripheral compartment. Sometimes a tri-phasic profile may appear (i.e. three compartment) if the distribution equilibrium into certain tissue(s) is achieved much slower than the other peripheral compartment.

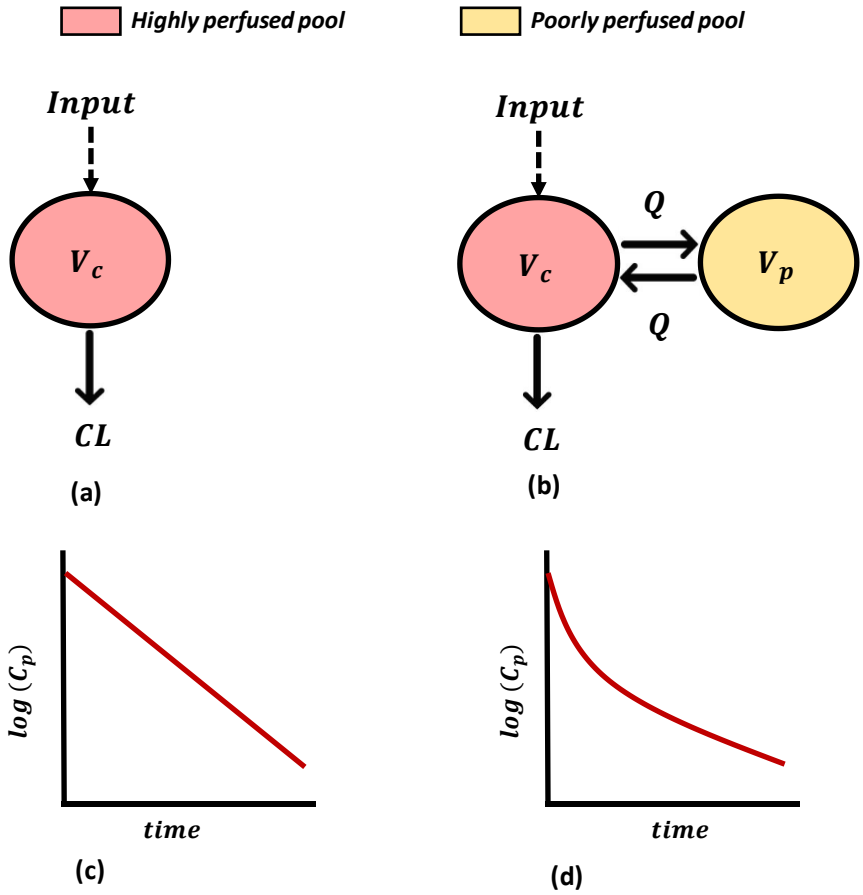

Figure 1.1 Schematics of one (a) and two (b) compartment models and their signature concentration-time profiles in (c) and (d) respectively.

V_c volume of central compartment, V_p volume of peripheral compartment, CL elimination clearance, Q distribution clearance, C_p drug concentration in plasma.

1.1.3. PD model

In quantitative pharmacology, the key assumption is that the pharmacological effect of a drug is related to its concentration at the site of action. This means that different concentrations of the same drug would produce different levels of effect in a patient. A PD model mathematically relates the drug effect to its concentration, thereby facilitating prediction of the effect of a drug at a given concentration. The mathematical constants that relate these two variables (i.e. effect and concentration) are known as PD parameters. In most cases, measurement of drug concentration at the site of action is not feasible in clinical studies. Therefore, PD model usually relates the drug effect to its concentration in plasma (blood) which is an easily accessible body fluid [2].

Typically, the concentration-effect relationships (defined by PD models) are found to be non-linear, probably due to the non-linear nature of the underlying biological processes (e.g. drug-receptor interaction [17]). For example, a general model for describing concentration-effect relationship is a simple E_{max} model (Eq 1.2) where E and C_p represent the drug effect and the plasma concentration respectively, and the PD parameters are maximum drug effect (E_{max}) and concentration for half-maximal effect (C_{50}). The underlying assumption is that the drug concentration at the site of action is in equilibrium with the plasma concentration (C_p).

$$E = \frac{E_{max} \times C_p}{C_{50} + C_p}$$

Eq 1.2 Simple E_{max} model defining concentration-effect relationship

The non-linearity of this equation is evident in the plot of drug effect (in percentage of E_{max}) against increasing values of C_p (Figure 1.2a). Here, the higher the drug concentration (C_p) the larger the effect is (E), which eventually reaches an asymptote to maximal effect (E_{max}). When C_p varies over several

orders of magnitude, then a semi-logarithmic plot (Figure 1.2b) helps to visualise the data better.

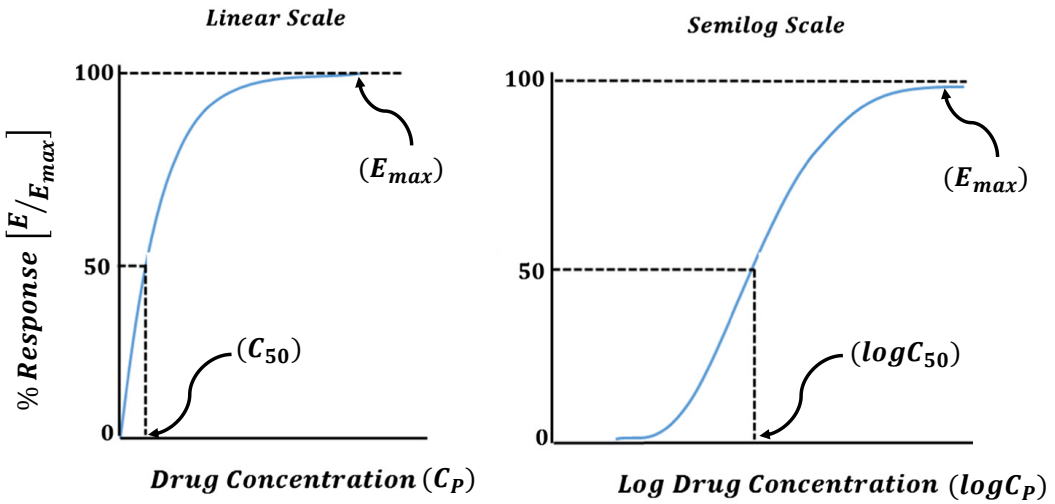

Figure 1.2 A typical concentration-effect profile simulated from a simple E_{max} model demonstrating the non-linearity in the relationship with respect to drug concentration; (a) linear scale (b) semi-logarithmic scale.

1.1.4. PK-PD model

PK-PD model describes the time course of drug action by mathematically relating dose and the effect via linking dose vs. concentration time course and concentration vs. effect relationships [3, 18, 19]. The type of chosen (PK-PD) link model primarily depends on the observed time courses of plasma concentration and effect of the drug and rest is dependent on available biological information.

When the peak effect occurs nearly at the time of peak plasma concentration, a direct (i.e. immediate) effect model is considered. A direct effect model assumes an instantaneous equilibrium between plasma and the site of action, which implies a proportional change in concentrations between plasma and site of action throughout the time course of the drug. This is the simplest circumstances where the PK model that describes the time course of C_p (e.g. Eq 1.1) can serve as the link model and the PK-PD model can be defined by Eq 1.3 (assuming an E_{max} model for PD).

$$E(t) = \frac{E_{max} \times C_p(t)}{C_{50} + C_p(t)} \qquad where, E(0) = 0, C_p(0) = \frac{Dose}{V}$$

Eq 1.3 A simple direct effect PK-PD model

In many cases, the peak effect of the drug occurs at a much later time point than that of the peak plasma concentration. This typically results in a counter-clock wise hysteresis loop when drug effects are plotted (in the Y-axis) against corresponding plasma concentrations (in the X-axis). Under such circumstances, an indirect (i.e. delayed) link model is applied to model the delay in drug action. A usual way of modelling such delay is to incorporate a link model to describe the time course of drug concentration in a hypothetical effect compartment (C_e) [20, 21] that describes the drug distribution to the 'biophase' [22]. A 'biophase' model assumes a non-equilibrium (or delayed equilibrium) distribution of drug between plasma and the effect site. For example, the link model for the simple one compartment PK by IV bolus administration (shown in Eq 1.1) can be written as Eq 1.4, where the first order rate constant k_{eo} determines the rate of disappearance of drug from the effect compartment. The rate at which the effect compartment achieves steady state is therefore related only to the rate constant k_{eo}. The amount of drug in the effect compartment is assumed to be negligible and therefore distribution to the effect compartment does not affect the mass balance in the equation for PK. Then the PK-PD model can be written as Eq 1.5.

$$\frac{dC_e}{dt} = k_{eo} \times (C_p - C_e) \qquad where, C_e(0) = 0$$

Eq 1.4 Link model for hypothetical effect compartment

$$E(t) = \frac{E_{max} \times C_e(t)}{C_{50} + C_e(t)} \qquad where, E(0) = 0, C_e(0) = 0$$

Eq 1.5 An indirect effect PK-PD model where effect is linked to the concentration of a hypothetical effect compartment (C_e) by a simple Emax relationship.

Sometimes, the delay can be modelled by describing the influence of drug on the natural turn-over of a relevant biological process (e.g. prothombin complex activity) in the body that results in the clinical expression of 'effect' [2]. Such PK-PD model is known as turn-over model or indirect response model [23]. A general format of the biological turn-over process is shown in Eq 1.6. The zero order rate R_{in} and the first order rate constant R_{out} describe the natural production and the degradation of the biological marker which is modulated by the drug to elicit its effect. The drug can either stimulate or inhibit any one of these two physiological parameters (R_{in}, R_{out}), which is modelled by factoring in either a stimulatory (S) or inhibitory (I) PD model into the respective parameters. The general format of the stimulatory and inhibitory PD models are shown in Eq 1.7 and Eq 1.8 respectively.

$$\frac{dE}{dt} = R_{in} - R_{out} \times E$$

Eq 1.6 A general model for describing biological turn-over processes

$$S = 1 + \frac{E_{max} \times C_p(t)}{C_{50} + C_p(t)}$$

Eq 1.7 Structure of the stimulatory PD model for incorporation into biological turn-over model

$$I = 1 - \frac{E_{max} \times C_p(t)}{C_{50} + C_p(t)}$$

Eq 1.8 Structure of the inhibitory PD model for incorporation into biological turn-over model

Therefore, a delayed PK-PD model for a one compartment PK with IV administration where drug distribution to the site of action is instantaneous can be defined by one of the suitable models from Eq 1.9, Eq 1.10, Eq 1.11 and Eq

1.12 in addition to the PK model in Eq 1.1. Selection of the most appropriate PD model should be guided by prior knowledge of the drug pharmacology.

$$Stimulation\ of\ input: \qquad \frac{dE}{dt} = R_{in} \times (S) - R_{out} \times E$$

Eq 1.9 An indirect response PK-PD model with stimulation of input

$$Stimulation\ of\ output: \qquad \frac{dE}{dt} = R_{in} - R_{out} \times (S) \times E$$

Eq 1.10 An indirect response PK-PD model with stimulation of output

$$Inhibition\ of\ input: \qquad \frac{dE}{dt} = R_{in} \times (I) - R_{out} \times E$$

Eq 1.11 An indirect response PK-PD model with inhibition of input

$$Inhibition\ of\ output: \qquad \frac{dE}{dt} = R_{in} - R_{out} \times (I) \times E$$

Eq 1.12 An indirect response PK-PD model with inhibition of output

The inter-relationship between PK and PD in a quantitative framework has been described in Figure 1.3. Notably, both PK and PD parameters are inherent properties of a drug within a specific population, and thus are not subject to external modification, but the dose (and/or regimen) can be adjusted. Therefore, an optimal pharmacological response (i.e. safe and effective treatment) can be achieved by modifying the dose and/or dosing regimen, if the PK and PD of the drug have been inter-linked appropriately. The PK exposure that produces the desired pharmacological response is known as therapeutic exposure.

The primary goal of quantitative clinical pharmacology is to predict the right dose and regimen for patients by quantifying the relationship between dose and the drug effect by developing a PK-PD model. This would help predict the pharmacological response within a standard individual at various doses and dosing regimens. However, in reality, individual patients hardly demonstrate standard characteristics such as body size (e.g. non-obese vs.

obese), age (e.g. adult vs. children), health status (e.g. normal vs. impaired organ function), etc. that affect the relevant physiology, and hence causes between-subject variation in PK and/or PD parameters. Such characteristics that reflect the sources of between-subject variability (BSV) of the PK and/or PD parameters are known as covariates. Therefore, identification of relevant covariates and quantification of their influence on the model parameters are key objectives of quantitative clinical pharmacology. Successful identification of covariates can help predict the right dose for the right patient, thus allowing dose scaling for optimal drug exposure and effect.

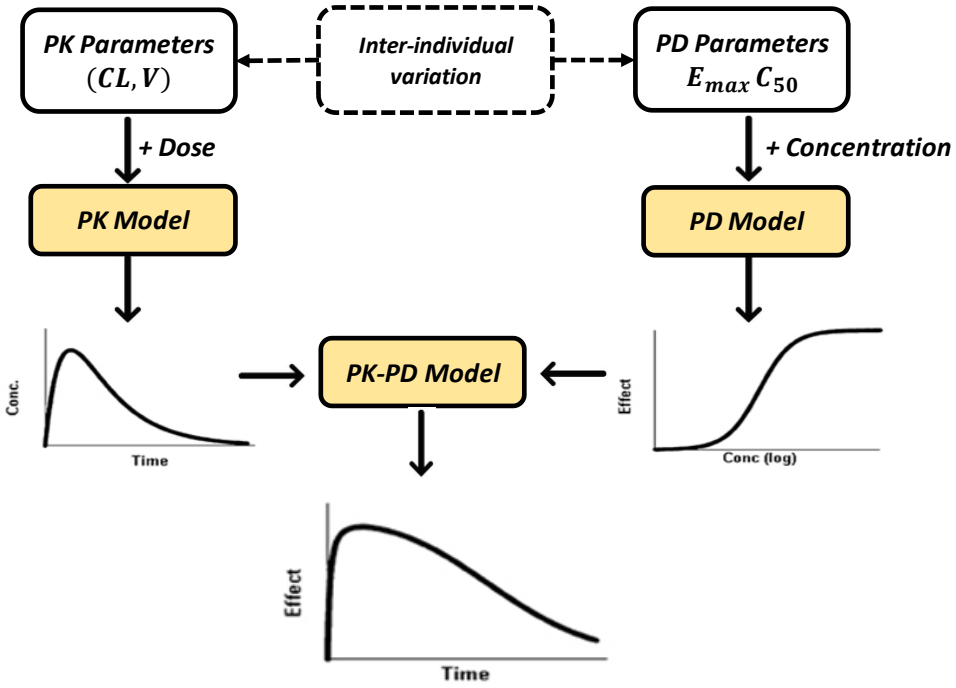

Figure 1.3 A schematic representation of the PK-PD modelling concept within quantitative pharmacology framework.

The PK and the PD models predict the concentration w.r.t. time and effect w.r.t. concentration. When connected, the PK-PD model predicts the time course of the drug effect. Both models are subject to inter-individual variation in their corresponding PK and PD parameters. The overall goal is to estimate these parameters, predict their inter-individual variations so that dose can be adjusted accordingly in order to achieve the therapeutic effect.

1.1.5. Basis of dose scaling

A fixed amount of dose that has proven for effectiveness in one particular population may not produce the desired effects in another population if significant variation in the PK and/or PD parameters was expected in the target population. Such situations are commonly encountered by the clinician when newly approved drugs are used in clinical practice. Due to the highly controlled nature of clinical trials, standard adult participants are studied during drug development (with few exceptions), and doses are approved based on observed therapeutic response in the standard adult population [24]. As a result, the approved doses do not necessarily produce optimal responses in other populations such as children, the obese, etc. This is because of the differences in relevant covariates (e.g. body size, age) in the target populations that lead to different PK exposures. In such circumstances, the dose is scaled according to the change in the covariate(s) from the standard population. For example, body weight is often a significant covariate of CL and thus body weight normalised doses are usually used clinically [25].

For dose scaling purposes, it is assumed that the exposure-response relationship remains unchanged between the patient groups (e.g. children vs. adult), and only the dose-exposure relationship changes due to the changes in PK parameter(s) [26]. Under this assumption, dose scaling actually simplifies to scaling of PK parameter(s) by the covariates in the target population. Since, CL is the sole PK parameter that determines the maintenance dose, scaling of CL is needed to achieve a desired steady state drug exposure in the plasma upon multiple dosing.

1.1.6. Maintenance dose

Under normal circumstances such as first order elimination, the rate of drug elimination is directly proportional to the plasma concentration (C_p) of the drug assuming the drug rapidly distributes within the water space of plasma and the eliminating organ(s). Here, CL is the proportionality constant (Eq 1.13, Eq 1.14).

$$Rate\ of\ Elimination \propto C_p$$

Eq 1.13 Drug elimination following first order kinetics

$$Rate\ of\ Elimination = CL \times C_p$$

Eq 1.14 Quantifying rate of drug elimination following first order kinetics

For chronic therapy, a constant drug exposure is desired so that the effectiveness of the drug is maintained. After a single administration, the drug exposure in the body decreases with time, and the amount of drug that is present at a particular time point depends on its elimination half-life ($t_{1/2}$). At completion of every half-life, 50% of the drug is eliminated from the body, which means that after 5 half-lives the drug will be almost completely eliminated from the body. Any successive dosing before completion of this wash-out period would cause the drug to accumulate inside body, and the extent of accumulation depends on the time and amount of successive dose administration. For example, if the same amount of dose is repeatedly administered at the completion of every half-life, then approximately equal amount of the dose will be accumulated inside the body after 5 doses (as 50% of dose is accumulated at every dosing interval). Due to drug accumulation after every dose, both the peak ($C_{p,max}$) and trough ($C_{p,min}$) concentrations would continue to increase until 5 doses, and further dosing would cause the plasma concentration to fluctuate between a fixed window of peak ($C_{p,ss,max}$)and trough ($C_{p,ss,min}$) concentrations. This state is known as steady

state (Figure 1.4) where the average of the peak and trough plasma concentrations ($C_{p,ss,avg}$) remains constant over time and commonly termed as steady state plasma concentration. This reflects a steady state exposure of the drug that is intended to be maintained throughout the duration of chronic therapy, and the dose that yields this steady state exposure is known as maintenance dose [1]. At steady state C_p in Eq 1.14 can be replaced by $C_{p,ss,avg}$ to form Eq 1.15.

$$Rate\ of\ Elimination = CL \times C_{p,ss,avg}$$

Eq 1.15 Rate of drug elimination at steady state after multiple doses

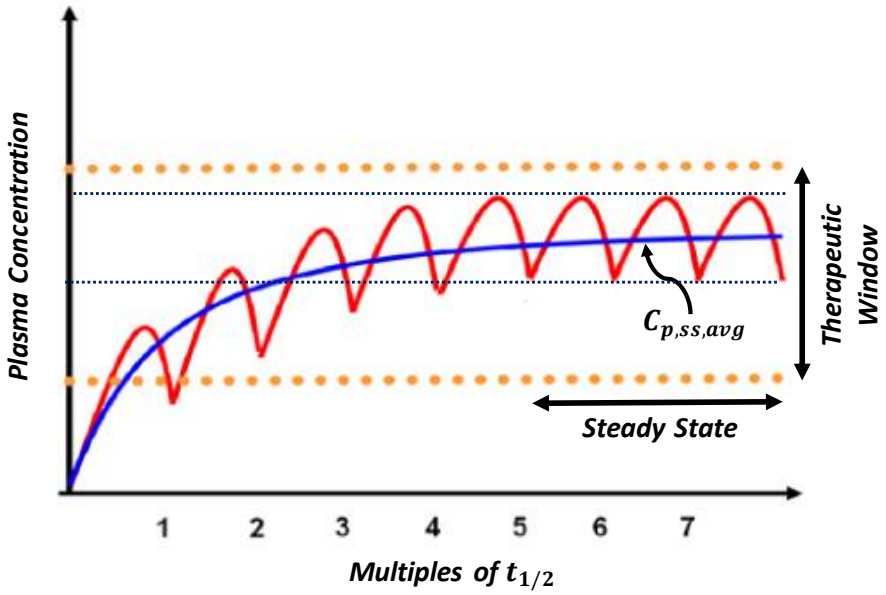

Figure 1.4 Achievement of steady state exposure upon repeated administration of a maintenance dose at every half-life.

At steady state, the drug exposure becomes constant (i.e. $C_{p,ss,avg}$) because approximately equal amount of the of the maintenance dose is remained in the body at every dosing interval, due to accumulation. This implies that the rate of input (i.e. dose) is equal to the rate of output (i.e. elimination). Therefore, Eq 1.15 can be rewritten as Eq 1.16.

$$Rate\ of\ Input = CL \times C_{p,ss,avg}$$

Eq 1.16 General relationship between rate of input and clearance at steady state

For a typical IV infusion, rate of input indicates the infusion rate (mass/unit time). But for IV bolus and oral administrations, rate of input refers to the amount of maintenance dose normalised to the dosing interval (τ). Therefore, Eq 1.16 can be rearranged as Eq 1.17 where F represents bioavailability (not applicable for IV).

$$Maitenance\ Dose = \frac{\tau \times CL \times C_{p,ss,avg}}{F}$$

Eq 1.17 Calculation of maintenance dose to achieve a target steady state concentration

When $C_{p,ss,avg}$ is known for a desired therapeutic effect, the maintenance dosing regimen (i.e. dose and interval) can be adjusted according (proportional) to the CL of the drug. This leaves maintenance dose scaling equivalent to CL scaling. The time to reach the steady state depends on relative magnitude of τ with respect to $t_{1/2}$ of the drug. The shorter the τ compared to the $t_{1/2}$, the sooner the steady state is reached. For scaling CL, the key is to identify its covariate(s) and how the covariate(s) influence(s) this parameter (parameter-covariate relationship) across the population. This is typically done by population pharmacokinetics (Pop-PK) modelling.

1.1.7. Covariates

Covariates are broadly defined as the intrinsic and extrinsic factors that influence the PK (and PD) parameters and thus describe the between-subject variability over these parameters to a significant extent. The intrinsic covariates are identifiable and measurable features of an individual (i.e. patient characteristics) that vary across the population such as body size, age, genotype, organ function (e.g. creatinine clearance), and patho-physiology (e.g.

serum albumin). The extrinsic covariates do not relate to the individual characteristics and can be modified externally, such as food, co-medication etc.

Another classification of covariates (including intrinsic and extrinsic) is based on their distributional properties, i.e. categorical and continuous covariates. The entire classification has been summarised in Figure 1.5. Categorical covariates takes the form of discrete values which are pre-assigned to define specific states of the patients. On the other hand, continuous covariates refer to some quantifiable characteristics that are measured on a scale, such as body weight is measured in kilogram scale.

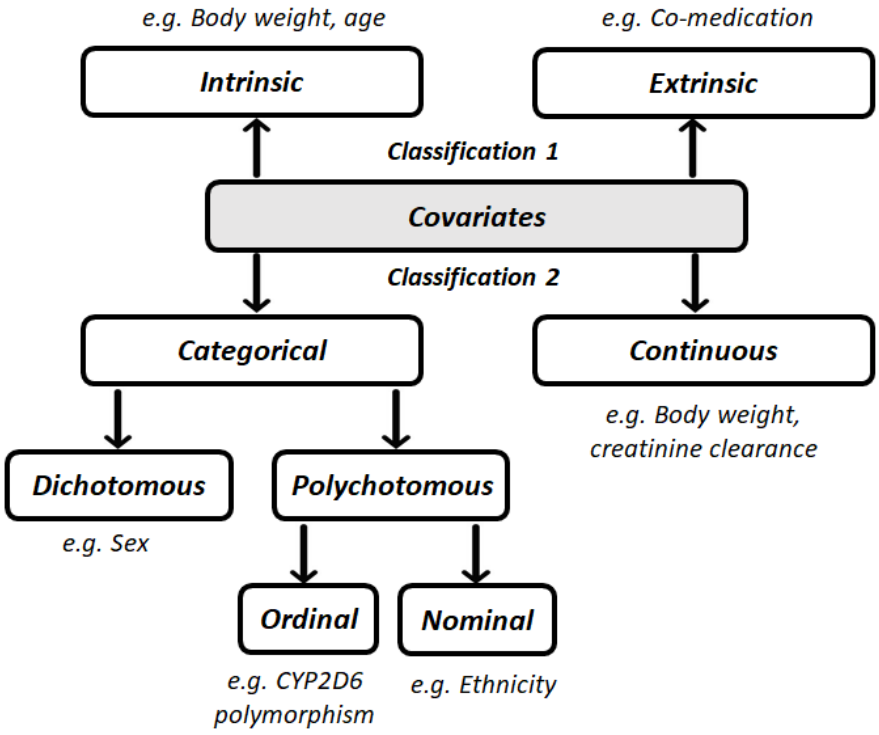

Figure 1.5 Summary of the overall classification system of covariates [27] .

1.1.8. Population pharmacokinetics modelling

Conventional PK studies in drug development include well controlled clinical studies involving a homogeneous population (i.e. with similar characteristics) and rich drug sampling designs. This type of approach is helpful in estimating the PK parameters. However, such well controlled studies

have limited ability to identify effects of relevant covariates on the PK parameters, which makes it challenging to extrapolate PK to different sub/special population, e.g. children, obese, and patients with impaired organ function. In this context, population pharmacokinetics (Pop-PK) studies are useful. Pop-PK studies mostly involve patients with wider range of characteristics such as body weight and age, with the exceptions of well controlled studies in early phase drug development, such as Phase 1 studies, where healthy adults within standard body size range are usually studied. Therefore Pop-PK studies are able to provide quantitative information about the PK variation in the respective target population(s), thereby giving the opportunity for dose scaling. Another advantage of Pop-PK study is that it can generate the required information from a sparse dataset (i.e. few samples per individuals).

There are several modelling approaches to analyse population PK data [28-31] such as the naïve pooled approach, the two stage approach, and the non-linear mixed effects approach. The naïve pooled method assumes that all observations arise from a single individual and hence can be interpreted as that no differences exist between individuals [32]. Because of this, naïve pooled method lacks the ability to estimate random effects parameters and the influence of significant patient covariates. Furthermore, it potentially causes biased estimation of fixed effects parameters. In the two stage approach, first the data from each individual is modelled separately in stage 1. In stage 2 the individual parameter estimates are combined in order to calculate the mean and variance of each parameter. Mixed effects refer to fixed effects parameters (e.g. mean CL in the population) and the variances of random effects that explains between-subject variability (BSV) of the parameters and the residual error in the data. The mixed effects approach combines all observed data and accounts for both population average effects and individual differences simultaneously.

In pop-PK modelling, the mean values of the PK parameters that correspond to a standard person in the population are estimated. However, within the population, individual PK parameters deviate from the standard values due to BSV. BSV has two components: predictable (BSVP) and unpredictable or random (BSVR) [33]. The predictable portion of the variability (BSVP) can be described by relevant covariates. Therefore, the larger the extent of BSVP the closer will be the population predictions of PK to the individual level. Therefore, covariate identification is a key objective of pop-PK modelling which is typically done in a non-linear mixed effects (NLME) modelling framework.

1.1.8.1. Non-linear mixed effects (NLME) modelling

1.1.8.1.1. The PK model

Pharmacokinetic model describes the rate of change of drug concentration (with respect to time) in the body. Under first order kinetics, the concentration changes exponentially with time, which is (mathematically) a non-linear process. Therefore, PK models are usually defined by a set of non-linear equations where time is the independent variable. Such non-linear equations that incorporate relevant PK parameters (e.g. CL, V) describe the concentration-time course of the drug in a standard individual that is representative of the population (i.e. population level prediction). This is known as structural model, which is defined by the fixed effects parameters. Fixed effects parameters also include covariate effects (if present) that extend the structural model predictions from population level to individual level by accounting for BSVP. However, concentration-time profiles of most individual participants in the study deviate from the predictions by the fixed effects parameters. In order to extend the model predictions to individual observations, random effects models are added to the structural model in a hierarchical manner [34].

The random effects models represent the stochastic components of the population PK model which usually represent a two stage hierarchy, viz., between-subject variability model (BSVR) and residual unexplained variability

(RUV) model. The BSVR model defines the distribution of the deviations of the individual PK parameters from their corresponding population values (after considering covariates). The RUV model is added which accounts for the differences of the predicted individual concentrations from the observations, i.e. intra-individual variation between the repeated measures. Such modelling approach is known as nonlinear mixed effects modelling (NLME) [35-37] that has different levels of hierarchy. Therefore, NLME modelling is basically a 'pharmaco-statistical' modelling framework where the structural model describes the pharmacology (here PK) of the drug that is accompanied by additional statistical models to describe the variation in the PK and individual observations. This makes NLME a powerful approach in predicting drug response at individual level in the population, providing the opportunity to adjust the dose based on patients' need.

1.1.8.1.2. Hierarchical models

A one compartment PK model with intravenous (IV) bolus input can be used for illustration purpose. The time course of the drug following administration of dose D can be described by Eq 1.18.

$$C_p(t) = \frac{D}{V} \times e^{-(\frac{CL}{V})\times t}$$

Eq 1.18 A one compartment PK model with intravenous (IV) bolus input

In two stage hierarchical modelling, this model in Eq 1.18 with two parameters ($p = 2$) is expressed as Eq 1.19 to describe the predictions by a function f, where $\hat{Y}_{ij}$ refers to the model predicted concentration of the drug in the i^{th} individual at j^{th} observation, $\boldsymbol{\varphi_i}$ represents the vector ($p \times 1$) of individual PK parameters in the i^{th} individual, and $\boldsymbol{x_{ij}}$ represents the vector of design variables like dose (D) and time (t) for j^{th} observation in the i^{th} individual. Here, a bold face notation indicates a vector or matrix.

$$\hat{Y}_{ij} = f(\boldsymbol{x_{ij}}, \boldsymbol{\varphi_i})$$

Eq 1.19 General model for individual level prediction of observations in two stage hierarchical modelling

The observed concentrations ($Y_{ij,obs}$) differ from the predicted ones ($\hat{Y}_{ij}$) by a residual unexplained error (RUV). The RUV model can be an additive (Eq 1.20) or multiplicative (Eq 1.21) error model or a combined error model (Eq 1.22). The additive error ${\epsilon_{ij}}_{add}$ and the multiplicative error ${\epsilon_{ij}}_{prop}$ are assumed to be normally and log-normally distributed around a mean of zero and a variance-covariance matrix $\boldsymbol{\Sigma}$, where σ_{add} and σ_{prop} represent their standard deviations respectively. An additive error model assumes a constant error for the entire range of observations. A multiplicative model assumes a constant coefficient of variation (CV) and implies a proportional error with respect to the observations. Further, combined error model assumes an additive type error in the lower observations but proportional error at larger values of observations. Typically the combined error model well suits the PK models and the additive errors mostly fits in the PD models [35, 38].

$$Y_{ij,obs} = \hat{Y}_{ij} + {\epsilon_{ij}}_{add}$$

Eq 1.20 Additive residual unexplained error (RUV) model

$$Y_{ij,obs} = \hat{Y}_{ij}.e^{\epsilon_{ij_{prop}}}$$

Eq 1.21 Multiplicative residual unexplained error (RUV) model

$$Y_{ij,obs} = \hat{Y}_{ij}.e^{\epsilon_{ij_{prop}}} + {\epsilon_{ij}}_{add}$$

Eq 1.22 Combined residual unexplained error (RUV) model

where, $\epsilon_{ij} \sim N(0, \boldsymbol{\Sigma})$, $\boldsymbol{\Sigma} = \begin{bmatrix} {\sigma_{add}}^2 & 0 \\ 0 & {\sigma_{prop}}^2 \end{bmatrix}$

In the second stage of hierarchy, the individual parameters ($\boldsymbol{\varphi_i}$) are defined by a function g Eq 1.23, where $\boldsymbol{\theta}$ is a vector (p × 1) of population mean parameters, $\boldsymbol{Z_i}$ is a scaler or vector of covariate(s), and $\boldsymbol{\eta_i}$ is a vector (p × 1) of random errors that represent the differences between the i^{th} individual's parameter values $\boldsymbol{\varphi_i}$ from the population mean parameter values $\boldsymbol{\theta}$. The random error $\boldsymbol{\eta_i}$ is assumed to be log-normally distributed around a mean of zero and a variance-covariance matrix $\boldsymbol{\Omega}$, where ω_{CL} and ω_V represent the standard deviations of the $\boldsymbol{\eta_i}$ distributions for the parameters CL and V respectively.

$$\boldsymbol{\varphi_i} = g(\boldsymbol{\theta}, \boldsymbol{Z_j}, \boldsymbol{\eta_i})$$

Eq 1.23 General model for individual level prediction of parameters in two stage hierarchical modelling

$$\text{where,} \quad \boldsymbol{\eta_i} \sim N(0, \boldsymbol{\Omega}) , \quad \boldsymbol{\Omega} = \begin{bmatrix} {\omega_{CL}}^2 & 0 \\ 0 & {\omega_V}^2 \end{bmatrix}$$

1.1.8.1.3. Estimation

In non-linear regression, the parameters are estimated by an iterative process due to unavailability of analytical solutions through approximations [39]. The idea of using NLME modelling in clinical pharmacology was conceived by Dr Lewis Sheiner and Dr Stuart Beal at University of California, San Francisco and was implemented by developing the software NONMEM [40, 41]. They used a maximum likelihood estimation (MLE) based estimation method that used a first-order Taylor approximation to linearise the model around the mean value of $\boldsymbol{\eta_i}$ [42-44]. This means during a step of search for a combination of parameters, all individuals have the same parameter values. This method is known as 'first-order approximation' (FO) method, which was implemented in the earlier versions of NONMEM. However, an advanced version of the approximation, i.e. 'first-order conditional estimation' (FOCE), has been successively implemented in the latter versions of NONMEM.

The MLE approach in FO method calculates the likelihood function of the j^{th} observation in the i^{th} individual (L_{ij}) as shown in Eq 1.24, where ${\sigma_j}^2$ represents the variance of the j^{th} observation. Therefore, the likelihood (or probability) of all the n_i number of repeated observations in the i^{th} individual (L_i) is the product of the likelihoods of the individual observations (L_j) as per Eq 1.25. Further, L_i can be rearranged to be represented as Eq 1.26. From there, -2 times of log-likelihood (-2LL) can be derived as per Eq 1.27.

$$L_{ij} = \frac{1}{\sqrt{2\pi{\sigma_j}^2}} e^{-\frac{1}{2{\sigma_j}^2}\left(Y_{ij,obs}-\hat{Y}_{ij}\right)^2}$$

Eq 1.24 Likelihood of the j^{th} observation in the i^{th} individual

$$L_i = \prod_{j=1}^{n_i} \frac{1}{\sqrt{2\pi{\sigma_j}^2}} e^{-\frac{1}{2{\sigma_j}^2}\left(Y_{ij,obs}-\hat{Y}_{ij}\right)^2}$$

Eq 1.25 Likelihood of the i^{th} individual

$$L_i = \prod_{j=1}^{n_i} (2\pi.{\sigma_j}^2)^{-\frac{1}{2}} . \; e^{-\frac{1}{2{\sigma_j}^2}\left(Y_{ij,obs}-\hat{Y}_{ij}\right)^2}$$

Eq 1.26 Likelihood of the i^{th} individual (rearranged)

$$-2LL_i = n_i.\log(2\pi) + \sum_{j=1}^{n_i}\left[\log({\sigma_j}^2) + \frac{\left(Y_{ij,obs}-\hat{Y}_{ij}\right)^2}{{\sigma_j}^2}\right]$$

Eq 1.27 Equation for minus two times of log-likelihood (-2LL) in i^{th} individual

Since the first term of Eq 1.27 is a constant, minimisation of the second term would maximise the likelihood L_i in the individual. Therefore, NONMEM minimises the value of the second term in the right hand side of Eq 1.27, which is known as objective function (OBJ). Further, assuming the variance ${\sigma_j}^2$ is constant which is denoted by σ^2, the OBJ for the i^{th} subject (OBJ_i) can be written as Eq 1.28. The overall OBJ of the dataset is the summation of OBJ_i for all N individuals (Eq 1.29). Therefore, OBJ depends on the squared error ($\left(Y_{ij,obs}-\hat{Y}_{ij}\right)^2$) weighted by the inverse of the variance σ^2. This means that a lower value of the OBJ reflects a better model fit.

$$OBJ_i = \mathrm{n_i}.\log(\sigma^2) + \sum_{j=1}^{n_i} \frac{\left(Y_{ij,obs} - \hat{Y}_{ij}\right)^2}{\sigma^2}$$

Eq 1.28 Calculation of individual NONMEM objective function ($\boldsymbol{OBJ_i}$) in FO

$$OBJ = \sum_{i=1}^{N} OBJ_i$$

Eq 1.29 Calculation of overall NONMEM objective function ($\boldsymbol{OBJ}$) in FO

In FOCE method [45], NONMEM primarily estimates the population parameters ($\boldsymbol{\theta}$) while it also estimates the empirical Bayes estimate (EBE) of the random variable $\boldsymbol{\eta_i}$. Therefore, NONMEM has two objective functions to minimise under FOCE: one for the parameters ($\boldsymbol{\theta}$), and the other for the EBEs ($\boldsymbol{\eta_i}$). The overall objective function for the i^{th} individual with total p number of parameters ($k = 1..\mathrm{p}$) is the summation of these two different objective functions, where θ_{ik} refers to the k^{th} parameter in the i^{th} individual, $\theta_{k,pop}$ refers to the population estimate of the k^{th} parameter and ${\omega_k}^2$ refers to the variance of the k^{th} parameter (Eq 1.30).

$$OBJ_i = \sum_{j=1}^{\mathrm{n_i}} \frac{\left(Y_{ij,obs} - \hat{Y}_{ij}\right)^2}{\sigma^2} + \sum_{k=1}^{\mathrm{p}} \frac{\left(\theta_{ik} - \theta_{k,pop}\right)^2}{{\omega_k}^2}$$

Eq 1.30 Calculation of individual NONMEM objective function ($\boldsymbol{OBJ_i}$) in FOCE

1.1.8.1.4. Covariate screening

Broadly, two types of covariate selection approaches have been discussed in the literature, viz. manual and automated [46-48]. In the manual selection approach, the modeller can control the selection of covariates based on the *a priori* knowledge; however, automated process incorporates the covariate(s) based on an algorithm. There is no consensus among the pharmacometrics community regarding the best method of covariate modelling. A common way is to look for correlation between the empirical Bayes estimates (EBEs) of the

base model vs. the available patient characteristics (e.g. body weight, age) [49, 50]. The EBEs refer to the η_i values that define the individual deviations of the parameter of interest. Therefore, observation of a reasonable correlation between EBEs of a parameter and a particular characteristic indicates a possible covariate effect on the parameter. This can be further confirmed if incorporation of the particular characteristic in the model (i.e. covariate model) eliminates the correlation. A more definitive way is to look for statistical significance followed by biological and clinical relevance [51, 52].

1.1.8.1.4.1. Covariate identification

A covariate needs to qualify a series of criteria to be incorporated into the population PK model.

Statistical significance: Successful identification of covariate(s) significantly drops the OBJ value that should also accompany the decrease in BSV of the parameter of interest and should be additionally guided by other diagnostics as appropriate [53]. These diagnostics primarily include graphical diagnostics such as goodness-of-fit plots (and/or residual based plots), but may include simulation based diagnostics as well, such as visual predictive check (VPC) with appropriate stratifications (e.g. age group, BMI group) as needed, whereas every diagnostic tool has its own limitation [54]. For example, EBE based diagnostics can become misleading in uninformative datasets due to the presence of η_i and/or ϵ-shrinkage (>20-30%) as shown by Savic and Karlsson [49]. A covariate should cause significant improvement in the overall model fit. In NONMEM, the extent of model fit is usually assessed by the OBJ. The lower the OBJ the better is the model fit. The statistical significance of the improvement in model fit is usually assessed by the likelihood ratio test. In likelihood ratio test, it is assumed that the decrease in OBJ between base model and the covariate model (ΔOBJ) is Chi-squared distributed. For nested models, it is usual to set the statistical significance criteria as >3.84 points drop in the ΔOBJ (for one additional parameter in the covariate model than the base model). This corresponds to a statistical *p-value* <0.05. For non-nested models,

other criteria such as the Akaike Information Criteria (AIC) [55] can be applied. AIC was developed on the concept of K-L information (Kullback-Leibler information) that quantifies the "distance" between the full reality and a model. Akaike found a formal relationship between the relative K-L distance and likelihood theory. He found that the maximized log-likelihood (***LL***) value was a biased estimate of relative K-L distance, but this bias was approximately equal to **p**, the number of estimable parameters in the approximating model. Therefore, Akaike found an estimator of relative K-L distance is approximately equal to $(LL - p)$. AIC refers to -2 times of the relative K-L distance that becomes equal to $(OBJ + 2\text{p})$. These criteria allow non-nested models having different number of parameters to be compared between each other by adding a penalty for the number of parameters (p).

Ribbing et al. [56] have highlighted that the main problem of choosing covariates based on statistical significance is selection bias. Selection bias refers to a higher covariate coefficient than its true value (i.e. effect size) when the respective covariate is statistically selected in the model. Selection bias can originate from two sources, viz. competition bias and stopping rule bias. Competition bias occurs when a covariate is selected from a pool of multiple correlated covariates that compete with each other for the parameter of interest. Although the overall contribution of competition bias on the selection bias is marginal, the presence of highly correlated covariates carries the risk of incorporating a false covariate in the model. This has been shown in the context of competition between total body weight and fat-free mass (highly correlated) as the covariate of clearance [57]. The majority of the selection bias comes from the stopping rule bias. Stopping rule is defined as the statistical significance criteria (e.g. $p < 0.05$) that has been traditionally used to conclude the success (or failure) of a clinical trial based on the clinical end point. It has been previously shown that decisions made with such stopping rule can inflate the effect size of the trial [58]. Similar influence has been observed in covariate selection also, where the stricter the stopping rule criteria (e.g. $p < 0.05$ vs. p

<0.01) the larger the selection bias would be. Stopping rule bias is particularly evident in low powered clinical studies.

By classical definition, power is the probability of not getting a type-II error $(1-\beta)$. For the context of covariate modelling, power refers to the probability that a true covariate is selected in the model when the covariate is chosen based on such stopping rule. The weaker the effect of a covariate (i.e. small effect size) the higher is the power required to incorporate the covariate in the model. Therefore, under-powered studies can inflate the effect size of a weak covariate if a strict stopping rule is applied. Similar inflation of effect size can occur for latent covariates whose data-type and distribution are not known *a priori* [59]. Because of this, population PK-PD studies need to be adequately powered if covariate identification is done by statistical significance. Otherwise, a biased covariate model would be incorporated that would compromise the predictive performance of the model during model extrapolation. Therefore, covariate identification must be justified by supporting evidence from biological perspective.

Biological plausibility: Apart from statistical significance, selection of a covariate must be justified by relevant biological information. For example, body size is known to directly (positively) influence drug clearance [60, 61] under normal body size and physiological range (obesity often confounds this positive influence). Therefore, the coefficient (i.e. effect size) of the covariate model is expected to be positive when body size descriptors are included as covariate; a negative estimate of the coefficient, if appeared statistically significant, should be rejected unless there is prior biological justification. In realty, clearance of many drugs may not be affected by obesity, such as midazolam, lidocaine, propranolol, verapamil or even, can be negatively influenced by obesity, such as triazolam [62]. This implies that the exponent can be of any value from negative to positive range (including zero); which needs to be appropriately justified by biology before accepting the estimated value. Further, the selection of the right body size descriptor (e.g. total body weight or

fat-free mass or body surface area) should be guided by appropriate biological justification. It is often hypothesised that fat-free mass is better correlated with clearance than total body weight [25] based on the fact that clearing organs increase in their size and/or capacity (that drive clearance) according to the change in fat-free mass. In spite of the known biology, FFM may not be statistically selected as the covariate on clearance in competition with WT, if the study design is not appropriate as shown by Han et al. [57]. Sometimes, biological plausibility can help preselect the covariates and incorporate in the base model from the beginning. For example, creatinine clearance is often an *a priori* covariate when modelling drugs that are renally eliminated.

Clinical relevance: In addition to the above criteria, the selected covariate needs to change the parameter of interest to substantial extent which could be clinically relevant to necessitate a dose adjustment [63]. An arbitrarily criteria of more than ±20% change in the parameter value within the inter-quartile range of the covariate is often considered relevant for dose adjustment purpose. A covariate that fails to influence the parameter to alter more than 20% (from its standard value) across its range in the population may not be meaningful for incorporation in the population PK model. On the other hand, a poor study design (e.g. narrow range) may lead to exclusion of a clinically relevant covariate due to lack of statistical significance. This has been shown for the case of enoxaparin [52] where the extent excreted (by kidney) unchanged is known to be 80%. However, a few clinical studies failed to identify creatinine clearance as the covariate of enoxaparin clearance due to inappropriate trial design.

1.1.9. Body size as covariate of clearance

The most commonly identified covariate of CL is body size. This is because the key physiological/anatomical variables that drive CL are known to vary with variation in body size. These variables are typically the size [64] and perfusion [65, 66] of the clearing organs, i.e. liver and kidney.

The change in CL in an individual (from the population standard) can be broadly expressed by Eq 1.31 [61]. The individual clearance (Cl_i) is the product of the population average (CL_{std}) and the three factors for maturation (F_{mat}), organ function (F_{func}), and body size (F_{size}).

$$Cl_i = CL_{std}.F_{mat}.F_{fun}.F_{size}$$

Eq 1.31 General equation of expressing change in the individual clearance from the population standard

The factor F_{mat} defines the maturational stage of drug elimination pathway(s) (i.e. ontogeny [67, 68]) in children. This is required since the physiological variables that are responsible for drug elimination (e.g. CYP expression or GFR) are not fully mature during childhood [61, 69]. So, for scaling for an adult the value of F_{mat} equals to 1.

The factor F_{func} refers to the functional status of clearing organs, i.e. kidney and liver. Organ function can be impaired by various pathological conditions that can exist within the organ (e.g. cirrhosis) or outside the organ (e.g. diabetes/obesity induced renal impairment) as well. Similarly, for scaling for an adult with a normal organ function the value of F_{fun} would be 1. Therefore, F_{size} remains the sole factor that plays a key role in scaling CL in adults whose organs are expected to function normally. F_{size} defines the influence of the change in the body size of an individual (WT_i) from the standard body size in the population (WT_{std}).

1.1.9.1. Scope of body size based dose scaling

The common target populations that are vulnerable to body size related change in drug PK are obese patients and children. Therefore, these two populations are subject to consideration for body size based dose adjustment.

1.1.9.1.1. Obese patients

Obesity has reached an epidemic proportion not only in Western societies but also in other parts of the world [70, 71]. Obesity refers to excessive adiposity in the body, defined as body mass index over 30 kg /m^2 [72]. Obesity co-exists with a range of co-morbidities which include: diabetes mellitus, cardiovascular disease, and hepatic and renal impairment [73]. Therefore clinicians are facing increasing number of obese patients in the clinic. Obese patients with no evidence of organ impairment often require higher maintenance drug doses than their non-obese counterparts. However, dosing guidelines for obese patients are often lacking since obese individuals are usually excluded from clinical trials during standard drug development [24]. Therefore, drug dose adjustments in obese patients are a common problem that is usually encountered in the post-approval stage.

However, some therapeutic areas require obese patients to be studied during the drug development stages. Such drug development programmes either directly target obesity as the primary therapeutic indication [74] or other therapeutic areas that are highly associated with obesity (e.g. hypercholesterolaemia [75]). A recent example of the latter case is non-alcoholic fatty liver disease (NASH) where more than ten drug candidates are currently in clinical development [76].

NASH is an advanced fibrotic and/or inflammatory stage of non-alcoholic fatty liver disease (NAFLD) that causes accumulation of substantial amount of intracellular fat in the liver (steatosis) [77, 78]. Currently, NASH severity is diagnosed through liver biopsy which is an invasive procedure, whereas liver fat measurement can be made by non-invasive imaging

techniques such as magnetic resonance imaging (MRI) [79, 80]. It has been reported that more than 80% of NASH patients are obese [78]. Current FDA guidance [81] for NASH drug development specifically recommends not to conduct extensive efficacy study directly in biopsy-confirmed NASH patients; instead a prior proof-of-concept study (Phase-IIa) in high risk patients (i.e. obese) is recommended. As per the guidance, only drugs that have demonstrated significant reduction of liver fat in the proof-of-concept study should be taken in Phase-IIb, where biopsy confirmed NASH patients can be studied. This indicates a new scope for dose translation from standard adults (First-in-human) to obese patients (Phase-IIa onwards) in drug development programmes.

1.1.9.1.2. Paediatric patients

Similar to the obese population, there has been a scarcity of clinical trials in paediatric populations as part of routine drug development. This is mostly because of ethical and logistical challenges typically encountered while conducting clinical studies in this special population and to some extent lack of financial incentive among pharmaceutical companies [82]. As a result, use of drugs in children has largely remained 'off-label' [82, 83], which makes drug dose adjustments in children challenging.

Maturation in the drug elimination mechanisms (i.e. ontogeny), in addition to body size and composition, are key considerations in paediatric dose selection. Failure to understand age-dependent maturation processes has resulted in serious adverse events in children in the past [84]. This has necessitated enactment of legislation in the Unites States of America (e.g. Best Pharmaceutical for Children Act 2002) and in Europe (Paediatric Regulation 2007) to minimise off-label use of drugs in children, thereby ensuring safe and effective therapy in this vulnerable group of patients [85-87]. These new laws have made paediatric clinical trials mandatory for new drug development programmes if the targeted population of the drug includes children.

As a result of this paediatric research initiative, a number of paediatric trials have been carried out in the USA by the pharmaceutical industries and the National Institute of Health (NIH); a total of 778 paediatric labelling changes have been made from February 1998 to March, 2019 due to this campaign [88]. Since these legislations also have the provision for allowing additional market exclusivity right (6 extra months) [89], pharmaceutical companies are incentivised to carry out more paediatric drug development studies. Unlike first-in-human (FIH) studies in adults, where the primary concern is safety (not necessarily efficacy), the first-in-children (FIC) studies need to demonstrate both safety and efficacy, since healthy children are not studied for ethical reasons [90]. This makes the FIC dose finding challenging. Therefore, significant research opportunities exist in this area.

1.1.9.2. Descriptors of body size

Conventionally, total body weight (WT) has been used as the descriptor of body size and F_{size} (see Eq 1.31) is calculated as the ratio of individual body weight (WT_i) to standard body weight in the population (WT_{std}). This corresponds to the 'mg per kilogram' dosing scheme that is commonly found in drug labels [25]. The choice of WT has become universal in clinical practice primarily because of its ease of measurement. However, there are other alternative size descriptors [91], e.g. body surface area (BSA), fat-free mass (FFM), ideal body weight (IBW), predicted normal weight ($PNWT$), and adjusted body weight (ABW) that may be more suitable to use in the obese. Among the alternative size descriptors, FFM has gained considerable interest because of its relevance to pharmacokinetics.

1.1.9.2.1. Total body weight

In the conventional 'mg per kilogram' system, the approved (adult) dose is multiplied by the ratio WT_i/WT_{std} where WT_{std} is often used as 70 kg [69]. This 'mg per kilogram' method assumes that drug clearance is proportional to WT and the dose proportionally scales with CL. However, this method tends to over dose obese patients that confounds the assumption.

It is generally hypothesised that CL increases with WT less than proportionally. This was supported by the observed relationship between basal metabolic rate (BMR) and WT across multiple species. Thus a similar non-linear relationship has been adopted for scaling CL by WT where the population CL (CL_{std}) is centred at WT_{std}, and is popularly known as *allometric* scaling (Eq 1.32). The underlying assumption of $allometric$ scaling is that CL (a parameter that describes the drug elimination capacity) is proportional to BMR. The term Exp refers to the exponent that describes the shape of the non-linearity. A value less than one for the exponent indicates a less than proportional scaling of CL to WT.

$$CL_i = CL_{std} \times \left[\frac{WT_i}{WT_{std}}\right]^{Exp}$$

Eq 1.32 Allometric scaling of clearance by total body weight

Although *allometric* scaling has been extensively used in both inter- and intra-species (i.e. human population) scaling of CL there is no consensus on the value of the exponent. Some researchers propose use of universal fixed values of the exponent that were historically observed in the BMR vs. WT relationship across species. Those observed values were $2/3$ [92] and $3/4$ [93]. Scaling by $WT^{2/3}$ is equivalent to scaling by BSA which is commonly used in dose selection in oncology. For scaling by $WT^{3/4}$, a theoretical framework was proposed by West et al. [94] by conducting a fractal analysis of the human vasculature from where the transport of essential materials takes place. Because

of this theoretical support, the use of 3/4 exponent has become ubiquitous in pharmacology.

However, other researchers do not agree with the existence of a universal value of the exponent that scales CL to WT. It is proposed that the value of the exponent depends on the data, i.e. empirical, hence "let the data speak" approach should be followed to determine the exponent [95]. Recently, It has been shown that the exponent can have a range of values for both inter- and intra-species scaling of CL [96, 97]. For intra-species scaling, the value of the exponent ranged from 0.5 to 1.2 [97]. A more detailed description of the origin of these exponent values and a brief account of the current conflict has been given in Chapter 2: . The presence of two different schools of thoughts around the value of the scaling exponent creates confusion among the pharmacometricians. Amidst this ongoing debate, it is currently unknown which method is likely to give the true exponent value.

Determining the true exponent value is critical in covariate model development, since it defines the effect of the covariate on the fixed effects (e.g. CL prediction). A falsely chosen exponent or a biased estimate of the exponent potentially cause bias in the estimation of CL when extrapolated outside the range of the population that was used to develop the model. For example, if the covariate model was developed in the standard adult WT range, a wrong exponent value (either chosen from the set of fixed values or estimated empirically) can result in biased CL prediction in children and obese adults who are the two extremes of the WT range. This has been shown in Figure 1.6 where CL values were simulated across the range of the population from an arbitrarily chosen CL_{std} of 70 mL/min. Simulations were conducted considering the whole range of plausible exponent values (i.e. 0.5, 0.67, 0.75, 1, 1.2) as found in the literature. It clearly demonstrates that the predictions do not deviate significantly around the standard body weight of 70 kg. However, the deviations are evident at the two extremes of WT range. As per the

simulation range (*WT*: 10-210 kg), the deviations can be as high as 2-fold in obese and 4-fold in children.

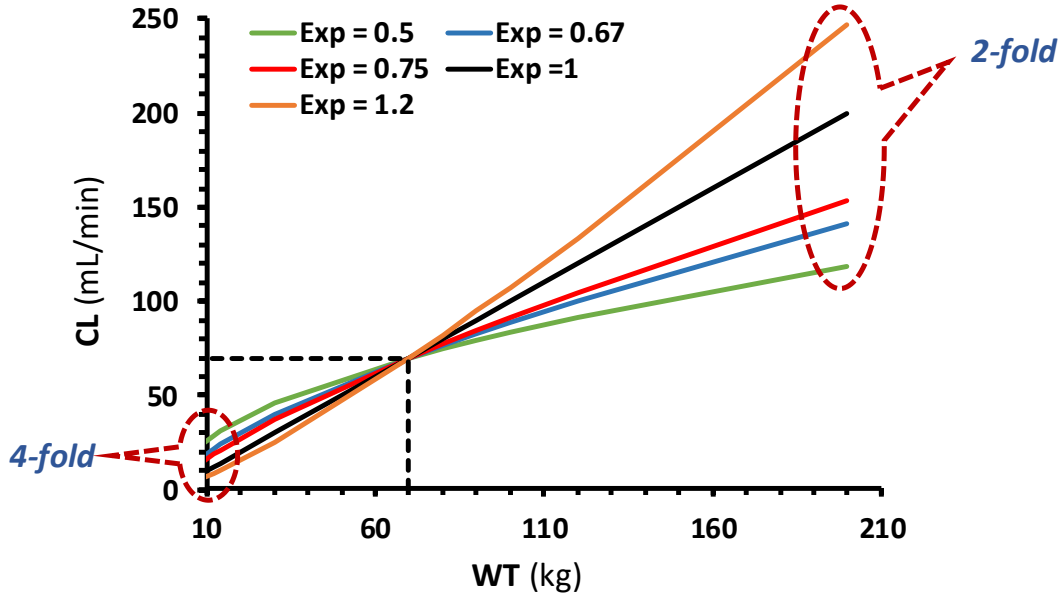

Figure 1.6 Simulation of *CL* using allometric model with different exponent values.

Therefore, if the purpose of the model is extrapolation of *CL* (e.g. designing first-in-children study), choosing the right exponent is the key for correct dose selection in the target population. In this context, a simulation-estimation based assessment is described in Chapter 2 in order to evaluate the current approaches of *allometric* scaling for their accuracy. This analysis would provide specific guidance to pharmacometricians on how to choose the right method in the right circumstances.

1.1.9.2.2. Fat-free mass

Fat-free mass *(FFM)* describes the lean component of the body excluding all fat and is essentially the sum of muscle mass, bones, non-adipose components of internal organs, and extracellular fluid and excludes fat in cellular structures. *FFM* is often referred to in the literature as lean body weight

(LBW) and used as a measure of non-fat weight. However, in the same individual FFM takes a slightly lower value than LBW (2-5%) as the latter includes the fat in bilayer lipid membranes, CNS, and bone marrow [98, 99]. Since the available body composition measurement techniques are not able to distinguish between these intrinsic fats from the rest of the body fat it is not possible to experimentally measure LBW. In contrast, FFM can be measured experimentally using various techniques and is used to approximate LBW.

1.1.9.2.2.1. FFM methods

Various experimental methods are available to measure FFM, e.g. bio-impedance analysis (BIA) , dual-energy X-ray absorptiometry [100]. These methods are quite cumbersome to use in regular practice. Some of the common issues with these methods include high cost, invasiveness, lengthy procedures, inadequate accessibility etc. Therefore, predictive models are developed to predict FFM from readily measurable patient characteristics (e.g. weight, height, and sex). However, these methods are useful for generating FFM data for the model development purpose.

Measuring FFM by each of these experimental methods is based on particular assumption(s) which may or may not be valid within and between populations. Because of the non-universality of these assumption(s), a particular method may need to be restricted for use in one particular population (e.g. adults) and another method to be used for other populations. Therefore, a systematic understanding of the available experimental methods is a prerequisite for their rational use in future research. In this context, a concise review of these methods has been written in Chapter 3. This review gives special emphasis on mathematical interpretation of the assumptions (and limitations) of these methodologies and thereby connecting them to each other in a common scientific framework.

1.1.9.2.2.2. FFM models

In regular practice, the use of FFM mostly depends on predictive models. Although a number of predictive models are available in the literature most of them were developed empirically. Empirical model development entirely relies on the regression of observed FFM against observable patient characteristics such as weight, height, and sex. Therefore, such models depend on the data and if used outside the population that was used for their development, can yield erroneous predictions of FFM. For example, the James model for FFM (Eq 1.33, Eq 1.34) [101] was developed empirically using a limited range of body size, and did not include sufficiently obese patients in their study. Because of this, the model yields unrealistic values of FFM beyond a certain body weight, which causes an inverted parabola like shape to the FFM vs. WT plot (Figure 1.7).

$$FFM_{male} = 1.1 \times WT - 128 \times \left(\frac{WT}{Ht}\right)^2$$

Eq 1.33 James model for FFM prediction in males

$$FFM_{female} = 1.07 \times WT - 148 \times \left(\frac{WT}{Ht}\right)^2$$

Eq 1.34 James model for FFM prediction in females

Later, Janmahasatian et al. [102] developed a FFM model based on the biological relationship between bioimpedance (Z) and body mass index (BMI). Bioimpedance is actually the measured resistance (R) of human body that is exerted against the flow of an high frequency AC current through the body. Therefore, bioimpedance indirectly reflects the body composition, i.e. proportions of various biomaterials that altogether cause the resistance. Such models that not only describe the data but also support a mechanism are more reliable for extrapolation purposes. Therefore, the Janmahasatian model (Eq 1.35, Eq 1.36), since its development has been extensively used in clinical pharmacology studies, and is widely recommended.

$$FFM_{Jan(male)} = \frac{9270 \times WT}{6680 + 216 \times BMI}$$

Eq 1.35 Janmahasatian model for *FFM* prediction in males

$$FFM_{Jan(female)} = \frac{9270 \times WT}{8780 + 244 \times BMI}$$

Eq 1.36 Janmahasatian model for *FFM* prediction in females

A comparative plot of the James model and the Janmahasatian model has been shown in Figure 1.7 where FFM values were simulated using the corresponding models over a range of body weights. For a given value of height, the James model starts falling down beyond a certain weight, whereas the Janmahasatian model continues to produce increasing values of FFM. This phenomenon warns about the risk of using empirical models, and the need for mechanism based models in practice.

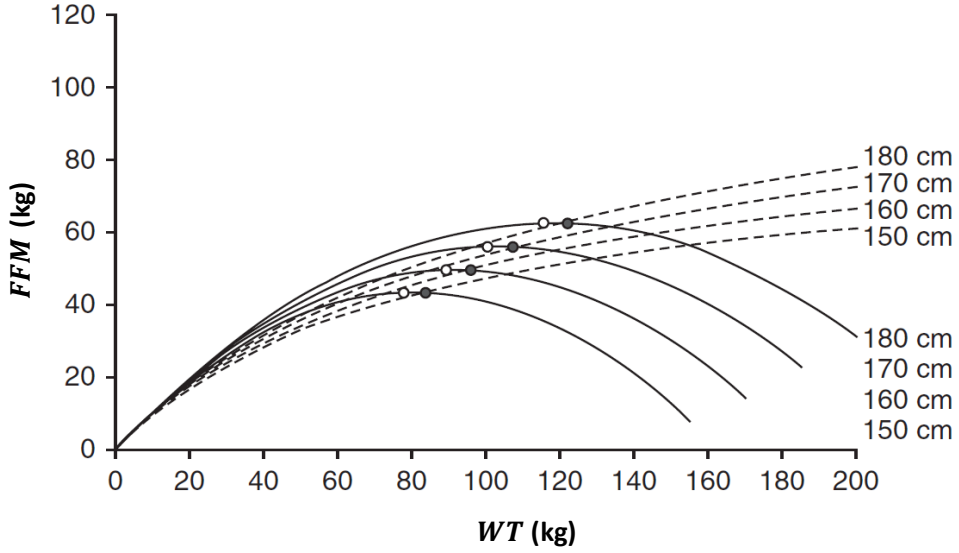

Figure 1.7 Simulation of *FFM* values from James model [101] and Janmahasatian model [102] at different heights of 150, 160, 170, and 180 cm. (reproduced from the report of La Colla et al. [103]).

However, the Janmahasatian model was developed in a population composed primarily of individuals with a European ancestry. The biological assumptions made thereof may not be valid in populations of other ethnic origins where a large inter-ethnic variation in body composition is expected. For example, it is widely reported that body composition widely varies between Asian Indians, Europeans, and Pacific Islanders. At a given BMI, Asian Indians have the highest percentage of body fat, while Pacific Islanders have the lowest body fat, with the Europeans being at the middle of the rank order [104]. This indicates the need for the validation of the Janmahasatian model in these populations. Recently, a validation study in an Indian population [105] has revealed that the model over-predicts FFM in Indians in comparison with BIA-measured FFM data. Therefore, there is potentially a need to extend the Janmahasatian model to other populations, and hence an extension of this model was developed in Chapter 4.

1.1.9.2.2.3. Relevance of FFM in clinical pharmacology

From a biological perspective, drug elimination exclusively takes place within the FFM component of the body, because the clearing organs are part of the FFM. So, variation in the size and/or capacity of the eliminating organs (that determine CL) are expected to follow the variation in FFM rather than WT. For example, it has been shown that glomerular filtration rate (GFR), which reflects the size and/or capacity of kidneys to eliminate drugs, varies proportionally with FFM rather than WT between normal and obese individuals [65]. Therefore, it is generally hypothesised that CL is better correlated with FFM than WT when body composition is altered along with size, e.g. obesity [25].

In an extensive review by Green and Duffull [91], it was shown that CL was best described by FFM as compared to other available size descriptors like WT, BSA, and IBW. The authors recommended FFM -based dose scaling of maintenance doses in the obese. As a result of growing interest in FFM, as a

measure of body size and composition, a few researchers have validated FFM based dose scaling by clinical studies with obese patients. Ingrande et al. [106] has established that the FFM based dose normalisation is the best way to scale the dose of propofol infusion in obese patients compared to a control group. Similar FFM based dosing recommendations were also made for other anaesthetics such as remifentanil [103] and dexmedetomidine [107].

1.1.9.2.2.4. Scaling by FFM

In spite of its biological relevance in scaling CL, the exact relationship between CL and FFM remains subject to dispute. Like WT, there is no consensus on the scaling exponent of FFM. As a result, a range of values can be found in the literature; some being fixed *a priori* (e.g. 1, 0.67, 0.75) and others are estimated through modelling of the data.

A recent meta-analysis of the literature was conducted by McLeay et al. [60] to determine the average value of the scaling exponent. Their analysis included 484 pharmacokinetic studies that reported a final covariate model of CL and body size. Since they did not have access to individual level data, they simulated individual CL values of all drugs across the human FFM range. The results suggest that FFM raised to an exponent of $2/3$ (0.67) best described the data. However, their analysis was based on a pooled dataset that covered a range of different categories of drug disposition, e.g. hepatic and renal elimination, low and high extraction drugs, etc. In drug development, the primary goal is to develop drugs with low-hepatic extraction in order to ensure less dose and dosing frequency in the clinic [108, 109]. Therefore to specifically determine the average value of the exponent for low-extraction drugs, a model based meta-analysis was conducted and described in Chapter 5 using literature reported individual data of CL and FFM.

The average value of the exponent, either in the literature or determined in this thesis (Chapter 5) actually refers to an empirical value, which has a

theoretical justification. In this context, the theoretical value of the exponent has been derived in Chapter 6 via modelling a new liver size descriptor, lean liver volume (LLV). LLV universally represents the functional size of the liver (devoid of any fat) that is primarily constituted by hepatocytes where drug elimination takes place. On the contrary, total liver volume (LV), which has been conventionally used as the liver size descriptor, is likely to over-estimate functional liver size in most obese patients. This is because more than 90% of obese patients have non-alcoholic fatty liver disease (NAFLD) that causes steatosis [110, 111].

Theoretically, LLV is expected to be the main driver of the variation in clearance (particularly for low-extraction drugs) between differently sized individuals where alteration in body composition is expected, e.g. obese vs. normal adults. Hence the LLV-FFM relationship is expected to define the CL-FFM relationship. A detailed description of this theoretical assumption has been provided in Chapter 6.

Finally, an additional use of the LLV model was explored in Chapter 7 in *in vitro-in vivo* extrapolation (IVIVE) of CL in the obese population. IVIVE based extrapolation of CL in the obese has been recently recommended [112-114]. However the current method of IVIVE uses LV as the scaler for functional liver size, which is likely to over-scale the CL due to presence of substantial liver fat in obese patients [110, 111, 115]. Here, LLV is expected to scale the CL better since it excludes all liver fat and more accurately describe functional liver size. A background on the science underlying these assumptions is provided in Chapter 7.

Overall, there is lack of consensus on the right exponent for scaling clearance (hence maintenance dose) by commonly used body size metrices, WT and FFM in traditional top-down approach of PK prediction (i.e. population PK modelling). More specifically, for WT based scaling, the conflict is on whether to fix the exponent at a plausible value (e.g. 0.75) or to estimate the value. On the other hand, for FFM based scaling, the current conflict is whether clearance

linearly scales to FFM nor not. For FFM, an additional complexity is choosing the correct method or model for its measurement or prediction respectively. In the case of the former, a concise understanding of the scientific framework of the available methodologies is currently lacking in the literature; and for the latter, a universally applicable model is currently unavailable. On the other hand, an alternative bottom-up approach can be implemented for scaling clearance in differently sized populations, e.g. obese by using IVIVE. However, for obese population, the currently used metric for liver size (i.e. total liver volume) is likely to over-predict clearance because of prevalence of non-alcoholic fatty liver disease (NAFLD). Therefore, lean liver volume (LLV) would be a more mechanistic descriptor of 'functional' liver size in this target population. However, there is currently no predictive models available for prediction of LLV, and no assessment has been done for its predictive performance in IVIVE.

1.2. Aims of the thesis

The overall aim of the thesis was to assess the methodologies that are currently being used to scale clearance (CL) to populations of different body size. The thesis has been divided into three parts as per the following:

***Part II*:** To assess scaling by body size. This part includes scaling by total body weight (WT) and was aimed to:

(Aim 1) Assess the influence of study design (and BSV) on choosing the allometric exponent (*Chapter 2*).

***Part III*:** To assess scaling by body size and composition. This part includes scaling by fat-free mass (FFM) and was aimed to:

(Aim 2) Systematically review the available methods and models for estimating fat-free mass (FFM) and interlinked them in a common scientific framework in order to understand their assumptions and limitations (*Chapter 3*).

(Aim 3) Develop an extended version of the Janmahasatian FFM model to extend its applicability in other ethnicities (*Chapter 4*).

(Aim 4) Estimate the average value of the exponent of FFM based scaling of clearance by conducting a model based meta-analysis of the literature data (*Chapter 5*)

***Part IV*.** To assess scaling by lean liver volume (LLV), a descriptor of functional liver size. This involved:

(Aim 5) Identifying the theoretical value of the allometric exponent for scaling CL by FFM, via identifying the lean liver volume (LLV) vs. FFM relationship (*Chapter 6*).

(Aim 6) Evaluating the potential use of the lean liver volume (LLV) model in *in vitro-in vivo* extrapolation (IVIVE) of clearance (*Chapter7*)

PART II

SCALING OF CLEARANCE BY BODY SIZE

Chapter 2: Choosing the allometric exponent in covariate model building

This chapter is based on the following peer-reviewed publication:

Sinha J, Al-Sallami HS, Duffull SB. *Choosing the allometric exponent in covariate model building*. Clinical Pharmacokinetics. 2019; 58(1): 89-100.

2.1. Introduction

Covariate identification is an integral part of population pharmacokinetic modelling in order to provide dosing recommendations for subpopulation(s) who might otherwise be at risk of sub-therapeutic or toxic exposure [50]. Successful incorporation of covariate(s) therefore facilitates an understanding of the predictable component of between subject variability (BSV) and hence improves the precision of dose selection and model predictions at the individual level. Body size is arguably the most important covariate of CL because of its biological and clinical relevance [61]. Total body weight (WT) has been conventionally used as the descriptor of body size. Models that link CL to WT have a common mathematical form as shown in Eq 2.1, which has been discussed in section 1.1.9.2.1 of Chapter 1: .

$$CL_i = CL_{std} \times \left[\frac{WT_i}{WT_{std}}\right]^{Exp}$$

Eq 2.1 Scaling of clearance by total body weight (same as Eq 1.32)

As per Eq 1.32 the value of the term Exp (exponent) determines whether the scaling of CL is linear ($Exp = 1$) or non-linear ($Exp \neq 1$) in relation to WT. Linear scaling is often depicted in the drug label (as 'mg/kg' dosing) and commonly practised in the clinic because of its simplicity of calculation. On the other hand, non-linear scaling of CL is adopted from the observed non-linear relationship between metabolic rate and body size across various animal species.

In 1880's, Max Rubner [92] observed that the mammalian basal metabolic rate (BMR) was proportional to $(WT)^{2/3}$ which is equivalent to scaling by body surface area (BSA). The Exp value of $2/3$ is widely used today in relation to oncologics and estimating GFR where normalisation by BSA is common. Later in 1932, Max Kleiber [116] showed that the BMR values of birds and mammalian species, spanning 3.7 orders of magnitude, aligned with a higher exponent of

WT which was approximately 3/4 (actually 0.737). Kleiber's 3/4 law was further supported in a wider weight range, mouse-to-elephant (~5 orders of magnitude) by Brody [117] and mycoplasma-to-blue whale (~27 orders of magnitude) by West et al. [93]. A theoretical basis of 3/4 exponent was also postulated by West et al. [94, 118] by introducing a general model for transport of essential materials via a space filling fractal network of branching tubes. The strong biological evidence and theoretical framework supporting 3/4 has made it the ubiquitous rule of biology.

In clinical pharmacology, under the assumption of a linear relationship between CL and BMR, this constant (Exp) is popularly known as the *allometric exponent* and hence is widely adopted for inter-species [119-122] and intra-species [61] scaling of CL. Debate on the value continues with the theoretical basis of 3/4 challenged by researchers [123, 124] who claimed that mammalian metabolic rate is scaled by $(WT)^{2/3}$ rather than $(WT)^{3/4}$. At this stage there remains no consensus over the theoretically correct value of the exponent [96, 125]. Some suggest, see Calvier et al. [97], that there is no universal value for this exponent in the population and the plausible range is 0.5 – 1.20. Hu and Hayton [96] who reviewed interspecies scaling of 115 xenobiotics over 3-4 species spanning four orders of magnitude of body weight reported a range of exponents between 0.29 – 1.2.

This leaves investigators with three overall approaches to solve the problem of scaling (1) to choose an Exp value based on their belief on the theoretical basis of the relation of CL to WT – in this approach CL is always dependent on WT to the power of a pre-defined value of Exp and this is not tested, (2) to choose a value of Exp from a set of mechanistically plausible values e.g. 1, 3/4 or 2/3 and include the relation between CL and WT if it is statistically significant (similar to method 1, CL is always considered to be dependent on WT), or (3) to estimate the value (i.e. let the data determine the value that best fits) as per empiricism [95, 126]. The second and third approaches require the investigator to have access to data that is sufficiently informative to

either select the correct exponent or provide an accurate and precise estimate of the exponent. Certainly, if there is no strong *a priori* belief in the relation between CL and WT, the empirical approach of estimation makes logical sense. The first approach is not considered here further as it is unaffected by experimental design. The assumption that underpins the second approach is that a universal exponent exists and it is contained in the set of plausible values (i.e. is one of the elements of $\{2/3, 3/4, 1\}$).

The work of Anderson and Holford [69] has shown that estimation, the third approach, can lead to an imprecise estimate of the allometric exponent in a regular clinical trial setting (e.g. approx. 100 patients). In their work they quantified the confidence interval on the exponent that, in many cases, included the range of $2/3$ to 1. In addition, we also see that statistical significance arising from low powered studies may occur because the effect size, by chance, is estimated to be larger than the true effect size [56, 58]. In this case the value of the parameter that describes the effect size will be inflated leading to erroneous inference from the analysis. This has been addressed by Ribbing et al. [56] for covariate selection and La Caze et al. [58] in a more general case.

The overall aim of this work was to evaluate the influence of BSV and study design on determination of the allometric exponent (Exp), when total body weight has considerable influence on CL.

2.1.1. Specific objectives

i. Objective 1: To assess the influence of between-subject variability (BSV) and study design on the power to select the true exponent from a set of *a priori* values.
ii. Objective 2: To assess the influence of between subject variability (BSV) and study design on the power to obtain unbiased exponent estimates.

We do not consider the precision of the estimate in this work as this has been adequately covered by Anderson and Holford [69].

2.2. Methods

2.2.1. General simulation-estimation setting

2.2.1.1. Platform

The studies in this paper are based on a stochastic simulation estimation (SSE) in a non-linear mixed effects modelling framework. All simulations were conducted using MATLAB and estimation using NONMEM (version 7.2, GNU-Fortran 95 compiler) on an AMD Opteron™ processor (2.30 GHz) and WfN platform. The First Order Conditional Estimation with interaction (FOCEI) method was used for all estimation runs.

In all scenarios, the nominal value of Exp used for simulation (see Table 2.1) was considered as the true value. The specific aims were then assessed by comparing the estimated parameter values against the true value. Simulations were conducted based on input-output (I/O) and covariate distribution models. No errors in trial execution were considered, such as patient related (e.g. dropouts) or investigator related (e.g. measurement error), for the simulations.

2.2.1.2. I/O Model:

Table 2.1 shows the essential components of the I/O model used for the simulations. A one-compartment intravenous bolus 'unit' model (dose = 1, volume = 1, half-life = 1) with linear elimination was used.

- *Fixed effect model:* $\theta_1, \theta_2, \theta_3$ represent the standard values of CL, the true Exp value and volume of distribution (V) of the population respectively. CL_i and V_i denote the individual values of CL and V, respectively, for the i^{th} individual. t_j and C_{ij} represent the time of the j^{th} observation and the predicted concentration at t_j for the i^{th} individual. Note all individuals had the same sampling design (see section 2.2.1.5). The covariate model for calculating $TVCL$ was as per Eq 2.1.

- *Random effects model:* Individual PK parameters, i.e. CL_i and V_i were assumed to be log-normally distributed. The between-subject differences in CL_i and V_i were denoted by $\eta_{i_{CL}}, \eta_{i_V}$ respectively, and were considered to be normally distributed with their standard deviations ω_{CL}, ω_V (where $\mathbf{\Omega}$ is the variance-covariance matrix). Three different levels of BSV were used for simulations, i.e. $\omega_{CL} = \omega_V = 0.2, 0.4, \text{and } 0.6$ in order to mimic low (20%), normal (40%), and high (60%) PK variability encountered in clinical studies that would affect the power to different extent [127].

- *Residual error model:* A combined residual error model was used for simulating observed concentrations ($C_{obs,ij}$), where $\varepsilon_{ij_1}, \varepsilon_{ij_2}$ represent the proportional and additive components, respectively. The proportional and additive errors were normally distributed with their standard deviations σ_1 and σ_2 respectively. The value of σ_1 was assumed to be 0.1 and the value of σ_2 was referenced to 10% of the population predicted average concentration (C_{avg}) and considered to be constant variance ($\mathbf{\Sigma}$ is the variance-covariance matrix).

Table 2.1 Input-output and covariate models for simulation

Model desciption	Random effects	Parameter values
$C_{ij} = \frac{D}{V_i} \times e^{-\left(\frac{CL_i}{V_i}\right) \times t_j}$	$\eta_i \sim N(0, \mathbf{\Omega})$	$\theta_1 = \ln(2)$
$TVCL = \theta_1 \times \left[\frac{WT_i}{WT_{std}}\right]^{\theta_2}$		$\theta_2 \in \{0.67;\ 0.75;\ 1\}$
		$\theta_3 = D = 1$
		$WT_{std} = 70$
$CL_i = TVCL \times e^{\eta_{i_{CL}}}$	$\mathbf{\Omega} = \begin{bmatrix} {\omega_{CL}}^2 & 0 \\ 0 & {\omega_V}^2 \end{bmatrix}$	$WT_i = \text{individual weight}$
		$\omega_{CL} = \omega_V \in \{0.2; 0.4; 0.6\}$
$V_i = \theta_3 \times e^{\eta_{i_V}}$	$\varepsilon_{ij} \sim N(0, \mathbf{\Sigma})$	$\sigma_1 = 0.1$
		$\sigma_2 = 0.1 \times C_{avg} = 0.02886$
$C_{obs,ij} = C_{ij} \times e^{\varepsilon_{ij_1}} + \varepsilon_{ij_2}$	$\mathbf{\Sigma} = \begin{bmatrix} {\sigma_1}^2 & 0 \\ 0 & {\sigma_2}^2 \end{bmatrix}$	$\left(C_{avg} = 0.2886\right)$

2.2.1.3. Covariate distribution model

Two different populations of non-obese individuals A and B, i.e. excluding and including children respectively were generated from NHANES III (The Third National Health and Nutrition Examination Survey,1988-1994) published by the CDC (Centres for Disease Control and Prevention, USA)[128]. Specific inclusion-exclusion criteria as mentioned in Table 2.2 were applied for the respective populations. This ensured plausible sets of covariates in all individuals. The demographic characteristics of the covariate distributions are described in

Table 2.2 Inclusion-exclusion criteria for generating two populations from NHANES database

Population	Subjects	Inclusion criteria	Exclusion criteria
A	Non-obese adults	Adults: age ≥18, BMI: 18-30 Children: age 3 to <18	Adults: WT < 35 Children: WT outside the 5th and 95th percentiles of growth chart [a]
B	Non-obese adults and children		

BMI = body mass index in kg/m^2, WT in kg, Age in years, [a] growth chart published by CDC [129]

Table 2.3 Demographic characteristics of the two different populations

Population	Number of individuals in NHANES database	Age range (year)	WT range (kg)
A	13106	18 – 90	35.1 – 109.9
B	Adults: 13106 Children: 7100	Adults: 18 – 90 Children: 3 to <18	Adults: 35.1 – 109.9 Children: 11.95 - 88

2.2.1.4. Design

Virtual cohorts of various sample sizes (N = 10, 20, 50, 100, 200, 500, 1000 subjects) were generated by non-parametric bootstrap from the individual subjects that meet the eligibility criteria for each of the populations A and B mentioned in Table 2.3, using MATLAB. Stratified sampling was performed for population B, with even sampling under the three predefined age groups (years), i.e. children (3 to 12), adolescents (>12 to <18), and adults (≥18) to ensure an equal proportion (about one-third) of individuals in each group. The three age groups were selected based on the FDA and EMA guidance [86, 130], with the exception of the lower bound of children, normally 2 years of age was changed here to 3 years of age to avoid the potential influence of ontogenic maturation.

2.2.1.5. Stochastic simulation-estimation scenarios

In Table 2.4, each group ID represents a specific simulation scenario, for which 1000 replicate concentration-time (C-T) datasets were simulated using the I/O and covariate distribution models. All virtual subjects provided samples at 0.25, 0.5, 1, 3 and 5 hour post-dose.

Table 2.4 Various groups representing specific simulation scenarios

$\theta_{2_{true}}$	Cohort ID [a]	ω_{CL} and ω_V	Group ID [b]	No. of Groups	Total
0.67	A_N	0.2, 0.4, 0.6	$AI_N^{0.67}, AII_N^{0.67}, AIII_N^{0.67}$	21	126
	B_N	0.2, 0.4, 0.6	$BI_N^{0.67}, BII_N^{0.67}, BIII_N^{0.67}$	21	
0.75	A_N	0.2, 0.4, 0.6	$AI_N^{0.75}, AII_N^{0.75}, AIII_N^{0.75}$	21	
	B_N	0.2, 0.4, 0.6	$BI_N^{0.75}, BII_N^{0.75}, BIII_N^{0.75}$	21	
1	A_N	0.2, 0.4, 0.6	$AI_N^1, AII_N^1, AIII_N^1$	21	
	B_N	0.2, 0.4, 0.6	$BI_N^1, BII_N^1, BIII_N^1$	21	

[a] N = 10, 20, 50, 100, 200, 500, 1000; [b] I, II, III refer to $\omega = 0.2, 0.4, 0.6$ respectively

2.2.2. Objective 1: Assessing the choice of exponent from a set of exponents

Three values of the exponent were considered (1, 0.67, 0.75) corresponding to the respective theoretical values (1, 2/3, 3/4). Each of the exponents was set to be the true value in turn and the other two exponents were false values. This yields three objective function values in NONMEM for the i^{th} replicate which were determined as OBJ_{true}, OBJ_{false1}, OBJ_{false2} from which the best model would be selected based on the AIC (Akaike Information Criteria) [55] value and the power computed as the proportion of time the correct exponent was chosen (as per Eq 2.2). The number of subjects required to achieve an arbitrary power of 80% (N_{80}) was interpolated to compare the powers of different comparisons of exponent.

2.2.3. Objective 2: Assessing estimation of the exponent

The true simulation value of the exponent was $\theta_2 = 0.75$ for all settings where the exponent was estimated. Following estimation from the i^{th} replicate, the respective OBJ values of base and covariate model (OBJ_{base}, OBJ_{cov}) and estimated value of θ_2 ($\hat{\theta}_2$) were recorded.

Covariate selection criteria: The covariate model was compared with the base model (i.e. model without WT) using the likelihood ratio test with one degree of freedom. A change in OBJ greater than 3.84 was considered statistically significant.

Power calculation: Power was calculated as the proportion of times that WT was found to be statistically significant out of 1000 replicates (Eq 2.2), given that the true model included WT as a covariate.

Bias calculation: Bias was calculated as the difference of the median estimated exponent ($\hat{\theta}_{2_{median}}$) from the true exponent ($\theta_2 = 0.75$) (Eq 2.3). The mean estimated exponent was calculated only from the runs in which the covariate model was statistically preferred over the null model.

The workflow of the entire SSE study is presented schematically in Figure 2.1. The MATLAB script for programming the entire SSE and the NONMEM files are available in section 0 to A1.5 of Appendix 1: for interested readers.

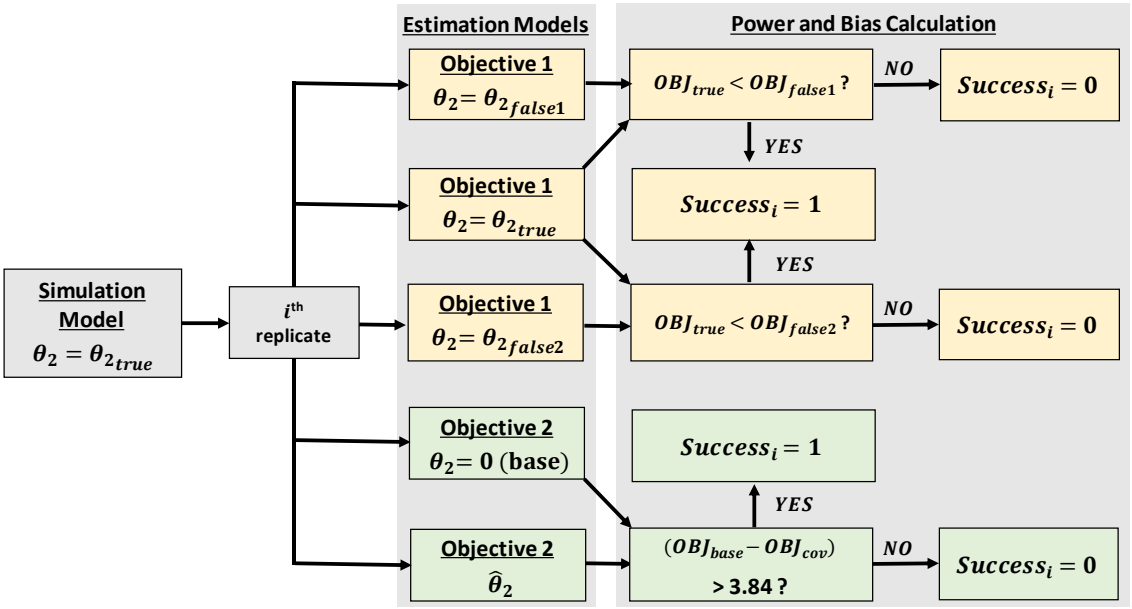

Figure 2.1 Schematic of simulation-estimation workflow including assessment for objective 1 and objective 2

Schematic of simulation-estimation workflow including assessment for objective 1 and objective 2. θ_2 *allometric exponent,* $\theta_{2_{true}}$ *true value of* θ_2 *used (0.67 or 0.75 or 1) for simulation and estimation;* $\theta_{2_{false1}}$ *and* $\theta_{2_{false2}}$ *false values of* θ_2 *used for estimation (For* $\theta_{2_{true}} = 0.67$, $\theta_{2_{false1}} = 0.75$ *and* $\theta_{2_{false2}} = 1$; *for* $\theta_{2_{true}} = 0.75$, $\theta_{2_{false1}} = 0.67$ *and* $\theta_{2_{false2}} = 1$; *for* $\theta_{2_{true}} = 1$, $\theta_{2_{false1}} = 0.75$ *and* $\theta_{2_{false2}} = 0.67$*);* $\hat{\theta}_2$ *estimate of* θ_2; OBJ_{true}, OBJ_{false1} *and* OBJ_{false2} *respective objective function values of the* i^{th} *replicate when* θ_2 *is fixed at* $\theta_{2_{true}}$, $\theta_{2_{false1}}$ *and* $\theta_{2_{false2}}$ *respectively for estimation;* OBJ_{base}, OBJ_{cov} *objective function values of base and covariate models respectively when* θ_2 *is estimated.*

$$Power(\%) = \sum_{i=1}^{1000} \frac{Success_i}{1000} \times 100$$

Eq 2.2 Calculation of for simulation-estimation scenarios

$$Bias\ (\%) = \frac{\left(\hat{\theta}_{2_{median}} - \theta_{2_{true}}\right)}{\theta_{2_{true}}} \times 100$$

Eq 2.3 Calculation of bias in the estimate of allometric exponent

2.3. Results

2.3.1. Objective 1: assessing choice of the exponent from a set of exponents

The power to detect the true value of the exponent from a range of *a priori* values for various scenarios are plotted in Figure 2.2. Power depends on sample size, BSV, the underlying population distribution of the covariate and the competing false exponent. Sample size and range of the covariate distribution had a positive relationship with power, whereas BSV had an inverse relationship. Studies with a wider range of WT distribution always had a higher power (i.e. population B was more powerful than population A) in selecting the true exponent under same setting. Similarly, and as anticipated, within the same WT distribution at a fixed sample size and BSV, the power was found to depend on the relative difference in the magnitude of the competing exponent. For example, in Figure 2.2a, with a true exponent of 0.67 at 40% BSV, 200 subjects resulted in ~60% power if the competing exponent was 0.75, which increased to ~80% if the competing value was 1. We see the values of N_{80} are in the similar range **(**at least not outside the two consecutive sample sizes tested) when the true and false values have been exchanged all other conditions being equal (see Table 2.5). For example, when the true coefficient is 0.67 and the false is 1 and vice versa, the N_{80} values are 170 and 150 respectively (with BSV = 40% and population A). Hence comparisons can be simplified to a comparison between the absolute differences of various sets of true and false exponents.

The range of N_{80} values under a certain covariate distribution gives a hint of clinical plausibility of choosing the correct exponent by this approach. We see it is almost impossible to distinguish 0.67 from 0.75 in almost any realistic study design for a drug with normal to high BSV (40 - 60%), even in studies that span children to adults (population B). The exception is a drug with an unrealistically low BSV (viz 20%) where a distinction is more likely to be able to be seen. In contrast, linear scaling appeared mostly distinguishable from the non-linear scaling based models for drugs with normal BSV.

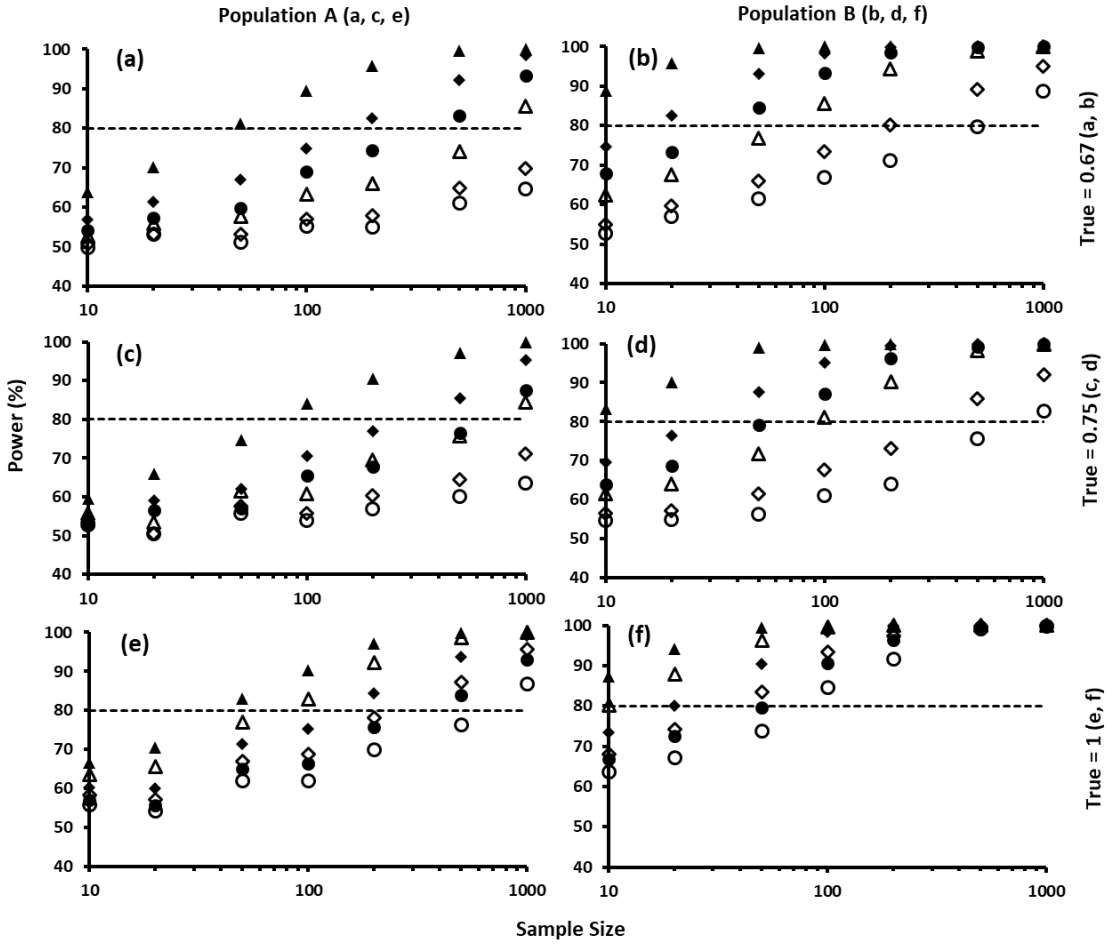

Figure 2.2 Power vs. sample size profiles at various BSV levels and weight distributions.

First (a, b), second (c, d) and third (e, f) rows of subplots represent power profiles for $\theta_{2_{true}}$ *= 0.67, 0.75 and 1 respectively. Sub-plots in the first (a, c, e) and second (b, d, f) columns represent population A (normal weight adults) and B (normal weight paediatric-adults) respectively. Triangles, diamonds and circles represent BSV values of 20%, 40% and 60%, respectively. Open (△,◇, ○) and filled (▲,◆, ●) markers under a specific shape represents powers when* $\theta_{2_{true}}$ *is competed by* $\theta_{2_{false1}}$ *and* $\theta_{2_{false2}}$ *respectively at the same BSV level. For* $\theta_{2_{true}} = 0.67$, $\theta_{2_{false1}}$ *is 0.75 and* $\theta_{2_{false2}}$ *is 1; for* $\theta_{2_{true}} = 0.75$, $\theta_{2_{false1}}$ *is 0.67 and* $\theta_{2_{false2}}$ *is 1; for* $\theta_{2_{true}} = 1$, $\theta_{2_{false1}}$ *is 0.75 and* $\theta_{2_{false2}}$ *is 0.67.*

Table 2.5 The N_{80} values at various scenarios calculated by linear interpolation.

True	Popu-lation	False								
		20% BSV			40% BSV			60% BSV		
		0.67	0.75	1	0.67	0.75	1	0.67	0.75	1
0.67	A	NA	760	50	NA	>1000	170	NA	>1000	390
	B		70	10		200	20		500	40
0.75	A	750	NA	80	>1000	NA	310	>1000	NA	660
	B	90		10	370		30	830		60
1	A	40	70	NA	150	260	NA	360	680	NA
	B	10	10		20	40		50	80	

N_{80} values were rounded off to nearest 10's multiple, NA not applicable

2.3.2. Objective 2: assessing estimation of the exponent

The objective was to evaluate the influence of study design (and BSV) on the bias of the allometric exponent. This objective evaluated two components, the power of the study to correctly determine weight as a covariate and bias in the estimate of the exponent when weight was included as statistically preferred over the base model.

The power to correctly select weight for a given sample size and covariate distribution is provided in Figure 2.3. In all simulations the true value of the exponent was arbitrarily set to 0.75 (the middle value from objective 1). A similar influence of BSV (inverse relationship) and range of the WT distribution (positive relationship) on power was observed as seen in objective 1. Although N_{80} values of objective 1 are higher than those of objective 2 under an equivalent scenario this is not, however, a fair comparison since in objective 1 we are determining the power to select the correct coefficient given that WT is

included in the model, whereas for objective 2 we are simply assessing whether WT would be included irrespective of the estimate of the coefficient. Therefore, the power calculation in objective 2 represents the power to answer a simpler question. However, even for objective 2 this difference becomes minimal as the range of covariate distribution increases and BSV decreases, since both approaches become similarly powered under these circumstances. The N_{80} value in the worst case situation (i.e. normal WT adult and 60% BSV) was approximately 200 (from Table 2.6). Most importantly, estimation of the exponent risks bias in the estimate of the exponent for underpowered studies. This bias is explored in Figure 2.4, where underpowered designs led to bias in the estimate of the exponent compared to the true value. For example, estimation with population A (normal weight adults) resulted in an overestimation of the exponent with a median value of 1.61 (true value = 0.75) with 10 subjects for normal BSV (i.e. a design that yielded 21% power). However, an improvement in power (87%) by increasing the sample size to 100 subjects led to an acceptably accurate estimate (median = 0.79) of the exponent. It is evident that estimation bias is linked to study power, irrespective of the cause of the low power whether due to sample size, range of the weight distribution, or BSV value of clearance. This is shown in Figure 2.5 where the median estimates of the exponent (expressed as % bias) are shown for all simulation scenarios. We observe that bias in the estimate depends on the study power and no further influence is seen of any of the study factors. We also see that the bias reaches negligible values when the power exceeds 80%.

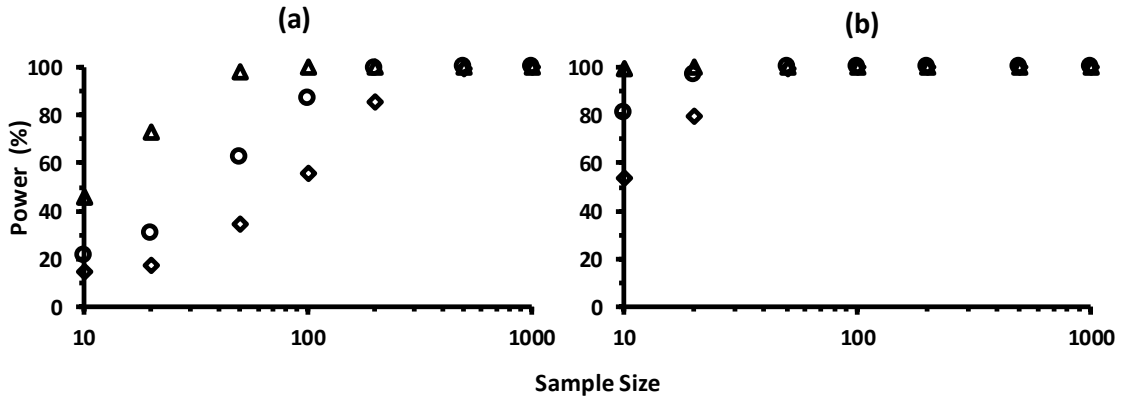

Figure 2.3 Influence of BSV on power of estimation ($\theta_{2_{true}}$= 0.75) in two different populations.

Subplots a and b represent population A (normal weight adults) and B (normal weight paediatric-adult subjects). Triangles (△), circles (○) and diamonds (◊) represent BSV values of 20%, 40% and 60%, respectively represent BSV values of 20%, 40% and 60%, respectively.

Table 2.6 Summary of power (%) and estimate bias (%) in the scenarios tested

Population	N	20% BSV		40% BSV		60% BSV	
		Power (%)	Bias (%)	Power (%)	Bias (%)	Power (%)	Bias (%)
A	10	46	39	21	115	15	193
	20	73	14	31	75	18	145
	50	98	2	63	26	35	65
	100	100	0	87	5	55	27
	200	100	1	99	1	85	7
	500	100	0	100	0	100	0
	1000	100	0	100	0	100	0
B	10	100	0	81	8	53	27
	20	100	0	97	0	79	9
	50	100	-1	100	-1	99	-2
	100	100	-1	100	-1	100	-2
	200	100	0	100	-1	100	-1
	500	100	0	100	0	100	0
	1000	100	0	100	-1	100	-1

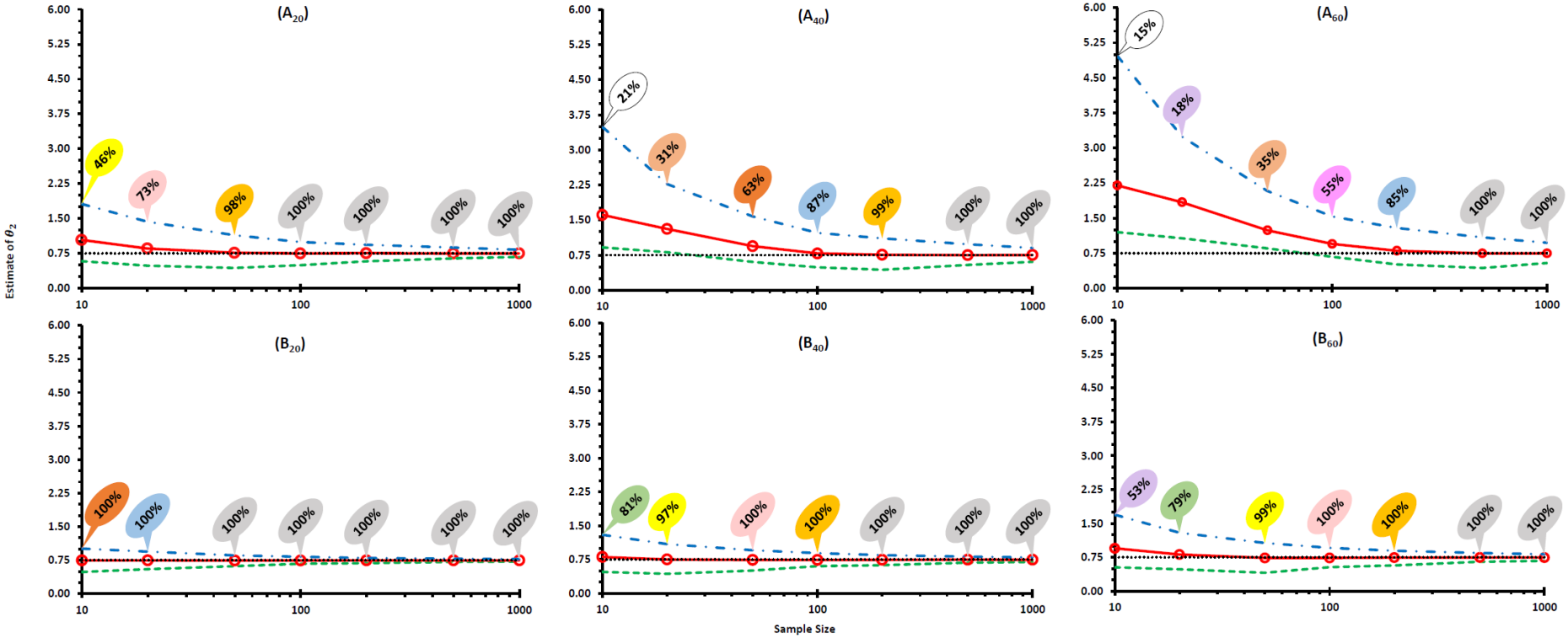

Figure 2.4 Estimate bias (95% confidence interval) vs. sample size profiles.

The y-axes on all subplots is the estimated θ_2 ($\theta_{2_{true}}$ = 0.75) and the x-axes show the sample size. The rows represent the different populations based on the distribution of the covariate, with the upper row being population A and the lower row the population B. The code shown above each subplot represents the covariate distribution and BSV (so A_{20} represents population A with BSV = 20%). The median (—O—), 2.5th (- - - -) and 97.5th percentiles (— · — · —) of estimates and true exponent (.....) are plotted for total 42 scenarios The balloons above each data point represent their respective power (%) and similar powers are shown with the same colour.

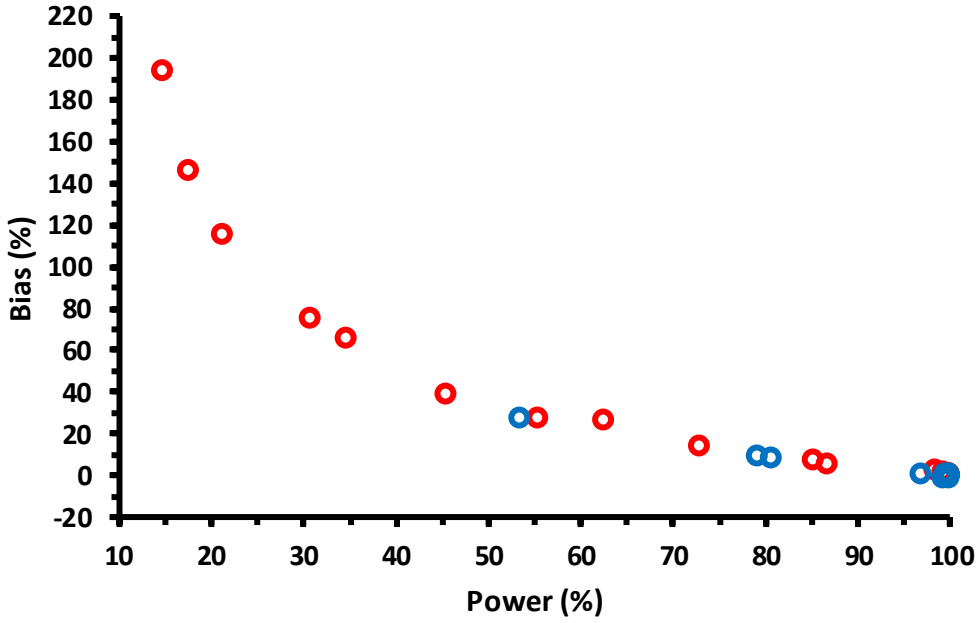

Figure 2.5 Influence of power on estimation bias of the allometric exponent ($\theta_{2_{true}}$= 0.75).

The open circles represent the median bias (%) at that power level. Bias (%) is calculated from each of the median estimates of all 42 scenarios described in Table 2.4. This figure includes simulations from all populations A (○) and B (○), BSV values (20%, 40% and 60%), and sample sizes (10, 20, 50, 100, 200, 500 and 1000).

2.4. *Discussion*

There is a lack of agreement amongst researchers in clinical pharmacology regarding inclusion of an allometric exponent in covariate modelling. This has led to an ongoing debate of 'theory', where a value is chosen *a priori*, versus empiricism, where the exponent is estimated from the data. In this study, we address the ability of the study design to support theory and empiricism.

The main findings of this work indicate that caution needs to be taken while building covariate models of clearance using data from regular clinical pharmacology studies. We are (arbitrarily) taking regular studies to involve <200 patients which preferentially exclude children and the typical value of BSV on CL is 40-60% [127]. In drug development setting, such studies typically

refer to late phase studies from phase 2b onwards. Such studies are not adequately powered to distinguish between choices of linear scaling ($\theta_2 = 1$) and theory based *allometric* scaling ($\theta_2 = 0.75$), and risks selection of wrong exponent. The number of subjects required to achieve a power of 80% (N_{80}) ranged from 260 to 310 (see Table 2.5). Recruiting a wider range of weights by including children in the cohort increases the power of correct selection, and studies with less than 100 patients will be adequate to correctly determine the exponent, under a balanced stratified design. Further, identification of the correct exponent from choices of theory based *allometry* ($\theta_2 = 0.75$) and BSA based scaling ($\theta_2 = 0.67$) is practically impossible with any sort of regular study design ($N_{80} \geq 1000$ in Table 2.5). Inclusion of paediatric patients in the cohort (who are 3 years of age or older and therefore avoiding ontological issues of maturation) improves the power, but the required number of participants will be as high as 800. Hence, data from regularly conducted clinical pharmacology studies should not be relied on to correctly choose the exponent from a set of *a priori* theoretical choices. Note that even adequately powered study carries the risk of incorporating an incorrect exponent, since the true exponent can be of any value and not necessarily be limited to the set of *a priori* values tested.

Of importance, however, is not the value of the exponent but rather how this affects our prediction of CL and therefore the likely dose selection and/or exposure. In Figure 2.6 we show the prediction error PE (%) of CL prediction when various false values of the exponent are chosen from a set of plausible values over a weight range of normal weighted individuals from ages 3 to adult. It is evident that false selection between BSA based scaling (exponent = $2/3$) and theory based allometry (exponent = $3/4$) is insignificant over the range of weights (i.e. within ±20% error). However, when comparing linear (exponent = 1) vs nonlinear (exponent = $2/3$) we see significant effects on clearance for individuals weighing below 40 kg (the median WT of a 12 year old male child as per the CDC growth chart [129]). The influence on adults is however negligible. This implies that power for choosing the correct *a priori*

value has little importance if the purpose is to extrapolate CL within a cohort of adults but is of considerable importance for scaling to children, particularly those less than 12 years.

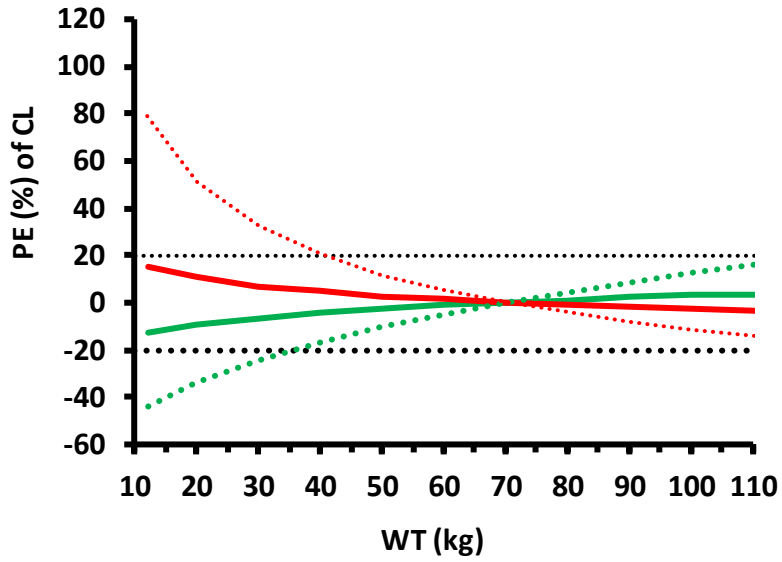

Figure 2.6 Influence of an incorrect choice of an exponent on weight on the value of clearance and its dependence on body weight.

The y-axis is the prediction error (PE) of clearance and the x-axis represents the weight range in population B, representing normal weighted subjects. The horizontal dotted lines (····) represent a ± 20% difference from the true value of clearance. The plot illustrates the influence of false selection of the exponent value. The red line (—), green line (—), dashed red line (····) and dashed green line (····) represent various combinations of true and false exponents, i.e. true = 0.75, false = 0.67, true = 0.67, false = 0.75, true = 1, false = 0.67, and true = 0.67, false = 1 respectively.

The alternative method explored here involved estimation of the exponent (as a continuous variable). We note that bias in estimating the exponent is evident when the power is less than 80% and hence there is a high risk of overestimating the true value for all studies where N < N_{80}. In this work, we show that bias in the estimate of the exponent directly depends on the study power and no additional variables contribute to this relation (Figure 2.5), either intrinsic (e.g. BSV) or extrinsic (e.g. covariate distribution, sample size). This direct influence of study power on the bias of the parameter estimates has been previously shown by Ribbing et al [56]. Their work

investigated the estimation bias for a coefficient for a covariate that enters the model linearly. This important work highlighted the influence of low power and quantified bias. In this work, we extend this consideration to parameters that occur in the exponent. We believe that these parameters are inherently more difficult to estimate since they enter the covariate model in a nonlinear manner. In this work we have also considered covariate distributions sourced from a database of patients that included children and adults which we hope will provide a robust assessment of the ability of various designs to inform the value of the exponent accurately and precisely.

The estimation approach appeared promising for typical clinical studies in terms of achieving required power [131-135]. It appears that a cut-off value of 80% power is adequate in order to restrict the bias below a reasonable tolerance (<10%). Clinical pharmacology studies should be designed appropriately to achieve this level of power, if the plan is to estimate the exponent and potentially extrapolate the results to other cohorts. Results of objective 2 suggest that most regular studies involving about 100 to 200 adults (resembling population A) are fit for the purpose of estimating the exponent reasonably (see 40% and 60% BSV and population A in Table 2.6). For example, a sample size of about 100 adults would estimate the exponent to be 0.79 (true value is 0.75) corresponding to 5% bias in Table 2.6 considering a normal PK variability (40%). This much bias in the exponent is sufficient to limit the error in CL prediction within ±3% across the body weight range of population A (35 to 110 kg). Therefore, a minimum sample size of about 100 to 200 is needed for obtaining an unbiased estimate of the exponent, if only adults are included in the study.

For studies that include children (typically >2 years of age to avoid variability due to ontogeny) the sample size requirements can be relaxed. This is evident from the results with population B, where about 10 to 20 participants with about equal proportions of children (33%), adolescent (33%) and adults (34%) was found to be sufficient to obtain an unbiased estimate of the

exponent. For example, assuming normal PK variability (40% BSV on CL), 10 study participants consisting of 3 children, 3 adolescent and 4 adults would be expected to provide an estimate of the exponent within 8% of the true value (i.e. an estimate of 0.81 assuming a true value of 0.75) (see Table 2.6). Similar to population A, it is anticipated that this level of bias appears to be irrelevant in terms of prediction of CL (within ±10%) in the studied body weight range of population B (12 to 110 kg). Even though low sample sizes such as 10 is expected to yield an imprecise estimate of the exponent (90% CI: 0.30 – 1.18) which is similar to the observation made by Anderson and Holford [69], it depends on the purpose of the study whether this is acceptable. In case an unbiased and appropriate precise estimate of the exponent is required, a higher sample size of about 50, which resembles most of the clinical studies involving children and adults would be required. Overall, the estimation approach appeared promising for typical clinical studies conducted involving adults as well as children in terms of achieving required power [29-33]. However, the sample size requirements in Table 2.6 are not directly applicable for true values other than 0.75. To be precise, sample size requirement will decrease if the 'true' value is greater than 0.75, but if the 'true' values is less than 0.75, the sample size requirement will be higher. However, the key finding of Objective 2 will not change, i.e. the bias vs. power profile is universal and does not depend on the 'true' value.

We explore the influence of bias in the estimate of the exponent on CL in Figure 2.7. In this plot we show prediction error (PE%) of clearance for a given range of study powers. We assume, for the purposes of illustration that the true exponent was 0.75 (note any value could be chosen and illustrate the same trends). We simulate the PE% at four representative weights 14 kg, 40 kg, 64 kg and 110 kg, representing typical values of weight for a 3 years and 12 years old children, adult and large frame adult, respectively. It is evident that a study power of > 80% results in negligible bias in all patient groups, indicating that extrapolation of CL for these types of study is likely to be without significant issues. In addition, it is apparent that for individuals that are close to the

weight standard value (WT_{std}) used in the calculation of CL, the less influence the power has on the value of CL via estimation of the allometric exponent. The larger the difference of individual body weight from standard weight however caused significant bias in the value of CL, which was typically obvious when power < 70%. In contrast to the findings for *a priori* selection of the exponent (objective 1), where under powered studies are less likely to produce an error in CL for patients above 12 years, the bias of the estimate of the exponent can potentially influence the CL extrapolation to all age groups. The influence in the case where the exponent is estimated depends on how far the individual is from the reference value for weight. For example, the influence of the bias in the estimate of the exponent at 30% power is <10% error in the case of a 64 kg individual when the reference body weight is 70 kg. However had the reference body weight been 10 kg then the bias of the estimate at 30% study power would be >93 %. In either case the issue will be seen at the extremes of weight with respect to the reference rate.

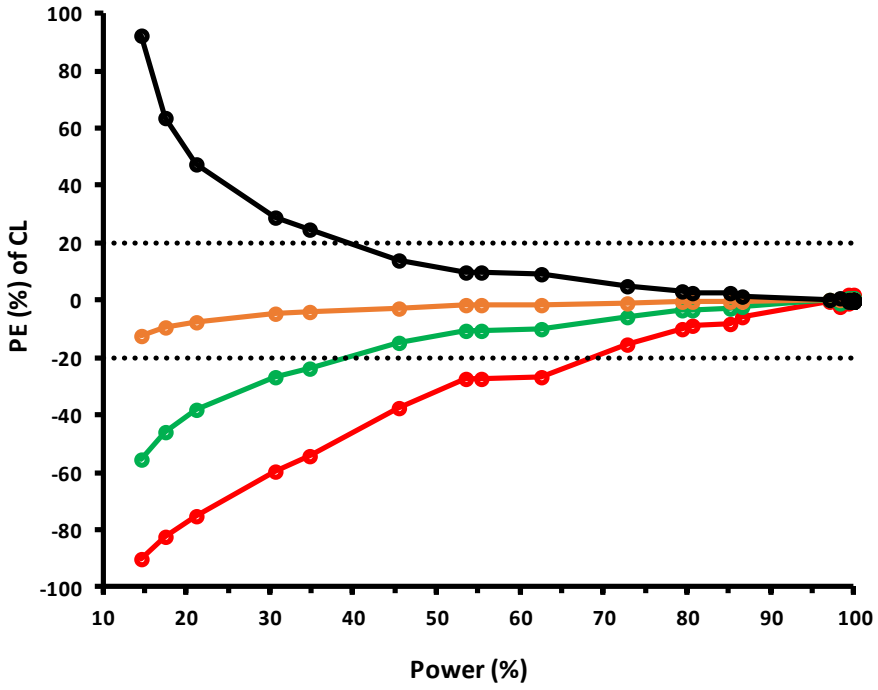

Figure 2.7 Influence of study power on the prediction error in clearance, based on the dependence of clearance on allometrically scaled weight, where the exponent is estimated as part of the analysis.

The y-axis is the prediction error (PE) of clearance and the x-axis represents the power of the study scenarios under objective 2 (see Table 2.4). For each value of power, four clearance PEs are shown, for body weights of 14 kg (), 40 kg (), 64 kg () and 110 kg (). The horizontal dotted lines represent ± 20% prediction error in clearance.

In this work only total body weight was considered as a covariate on CL; age and/or obesity related (patho)physiological changes that can potentially influence clearance were not considered. Hence, improvement in the power by including children (population B) purely reflects the benefit of involving a wider range of normal weights of participants in the study. This, also implies that involving overweight and obese adults, in spite of producing a wider range of weight in the study may not produce similar improvement in the power, as seen with population B. This is because this study does not address the influence of body composition related changes in (patho)physiology (e.g. renal damage, altered enzyme/transporter activity, altered protein binding) on clearance, which is not well understood. However, for readers' interest additional scenarios with all-comer adult population (including obese) were explored and can be found in section A1.1 of Appendix 1: . In addition, an all-comer study involving children and adults (i.e. not stratified to the FDA/EMA guidelines) is also provided in this additional section.

2.5. Conclusions

This study has evaluated the influence of study design on the two current strategies for determining the properties of allometric scaling of clearance by weight; (1) the power to correctly select the exponent from a set of *a priori* values and (2) the power to obtain unbiased exponent estimates. In both cases, there is a risk of building a misspecified model by incorporating an incorrect value (either *a priori* or by estimation) which is particularly evident in studies with power <80%. Misspecification of the exponent does not affect the accuracy of the prediction of CL within the study population, but it will lead to potential issues when extrapolated to new populations, e.g. from adults to children. It seems that a study power of 80% or more is required for model extrapolation purpose and this is irrespective of the method used to determine the allometric exponent and the covariate distribution within the study cohort. Overall, the

sample size requirement to achieve 80% power when estimating the exponent was smaller than when the exponent was chosen from a range of *a priori* choices. Clinical studies that involve only adults with at least 100 to 200 participants or includes children (more than 2 years of age), adolescents and adults in equal portions with at least 50 participants (in total) appear to provide adequate power and precision for estimation of the exponent. If practical or operational constraints, such as a limited sample size or a narrow weight range, hinder the ability to achieve an appropriate study power then it may be necessary to rely on prior information about the likely value of the exponent rather than letting the data speak to the value. However, this will also carry a risk of incorporating an incorrect exponent if the *a priori* choice is not correct.

PART III

SCALING OF CLEARANCE BY BODY SIZE COMPOSITION

Chapter 3: A review of the methods and mathematical models used in the measurement of fat-free mass

This chapter is based on the following peer-reviewed publication:

Sinha J, Duffull SB, Al-Sallami HS. *Review of the methods and associated mathematical models used in the measurement of fat-free mass.* Clinical Pharmacokinetics. 2018; 57(7): 781–795.

3.1. Introduction

Body size-based drug dosing which is often found in drug labelling typically refers to total body weight (WT) as the size measure. However, the emphasis on FFM as an alternative size descriptor for dose scaling is increasing [24, 25, 91, 126, 136-138]. Various experimental methods are available to measure FFM. These measurements can be used to develop mathematical models to predict FFM from readily measurable patient characteristics (e.g. weight, height, and sex). However, measuring FFM by each of these experimental methods is based on particular assumption(s) which may or may not be valid within and between populations. Because of the non-universality of these assumption(s), a particular method may need to be restricted for use in one particular population (e.g. adults) and another method used for other populations. Therefore, a systematic understanding of the available experimental methods is a prerequisite for their rational use in future research. Compared to the reviews already published on this topic [100, 139-143], the current review presents the mathematical underpinnings and assumptions associated with FFM measurement methods and the clinical implications of such assumptions.

Therefore, the aim of this review is to provide a scientific framework for FFM determination by various measurement methods with special emphasis on mathematical interpretation, and to illustrate how they differ and relate to each other in terms of their assumptions and limitations.

3.2. Methods for body composition analysis

There are six distinct methods (sections 3.2.1 to 3.2.6) of body composition analysis which are widely used in various populations. They are densitometry, hydrometry, bio-impedance analysis, whole body counting, dual-energy X-ray absorptiometry, and medical imaging. These are built on different physical and/or biological principles (e.g. body density, X-ray attenuation) and simplified based on some key assumptions. This section describes the

methodological details of these techniques, with special emphasis on their mathematical calculations.

3.2.1. Densitometry

3.2.1.1. Principle:

From a body composition perspective, the human body can be divided into two components: fat mass (FM) and fat-free mass (FFM) and thus total body mass (BM) can be expressed by Eq 3.1.

$$BM = FM + FFM$$

Eq 3.1 Components of human body from body composition perspective

The major portion of FFM constitutes of water in addition to proteins, carbohydrate and minerals. Thus FM and FFM are assumed to be two immiscible phases in the body (see Figure A2.1 in Appendix 2:) which allows the volume to be summed as Eq 3.2 similar to mass in Eq 3.1.

$$V_B = V_F + V_{FF}$$

Eq 3.2 Components of body volume

V_B denotes total body volume and V_F and V_{FF} represent the volumes of fat and fat free components, respectively.

Since volume can be expressed as mass divided by density, Eq 3.2 can be rewritten as Eq 3.3 below, where $\rho_{\mathrm{BM}}, \rho_{\mathrm{FM}}$, and ρ_{FFM} represent densities of BM, FM and FFM, respectively.

$$\frac{BM}{\rho_{BM}} = \frac{FM}{\rho_{FM}} + \frac{FFM}{\rho_{FFM}}$$

Eq 3.3 Body volume in terms of mass and density

Further rearrangement of Eq 3.3 and incorporating fractional fat mass (f_{FM}) and fractional fat-free mass (f_{FFM}) result in Eq 3.6 below (detail derivation is shown in section A2.1 of Appendix 2:).

$$\frac{BM}{\rho_{BM}} = \frac{BM \times f_{FM}}{\rho_{FM}} + \frac{BM \times f_{FFM}}{\rho_{FFM}}$$

Eq 3.4 Body volume in terms of mass, fractional mass and density

$$\frac{1}{\rho_{BM}} = \frac{f_{FM}}{\rho_{FM}} + \frac{f_{FFM}}{\rho_{FFM}}$$

Eq 3.5 Body volume in terms of fractional mass and density (rearranged)

$$f_{\mathrm{FM}} = \frac{1}{(\rho_{\mathrm{FFM}} - \rho_{\mathrm{FM}})} \times \left(\frac{\rho_{\mathrm{FM}} \times \rho_{\mathrm{FFM}}}{\rho_{\mathrm{BM}}} - \rho_{\mathrm{FM}}\right)$$

Eq 3.6 Equation for fractional fat mass

The densities of FM and FFM were derived from adipose tissue samples during surgery and by chemical analysis of human cadavers. Mean values were ρ_{FM} = 0.90 g/mL [144], ρ_{FFM} = 1.10 g/mL [145] (detailed calculations are shown in sections A2.2.1 and A2.2.3 of Appendix 2:). Using these values, Eq 3.6 can be simplified to Eq 3.7 which is known as Siri's equation [146] in body composition research.

$$f_{\mathrm{FM}} = \left(\frac{4.95}{\rho_{\mathrm{BM}}} - 4.5\right)$$

Eq 3.7 Siri's equation of body composition

Often, body mass (BM) is referred to as total body weight (WT). Therefore, FFM can be derived by measuring WT using Eq 3.8 and Eq 3.9.

$$FM = WT \times f_{FM}$$

Eq 3.8 Calculation of fat mass

$$FFM = WT - FM$$

Eq 3.9 Calculation of fat-free mass

3.2.1.2. Methodology:

Using an *a priori* known values of ρ_{FM} and ρ_{FFM}, FFM can be calculated by Eq 3.6, Eq 3.8 and Eq 3.9 if the total body density (ρ_{BM}) is known. Total body density can be determined by the ratio of WT and V_B. WT can be measured easily using a weight machine whereas the measurement of V_B is more involved (sections 3.2.1.2.1 and 3.2.1.2.2). Alternatively, ρ_{BM} can be directly predicted by anthropometric measurements as described in 3.2.1.2.3.

3.2.1.2.1. Hydrostatic weighing

The experimental system consists of a tank of water and a weight scale. The subject's weight is taken first outside water (WT_{air}) followed by weighing under water (WT_{water}). For WT_{water} determination, the subject exhales maximally, submerges completely in the water, and body weight is recorded on the scale. The reduction in the weight (ΔWT) due to underwater weighing is calculated by Eq 3.10.

$$\Delta WT = WT_{air} - WT_{water}$$

Eq 3.10 Reduction in the weight due to underwater weighing

According to Archimedes' principle, ΔWT is equal to the upward buoyant force which is exerted on the subject's body while immersed inside the water and this is equal to the weight of the water displaced by the subjects' body. Since the displaced water volume is equal to the total body volume of the subject, ΔWT is equal to V_B at 4˚C, the temperature at which water density is 1 g/mL. Since, under-water weighing is carried out in water at 30˚C, a water density correction needs to be considered at this temperature to obtain ρ_{BM} (Eq 3.11). The density of water at 30˚C is 0.9957 g/mL.Residual air (V_R) trapped in the lung is a significant source of error for ρ_{BM} measurement by hydrostatic weighing and needs to be accounted for by subtracting it from the calculated body volume [147]. Closed circuit oxygen dilution technique is commonly used for measuring V_R.

$$\rho_{BM}(g/mL) = \frac{WT_{air}\ (kg)}{\frac{\Delta WT\ (kg)}{0.9957} - V_R(L)}$$

Eq 3.11 Calculation of body density by underwater weighing

Hydrodensitometry can be used to measure body density with good precision provided that the operators are well trained. In spite of the consistency in body density measurement, hydrostatic weighing is not preferred in children, elderly, disabled and other special populations due to its experimental difficulties [147].

3.2.1.2.2. Air displacement plethysmography

A relatively recent technique of air displacement plethysmography for measurement of body density obviates the need for underwater weighing. BOD POD® [148] differs from underwater weighing in that it uses air instead of water to measure body volume, based on the physical relationship between pressure and volume change in a thermally insulated system (Eq 3.12). This relationship allows for the derivation of an unknown volume by directly measuring pressure.

$$\frac{P_1}{P_2} = \left(\frac{V_2}{V_1}\right)^{\gamma}$$

Eq 3.12 Physical relationship between pressure and volume

V_1 and V_2 represent the respective volumes of a gas at two different pressures of P_1 and P_2 and γ is a gas specific constant whose value is 1.4 for air [149]

The BOD POD® device is comprised of a 'test' chamber and a 'reference' chamber, which are separated by a diaphragm [149]. The subject is seated in the test chamber and the diaphragm oscillates to produce a slight change in volume and, consequently, pressure in each chamber. The subject's volume is obtained by the difference in pressure in the presence and absence of the

subject in the test chamber. When the volume is increased in one of the chambers, it is decreased by the same amount in the other chamber, and vice versa. The pressure in each of the two chambers changes accordingly, and the magnitude of the pressure change indicates the relative size of each of the chambers. The pressure change is roughly ± 0.005 m H_20, and is rarely noticeable to the subject (comparable to the change in pressure while moving from the first floor to the second floor in an elevator). In this method the BOD POD® measures the pressure change and then under ideal gas properties as per Eq 3.12 is able to compute the respective apparent volumes of each chamber.

Unlike hydrostatic weighing, the subject breathes normally inside the instrument during experiment. But the air inside the lung (lung volume) and in contact with hair, clothing, and skin surface closely follows isothermal processes and thus is more compressible than in the rest of the test chamber under adiabatic condition. This leads to error in V_B measurement and needs to be corrected for. The body density is calculated by using Eq 3.13 [149]:

$$\rho_{BM} = \frac{WT}{V_B + 0.40 \times V_L - \delta \times BSA}$$

Eq 3.13 Calculation of body density by BOD POD

Due to isothermal compression, the lung volume (V_L) appears 40% larger than it is, and consequently underestimation of V_B occurs by 40% of V_L and hence added to the measured V_B. For this reason, V_L is also determined in the BOD POD®. V_L is determined as per usual pulmonary function tests [150]. The effect of clothing and hair is handled by wearing minimal clothing (e.g. bathing suit) and swim cap respectively. The effect of surface area causes overestimation of V_B and therefore corrected by subtracting a factor called surface area artefact (SAA). SAA is calculated automatically by the instrument by multiplying subject's body surface area (BSA, calculated by Dubois formula [151]) with an instrument specific constant 'δ' (L/m^2). This technique overcomes the difficulties associated with underwater weighing.

3.2.1.2.3. Anthropometry (Skinfold Thickness):

Skinfold thickness has been explored to predict body density. This approach is based upon two assumptions: the thickness of the subcutaneous adipose tissue reflects a constant proportion of total body fat and the sites selected for measurement represent the average thickness of the body's subcutaneous adipose tissue [139]. The measurement of skinfold thickness is made by grasping the skin and adjacent subcutaneous tissue between the thumb and forefinger, shaking it gently to exclude underlying muscle, and pulling it away from the body just far enough to allow the jaws of the calliper to impinge on the skin. Multiple readings are made at each site to improve the accuracy and the reproducibility of the measurements.

Jackson et al. [152, 153] proposed a generalised regression equation for males and females. In their work, they used a quadratic regression model over the sum of seven skinfold measures (chest, axilla, triceps, sub-scapula, abdomen, supra-iliac and front thigh) and incorporated age, waist, forearm circumference, and gluteal circumference as additional independent variables. Their predictive models are shown in Eq 3.14 and Eq 3.15.

$$\rho_{\mathrm{BM}} = 11010 \times 10^{-4} - 4.115 \times 10^{-4} \times X_1 + 0.0069 \times 10^{-4} \times (X_1)^2 - 2.2631 \times 10^{-4} \times X_2 - 59.239 \times 10^{-4} \times X_3 + 190.632 \times 10^{-4} \times X_4$$

Eq 3.14 Jackson's model for body density for males

$$\rho_{\mathrm{BM}} = 11470 \times 10^{-4} - 4.293 \times 10^{-4} \times X_1 + 0.0065 \times 10^{-4} \times (X_1)^2 - 0.9975 \times 10^{-4} \times X_2 - 6.2415 \times 10^{-4} \times X_5$$

Eq 3.15 Jackson's model for body density for females

X_1 = sum of seven skinfolds, X_2 = age, X_3 = waist circumference, X_4 = fore arm circumference, X_5 = gluteal circumference.

3.2.2. Hydrometry

3.2.2.1. Principle:

In the hydrometry setting, water is assumed to constitute a constant fraction of FFM. It is, therefore, possible to estimate FFM if total body water can be measured experimentally. Total body water (TBW) can be measured either by measuring the dilution space of an isotope labelled water or of a non-aqueous compound which freely distributes in body water. Knowing TBW, FFM can be calculated by Eq 3.16 using a standard value of $R_{\text{water/FFM}} = 0.73$, based on the reported experimental value of FFM hydration using human cadavers [154]. Detailed calculation of cadaver analysis is shown in section A2.2.2 of Appendix 2: .

$$FFM\ (Kg) = \frac{TBW\ (Kg)}{R_{water/FFM}}$$

Eq 3.16 Relationship between total body water and fat-free mass

3.2.2.2. Methodology:

Various methods have been proposed to approximate TBW. These are discussed in sections 3.2.2.2.1 and 3.2.2.2.2 and calculated by Eq 3.17-Eq 3.21.

3.2.2.2.1. Isotope dilution

The tracers used for determination of TBW are either tritiated water (^3H_2O), deuterated water (^2H_2O), or stable ^{18}O-labelled water ($H_2{}^{18}O$). The tracer is administered orally or by intravenous (IV) injection and allowed to equilibrate for 2-6 h depending on the tracer used and the health status of the subject. After equilibration a single fluid sample is taken (typically blood or saliva) for analysis and the urine is also collected and analysed for calibration purposes. The underpinning assumption is that different isotopes of water are indistinguishable to the body.

Selection of bioanalysis technique of the tracer depends upon the tracer used in the experiment. Tritium (^{3}H) estimation is very easy in the biological sample by using scintillation counting but it emits radiation which limits its use particularly in children and women during pregnancy or during child bearing age. In contrast, non-radioactive isotopes such as ^{2}H and ^{18}O are safer in this context, but their analysis usually involves mass spectrometry (LC-MS) which often limits their use in clinical practice. Upon measurement of the concentration of tracer, the TBW is then calculated using Eq 3.17, based on the dilution space of the tracer.

$$TBW = \frac{Amount\ of\ tracer\ ingested - Amount\ of\ tracer\ in\ urine}{[tracer]_{blood}}$$

Eq 3.17 Calculation of total body water by isotope dilution

N.B. For tritium dilution, the amounts and concentration in Eq 3.17 would be replaced by radio activity

Isotope dilution is a relatively lengthy process requiring the time to reach steady state, which can vary across subjects leading to potential errors. Typically multiple samples are taken to avoid these issues.

3.2.2.2.2. Non-aqueous compound dilution

TBW can be indirectly measured by separately measuring extracellular water (ECW) and intracellular water (ICW) and by Eq 3.18.

$$TBW = ECW + ICW$$

Eq 3.18 Components of total body water

Bromide (Br^{-}) and chloride (Cl^{-}) are distributed primarily in the ECW. Therefore, ECW is typically measured either using dilution of Br^{-} or by measuring chloride space (volume of distribution). Essentially both of these techniques use the estimated volume of distribution of the species in question as the value for ECW.

Br^- is usually administered in the form of sodium bromide (NaBr) orally or as an IV injection in isotonic saline. A blood sample is collected post-equilibrium, 3-4 h later. Since Br^- has a long biological half-life of ~12 days, very insignificant amount is lost by the time of collection and hence no correction for the amount excreted is required. Eq 3.19 can be used to calculate the volume of ECW (ECW_{Br}) using the corrected Br^- dilution space. No correction for bioavailability is required for oral administration because of its complete absorption [155].

$$ECW_{Br}(L) = \frac{dose\ amount}{[Br^-]_{serum}} \times \beta_1 \times \beta_2 \times \beta_3$$

Eq 3.19 Calculation of extra-cellular water volume by bromide space

The correction factors β_1, β_2 and β_3 are fixed constants. β_1 accounts for the limited distribution of administered Br^- into non-extracellular space (primarily erythrocytes), β_2 denotes the water content (~94%) in serum [156, 157] and β_3 is the ratio of $[Br^-]_{serum}$ to $[Br^-]_{ECW}$. The ratio β_3 is used to correct for the equilibrium shift caused by the presence of charged plasma proteins in the intra-vascular space and was found to be similar for both Br^- and Cl^-. The values of β_1, β_2 and β_3 used in literature are 0.90, 0.94 and 0.95 respectively [156-159].

Total body Cl^-content ($TBCl$) is estimated by delayed γ-neutron activation in order to measure the chloride space. In delayed γ -neutron activation, placing a subject within a neutron beam from an external source produces short-lived radionuclides of Cl^-atoms in the body, which decay during the next ~5-20 minutes by releasing a characteristic γ -ray. The count is measured by using thallium-doped sodium iodide (NaI[TI]) scintillator which has adequate energy resolution. The measured count is converted to the absolute $TBCl$ amount using calibration curve of absolute amount vs. measured count, prepared with prior standards having known amount of Cl^- [100]. Eq 3.20 is used to calculate the ECW using corrected Cl^- space (ECW_{Cl}) , which uses the

same correction factors as in Eq 3.19, since Cl^- shares similar non-extracellular distribution and equilibrium shift as applied for Br^-.

$$ECW_{Cl}(L) = \frac{TBCl\ (mmol)}{[Cl^-]_{serum}\ (mM)} \times \beta_1 \times \beta_2 \times \beta_3$$

Eq 3.20 Calculation of extra-cellular water volume by chloride space

ICW can be quantified and distinguished from ECW on the basis of compartment specific cation/anion patterns. Since, potassium (K^+) is mostly restricted to the intracellular space (~97%), its dilution space can give good approximation of ICW. Total body potassium (TBK) can be measured by ^{40}K whole body counting (Eq 3.28 in section 3.2.4) and ICW can be estimated by dividing TBK with intracellular K^+ concentration ($[K^+]_i$) using Eq 3.21. The most commonly used value of $[K^+]_i$ is 150 mmol/L [160-162].

$$ICW\ (L) = \frac{TBK}{[K^+]_i}$$

Eq 3.21 Calculation of intra-cellular water volume by total body potassium

3.2.3. Bio-impedance Analysis (BIA)

3.2.3.1. Principle:

For a solid conductor, the resistance (R) is a measure of the extent to which the solid element opposes the flow of electrons. Body fluids are rich in electrolyte ions (Na^+, K^+ etc.), which conduct electricity and impose resistance (R) opposite to the current flow. A direct current (DC), when applied to the body, only passes through the ECW because of the lipid based cell membrane barrier which acts as insulator. In contrast, if an alternating current (AC) is applied, the cell membrane acts as capacitor in an electrical circuit, which accumulates then discharges electrical charge with each cycle of the AC

current. The resistance produced by the capacitor is known as reactance (X_c) and is defined by Eq 3.22.

$$Reactance\ (Ohm) = \frac{1}{2\pi \times Frequency\ (Hz) \times Capacitance\ (Farads)}$$

Eq 3.22 Relationship between reactance, capacitance and frequency

The magnitude of reactance (X_c) depends inversely on the frequency of the applied AC current, whereas resistance (R) is constant across frequencies. The overall resistance to current flow through our body, which is known as (bio)-impedance (Z), has two components R and X_c and is defined by Eq 3.23 [163]

$$Z^2 = R^2 + X_c^2$$

Eq 3.23 Relationship between bio-impedance, resistance and reactance

At lower frequency (<5 kHz), the magnitude of X_c is high and thus it opposes the current flow through the ICW. But, at higher frequency range (50-100 kHz), the reactive component (X_c) becomes negligible and thus the impedance (Z) is mainly due to the resistance ($Z \approx R$), which allows the current to flow through ICW as well (Figure A2.2 of Appendix 2:)

3.2.3.2. Methodology:

Single frequency BIA is carried out to determine TBW and FFM, where a high frequency (typically 50 kHz) AC current (800 μA) is applied to a subject's body by a tetra-polar BIA instrument (Figure A2.3 of Appendix 2:). Two source electrodes are placed for applying current and two detection electrodes are placed to record the voltage drop due to impedance, a function of both R and X_c [163-166]. Typically BIA electrodes are placed as per hand-to-foot arrangement

as shown in Figure A2.3, but some BIA instruments use hand-to-hand or foot-to-foot electrode placement as well [167].

For a cylindrical conductor (Figure 3.1) with specific resistivity φ (ohm-cm), length L (cm), cross-sectional area A_c (cm^2) and volume V_c (mL), the Z or R are defined by Eq 3.24, from where Eq 3.25 can be derived for the solution of V_c.

$$R \text{ or } Z \text{ (ohm)} = \frac{\varphi \times L}{A_c} = \frac{\varphi \times L^2}{A_c \times L} = \frac{\varphi \times L^2}{V_c}$$

Eq 3.24 Resistance of a cylindrical conductor

$$V_c(\text{mL}) = \frac{\varphi \times L^2}{R \text{ or } Z}$$

Eq 3.25 Calculation of volume of a conductor from its resistance

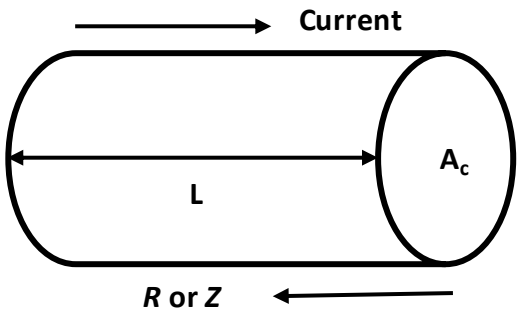

Figure 3.1 Representation of electric current flow through cylindrical conductor against the resistance or impedance.

L length, A_c cross-sectional area, Z impedance, R resistance

V_c and L can be imagined as the volume of TBW or FFM through which current flows exclusively and height (Ht) of an individual, respectively. Therefore it follows that if the value of R or Z can be determined by BIA then the volume of TBW or FFM can be estimated. If TBW is estimated instead of FFM, it can be used to predict FFM indirectly by previously described Eq 3.16. Since human body does not represent a series of cylinders, an equation needs to be developed that links experimentally determined bio-impedance to TBW or FFM. This is typically accomplished by from $Ht^2/_R$ or $Ht^2/_Z$ as the starting

point with additional anthropometric characteristics included as required. Eq 3.26 represents the general format of the equations for predicting TBW or FFM reported commonly in the literature [163, 167, 168], where the coefficients (θ_1,θ_2, θ_3, θ_4) and intercept (θ_5) values are estimated. The value of a particular coefficient(s) could be zero if poor correlation is demonstrated.

$$\text{TBW} = \theta_1 \times \left[\frac{\text{Ht}^2}{R \text{ or } Z}\right] + \theta_2 \times [\text{Sex}] + \theta_3 \times [\text{WT}] + \theta_4 \times [\text{Age}] + \theta_5$$

Eq 3.26 General format of the equations for predicting total body water from bioimpedance

Janmahasatian et al. [102] developed a mathematical model (Eq 3.27) for predicting FFM directly from measured Z which obviates the need of predicting TBW. They first developed a model for predicting bio-impedance ($\hat{Z}$) from WT and Ht. In the next step, they developed FFM prediction model using the model predicted $\hat{Z}$ estimates using mechanistic basis. Their model can be used for predicting FFM directly from BIA derived Z value or from WT and Ht without BIA data.

$$FFM = 9.27 \times 10^3 \times \frac{Ht^2}{Z}$$

Eq 3.27 Janmahasatian's equation for predicting FFM from bioimpedance

FFM is in kg, Ht is in metres and Z is in ohms.

3.2.4. Whole Body Counting

3.2.4.1. Principle:

The whole body scans obtained from whole body radioactivity counters installed at nuclear plants and laboratories were found to have natural background signal from the body. With the development of scintillation detectors with adequate energy resolution, one of the naturally emitted signals was identified as potassium (^{40}K). Naturally-occurring potassium contains

three isotopes among which the ^{40}K isotope is radioactive and constitutes a very small constant proportion of potassium (93.1% ^{39}K, 6.9% ^{41}K, 0.0118% ^{40}K). Therefore, total body potassium (TBK) can be determined by measuring the ^{40}K content in the body (Eq 3.28). A whole body scan takes 5-20 minutes using detectors with high energy resolution to selectively record γ-rays of 1.46 MeV energy emitted from ^{40}K.

$$TBK\ (mmol) = \frac{Radioactive\ K\ content\ (mg)}{0.000118 \times 39.102\ (mg/mmol)}$$

Eq 3.28 Measurement of total body potassium from whole body counting

0.000118 is the mass fraction of radioactive ^{40}K and 39.102 is the molecular weight of potassium. Of note here, the value of TBK determined by Eq 3.28 is used in Eq 3.21 to calculate ICW.

Potassium is mostly (97%) restricted to intra-cellular space which is exclusively present within the FFM portion of the body, and therefore the TBK value can be used to estimate FFM (Eq 3.29) assuming that TBK constitutes a constant proportion of FFM. The standard TBK to FFM ratio ($R_{\mathrm{TBK\,/\,FFM}}$) used in body composition research is 68.1 mmol/kg of FFM used for both sexes [140]. This value was determined from human cadaver studies and discussed further in section A2.2.4 of Appendix 2: .

$$FFM\ (kg) = \frac{TBK\ (mmol)}{R_{TBK\ /\ FFM}}$$

Eq 3.29 Measurement of fat-free mass from whole body counting data

FFM values extrapolated from TBK data depend on the ratio; $R_{\mathrm{TBK\,/\,FFM}}$. Variations in this ratio were reported in the literature (discussed in detail in section A2.4 of Appendix 2:) which suggests that this ratio is not constant across populations. Therefore, FFM extrapolated from TBK data might become erroneous if a universal value of $R_{\mathrm{TBK\,/\,FFM}}$ is used.

3.2.4.2. Methodology of counting:

The subject is placed in a supine position on the table, and scanning is performed through radioactivity detectors placed at anterior and posterior sides of the subject. The detector possesses high quality energy resolution to discriminate the γ-rays emitted from ^{40}K and from other naturally occurring radioisotopes inside body. Thallium-doped sodium iodide (NaI[TI]) scintillator is best suited for this purpose [169]. The counting takes 5-20 minutes depending upon number of detectors used.

3.2.5. Dual-energy X-ray absorptiometry (DXA):

3.2.5.1. Principle:

The underlying concept of DXA is similar to that of the regular diagnostic X-ray radiography, which states that X-ray absorption *in vivo* is a function of tissue composition and X-ray wavelength. DXA employs two monochromatic X-ray beams i.e. a low (40 keV) and a high (70 keV) energy beam and it employs a photo-detector with electronic transmission to record the attenuation of beam intensities (Figure 3.2). DXA divides the whole human body into several thousands of small squares (usually 1 mm× 1 mm), known as pixel (about 21,000 pixels) and records the respective attenuation ratios (denoted as '*r*' later in this section) of low to high energy beams for each of the pixels. The primary objective of DXA is to solve the fractional mass of lean tissue out of the attenuation data from all the pixels by using mathematical approximation. The effective radiation dose used in DXA is about 5 times lower than that used in a regular diagnostic chest X-ray radiography [170] which makes it a safer way of studying body composition in special populations (e.g. children). This corresponds to an average radiation exposure that a person receives in 1-2 days from natural sources [171].

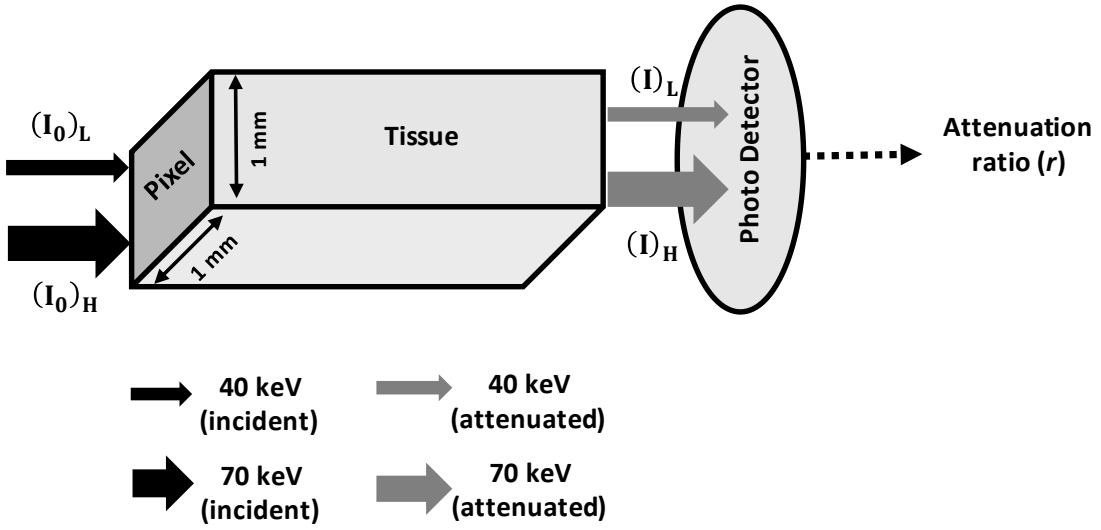

Figure 3.2 Schematic of a pixel composed of mixture of tissue components.

Two monochromatic X-ray beams passes through the pixel. $(I_0)_L$ and $(I_0)_H$ denote the intensities of low and high energy incident beams respectively. $(I)_L$ and $(I)_H$ denote the intensities of low and high energy transmitted beams. Every pixel represents fractional masses and masses of a individual components, i.e. lean, fat and bone mineral

Using DXA, one assumes that the body is composed of three major constituents, i.e. fat, lean tissue and bone mineral, where fat and lean together constitute the soft tissue. Each of these tissues, being distinct in terms of composition, possesses a characteristic attenuation ratio (r) of the 40 keV to 70 keV intensity beams, which are known *a priori*. These ratios are denoted here as r_{fat}, r_{lean} and r_{bone} for fat, lean and bone mineral respectively. Their known theoretical values are 1.21, 1.36 and 2.86 respectively, which were calculated by Pietrobelli et al. [172] using the elemental composition (e.g. C, H, O, N) of respective tissues and the known attenuation of each of the elements. The authors further estimated r_{fat} and r_{lean} to be 1.20 and 1.40 experimentally by using animal tissues. The observed r values of the pixels from a DXA scan differs from these standard values because they are mixture of two or three of these standard tissues with (almost) infinite sets of fractional compositions. For example, if a pixel is composed of fat and lean tissue its r value would be between 1.20 and 1.36. Similarly, if a pixel is made of lean and bone, its r value

would fall between 1.36 and 2.86. Moreover, because of infinite sets of possible compositions, r values can hold any number within the specific range.

DXA involves a two stage process (Figure 3.3). In the first stage, pixels related to bone mineral are separated from the non-bone pixels of a whole body scan. This is performed based on a threshold value of 'r', below which non-bone or soft tissue pixels appear. The soft tissue pixels are a two-component system of lean and fat tissue. The fractional mass of lean tissue in each (i^{th}) soft tissue pixel (f_{lean_i}) is derived from the measured r values $\left(r_{\text{ST}_i}\right)$ using Eq 3.30 (for derivation, refer to section A2.3 of Appendix 2:). The average fraction of lean tissue in the whole body's soft tissue mass, i.e. $f_{lean\,(ST)}$ is then determined by dividing the sum of all f_{lean_i} values by the total number (N_{ST}) of soft tissue pixels (Eq 3.31).

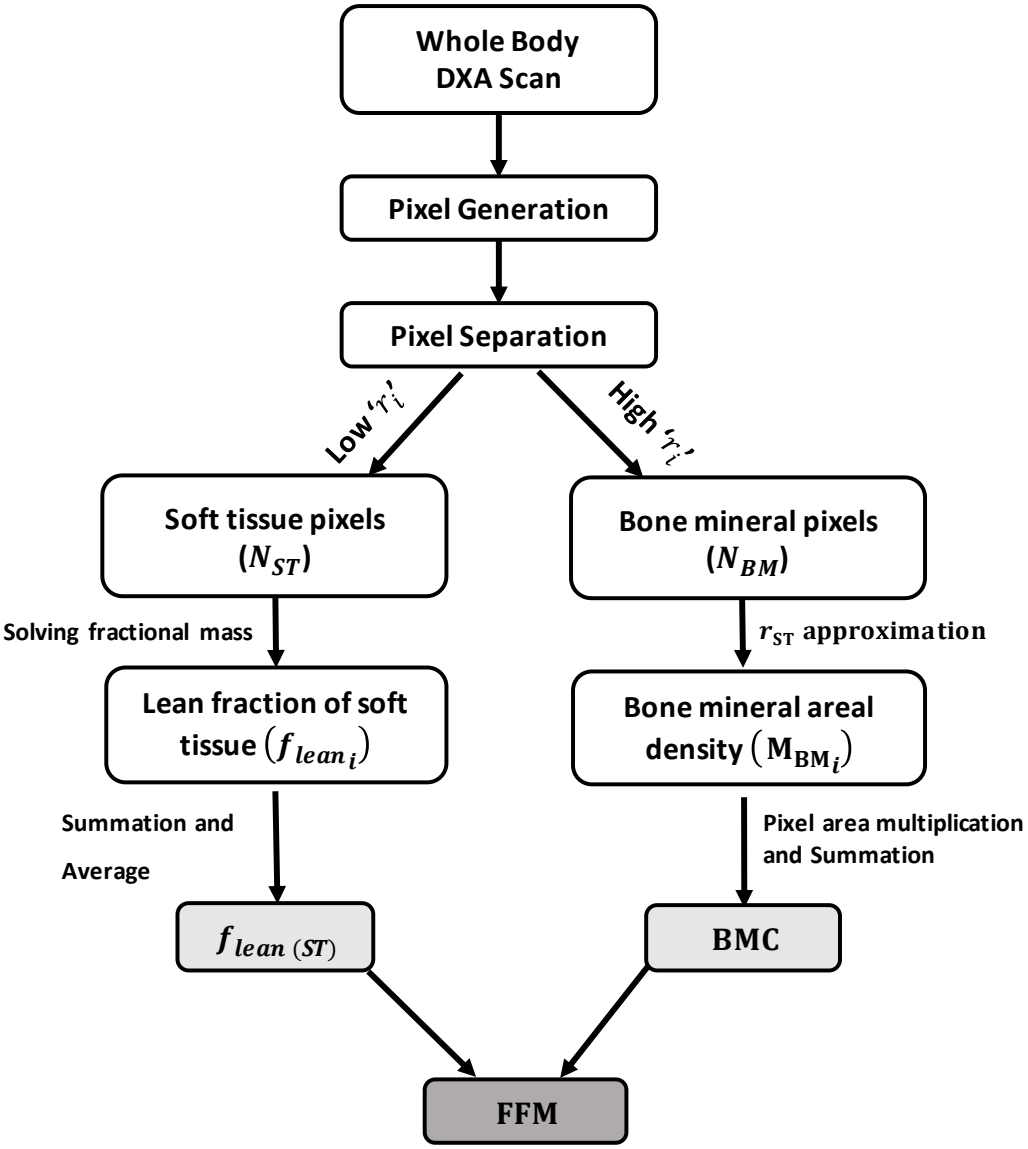

Figure 3.3 Summary of DXA workflow covering various steps from whole body scan to FFM estimation.

The total number of pixels generated in the whole body DXA scan is equal to the sum of N_{ST} and N_{BM}. r_i attenuation ratio of the i^{th} pixel, r_{ST} approximated attenuation ratio of soft tissue in the bone mineral pixels, $f_{lean\ (ST)}$ average fraction of lean tissue in the whole body's soft tissue mass, BMC bone mineral content, FFM fat-free mass

$$f_{lean_i} = \frac{r_{\mathrm{ST}_i} - r_{fat}}{r_{lean} - r_{fat}}$$

Eq 3.30 Calculation of fractional mass of lean tissue in soft tissue pixel in DXA

$$f_{lean\ (ST)} = \frac{\sum_{i=1}^{N_{ST}} f_{lean_i}}{N_{\mathrm{ST}}}$$

Eq 3.31 Calculation of average fraction of lean tissue in the whole body's soft tissue mass in DXA

In the second stage, bone mineral content (BMC) is calculated by Eq 3.32 (for derivation, refer to section A2.3 of Appendix 2:) using attenuations from the bone mineral containing pixels which remained above the threshold 'r' value.

$$BMC\ (g)\ = \sum_{i=1}^{N_{BM}} M_{BM_i}(g/cm^2) \times Pixel\ Area_i\ (cm^2)$$

Eq 3.32 Calculation of bone mineral content in DXA

M_{BM_i} and N_{BM} represent the bone mineral areal density (g/cm^2) of the ith pixel and the total number of bone mineral pixels.

The bone containing pixels usually constitutes 40-45% of the total 21000 pixels recorded in a typical whole body DXA scan [173]. Once the BMC mass is determined, the weight of soft tissue (WT_{ST}) and FFM can be calculated by Eq 3.33 and Eq 3.34 respectively.

$$WT_{ST}\ (g) = (WT - BMC)$$

Eq 3.33 Calculation of weight of soft tissue in DXA

$$FFM\ (kg) = WT_{ST}\ (kg) \times f_{lean\ (ST)} + BMC\ (kg)$$

Eq 3.34 Calculation of fat-free mass in DXA

3.2.5.2. Methodology of scanning:

For a whole body scan, the subject lies in a supine position in the centre of the scanning table. The X-ray source, located at the posterior position of the

subject emits radiation which passes through the subject's body and is captured by the detector placed anteriorly. A whole body scan requires 5-30 minutes depending upon the instrument used. The subject must avoid movement during the scan.

3.2.6. Medical Imaging

Medical imaging is also a very useful tool in body composition research. Computed tomography (CT) and magnetic resonance imaging (MRI) are the two radiological techniques primarily used for this purpose.

Principle of CT:

The working principle of CT is similar with that of DXA, as both measure the differential attenuation (tissue dependent) of X-ray as it passes through the body. The difference lies with the effective dose of the applied radiation and the methods used for image detection and analysis. CT effective dose is many fold higher than regular X-ray radiographic doses and thus significantly higher than DXA. This imposes potential risk to the patient, particularly upon repeated exposure. A DXA-generated pixel represents an infinite depth of a tissue mixture (therefore volume cannot be determined), whereas CT-derived pixels correspond to a specific depth (known *a priori*) from where volume can be calculated. This is accomplished by dividing the whole body into hundreds of axial slices and assigns distinct pixels on every slice to reconstruct high resolution images of a particular tissue on every slice. Therefore in CT, every pixel represents a 3D voxel which corresponds to the slice thickness (usually 10 mm) and inter-slice distance, whereas DXA works with 2D pixel. Tissue volume is then calculated by adding up the volumes of that tissue on every slice and the interpolated inter-slice volumes (discussed later under 3.2.6.2). In contrast to DXA, CT is based on estimating the volume of adipose tissue rather than bone mineral mass and fractional lean mass. DXA and CT derive the mass of tissues in exactly opposite ways. DXA determines the (areal) density (g/cm^2)

of bone mineral first, which is then multiplied by a known geometric variable, i.e. pixel area (cm^2) to estimate the mass of bone mineral (g). On the contrary, CT determines the geometric variable i.e. volume of adipose tissue (cm^3) first, which is then multiplied by the known (*a priori*) value of adipose tissue density (g/cm^3) in order to derive the adipose tissue mass (g). Also, unlike DXA CT is not strictly dependent on two particular monochromatic X-ray beams of specific energy.

3.2.6.1. Principle of MRI:

MRI has been proposed as an alternative technique which avoids the health risk associated with ionising radiation. This technique is based on the interaction between hydrogen nuclei (protons) and the magnetic field generated by the MRI instrument. The MRI induces a strong magnetic field that is about 50,000 times stronger than earth's magnetic field (1.5 Tesla vs 3.2×10^{-5} Tesla), whereby the spin of all hydrogen nuclei aligns with the applied magnetic field. Once the magnetic alignment is achieved, a pulse radio frequency (RF) is applied which is well absorbed by the protons and upon cessation of the RF pulse, the excited protons return to their original position by releasing energy in the RF range. This radiating energy travels through the tissue and gets attenuated before it is captured by the detector placed in the MRI scanner. The extent of signal attenuation is tissue specific. Therefore the MRI system is able to distinguish various types of tissues by constructing images based on variable signal attenuation.

3.2.6.2. Methodology of image analysis:

Images are generated during the scan by dividing the subject's body into several axial slices along the longitudinal axis. Once image acquisition is completed, both CT and MRI images can be analysed using a common method. The attenuation is expressed as CT number (measured in Housenfield units

[HU]), which is a measure of attenuation relative to water, defined as 0 HU. The image is constructed by many pixels (usually 1 mm × 1mm) which have a defined CT number based on a grey scale which gives contrast to the image. Every pixel represents a voxel element with a specified depth. The extent of attenuation is dependent on the physical density of a particular tissue; with lower density represented by lower CT numbers, relative to water (HU=0). For example, pixels of adipose tissue range from -190 to -30 HU and for skeletal muscle from 30 to 100 HU. Each pixel is then segregated based on the CT number using interactive image analysis software that utilises image segmentation algorithms like 'histogram analysis' or 'edge detection' [174]. Once the edges of different tissues have been identified and demarcation lines are drawn, the analyser applies colour coding to provide visual differentiation of regions of tissues and thereby, to calculate the surface area contributed by a particular tissue on that image.

Acquisition and analysis of contiguous images of whole body scan is time consuming and expensive. Therefore in actual practice, axial images are typically collected along with inter-slice gaps (e.g. space between the upper surface of one image and lower surface of adjacent image) ranging from 20 to 40 mm as described in Figure 3.4. Image_i and Image_{i+1} are two consecutive image slices with an inter-slice distance (l) of 40 mm and image thickness (t) of 10 mm. The surface areas (cm^2) of the adipose tissue (shown in grey colour) on two images are Area_i and Area_{i+1} respectively ($\text{Area}_i > \text{Area}_{i+1}$), N_s is the total number of image slices generated and V_{AT} is the total volume (cm^3) of adipose tissue in the body. V_{AT} is then calculated from the areas of adipose tissue on consecutive images and the inter-slice distance. Three different geometrical models are in place for volume calculation, which mainly differ in their assumptions of the inter-slice volume interpolation [174]. However, all models assume that the change in cross-sectional area of adipose tissue between two consecutive images is linear. The parallel trapezium model (Eq 3.35) [175] is one

of the geometrical models used for this purpose. It assumes that the irregular shapes of the adipose tissues in the axial images are trapezoids.

$$V_{\mathrm{AT}} = \frac{l}{2} \times \sum_{i=1}^{N_s} \mathrm{Area}_i$$

Eq 3.35 Calculation of adipose tissue volume by medical imaging

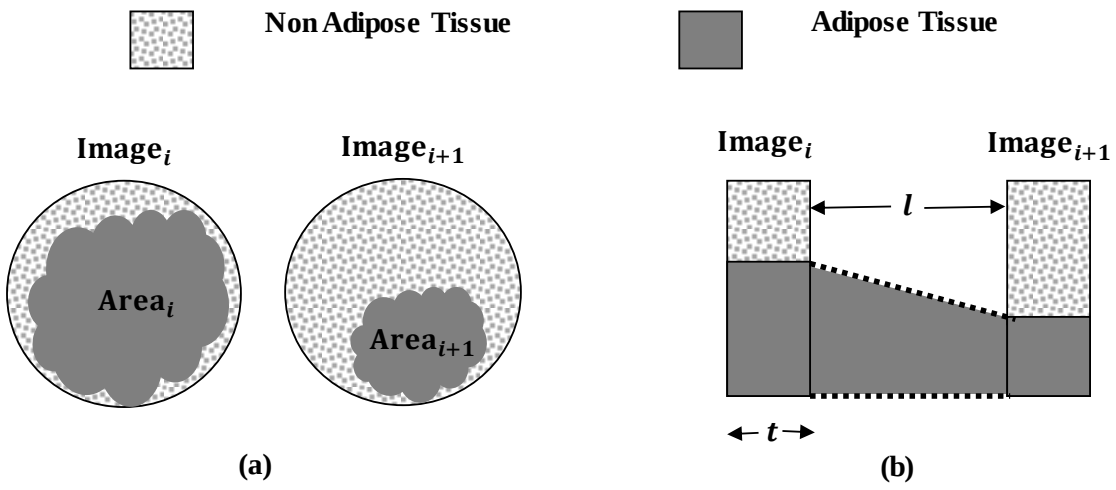

Figure 3.4 Schematic representation of CT/MRI image slices

(a) Schematic representation of two consecutive CT/MRI image slices and areas covered by adipose tissue ($Area_i$, $Area_{i+1}$) and non-adipose tissue. (b) Total volume of adipose tissue (dark shaded) contributed by two slices (t slice thickness) and the inter-slice gap (l) assuming a linear interpolation (dotted line). The tissues in each slices are geometrically irregular, which are approximated by various assumptions made in the mathematical models for volume calculation

The FM weight can be calculated by Eq 3.36 by knowing the adipose tissue density (ρ_{AT}) and fractional fat content (f_{AT}) and finally the FFM by using Eq 3.9. Apart from fat, adipose tissue also contains water, protein, minerals and thus holds a slightly higher density than ρ_{FM}. A density of 0.95 g/mL and 80% fat content ($f_{\mathrm{AT}} = 0.80$) of adipose tissue is usually assumed in the literature for calculating its volume from imaging studies [99, 176, 177].

$$\mathrm{FM} = V_{\mathrm{AT}} \times \rho_{\mathrm{AT}} \times f_{\mathrm{AT}}$$

Eq 3.36 Calculation of fat-mass by medical imaging

3.3. An overarching framework to quantify FFM

Although each method of FFM measurement is distinct with respect to its working principle and operation, their interim outcomes are interrelated. We provide an overarching scheme of how the methods interrelate in Figure 3.5 and the interlinks between parameters of various methods through specific Equation numbers in Figure 3.6. Examples of their use in calculations of FFM using standard values are summarised in Table A2.5 of Appendix 2: . Each of the physiological variables measured by most of the methods discussed here i.e. fat mass (FM), total body water (TBW) and total body potassium (TBK) links multiple methods. For example, both densitometry based methods (hydrostatic weighing, BOD POD®, skinfold thickness) and imaging based methods (CT, MRI) determine the same physiological estimate i.e. fat mass, which is subtracted from total body weight (WT) to calculate FFM. Similarly, total body water is the common outcome determined by hydrometry based methods (isotope dilution, ICW and ECW measurement) and bioimpedance analysis (BIA) from which FFM is calculated using the ratio $R_{\mathrm{water/FFM}}$. Again, the intracellular water is measured from the total body potassium measurement, which is a part of whole body counting, another FFM measuring method. In whole body counting, FFM can be directly calculated from TBK using the ratio $R_{\mathrm{TBK/FFM}}$ without the need of estimating TBW. On the other hand, DXA measures unique variables i.e. $f_{lean\,(ST)}$ and BMC which are not shared by any other methods. The FFM model by Janmahasatian et al. appears in the framework (Figure 3.5) because it involved the development of a BIA prediction model which was subsequently used to develop a FFM prediction model.

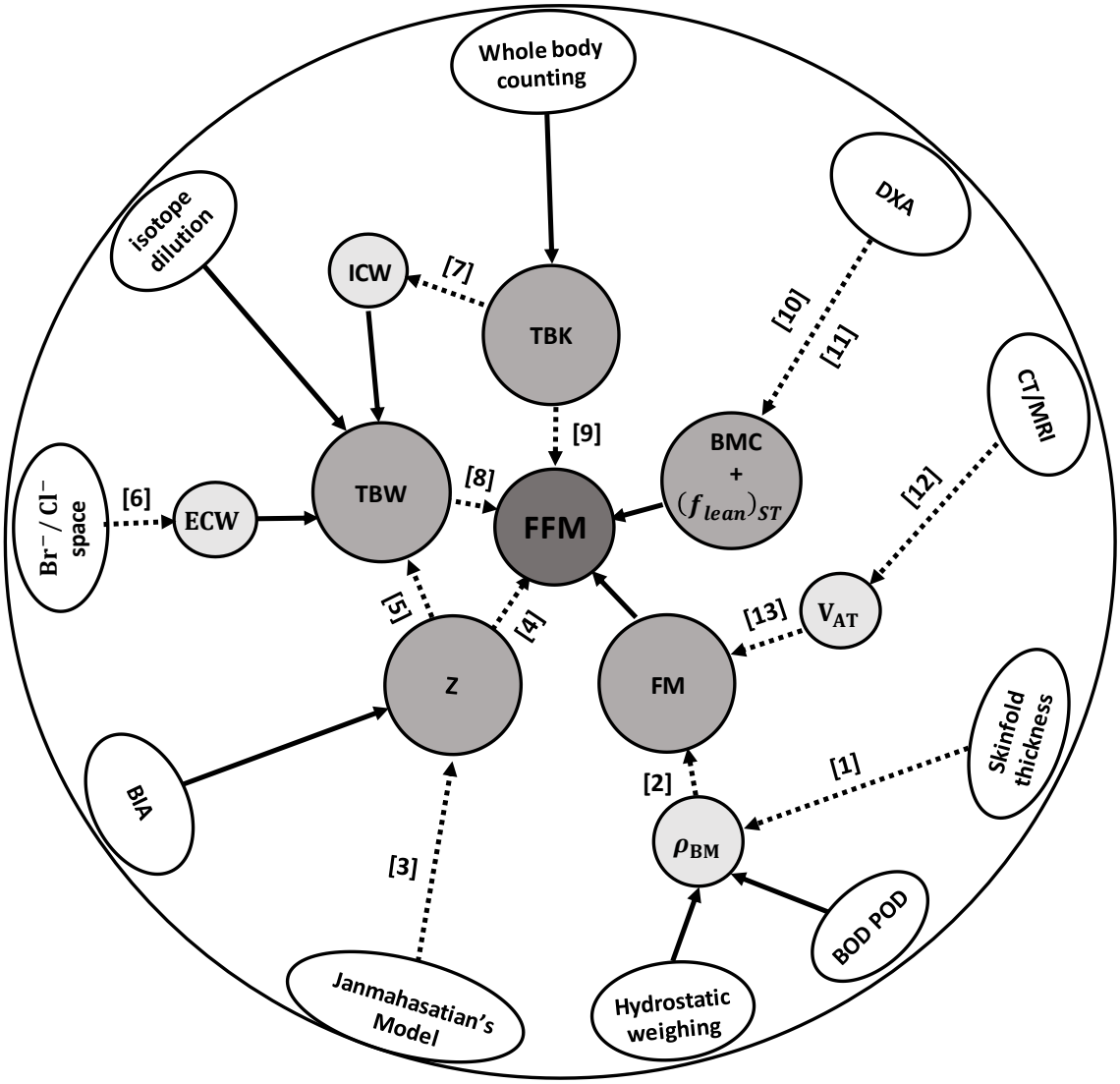

Figure 3.5 Summary of various body composition measurement methods and how they contribute to understanding of FFM.

The circles surrounding FFM (darker shade) in the centre represent the parameters from which FFM can be directly calculated. Smaller circles towards peripheri (lighter shade) represent the parameters required to derive the parameters within the darker circles. A continuous arrow represents a direct calculation, but a dashed arrow represents an indirect derivation based on assumption(s) and/or a predictive equation.Unlike other methods each of which derives a single outcome, DXA derives two parameters, i.e. $f_{lean\,(ST)}$ and BMC, in order to derive FFM. Each of the numbers from [1] to [13] against the dashed arrows represents the specific basis of the calculation related to that indirect step: [1] based on population specific regression equation; [2] based on assumed value of ρ_{FM} and ρ_{FFM}; [3] based on the model developed by Janmahasatian et al. which can predict Z (bioimpedance) using body weight and height; [4, 5] based on population specific regression equation [6] Br^-/Cl^-dilution space is an approximation of ECW; [7] K^+ space is used as an approximation of ICW with an assumed value of $[K^+]_i$; [8] value of $R_{water/FFM}$ needs to be assumed; [9] assumed value of $R_{TBK/FFM}$; [10] $f_{lean\,(ST)}$ estimation is dependent on assumed/measured values of r_{fat} and r_{lean}; [11] approximation of r_{ST} value needs to be made for determining BMC; [12] based on assumption

for interslice volume interpolation of adipose tissue; [13] depends on assumed values of f_{AT} and ρ_{AT}. ECW extracellular water, ICW intracellular water, TBW total body water, TBK total body potassium, Z impedance, $f_{lean\,(ST)}$ average fraction of lean tissue in the whole body's soft tissue mass, BMC bone mineral content, FFM fat-free mass, FM fat mass, V_{AT} total volume of adipose tissue in body, ρ_{BM} total body density, DXA dual-energy X-ray absorptiometry, CT computed tomography, MRI magnetic resonance imaging, BIA bio-impedance analysis, and BOD POD® represents air displacement plethysmography.

<table>
<tr><th>Methods</th><th colspan="6">Interlinks between outcomes with specific Equation</th></tr>
<tr><td>Hydrostatic weighing</td><td>Eq 3.11</td><td rowspan="3">ρ_{BM}</td><td rowspan="3">Eq 3.6 and Eq 3.8</td><td rowspan="5">FM</td><td rowspan="5">Eq 3.9</td><td rowspan="11">FFM</td></tr>
<tr><td>BOD POD®</td><td>Eq 3.13</td></tr>
<tr><td>Skinfold thickness [a]</td><td>Eq 3.14, Eq 3.15</td></tr>
<tr><td>CT/MRI</td><td>Eq 3.35</td><td>V_{AT}</td><td>Eq 3.36</td></tr>
<tr><td rowspan="2">BIA</td><td rowspan="2">NA[b]</td><td rowspan="2">Z</td><td colspan="2">Eq 3.27</td></tr>
<tr><td>Eq 3.26</td><td rowspan="5">TBW</td><td rowspan="5">Eq 3.16</td></tr>
<tr><td>Isotope dilution</td><td>Eq 3.17</td><td colspan="2"></td></tr>
<tr><td>Br^-/ Cl^- space [c]</td><td>Eq 3.19, Eq 3.20</td><td colspan="2">ECW</td><td rowspan="3">Eq 3.18</td></tr>
<tr><td rowspan="2">Whole body counting</td><td rowspan="2">Eq 3.28</td><td rowspan="2">TBK</td><td>Eq 3.21</td><td>ICW</td></tr>
<tr><td colspan="2">Eq 3.29</td></tr>
<tr><td>DXA[d]</td><td>Eq 3.31, Eq 3.32</td><td colspan="3">$f_{lean\ (ST)} + BMC$</td><td>Eq 3.33, Eq 3.34</td></tr>
</table>

[a] Eq 3.14 and Eq 3.15 are for men and women respectively; [b] Not applicable since Z is directly read from BIA instrument; [c] Eq 3.19 *and* Eq 3.20 are for ECW_{Br} and ECW_{Cl} respectively; [d] Eq 3.31 and Eq 3.32 are for $f_{lean\ (ST)}$ and BMC respectively.

Figure 3.6 Interconnections between various methods through specific equations.

Shaded outcomes represent the outcomes required to calculate FFM as described in Figure 3.5. The non-shaded boxes represent the equations that link the methods or outcomes. The equation numbers represent those from the text. ECW extracellular water, ICW intracellular water, TBW total body water, TBK total body potassium, Z impedance, $f_{lean\ (ST)}$ average fraction of lean tissue in the whole body's soft tissue mass, BMC bone mineral content, FFM fat-free mass, FM fat mass, V_{AT} total volume of adipose tissue in body, ρ_{BM} total body density, DXA dual-energy X-ray absorptiometry, CT computed tomography, MRI magnetic resonance imaging, BIA bio-impedance analysis

3.4. Prediction Models for FFM

Another way of determining FFM is by the use of predictive models which have been extensively published in the literature [101, 102, 178-185]. These models utilise measurable patient characteristics (e.g. WT, Ht, age, sex) to predict FFM and thus preferred for determining individual FFM in pharmacokinetic analyses and in clinical practice. However, the mathematical relationship between FFM and such patient characteristics were mostly empirically derived based on regression analysis of measured FFM (e.g. using DXA or BIA) in relation to patient characteristics such as WT, Ht, and age. Empirical models are mostly data-driven which hinders their use in new populations. For instance, the model by James et al. [101] results in under prediction of FFM once a certain value of WT is exceeded, which can lead to under-dosing in obese patients [25, 103]. This is because the range of WT that was used during model development was narrow, mostly excluding obese and there was no biological mechanism supporting the mathematical relationship used in the model. Later, Janmahasatian et al. [102] developed a model in adults with a wide range of age (18-82 years), body weight (40.7-216.5 kg), BMI (17.1-69.9 kg.m^2) and assumed a more mechanistic relationship between FFM and other size variables. Janmahasatian's model has been used commonly for FFM calculation in pharmacokinetic analyses. More recently, Al-Sallami et al. [185] extended Janmahasatian's adult FFM model to include children of 3 years and above by introducing a maturation model. This model might help in predicting the body composition driven change in clearance in children. A list of various published FFM models is in Table A2.6 of Appendix 2: .

3.5. *Limitations of assumptions and operations and their clinical implications*

It is important to use a particular FFM measuring method in situation(s) where its assumption(s) and operational requirement(s) are largely met. In this section, a discussion of the methods in terms of assumptions and operational challenges is provided. This is intended to provide a guide for the choice of method when measuring FFM experimentally and subsequent application to pharmacokinetic studies.

Of note, none of the existing methods measures FFM directly. Instead, FFM is derived indirectly from an experimental measurement (e.g. ρ_{BM}) by factoring in certain parameters. Although the typical values used for these parameters (e.g. ρ_{FFM}=1.10 g/mL) are the key assumptions for FFM derivation they may not be constant across the populations. Their values can deviate from the standard values as a result of (patho)physiological changes (e.g. structural maturation or abnormal hydration) caused by age [154, 186, 187], pregnancy, disease [159, 188, 189] and even by therapeutic intervention [190, 191]. A detailed discussion about deviations in the assumed constants can be found in section A2.4 of Appendix 2: . Therefore, caution must be used while selecting a particular method in a particular population, where alteration in the required parameter values are suspected. Parameter values can also differ within a population. This natural variability can potentially cause measurement errors in certain methods, e.g. at least 4% error in FM estimation by densitometry[98]. On the other hand, variation in the level of body hydration within the natural range is not expected to cause significant variation in DXA-derived FFM measurement [173].

Further to the biological variation between and within populations, the use of these methods may be impacted by operational challenges. These include practical and safety aspects of use and are discussed in detail in section A2.5 and Table A2.7 of Appendix 2: . In this context, anthropometry, BOD POD, BIA, and DXA appear reasonably acceptable for most situations due to

their relative safety and ease of use. However, anthropometry and BOD POD® may not be the method of choice where a biological variation in ρ_{FFM} is expected e.g. children. Similarly, BIA is not recommended if abnormal hydration is suspected, e.g. younger children, pregnant women, and critically ill patients. Use of DXA is more acceptable in this regard since it is least susceptible to biological variation in hydration. Therefore, DXA has been indicated as the standard method for assessing body composition in most patient groups [173].

Alternatively, FFM prediction models are available and are used in certain situations in clinical practice. Models in current use include the adult FFM model developed by Janmahasatian et al. [102] which was based on FFM measurements using BIA and DXA. The paediatric FFM model developed by Al-Sallami et al. [185] was based on FFM measuremenst using DXA. Of note, neither of these models extends to patients at the extremes of age (under 3 years or over 82 years).

3.6. Relevance of FFM in clinical pharmacology

Most size-based dosing recommendations stipulate total body weight (WT) as a scaler on a 'dose per kilogram' basis. This is because WT is relatively easy to measure and often correlates well with drug clearance especially in subjects with normal weight. Clearance (CL) depends on the intrinsic elimination capacity of the various eliminating organ(s) and their perfusion which often correlates well with WT in normal weighted individuals. However, excess fat mass does not contribute to drug elimination hence scaling drug clearance based on WT in the obese can potentially result in over-prediction of the maintenance dose. Obese subjects are often excluded from the various stages of drug development [24], despite the increasing prevalence of obesity worldwide [70, 192]. This has necessitated the development of alternative descriptors of size including FFM which is expected to correlate better with drug CL [24, 25, 91, 126, 136-138]. Of note, at least empirically, FFM has shown non-

linear correlation with CL according to a recent review by McLeay et al. [60] in which various body size descriptors were analysed as covariates on CL. Findings of this study (Figure 3.7) suggest that FFM raised to the power of $2/3$ best described the overall increase in CL with body size compared to other established size metrics. Although LBW and FFM continue to be used interchangeably in the literature LBW can not be measured experimentally and is approximated by FFM. Bedside determination of FFM in the clinic is possible through the use of either BIA or FFM prediction models.

Along with CL, volume of distribution (V) also plays a key role in determining loading dose and scaling of V is also important for dose optimisation in obese patients. Conventionally, V is scaled linearly with WT irrespective of body size. However, the absolute V (in Litres) of low to moderately lipophilic drugs (e.g. non-depolarising neuromuscular blockers) are less likely to be affected by obesity and hence suggested for FFM based scaling [138]. Clinically, FFM -based dosing has been demonstrated for daptomycin [193], propofol [106], remifentanil [103] and dexmedetomidine [107] in morbidly obese patients. Therefore, FFM based dosing is increasingly being adopted in clinical pharmacology and accurate prediction of individual FFM is of utmost importance.

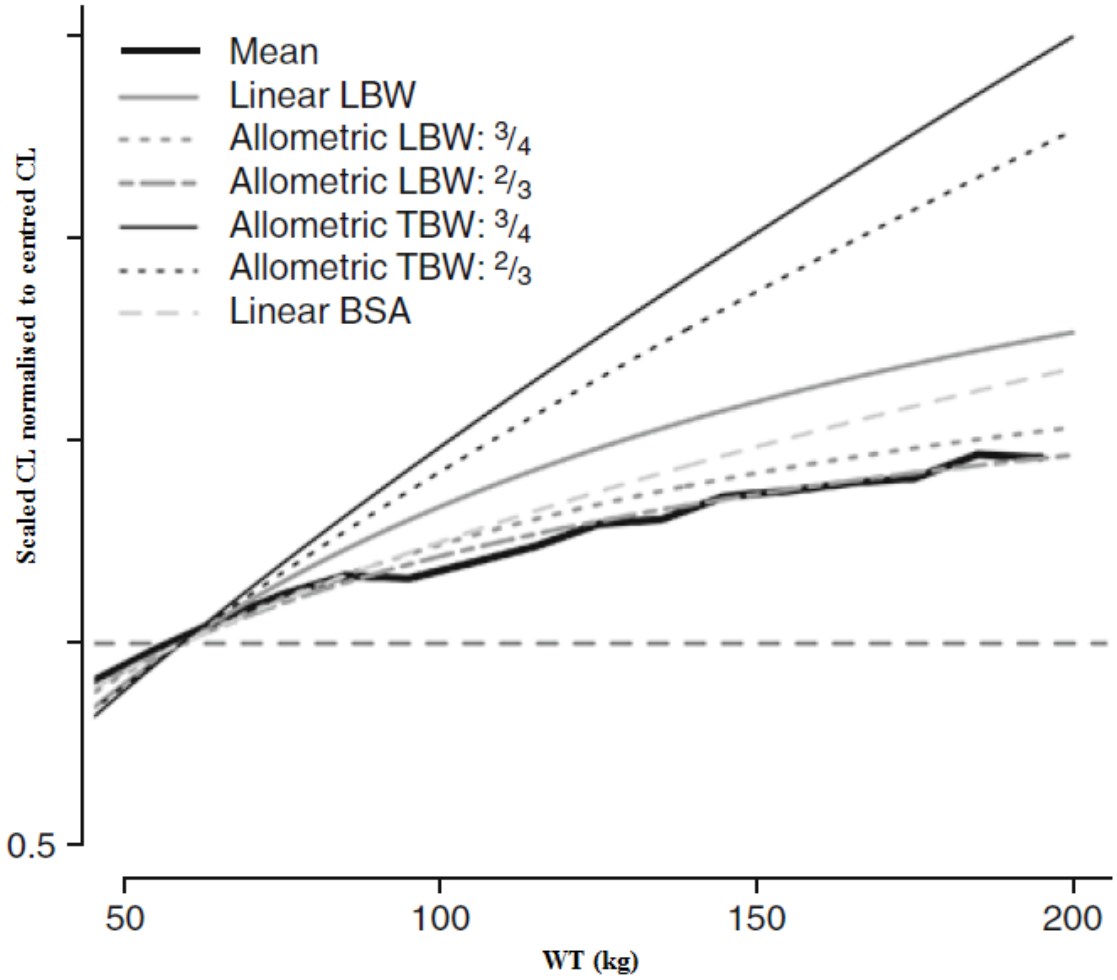

Figure 3.7 Meta-analysis result of relationship between various size metrics with *CL*

Mean scaled CL values (normalised to the centred CL) across the WT range from 121 studies (which reported various size metrics as covariate of CL in adults) are plotted on the y-axis (thick dark line). Various other size metrics scaled across the WT range are also overlaid. LBW refers to FFM and TBW refers to WT in the context of this thesis. (Centring: TBW= 59 kg, LBW = 50.45 kg, BSA = 1.72m^2). WT total body weight (TBW represents WT in this figure), LBW lean body weight, BSA body surface area. Modified with permission from original work published by McLeay et al. [60]

3.7. Discussion and Conclusion

Body size is one of the most important covariates to describe drug pharmacokinetics. WT is an appropriate size descriptor if body composition remains constant over all sizes. However, body composition is not constant over the WT range thus WT-based dosing regimens are not appropriate for obese patients. FFM has been gaining popularity in clinical pharmacology as it describes body size without the excess fat mass which is not thought to contribute to drug metabolism and excretion. However, unlike WT, FFM is not a directly measurable characteristic, hence accurate FFM measurement is required. There are numerous methods for measuring FFM which are highly variable in terms of their working principles and assumptions. These are thoroughly discussed in this review with special emphasis on their interrelationship on a physiological framework and will help rationalising their use. These methods can then be used to develop predictive mathematical models that can predict FFM from readily measurable patient variables.

Although predictive models for FFM are used in population PK analyses and size-based dose recommendations, these models can not be extrapolated to special populations such as infants or patients suffering from cachexia. Extrapolating FFM to these populations using the available models may result in prediction bias. In such situations, where the available models do not appear suitable, new models need to be developed. Future model development processes need to measure FFM experimentally and hence the choice of method should be determined based on proper scientific justification. The technical details described in this review will help researchers in selecting fit-for-purpose methods to determine FFM in order to develop predictive models for relevant patient populations.

Chapter 4: An extended framework of Janmahasatian's fat-free mass model for universal application across populations of different ethnicities

4.1. Introduction

As discussed in Chapter 3, measurement of FFM involves methodologies which are often too cumbersome to be implemented in regular practice. The use of FFM is therefore based on the availability of predictive equations. Among the available FFM models, the model developed by Janmahasatian et al. [102] has been widely recommended and used extensively. The semi-mechanistic model (for adults) is shown in Eq 1.35 and Eq 1.36 in Chapter 1: . Janmahasatian's model has recently been extended to predict FFM in children to 3 years of age [185].

Janmahasatian's model was built from healthy volunteers whose ancestry predominantly originated from Europe. A key assumption in this model is a linear relationship between bioimpedance (Z) and body mass index (BMI) which was supported in their study population. It is unknown whether this relationship will hold true for all ethnic groups. Rush et al. [104] have reported that the percent fat mass and BMI have a curvilinear (not linear) relationship, and moreover the relationship varies between populations of different ethnic origins. This implies that percent fat mass values are different in different ethnic populations once normalised to BMI. In particular it was shown in their work that people from India had on average 7.6% (95% CI: 5% – 10.2%) higher fat mass component than Europeans for a given BMI value and in contrast that people from the South Pacific (e.g. Samoa) had about 3.8% (95% CI: 1.4% – 6.1%) lower fat mass component than Europeans. This implies that Asian Indians have lower FFM compared to European adults at an equivalent BMI. We anticipate therefore that people of other ethnicities (e.g. India) may challenge the linear assumption seen in the original (Janmahasatian) FFM model. Therefore, FFM_{Jan} which follows the European body composition pattern is expected to over-estimate FFM in Indians. A recent study by Srigiripura et al. [105] evaluated the Janmahasatian model which resulted in bias in FFM predictions for Indian people (Figure 4.1). Their work reported over-estimation of FFM in the Indian population by Janmahasatian model when compared to the BIA measured values (FFM_{BIA}). However, the authors did not mention which regression equation was used to extrapolate FFM from the BIA measured Z data, and the equation's validity

in the study population. The mean error [95% CI] of the prediction ($FFM_{BIA} - FFM_{Jan}$) was -3.76 [(-7.96) – (0.44)] kg. This could be due to the non-universality of the body composition vs. BMI relationship which was not considered in the FFM_{Jan} model. Therefore, the use of Janmahasatian's model in other populations requires prior qualification.

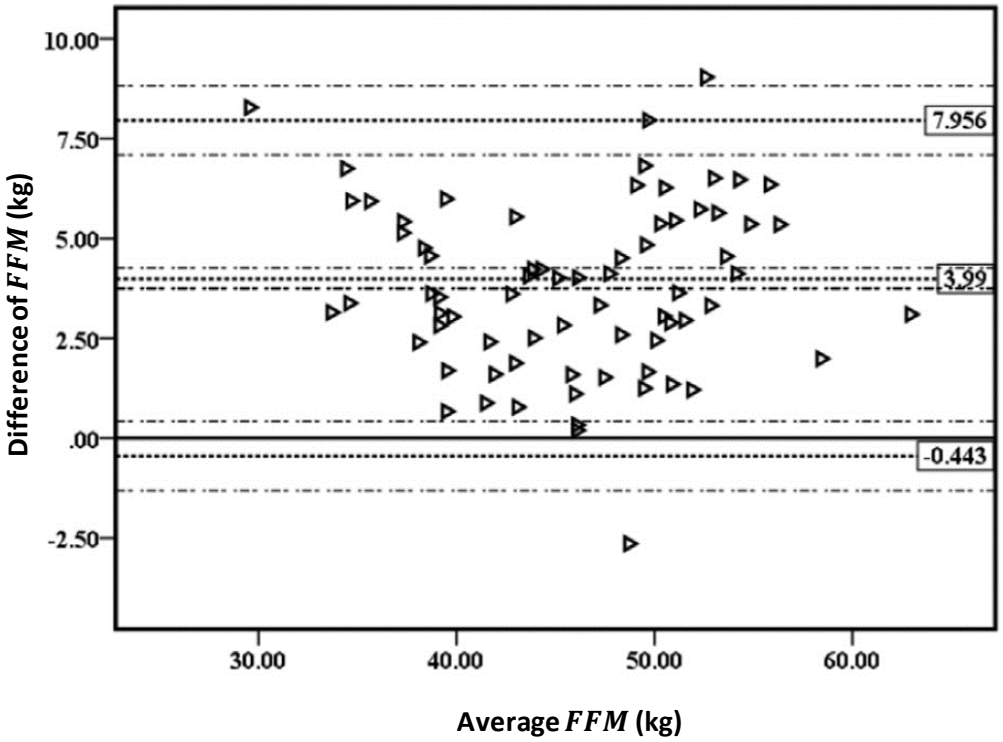

Figure 4.1 Bias in FFM prediction by Janmahasatian's model in Indian population

The difference in FFM prediction by Janmahasatian's model compared to the BIA measured FFM values are plotted in y-axis and the average of corresponding model predicted and measured FFM values are plotted in x-axis. The figure has been reproduced from the report of Srigiripura et al. [105].

In the current work we describe an extension of the Janmahasatian equation that relaxes the linearity assumption in the use of bioimpedance to provide an equation that is universal across populations. The revised model was termed an extended FFM model (FFM_{Ext}).

Objective-1: To derive an extended version of FFM model structure (FFM_{Ext}) that would incorporate estimable ethnicity specific parameter(s).

Objective-2: To estimate the ethnic specific parameters from the extended FFM equation to describe an Indian population.

4.2. Methods

4.2.1. Objective-1: Extension of the FFM equation to include ethnic specific parameters

For this objective, one of the biological assumptions that underpinned Janmahasatian's model development was revisited. From here, the original assumption of linearity was relaxed to accommodate ethnic differences and provide specific parameters that can be estimated in future studies. This objective yields the extended FFM equation (FFM_{Ext}).

4.2.1.1. Bioimpedance and Janmahasatian's assumption

The body is comprised of both conducting (e.g. charged ions) and non-conducting materials (e.g. fat). When an AC current flows through the body, it experiences two types of opposition to its flow, i.e. resistance (R) produced by the conducting materials and reactance (X_c) produced the non-conducting materials. Bioimpedance (Z) refers to the overall inhibition against the AC current flow which depends on both R and X_c (Eq 4.1). Reactance (X_c) is inversely proportional to the capacitance (of the non-conducting material) and also, to the frequency of the AC current. At high frequency range as in BIA (typically, 50 kHz), X_c becomes negligible, thus Z becomes approximately equal to R. Therefore BIA in this setting reflects the resistance (R) of the body. The magnitude of the electrical resistance produced by different bio-materials is different and hence the total resistance to a flow of current provides an indication of the composition for a given size. Therefore, Z (essentially a measure of resistance) is an indirect measure of body composition. The assumption that the fat type or content, for a given composition based on BMI, is similar across ethnic groups is predicated in the use of Janmahasatian's model.

$$Z = \sqrt{R^2 + {X_c}^2}$$

Eq 4.1 Relationship between bioimpedance, resistance and reactance (same as Eq 3.23)

For a cylindrical conductor R is a function of specific resistivity (φ), length (L) and cross-sectional area (A) as in Eq 4.2. Every conductor has a distinct φ value.

$$R\ (\approx Z) = \frac{\varphi \times L}{A}$$

Eq 4.2 Electrical resistance of a cylindrical conductor

When Janmahasatian et al. applied this principle to the human body, it was assumed that the body was approximated by a series of cylinders with total L is equivalent to height (Ht). Eq 4.4 was derived from Eq 4.2. (where, V is body volume, WT is total body weight and ρ_{BM} is body density). The intermediary step (Eq 4.3) is shown here.

$$Z \approx R = \frac{\varphi \times L}{A} = \frac{\varphi \times L^2}{V} = \frac{\varphi \times L^2}{WT/\rho_{BM}} = \frac{\varphi \times \rho_{BM}}{WT/L^2} = \frac{\varphi \times \rho_{BM}}{WT/Ht^2}$$

Eq 4.3 Rearrangement of equation of resistance with respect to human body

$$\therefore Z = \frac{\varphi \times \rho_{BM}}{BMI}$$

Eq 4.4 Relationship between bioimpedance and BMI

As per Eq 4.4, if (and only if) φ and ρ_{BM} (or their product) are constant across the human body size range (i.e. BMI range), then Eq 4.5 holds. This was a fundamental assumption in Janmahasatian's model and one that proved reasonable in the population that they studied.

$$Z_{Jan} \propto BMI^{-1}$$

Eq 4.5 The key assumption of Janmahasatian's model: proportional relationship between bioimpedance and BMI

From Eq 4.5, Janmahasatian et al. derived the structure of the Z_{Jan}'s model as Eq 4.6, where θ_1 and θ_2 are the intercept and proportionality constant. In this expression both θ_1 and θ_2 are functions of φ and/or ρ_{BM}.

$$Z_{Jan} = \theta_1 + \theta_2 \times BMI^{-1}$$

Eq 4.6 Janmahasatian's linear model structure for bioimpedance

By regressing observed Z values against BMI, estimates of θ_1 (male: 216, female: 244) and θ_2 (male: 6680, female: 8780) were obtained. In the next step, observed FFM was estimated as proportional to Ht^2/Z_{Jan} with the estimated proportionality constant θ_3 (Eq 4.7). Then, Z_{Jan} from Eq 4.6 was substituted into the Eq 4.7, which depicts a previously accepted relationship, to develop the final FFM_{Jan} model (Eq 4.10). Note Eq 4.10 can be expressed as Eq 1.35 and Eq 1.36 of Chapter 1: .

$$FFM_{Jan} = \theta_3 \times \frac{Ht^2}{Z_{Jan}}$$

Eq 4.7 Janmahasatian's model structure for fat-free mass with respect to bioimpedance

$$FFM_{Jan} = \frac{\theta_3 \times Ht^2}{\theta_1 + \theta_2 \times BMI^{-1}}$$

Eq 4.8 Janmahasatian's model structure for fat-free mass with respect to BMI and height

$$FFM_{Jan} = \frac{\theta_3 \times Ht^2 \times BMI}{\theta_1 \times BMI + \theta_2}$$

Eq 4.9 Janmahasatian's model structure for fat-free mass with respect to BMI and height (rearranged)

$$FFM_{Jan} = \frac{\theta_3 \times WT}{\theta_2 + \theta_1 \times BMI}$$

Eq 4.10 Janmahasatian's model structure for fat-free mass with respect to BMI and WT

4.2.1.2. Extended assumption

The composition of the human body (i.e. proportions of various conducting materials.) changes as body size changes. This also results in changes to fat content (composition or amount), which across ethnic groups does not support a universal constant φ and ρ_{BM} (i.e. body density) for a given value of BMI in humans. This implies, that the electrical impedance theory needs accommodate the potential (special) case of 'biodiversity'-impedance. This can be accommodated by relaxing the assumption of proportionality between Z and BMI^{-1} (of Eq 4.6) as shown in Eq 4.11. This would also enable the extended FFM model (FFM_{Ext}) to account for ethnicity specific differences in the non-linearity (should they exist) by estimating the set of additional composition factors $\Psi\ \{\psi_1;\ \psi_2;\ \psi_3\}$.

$$Z_{Ext} = \psi_1 \times \theta_1 + \psi_2 \times \theta_2 \times BMI^{(-\psi_3)}$$

Eq 4.11 Extended non-linear model structure for bioimpedance

In this work, of development of the FFM_{Ext} model, it was also assumed that the FFM to Z relationship was universal (Eq 4.12), as used by Janmahasatian et al. (Eq 4.7).

4.2.1.3. Derivation of FFM_{Ext} model

$$\because FFM_{Ext} = \theta_3 \times \frac{Ht^2}{Z_{Ext}}$$

Eq 4.12 Extended model structure for fat-free mass

By replacing Z_{Ext} (as per Eq 4.11) in Eq 4.12,

$$FFM_{Ext} = \frac{\theta_3 \times Ht^2}{\psi_1 \times \theta_1 + \psi_2 \times \theta_2 \times BMI^{(-\psi_3)}}$$

Eq 4.13 Extended rearranged model structure for fat-free mass

by multiplying with BMI,

$$FFM_{Ext} = \frac{\theta_3 \times Ht^2 \times BMI}{[\psi_1 \times \theta_1 + \psi_2 \times \theta_2 \times BMI^{(-\psi_3)}] \times BMI}$$

Eq 4.14 Extended rearranged model structure for fat-free mass (continued)

$$\therefore FFM_{Ext} = \frac{\theta_3 \times WT}{\psi_1 \times \theta_1 \times BMI + \psi_2 \times \theta_2 \times BMI^{(1-\psi_3)}}$$

Eq 4.15 Extended rearranged model structure for fat-free mass with respect to BMI and WT

The extended FFM model was derived as Eq 4.16.

$$\boldsymbol{FFM_{Ext} = \frac{\theta_3 \times WT}{[\psi_1 \times \theta_1 \times BMI^{\psi_3} + \psi_2 \times \theta_2] \times BMI^{(1-\psi_3)}}}$$

Eq 4.16 Final extended rearranged model structure for fat-free mass

If $\Psi\{\psi_1, \psi_2, \psi_3\} = 1$ (i.e. no change in composition) then FFM_{Ext} model (Eq 4.16) simplifies to FFM_{Jan} model (Eq 4.10). Otherwise, for other populations, ethnicity specific estimated values of $\psi_1, \psi_2 \; and \; \psi_3$ can be estimated.

4.2.2. Objective-2: Application of the extended FFM model in Indians

Here, the ethnicity specific composition parameters, the vector Ψ were incorporated in the FFM_{Ext} model structure and were estimated for an Indian population, providing an extended FFM model for Indians $FFM_{Ext(Ind)}$.

For objective-2, a reference model to describe the FFM in the Indian population was identified. Simulations from this model were used to calibrate the Ψ parameters from the FFM_{Ext} model using nonlinear regression for their estimation.

4.2.2.1. The reference FFM model for the Indian population

Derivation of an extension to the FFM_{Jan} model was developed based on a reference equation that has been shown to provide acceptably accurate estimates of FFM in the Indian population. The reference equation was based on the model developed by Kulkarni et al. [194]. Kulkarni's model (FFM_{Kul}) was developed and validated in a large cohort (N=2200, 36% female) of healthy Indian adults (age: 18 - 79 years) covering a wide range of BMI (14 - 44 kg/m^2).

Briefly, in their study [194], the participants were randomly assigned to the prediction and the validation group which comprised of 60% and 40% of the sample size respectively. The data of the prediction group was used for model development, which was done by simple linear regression analysis of dual energy X-ray absorptiometry (DXA) measured FFM data (single measurements) against simple anthropometric variables WT, Ht and age. The model equations are shown in Eq 4.17 and Eq 4.18 for males and females respectively. The mean error of prediction (standard deviation) of these models, when applied to their validation dataset were 0.28 (1.96) kg and 0.02 (1.64) kg for males and females respectively.

Later, the Kulkarni model for males (Eq 4.17) was externally validated in the study by Srigiripura et al. [105], where they assessed the predictive performances of the model in 72 Indian male patients (age: 40 - 74 years, BMI: 13.67 – 33.12 kg/m^2) against the BIA measured FFM data. They found that the mean error (standard deviation) of prediction by the Kulkarni model was 0.33 (2.35) kg in the dataset, which was similar to Kulkarni's validation result (0.28 kg) as mentioned above. Based on these findings, the Kulkarni's model (FFM_{Kul}) was used as the reference model on the assumption that FFM_{Kul} reasonably approximates the true FFM in Indian adults (among the available models).

$$FFM_{Kul\,(male)} = -15.605 - (0.032 \times Age) + (0.192 \times Ht) + (0.502 \times WT)$$

Eq 4.17 Kulkarni's fat-free mass model for Indian males

$$FFM_{Kul\,(female)} = -13.034 - (0.018 \times Age) + (0.165 \times Ht) + (0.409 \times WT)$$

Eq 4.18 Kulkarni's fat-free mass model for Indian females

4.2.2.2. Simulation of FFM data from the reference model

The reference equations (Eq 4.17 & Eq 4.18) were used to simulate FFM measurements (without error) to provide a calibration for the composition parameters of the FFM_{Ext} model. The simulation data was based on a database of N=100 patient volunteers (demographics are summarised in Table 4.1) that arose from a retrospective study described briefly here and reported elsewhere [195]. The primary objective of this study was to measure liver fat by computerised tomography (CT). Patient characteristics including sex, Ht, WT, age were collected for one hundred adult Indian patients consisting of 30 females and 70 males aged 18-60 years. The study was conducted at the PSG Hospital, Coimbatore, India. All subjects had normal liver or kidney function tests, and were not undergoing any treatment for a medical condition related to the liver or kidney, not pregnant, and not breastfeeding.

In this study a single FFM value was simulated per subject and each subject was included in the simulated data once only. The data that were generated from this simulation were denoted FFM_{Kul}.

Table 4.1 Summary of patient characteristics that was used for simulation of FFM data.

Characteristics	Female (N=30) Median (range)	Male (N=70) Median (range)
Age (year)	37 (23 - 59)	39 (18 - 66)
Height (cm)	155 (143 - 170)	166 (148 - 197)
Weight (kg)	70.4 (46 - 118)	79.3 (45 - 128)
BMI (kg/m^2)	29.6 (18 - 43.9)	28.5 (16.9 - 51.8)
FFM_{Kul} (kg)	40.0 (29.6 - 61.6)	56.1 (34.7 - 81.2)
FFM_{Jan} (kg)	40.8 (30.8 – 56.1)	57.1 (38.0 – 75.5)

FFM fat-free mass, BMI body mass index, FFM_{Kul} fat-free mass calculated by Kulkarni's model [194], FFM_{Jan} fat-free mass calculated by Janmahasatian's model [102], These patients characteristics were part of a retrospective study that was reported elsewhere [195]

4.2.2.3. Model development

The FFM_{Kul} data were modelled within a nonlinear regression framework. The first-order approximation method (FO) in NONMEM was used (version 7.3). As indicated in section 4.2.2.2, there were no repeated measures in this data set. Model selection was based on Akaike Information Criteria (AIC) [55], where a lower AIC value was indicative of a better description of the data. Model evaluation as done by goodness-of-fit (GoF) plots of observed vs. predicted values of FFM.

The model for $FFM_{Ext(Ind)}$ estimation is shown in Eq 4.19 (adapted from Eq 4.16). The subscript 'i' denotes the i^{th} individual's value. The sex specific values of $\theta_1, \theta_2, \theta_3$ were fixed as per Janmahasatian's model (see Eq 4.10 and the values in Eq 1.35 and Eq 1.36). The three composition (aka ethnicity) parameters ψ_1, ψ_2, ψ_3 were estimated for Indians, along with the variance parameter of the residual error model. Sex was tested as covariate for Ψ parameters, which is similar to the original Janmahasatian model. Finally an additive error model was considered where the standard deviation was defined by σ.

$$FFM_{Ext(Ind)_i} = \frac{\theta_3 \times WT_i}{\left[\psi_2.\theta_2 + \psi_1.\theta_1.BMI_i^{\psi_3}\right] \times BMI_i^{(1-\psi_3)}}$$

Eq 4.19 Structure of fat-free mass model in Indians

4.3. *Results*

The FFM_{Jan} was demonstrated to deviate from the FFM_{Kul} as shown in Figure 4.2. Overall, FFM_{Jan} estimates were higher than the FFM_{Kul} estimates, particularly in males as shown in Table 4.2.

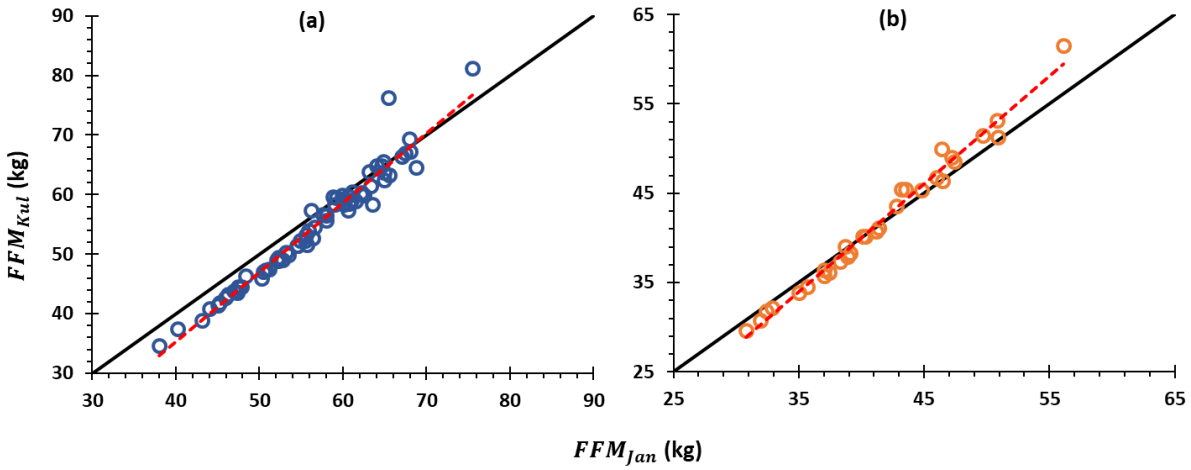

Figure 4.2 Deviation in *FFM* prediction in Indian males (a) and females (b) by Janmahasatian's model and Kulkarni's model.

The solid line and the dotted line represent the line of unity and the linear regression line respectively.

Table 4.2 Bias (ME) and precision (RMSE) of Janmahasatian's *FFM* model in Indian patients

Sex	ME [95% CI] in kg	RMSE in kg
Male	-1.9 [(-2.6) – (-1.2)]	3.0
Female	0.3 [(-0.2) – 0.9]	1.6

ME mean error, RMSE root mean squared error

A summary of model selection is shown in Table 4.3. When, sex was considered as a covariate on ψ_1 (Model-2), it caused massive drop (about 141 unit) in the AIC value compared to the base model (Model-1). Further, considering sex as a covariate on ψ_2 (Model-3) significantly improved the model fit. However, considering sex on ψ_3 (Model-4) did not further improve the model fit (as AIC was increased), thus keeping Model-3 as the current best choice. Since, the estimates of ψ_1 in Model-3 were negligible, these were fixed to 0 (Model-5), which further lowered the AIC value by about 7 unit and produced similar estimates as compared to Model-3. Therefore, Model-5 was considered as the final model. Summary of the parameter estimates of the final model is shown in Table 4.4. GoF plots of the final model are shown in Figure 4.3.

Table 4.3 Summary of extended FFM model selection for Indians.

Model No.	Covariate on Ψ	AIC	ΔAIC	ψ_1		ψ_2		ψ_3		σ (kg)
1	-	154.06	-	0.87		2.34		1.21		1.26
2	Sex on ψ_1	12.97	-141.09	0.20	0.02	0.86		0.78		0.62
3	Sex on ψ_1 and ψ_2	-37.96	-50.93	0.02	0.02	0.78	0.71	0.72		0.47
4	Sex on ψ_1, ψ_2 and ψ_3	-37.77	0.19	0.01 (Male)	0.01 (Female)	0.780 (Male)	0.69 (Female)	0.72 (Male)	0.72 (Female)	0.47
5	**Sex on ψ_2**	**-44.94**	**-6.98** [a]	**0 (FIXED)**		**0.77 (Male)**	**0.70 (Female)**	**0.72**		**0.47**

$FFM_{Ext(Ind)}$ extended fat-free mass in Indians; θ_1, θ_1 and θ_3 are Janmahasatian's model parameters (fixed), WT total body weight; BMI body mass index; Ψ $\{\psi_1, \psi_2, \psi_3\}$ ethnicity specific body composition parameters; AIC Alaike Information Criteria; σ standard deviation of additive error; [a] (Model 5 – Model 3); ΔAIC represents the difference between the two consecutive models unless otherwise stated; the drop and gain in AIC values (compared to the previous model) is represented by negative and positive signs respectively

Table 4.4 Parameter estimates (%RSE) of the final $FFM_{Ext(Ind)}$ model

Sex	ψ_1	ψ_2	ψ_3	σ (kg)
Male	0 (fixed)	0.77 (3.2)	0.72 (1.3)	0.47 (12.4)
female		0.70 (3.3)		

The (final) extended models for FFM prediction in Indians can be written as Eq 4.20 and Eq 4.21 respectively. Here we preserve the previous Janmahasatian parameter values in order to allow comparisons.

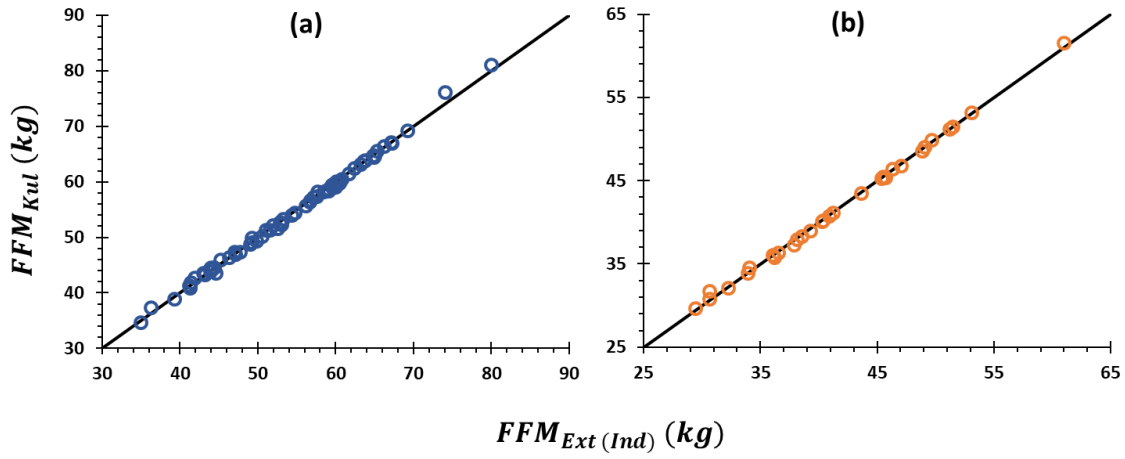

Figure 4.3 GoF plots of model fit of the final $FFM_{Ext(Ind)}$model in Indian males (a) and females (b).

The solid line represents the line of unity.

$$FFM_{Ext(Ind)} = \frac{9270 \times WT}{0.77 \times 6680 \times BMI^{0.28}}$$

Eq 4.20 Final extended fat-free mass model for Indian males

$$FFM_{Ext(Ind)} = \frac{9270 \times WT}{0.70 \times 8780 \times BMI^{0.28}}$$

Eq 4.21 Final extended fat-free mass model for Indian females

4.4. Discussion

In this work, we have revisited the basic assumption of Janmahasatian's FFM model structure, and extended it to accommodate ethnicity specific correction factors (i.e. parameters), which are estimable when FFM data is available for a new population. We further showed an application of the extended FFM model structure (FFM_{Ext}) by developing the extended FFM model for the Indian population ($FFM_{Ext(Ind)}$).

Janmahasatian et al. assumed a linear (i.e. proportional) relationship between bioimpedance (Z) and BMI (Eq 4.6), on which their FFM model (FFM_{Jan}) was subsequently built. In this work, this assumption was relaxed to accommodate a potential non-linear relationship (Eq 4.11), since the constancy of specific resistivity (φ) and body density (ρ_{BM}) over the body size range for all ethnic groups is unlikely. Changes in φ and/or ρ_{BM} with changes in BMI are likely to be due to altered proportions of various bio-materials (e.g. fat, proteins, minerals), i.e. change in body composition for a given reference size. This extended assumption of non-linear relationship is further supported by the observation made by Rush et al. [104, 196, 197] and Deurenberg et al. [198] in their multiple studies. These authors quantified human adult body composition of different ethnicities by standard body composition analysis methods such as BIA and DXA, and consistently found that it follows a curvilinear relationship with BMI. Most importantly, the key conclusion of their studies was that the body composition vs. BMI relationships differed widely across a range of different ethnic populations, i.e. European (Caucasian), Asian Indian, Māori and Pacific Islander (or Polynesian). In general, at a fixed BMI, the degree of adiposity was found to be the highest in Asian Indians, and the lowest in Pacific Islanders, while the Europeans fell in the middle of the rank order. This was partly explained by the difference in muscularity and fat distribution among the populations. For example, it is reported that Asian Indians have more abdominal fat deposition than their European and Pacific Island counterparts.

Based on apparent interethnic differences in body composition, given a reference size it is highly unlikely that the estimated relationship of Z with BMI in European population (Eq 4.6) as adopted in FFM_{Jan} model, would remain universal. The extended FFM model structure (FFM_{Ext}), in this regard will provide a useful extension to the scope of Janmahasatian's model. This is because the FFM_{Ext} model not only aligns with the mechanistic features of Janmahasatia's model but also incorporates the potential non-linear body composition patterns respectively by incorporating estimable parameters $\Psi\{\psi_1, \psi_2, \psi_3\}$.

This work was based on the use of a reference model, Kulkarni's model (FFM_{Kul}) [194], to calibrate the current FFM_{Ext} model. The reference model has been previously evaluated, both internally and externally [105] and shown to perform well in Indians. However, the FFM_{Kul} model was developed empirically by simple linear regression without accounting for any underlying mechanism, and hence may not be advisable for extrapolation to a broader population range. Therefore, the extension of Janmahasatian's model, incorporates both the predictive performance of the FFM_{Kul} model and due to its mechanistic nature the ability to extrapolate to other populations.

The final $FFM_{Ext(Ind)}$ model estimates (Table 4.4) indicate a non-linear body composition vs. BMI relationship in Indians (i.e. $\psi_3 = 0.72$) that is different than the (assumed) linear one in Europeans (i.e. $\psi_3 = 1$), whereas the extent of non-linearity between males and females are similar. The final model significantly improved the individual predictions ($FFM_{Ext,Ind}$) close to the reference model (Figure 4.3) when compared with FFM_{Jan} predictions (Figure 4.2). Further, 3D plots (Figure 4.4) of the final $FFM_{Ext(Ind)}$ model (Eq 4.20, Eq 4.21) and the FFM_{Jan} model (Eq 1.35, Eq 1.36 of Chapter 1:) were generated to understand how they are likely to deviate from each other over a range of values of WT and Ht that extend outside the current study population (Table 4.1). Overall there was a trend of larger FFM_{Jan} estimates than $FFM_{Ext(Ind)}$

(more in males than females) in low to moderate BMI zone, whereas the trend flipped over at higher BMI zone.

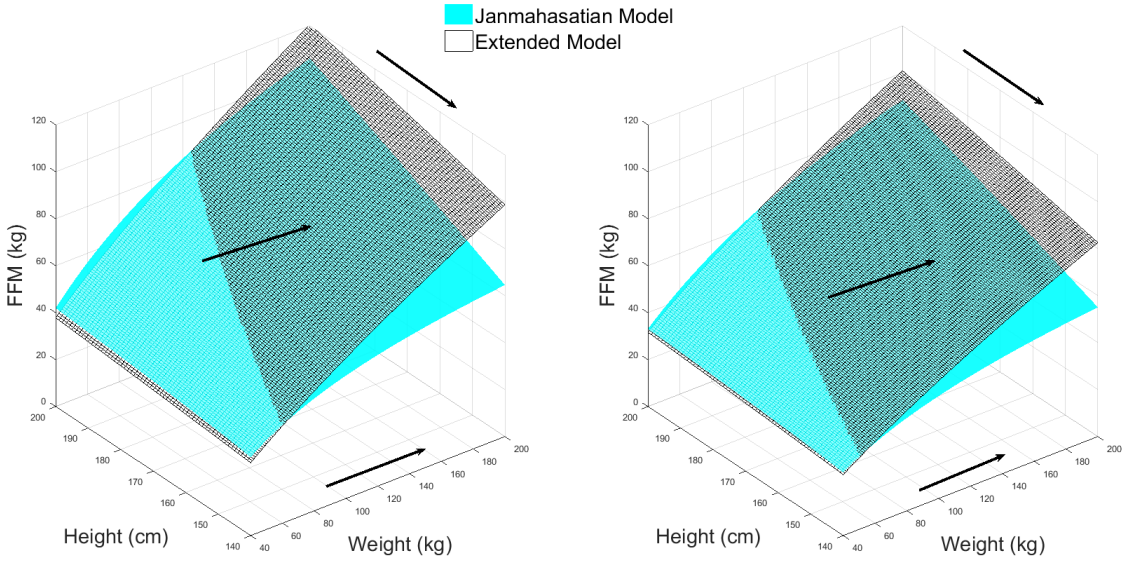

Figure 4.4 3D plots of the final $FFM_{Ext(Ind)}$ model and FFM_{Jan} model in Indian males (a) and females (b).

The black arrows represent the directions of low to high BMI zones.

So, further analysis was aimed to identify the deflection point on the BMI axis. As per the model, the deviation in FFM prediction between these two models is actually caused by the difference in their predicted bioimpedance estimates (i.e. Z_{Jan} vs. Z_{Ext}). Therefore, Z_{Jan} and Z_{Ext} values were simulated over a range of BMI values (Figure 4.5) using Eq 4.6 and Eq 4.11. The points of deflection were identified to be 32 and 28 kg/m² for males and females respectively, which were close to the standard BMI cut-off for obesity, i.e. 30 kg/m². This implies, FFM_{Jan} model is likely to over-estimate FFM in non-obese Indians, whereas it is likely to under-estimate in obese. This is in line with the validation study by Srigiripura et al. who observed over-estimation of FFM by Janmahasatian model where the BMI of their study population ranged from 14 – 33 kg/m². Future validation studies involving obese Indians are required to confirm the validity of these models. Once the extended FFM model has been

validated in Indians, then the model can be extended to other ethnicities as well.

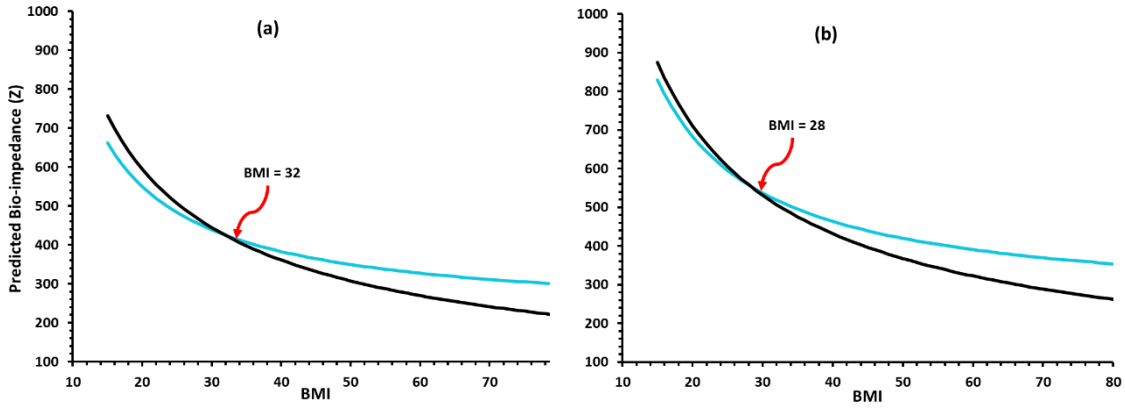

Figure 4.5 Predicted bio-impedance (Z) vs. BMI plots in males (a) and females (b).

The blue and the black lines represent the predictions by Janmahasatian's model (Z_{Jan}) and extended model (Z_{Ext}) respectively.

The advantage of the extended model is that it obviates the need of measuring FFM for future FFM model development. This is because the extended model corrects the Janmahasatian model at the root cause level, i.e. difference in body composition pattern, which (if uncorrected) can eventually cause model misspecification in the original model, if is used outside the European population, as seen with Indians. Therefore, future FFM model development in other ethnicities would only need to have the BIA data (i.e. Z) and estimate the body composition parameters Ψ thereof, by simply doing a non-linear regression analysis using the equation: $Z_{Ext} = \psi_1 \times \theta_1 + \psi_2 \times \theta_2 \times BMI^{(-\psi_3)}$ (Eq 4.11). Then, the extended FFM model can be derived simply plugging in the Z_{Ext} equation in Eq 4.12, as shown in section 4.2.1.2. Therefore, the proposed FFM_{Ext} model would be a highly clinically relevant approach for the future body composition research. This would enable the researchers develop FFM models with only BIA data in hand, which is a much easier procedure to carry out than the cumbersome FFM measuring methods like

DXA. Even, the ease and portability of BIA has made it the choice of method for large epidemiological surveys.

4.5. Conclusion

In conclusion, the original assumption of FFM_{Jan} model was extended to accommodate ethnicity driven variation in body composition, and an extended model structure (FFM_{Ext}) was derived. The FFM_{Ext} model structure was used to develop an extended FFM model for Indians ($FFM_{Ext(Ind)}$). The FFM_{Ext} model structure can be applied to develop extended FFM models in other relevant populations once FFM data or bioimpedance (Z) data become available.

Chapter 5: Identifying the average relationship between clearance and fat-free mass: A model based meta-analysis

5.1. Introduction

Fat-free mass (FFM) has been proposed as an alternative dose scalar to body weight (WT) [24, 91, 103, 106, 107, 126, 136-138] as it accounts for the change in body size and composition in contrast with WT which only accounts for body size. Dose scaling by FFM actually simplifies to scaling of CL by FFM when drug response links to exposure. However, the nature of the scaling relationship between CL and FFM is not universal in the literature.

There is a general belief that CL proportionally scales to FFM. A proportional relationship has been speculated [25] probably due to the fact that drug eliminating organs are exclusive parts of the lean portion of the body; hence changes in organ size and/or capacity would occur according to the change in FFM. However, there is limited theory to impute proportionality in the CL vs. FFM relationship.

McLeay et al. [60] have empirically determined the average value of the allometric scaling exponent to be $2/3$ which suggests a less than proportional scaling of CL by FFM. A non-linear (i.e. less than proportional) scaling of CL by FFM in the obese has been justified by some researchers [126, 199] on the ground that it is equivalent to the theoretical allometric scaling (by WT) with an additional correction for body composition. This is presumably, because allometric scaling estimation was made on normal physiological considerations which do not include obesity.

On the other hand, the empirical value (i.e. $2/3$) was determined by pooling data from drugs with different (hepatic and renal) elimination pathways, which might have confounded the result (i.e. the empirical estimate of the exponent). For example, it is likely to be confounded by including renally cleared drugs as glomerular filtration rate (GFR) is known to scale to body surface area (BSA) which is equivalent to scaling by $WT^{2/3}$. Additionally, within the hepatic elimination category, drugs under low and high extraction sub-categories may scale differently to the same body size metric, since their

clearances are rate limited to different physiological variables (i.e. hepatic intrinsic clearance and blood flow respectively). For the high extraction category, it is not clear whether clearance scales with body size or not. Several high extraction drugs have been found to have no influence of increase in body size on their clearance, such as propranolol, lidocaine, verapamil, sufentanil, and paclitaxel. It has been hypothesised that liver blood flow does not increase with obesity (in spite of increase in cardiac output) due to increased peripheral resistance and/or narrowing of hepatic sinusoids due to fatty infiltration (see section page 175 of section 8.1 for a detail discussion). Therefore, pooling data from high extraction compounds also might have confounded the empirical estimate of the exponent (as stated above for renally cleared drugs). On the other hand, drugs under low extraction category, have an obvious influence of body size on their clearance. This is because, their clearance approximates to the intrinsic clearance (CL_{int,u_H}) or the metabolic capacity of the liver, which has a direct influence of liver size (see Eq 6.1 and 6.14 in Chapter 6). Since liver size increases with obesity, it is expected that clearance of low extraction drugs would have an influence of body size. In obesity, since FFM more accurately describes the body size (than WT) from where drug elimination occurs, the relationship between clearance of low extraction drugs and FFM needs to be identified. Further to it, in drug development, a key goal is to develop drugs with low-hepatic extraction in order to ensure less dose and dosing frequency in the clinic. This necessitates re-determination of the empirical value of the allometric exponent by further sub-group analyses, and thereby explore whether the elimination pathway has implications on selection of the allometric exponent for scaling CL by FFM.

Therefore, the objective of this work is to estimate the scaling relationship between CL and FFM by a model based meta-analysis for low clearance drugs that are hepatically cleared.

5.2. Method

5.2.1. Data

This work was based on a thorough review of the literature non-systematic review (i.e. not at par with PRISMA guideline) using an appropriate search strategy followed by a model based meta-analysis.

The literature search was carried out using MEDLINE to identify reports of individual CL and FFM data using the specified keywords below. Further, inclusion and exclusion criteria were applied identify relevant publications. Note the data were not predicated on the requirement that a statistically significant relationship was or was not found between FFM and CL and hence the risk of publication bias is expected to be minimal. The data that were required for this analysis was either individual tabulated data of FFM values (or covariates weight, height and sex in order to compute FFM) and CL values or a plot of CL versus FFM from which data pairs could be extracted digitally.

Search keywords: "((NONMEM OR ((population AND (model* OR analys*)) OR (non AND linear AND mixed AND effect*))) AND ((fat AND free AND (weight OR mass)) OR (lean AND body AND (weight OR mass))) AND (PK OR pharmacokinetic* OR clearance)"

5.2.1.1. Inclusion criteria:

- Full text articles only
- Only human studies,
- Only reports in English
- Only adult participants (i.e. >18 years of age)
- Reports that provide individual values of CL and FFM or where FFM could be calculated at the individual level (using sex, body weight, and height)

5.2.1.2. Exclusion criteria:

- Drugs that are significantly eliminated by kidney (>20%) and/or by other extra-hepatic mechanism such as plasma instability; non-specific metabolism (e.g. carboxyl esterase, protease); and target mediated drug disposition (TMDD).
- Drugs that are known to demonstrate non-linear and/or time varying elimination due to auto-inhibition and induction of metabolic enzyme(s) respectively.
- Drugs that have a high systemic clearance above 30 L/hr and/or are substrates of polymorphic enzymes such as CYP2D6.

Articles which reported individual CL and FFM data (either in tabular or graphical format) were selected. Where a graphical format was provided, individual level data were extracted using the software programme Plot Digitizer (version 2.5). The data were then collated for analysis.

Individual data of all the drugs were pooled to form a single dataset for analysis. In the input data file (.csv), each drug was assigned an ID, and the CL values under each drug was considered as the repeated dependent variable measures and FFM the explanatory variable. For drug(s) where CL values of multiple metabolic pathways (e.g. acetaminophen) were separately reported, each pathway was considered as a distinct ID in the data file. If sufficient multi-pathway data were available then an additional level of between-occasion

variability would be considered. For each drug, the average CL value (CL_{mean}) was calculated and recorded in the dataset, which was used as an *a priori* drug specific normalising constant during the modelling step. The hierarchical model for the data is described below (Eq 5.1, Eq 5.2 and Eq 5.3)

Individual level model:

$$Y_{ikj} = f\left(\boldsymbol{\theta_{ik}}, x_{ikj}, CL_{mean_i}\right) + \varepsilon_{ikj}$$

Eq 5.1 Individual level model of CL and FFM

Y_{ikj}: CL of the i^{th} drug in the k^{th} occasion (i.e. article) at the j^{th} observation (i.e. patient), $\boldsymbol{\theta_{ik}}$: Vector of individual level parameters for the i^{th} drug in the k^{th} occasion, x_{ikj}: Represents FFM for the i^{th} drug in the k^{th} occasion at the j^{th} observation, $CL_{mean_{ik}}$: Represents the calculated average clearance of the i^{th} drug (considered as a normalising constant) in the k^{th} occasion, ε_{ikj}: Residual error between the predicted and j^{th} observation of the i^{th} drug in the k^{th} occasion.

Between-occasion variability (BOV) model:

$$\boldsymbol{\theta_{ik}} \sim N(\boldsymbol{\theta_i}, \mathbf{K})$$

Eq 5.2 BOV model for CL and FFM

$\boldsymbol{\theta_i}$: Vector of individual level parameters for the i^{th} drug (average of k occasions),$\boldsymbol{K}$: Variance-covariance matrix of inter-occasion variability of θ_i parameters, BOV model was only applicable if data of the same drug comes from multiples sources (i.e. articles).

Between-subject variability (BSV) model:

$$\boldsymbol{\theta_i} \sim N(\boldsymbol{\theta}, \boldsymbol{\Omega})$$

Eq 5.3 BSV model for CL and FFM

$\boldsymbol{\theta}$: Vector of population level parameters $[\theta_1, \theta_2, \theta_3]$. Their descriptions are given in section 5.2.2.1 and in Table 5.1,$\boldsymbol{\Omega}$: Variance-covariance matrix of between-subject variability of $\boldsymbol{\theta}$ parameters.

5.2.2. Model development

The data were analysed in a nonlinear mixed effects modelling framework due to the presence of repeated measures and the model may incur inclusion of statistical nonlinearity. Modelling was performed using NONMEM (version 7.3) and a three stage hierarchical modelling framework. An input-

output (I/O) model was used to scale individual clearance with FFM (x_{ikj}) by using the individual level parameters ($\boldsymbol{\theta_{ik}}$) as in Eq 5.1. A combined error model (proportional + additive) was applied to quantify the residual unexplained variability (RUV) over the observations, i.e. intra-individual variability. A BOV model was assumed to obtain the individual level parameters at the k^{th} occasion ($\boldsymbol{\theta_{ik}}$) from the average of all the occasions ($\boldsymbol{\theta_i}$) as shown in Eq 5.2. The average individual parameters were obtained from the population parameter ($\boldsymbol{\theta}$) by assuming a between-subject variability (BSV) model (Eq 5.3). The first-order conditional estimation with interaction (FOCEI) method was used for parameter estimation. Here, a model for BOV would be considered if individual CL and FFM data for a particular drug (i.e. ID) came from multiple sources (i.e. articles).

5.2.2.1. Model description

A summary of the general model equations are shown in Table 5.1. In the absence of multiple references for the same drug then BOV would be omitted. Three population level parameters (fixed effects) were considered, i.e. θ_1, θ_2, and θ_3. Here, θ_1 refers to the ratio between standard population CL (unknown) and $CL_{mean_{ik}}$ (known) for a drug; e.g. θ_1 will be 1 if the observed $CL_{mean_{ik}}$ equals to population CL. The parameters θ_2 and θ_3 represent the scaling exponent and the intercept of clearance with respect to FFM at the population level. For all fixed effects parameters θ_1, θ_2, and θ_3, BSV models were applied to account for the random inter-individual differences by which drug specific parameters θ_{1_i}, θ_{2_i}, and θ_{3_i} were obtained respectively. A BOV model was assumed to discern the drug specific parameter values for the for the k^{th} publication (if exists), i.e. $\theta_{1_{ik}}$, $\theta_{2_{ik}}$, and $\theta_{3_{ik}}$ respectively. Proportional error models were used to account for BSV, where η_{i1}, η_{i2}, and η_{i3} were the random errors of θ_1, θ_2, and θ_3 respectively, and were log-normally distributed. The distributions of η_{i1}, η_{i2}, and η_{i3} were defined by the variance-covariance matrix $\boldsymbol{\Omega}$, where ω_1, ω_2, and ω_3 refer to their respective standard deviations from a mean zero. Similarly, proportional error models were used to account for BOV,

where η_{k1}, η_{k2}, and η_{k3} were the random errors of θ_{1_i}, θ_{2_i}, and θ_{3_i} respectively, and were log-normally distributed. The distributions of η_{k1}, η_{k2}, and η_{k3} were defined by the variance-covariance matrix **K**, where κ_1, κ_2, and κ_3 refer to their respective standard deviations from a mean zero. At the individual level (i.e. for i^{th} drug at k^{th} occasion), an I/O model was used to describe the expectations of repeated measurements of clearance at the j^{th} observation of FFM (CL_{ikj}). The I/O model consisted of a coefficient term and an exponent (non-linear) term with and without an intercept term θ_3. Finally, the RUV model was considered to describe the intra-individual variations of the observations ($CL_{ikj,obs}$) from the I/O model expectations (CL_{ikj}). For RUV, both additive and combined error model was used where ϵ_{ikj_1} and ϵ_{ikj_2} refer to the additive and the proportional errors respectively. The distribution of ϵ_{ikj_1} and ϵ_{ikj_2} was defined by the variance-covariance matrix $\boldsymbol{\Sigma}$, where σ_1 and σ_2 refer to their respective standard deviations with a mean zero. Additionally, a drug specific proportional error (η_{i4}) was also tried which was distributed with standard deviation ω_4 and mean zero.

Table 5.1 Model equations for the meta-analysis

Fixed Effects Parameters: θ_1, θ_2, θ_3 (population level)
BSV Model
$\theta_{1_i} = \theta_1 \times e^{\eta_{i1}}$ $\theta_{2_i} = \theta_2 \times e^{\eta_{i2}}$ $\theta_{3_i} = \theta_2 \times e^{\eta_{i3}}$ Where, $\eta_i \sim N(0, \boldsymbol{\Omega})$ and $\boldsymbol{\Omega} = \begin{bmatrix} {\omega_1}^2 & \cdots & 0 \\ \vdots & \ddots & \vdots \\ 0 & \cdots & {\omega_4}^2 \end{bmatrix}$
BOV Model (if applicable)
$\theta_{1_{ik}} = \theta_{1_i} \times e^{\eta_{k1}}$ $\theta_{2_{ik}} = \theta_{2_i} \times e^{\eta_{k2}}$ $\theta_{3_{ik}} = \theta_{3_i} \times e^{\eta_{k3}}$ Where, $\eta_k \sim N(0, \mathbf{K})$ and $\mathbf{K} = \begin{bmatrix} {\kappa_1}^2 & 0 & 0 \\ 0 & {\kappa_2}^2 & 0 \\ 0 & 0 & {\kappa_3}^2 \end{bmatrix}$
I/O model (Individual level)
$CL_{ikj} = \theta_{3_{ik}} + \theta_{1_{ik}} \times CL_{mean_{ik}} \times \left(\frac{FFM_{kj}}{FFM_{std}}\right)^{\theta_{2ik}}$
RUV Model
$CL_{ikj,obs} = CL_{ikj} \times e^{\epsilon_{ikj_2}} + \epsilon_{ikj_1}$ $CL_{ikj,obs} = CL_{ikj} + \epsilon_{ikj_1} \times e^{\eta_{i4}}$, where variance of η_{i4} is ${\omega_4}^2$ (defined in $\boldsymbol{\Omega}$) Where, $\epsilon_{ikj} \sim N(0, \boldsymbol{\Sigma})$ $\boldsymbol{\Sigma} = \begin{bmatrix} {\sigma_1}^2 & 0 \\ 0 & {\sigma_2}^2 \end{bmatrix}$

5.2.2.2. Model selection and evaluation

Various fixed effects models (e.g. fixing or estimating parameter) and random effects models (e.g. with or without BSV on θ_2, additive or combination RUV models) were tested. Model selection was done based on log-likelihood ratio test (LRT), where a decrease in the NONMEM objective function (ΔOBJ) > 3.84 was considered statistically significant (*p-Value* <0.05)

for one parameter difference. The final model was evaluated by the observed vs. the predicted (i.e. the goodness-of-fit) plots.

5.3. Results

5.3.1. Data

The flow chart of the article screening process is shown in Figure 5.1. The initial search resulted in 221 articles. Out of these 221 articles, 88 articles were retained after applying the inclusion/exclusion criteria. Upon manually screening those 88 articles, 15 articles were found to contain individual level data for CL and FFM. Further applying the criteria to exclude significant extra-hepatic elimination and high clearance drugs resulted in 7 articles, which were eligible for analysis.

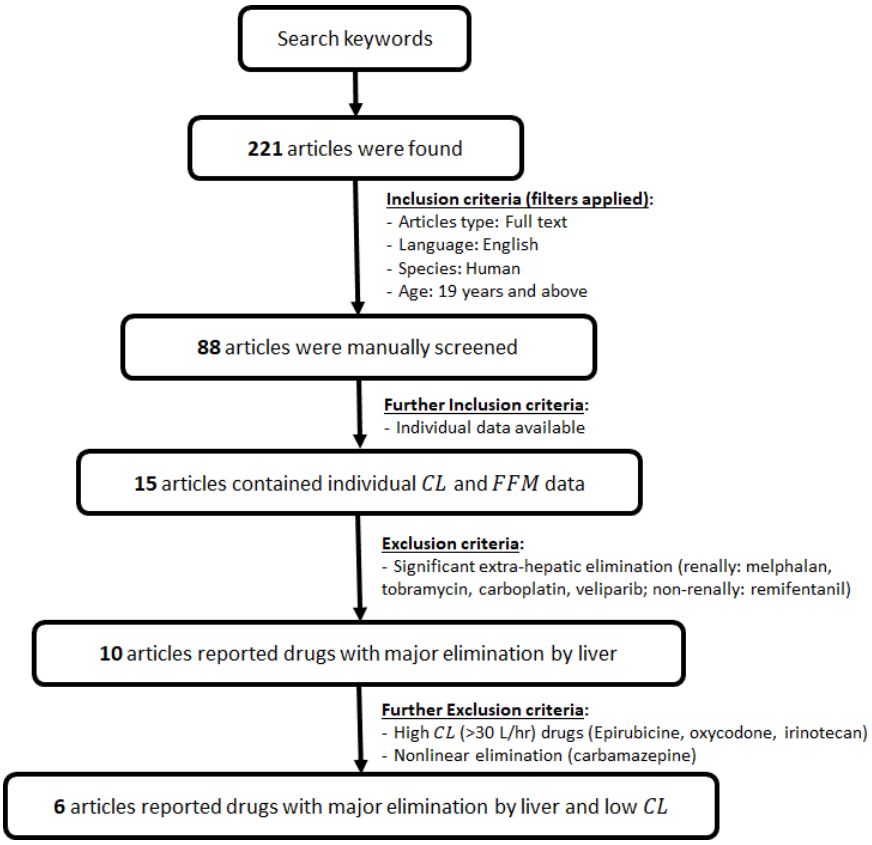

Figure 5.1 Summary of article screening following MEDLINE search

A summary of the chosen articles is provided in Table 5.2. None of the drugs were found from multiple articles. For acetaminophen, separate values of CL for three different metabolic pathways, i.e. glucuronidation (major), sulfation (minor) and CYP2E1 mediated oxidation (minor) were available for each patient. Since no drug data were sourced from more than 1 study then the BOV terms were dropped from the modelling. In addition, only 1 drug had repeated pathways unmeasured and therefore an additional level of BOV was not considered. The, CL values from each pathway of acetaminophen were assigned to a different ID in NONMEM input data file. Also, carabamazepine data were excluded from the modelling dataset because of its known property of enzyme induction. Hence, altogether 8 different IDs and 521 repeated measures were used in the NONMEM data set. Visualisation of individual CL vs. FFM data for all the 8 IDs is shown in Figure A3.1 of Appendix 3: .

Table 5.2 Summary of the literature extracted data that was used in modelling

Drug	Route	Sample Size (N)	FFM range (kg)	Average CL (L/hr)	Reference
Acetamenophen [a]	IV	28	35.9 - 96.2	13.3 [b] 3.9 [c] 1.2 [d]	[200]
Antipyrine	PO	17	32.0 – 62.0	1.6	[60]
Efavirenz	PO	71	35.6 – 75.0	6.6	[201]
Theophylline	PO	12	44.8 - 67.6	33.2	[202]
Ribavirin	PO	321	40.6 - 91.3	19.7	[203]
Moxifloxacin	IV	12	49.4 - 94.8	9.6	[204]

[a] CL for three metabolic pathways were separately reported for each patient, [b] glucuronidation, [c] sulfation, [d] oxidation, [e] excluded from modelling dataset

5.3.2. Model development

A summary of the model selection is given in Table 5.3. Additional models were tested and are summarised in Table 5.4. All modelling was considered within a two-stage hierarchical modelling. Initially, an intercept model (M1) was tried where the intercept θ_3 was estimated. The estimate of θ_3 was negligible and also, the associated estimate of CV% (ω_3) was 152% which appeared to be unrealistic. Moreover, excluding the θ_3 parameter (and ω_3) did not significantly worse the model fit in M2. Therefore, successive modelling (M2 onwards) excluded θ_3. Initially, an additive error was used to describe RUV (M1, M2); however inclusion of a combined error model (M3) significantly improved the fit. In M4, the BSV on parameter θ_2 was fixed to zero which significantly worsened the model fit as OBJ was increase by 25.53 points compared to M3. When an ETA-EPS error model was considered, i.e. using BSV in the residual error ($\epsilon \times e^{\eta}$), the fit of model M5 was significantly improved compared to M3 ($\Delta OBJ = -62.78$). The estimated exponent of M5 was 0.68 with a 45% BSV on it. Further, fixing the BSV of θ_2 to zero (M6) and considering correlation between ω_2, ω_3 (M7) did not improve the model fit compared to M5. The final model was therefore M5.

A sub-group analysis was done (Table 5.4) by excluding certain drugs based on their metabolic pathways to rule out if any particular pathway is influential towards the estimate of the exponent. First, oxidation pathway of acetaminophen was excluded (S1) since it has minute contribution on the overall elimination of the drug. In the next stage, its glucuronidation was excluded (S2) given the fact that a type of enzyme (i.e. cytosolic) isoform is involved in the process (aka phase-2) which is different that the regular microsomal metabolism by CYPs (aka phase-1). Exclusion of moxifloxacin was also tested (S4) since it is metabolised by phase-2 enzymes. Further, exclusion of both acetaminophen glucuronidation and moxifloxacin data (S5) and exclusion of all pathways of acetaminophen were also tried (S3). Irrespective of the exclusion of specific metabolic pathway or drug, the estimate of exponent

varied from 0.52 to 0.76. In subgroup analyses OBJ values were not compared as the number of records varied in different datasets.

The goodness-of-fit plot and the residual plot of M5 appeared reasonable (Figure 5.2). Therefore, M5 was considered as the final model. The signature profile of the $CL\ vs. FFM$ relationship has been shown in Figure 5.3.

Table 5.3 Summary of model selection in meta-analysis

Model	OBJ	ΔOBJ	θ_1	θ_2	ω_1 (CV%)	ω_2 (CV%)	σ_1 (L/hr)	σ_2 (CV%)
M1[a]	1150.98	-	0.99	0.64	4%	38%	1.8	-
M2	1151.17	0.19	0.99	0.64	4%	38%	1.8	-
M3	1130.35	-20.63 [b]	1.00	0.65	5%	35%	1.4	8%
M4	1155.89	25.53	1.00	0.60	5%	0 (fixed)	1.4	8%
Model	OBJ	ΔOBJ	θ_1	θ_2	ω_1 (CV%)	ω_2 (CV%)	ω_3 (CV%)	σ_1 (L/hr)
M5	1067.57	-62.78 [c]	0.99	0.68	3%	45%	0.67	1.1
M6	1082.16	14.59	1.01	0.56	4%	0 (fixed)	0.66	1.2
M7	1066.61	-0.96 [d]	0.99	0.71	3%	42% [e]	0.67[e]	1.1

[a] Estimates of intercept $\theta_3 = 0.02$ and its BSV $\omega_3 = 1.52$, [b] Calculated as (M1 – M3), [c] Calculated as (M3 – M5), [d] Calculated as (M5 – M7), [e] Correlation between ω_2 and ω_3 was estimated to be -0.42, ΔOBJ represents the difference between the two consecutive models unless otherwise stated; the drop and gain in OBJ values (compared to the previous model) is represented by negative and positive signs respectively.

Table 5.4 Summary of sub-group analyses.

Subgroup	OBJ	θ_1	θ_2	ω_1 (CV %)	ω_2 (CV %)	σ_1 (L/hr)	σ_2 (CV %)
S1	1087.33	1.00	0.61	4%	35%	1.4	51%
S2	978.49	1.00	0.61	4%	43%	1.01	64%
S3	962.08	1.01	0.52	5%	1%	1.3	53%
S4	1034.85	1.00	0.76	4%	39%	1.0	69%
S5	945.52	1.01	0.70	5%	37%	0.90	63%

S1 excluded acetamenophen-oxidation; S2 excluded acetamenophen -glucuronidation; S3 excluded all pathways of acetamenophen metabolism, S4 excluded moxifloxacin; S5 excluded acetamenophen -glucuronidation and moxifloxacin

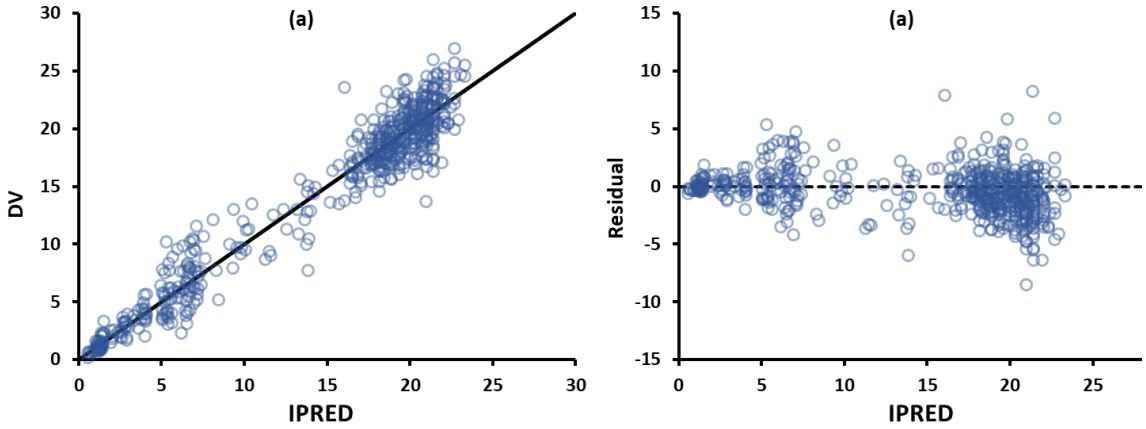

Figure 5.2 (a) Goodness-of-fit plot and (b) residual vs. IPRED plot of the final model (M5)

The solid black line represents the line of unity and the dotted line represents the zero residual.

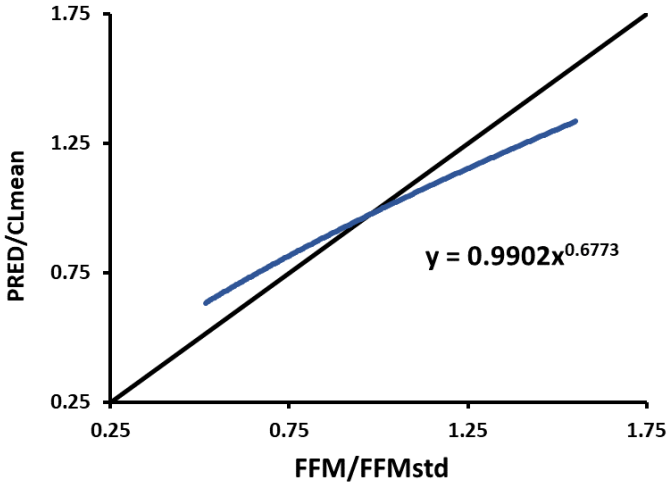

Figure 5.3 Normalised clearance (PRED/CL_{mean}) vs. normalised fat-free mass (FFM/FFM_{std}) plots

The solid black lines represent the line of unity.

5.4. Discussion

In this work, the average relationship between clearance (CL) and fat-free mass (FFM) was estimated from the literature data using a model-based meta-analysis (MBMA) method within the framework of non-linear mixed effects (NLME) modelling.

In clinical pharmacology, the traditional meta-analysis refers to the statistical analysis of a large collection of data from multiple pharmacokinetic (PK)-pharmacodynamic (PD) studies for the purpose of integrating the findings [205]. Model-based meta-analysis (MBMA) builds on traditional meta-analysis by further incorporating NLME models into it in order to describe the average findings, e.g. PK parameters and the variability. Meta-analyses can be based on either individual patient data (e.g. individual concentration-time course) or aggregate data (e.g. mean response or treatment effect). While individual patient data based meta-analyses are considered the gold standard [206], literature based meta-analyses are more often based on aggregate data due to limited accessibility to individual level data. Pooling data from multiple studies makes the analyses more informative in nature, increasing the precision of the

parameter estimates and also the statistical power to accurately identify the sources of variability (i.e. covariates) in the parameters of interest [207]. Overall, MBMA has been extensively applied in clinical pharmacology to address a range of questions. For example, new covariates of CL (that were not identified retrospectively) were identified for efavirenz [208] and docetaxel [209] from pooled phase-1 and phase-2 studies; a parent-metabolite PK model for vitamin D3 and its active metabolite 25-hydroxy vitamin D3 was developed [210]; and a guidance to optimally design phase-1 studies for therapeutic antibodies [211] using MBMA has also been proposed.

There was an *a priori* expectation that CL would vary in proportion to FFM (i.e. linear scaling) since drug elimination occurs in the lean portion of the body. The finding of Chapter 6: (next chapter) aligns with such expectation of linear scaling of clearance by FFM. However, the result of this analysis suggests that CL is scaled by FFM with an estimated exponent of 0.68 which indicates a less than proportional scaling. This estimate includes scaling of CL by $2/3$ power of body size which is a well-known scaling method in total body weight based scaling [123, 124].

The finding of this study aligns with the literature based meta-analysis reported by McLeay et al. [60]. Their meta-analysis derived the average scaling exponent to be $2/3$ (i.e. 0.67) when CL is scaled by FFM. It is noteworthy that their meta-analysis involved pooling drugs from a range of mechanisms (i.e. renal, hepatic, and mixed) and extents (i.e. low and high liver extraction ratios) of elimination, whereas this work particularly analysed the data coming from low-clearance drugs that are solely eliminated by liver and in the subgroup analysis only those that were eliminated by phase-1 metabolism (S5 in Table 5.4). Therefore, there is little theoretical explanation behind the similarity in these findings. While looking at the individual CL vs. FFM profiles (Figure A3.1 in Appendix 3:), a range of exponents were found among the drugs. This can be explained by 45% BSV over the estimate of the exponent (θ_2). The cause of this variation could not be understood by the current analysis.

The major limitation of this work was limited sample size, i.e. 8 IDs (N=8) out of 6 drugs were available for modelling. Such a small sized study is less likely to have adequate power to estimate the true parameter-covariate relationship as demonstrated by Ribbing et al. [56] and also covered under Chapter 2: [212] Therefore, the estimated exponent 0.68 should be interpreted and implemented cautiously, as it may not represent the true CL vs. FFM relationship across a wider range of drugs, unless validated by a larger meta-analyses in the future. Future studies are advised to include an *a priori* power analysis and increase the sample size accordingly in order to ensure adequate (>80%) power. In addition, the current study covered limited pathways of CYP metabolism (e.g. CYP2E1: acetaminophen, CYP2B6/2A6: efavirenz, CYP1A2: theophylline), and phase-2 metabolism (e.g. acetaminophen, moxifloxacin). Therefore, the current study provide limited support to extend the use of $2/3$ as the value of exponent for drugs that are metabolised by phase-1 and/or phase-2 metabolism in general. Thus future analyses should ideally include sufficient data covering other common pathways of drug metabolism (e.g. CYP 2D6, 2C9, 2C19), and possibly drug efflux (i.e. transporter mediated biliary secretion). Hence, in the absence of knowledge about the true relationship between CL and FFM, it will be prudent to estimate the exponent with the data empirically. However, if the study is under-powered (due to limited sample size and/or covariate range), estimation may lead to biased exponent as shown in Chapter 2: [212]. Under such circumstances, assuming the theoretical linear relationship (derived in Chapter 6:) or a value of $2/3$ might be a reasonable alternative. In this context, a theoretical basis of CL vs. FFM scaling exponent has been sought in Chapter 6: .

PART IV

SCALING OF CLEARANCE BY LEAN LIVER VOLUME

Chapter 6: Evaluating the relationship between lean liver volume and fat free mass

6.1. Introduction

The global prevalence of obesity and its related co-morbidities are rising [192, 213]. As a result, clinicians are faced with an increasing number of obese patients in their day to day practice [24]. Obesity is known to influence drug clearance (CL) due to changes in body size and composition, and hence alters the maintenance dose rate requirements [183, 214, 215]. However, quantification of dose requirements in the obese is rarely formally explored as obese subjects are often excluded from clinical trials during drug development.

Fat-free mass (FFM) has been proposed as an alternative dose scaler to body weight (WT) [25, 91, 103, 106, 107, 126, 136-138] as it accounts for the change in body size and composition in contrast with WT which only accounts for size. Dose scaling by FFM is underpinned by the scaling of CL by FFM, based on the assumption that dose and CL follow a proportional relationship; however, limited theory is available to impute linearity. Moreover, the nature of the scaling relationship is not universally proportional in the literature, and an empirical value of 0.67 was derived by McLeay et al. [60]. In line with the literature, the empirically estimated value of the exponent particularly for the low extraction drugs was 0.68 in Chapter 5, which again does not support a linear scaling of CL by FFM. Therefore, it is necessary to understand whether the empirically determined values can be supported by a theory. FFM based scaling is underpinned by the assumption that drug eliminating organs are constituents of FFM and their capacity to metabolise and/or excrete drugs (as determinant of CL) vary according to the variation in FFM across lean and obese individuals [136]. When the eliminating organ is the liver, CL of low clearance drugs approximates to the hepatic intrinsic clearance, i.e. CL_{int,u_H} (assuming a well-stirred model), which is believed to be proportional to $Liver\ Size$ (Eq 6.1) under certain assumption (see section 6.4 and Eq 6.14). Since $CL \propto Liver\ Size$, then the $Liver\ Size$ vs. FFM relationship that is denoted by a mathematical function f in Eq 6.2 would determine the theoretical relationship between CL and FFM, described by function g in Eq 6.3 (i.e. $f = g$). Therefore,

the theoretical scaling relationship between CL and FFM (i.e. g), whether linear (i.e. proportional) or non-linear, can be deduced by finding the relationship between $Liver\ Size$ and FFM (i.e. f).

$$CL\left(\approx CL_{int,u_H}\right) \propto Liver\ Size$$

Eq 6.1 Relationship between clearance and liver size

$$Liver\ Size = f(FFM)$$

Eq 6.2 Liver size as a function of fat-free mass.

$$CL = g(FFM)$$

Eq 6.3 Clearance as a function of fat-free mass.

Traditionally, total liver volume (LV) is used as descriptor of $Liver\ Size$. However, it is unclear if LV accurately describes the 'functional' $Liver\ Size$ in the obese. Here, we define 'functional' $Liver\ Size$ as the volume of liver from which drug elimination occurs. From a biological point of view, LV represents the summation of lean liver volume (LLV) and liver fat ($LFAT$) as shown in Eq 6.4. The lean portion of the liver primarily consists of metabolically active parenchymal tissue that almost exclusively contributes to drug elimination. In healthy livers, the presence of liver fat is negligible (<2% of LV) [216, 217] and thus LV is a sufficient approximation of 'functional' $Liver\ Size$. However, nearly 90% of obese patients have steatosis [110, 111], a pathological condition where liver fat is above 5% of LV and reported to be as high as 50% [79, 115, 218]. Therefore, we hypothesise that scaling of CL by FFM actually simplifies to the scaling of LLV by FFM.

$$LV = LLV + LFAT$$

Eq 6.4 Components of total liver volume.

The aim of this work was to investigate the relationship between LLV and FFM and therefore to identify the form of Eq 6.2.

6.2. Method

6.2.1. Data

One hundred adult Indian (Caucasian) patients consisting of 30 females and 70 males aged 18-60 years and scheduled to undergo a computerised tomography (CT) scan of the abdomen or neighbouring anatomical region were recruited in this study. The study was conducted at the PSG Hospital, Coimbatore, India and described by McLeay et al. elsewhere [195]. Subjects were stratified into three groups according to body mass index (BMI) with approximately equal number of subjects per group: normal (<25 kg/m^2), overweight (25-30 kg/m^2), and obese (>30 kg /m^2). Single measurements of lean liver volume (LLV) per patient were available from this study, along with patient characteristics such as sex, height (Ht), weight (WT), age, and clinical chemistry such as blood glucose and lipid profiles and liver and kidney functions. The LLV data was derived from the total liver volume (LV) and liver fat ($LFAT$) data, measured by a CT-based method which has been described in detail by McLeay et al. [195]. All subjects underwent ultrasonography screening of the abdomen prior to recruitment and were excluded if there was evidence of hepatic structural abnormality. Subjects were also excluded if they had abnormal liver or kidney function tests, were undergoing current treatment for a medical condition related to the liver or kidney, were pregnant, or were breastfeeding. Patient characteristics used for modelling are summarised in Table 6.1. Individual FFM was calculated from the patients' characteristics by using the equations developed by Janmahasatian et al. (Eq 6.5 and Eq 6.6) [102] and Kulkarni et al. (Eq 6.7 and Eq 6.8) [194]. However, FFM by Kulkarni's model

was used throughout the modelling work based on the assumption that it reasonably approximates the true FFM in Indian subjects [105] (discussed in Chapter 4:) Body surface area (BSA) was calculated by Du Bois formula [219].

$$FFM_{Jan\ (male)} = \frac{9270 \times WT}{6680 + 216 \times BMI}$$

Eq 6.5 Janmahasatian's model for fat-free mass in males (same as Eq 1.35)

$$FFM_{Jan\ (female)} = \frac{9270 \times WT}{8780 + 244 \times BMI}$$

Eq 6.6 Janmahasatian's model for fat-free mass in females (same as Eq 1.36

$$FFM_{Kul\ (male)} = -15.605 - (0.032 \times Age) + (0.192 \times Ht) + (0.502 \times WT)$$

Eq 6.7 Kulkarni's model for fat-free mass in males

$$FFM_{Kul\ (female)} = -13.034 - (0.018 \times Age) + (0.165 \times Ht) + (0.409 \times WT)$$

Eq 6.8 Kulkarni's model for fat-free mass in females

Table 6.1 Summary of patient characteristics in the study

BMI strata	Normal ($N = 30$)	Over weight ($N = 31$)	Obese ($N = 39$)
Characteristics:	**Median (range)**	**Median (range)**	**Median (range)**
Age (year)	34 (18-57)	39 (24-66)	41 (25-60)
$Height$ (cm)	164 (148-197)	164 (143-189)	164 (146-177)
$Weight$ (kg)	58 (45-74)	73 (54-91)	90 (70-128)
FFM (kg) [a]	43.7 (29.6-58.3)	51.4 (32.2-64.5)	59.2 (39.0-81.2)
FFM (kg) [b]	47.1 (30.8-63.5)	54.5 (32.9-68.8)	59.2 (38.6-75.5)
BMI (kg/m^2)	21.8 (16.9-24.7)	27.9 (25.2-29.8)	33.8 (30.1-51.8)
BSA (m^2)	1.6 (1.4-2.1)	1.8 (1.4-2.2)	2 (1.6-2.4)
LV (mL)	1065.9 (689.2-1835.4)	1394.1 (787.5-2161.2)	1799.8 (963-2630.1)
$LFAT$ (%)	0 (0-10.7)	1.7 (0-16.1)	9.9 (0-20)
LLV (mL)	1079.3 (711-1777.9)	1338.4 (789.9-2003)	1599.5 (962.5-2259.2)

FFM fat-free mass, BMI body mass index, BSA body surface area, LV total liver volume, $LFAT$ liver fat, LLV lean liver volume, [a] calculated by Kulkarni's model [194], [b] calculated by Janmahasatian's model [102]

6.2.2. Model development

Lean liver volume was modelled within a nonlinear regression framework using the first-order approximation method (FO) in NONMEM (version 7.3). Note there were no repeated measures in this data set. Covariates were selected based on the Akaike Information Criteria (AIC) [55], where a lower AIC value was indicative of a better description of the data. In the first stage, both *allometric* scaling (Eq 6.9) and linear scaling (θ_{size} fixed to 1) was used to identify the best size descriptor among WT, BSA, and FFM, with and without including sex. We define *allometric* here as any relationship that is not isometric, that is any nonlinear relationship between LLV and a measure of

body size. This was followed by testing clinical chemistry markers by linear models (Eq 6.10) using stepwise covariate modelling which involved forward selection (*p value* <0.05) followed by backward deletion (*p value* <0.01) steps. An additive residual error model (Eq 6.11) was used for modelling the data. Finally, biological plausibility was used to justify the selection of the final model.

$$LLV_i = \theta_{LLV} \times \left(\frac{Size_i}{Size_{std}}\right)^{\theta_{size}}$$

Eq 6.9 Allometric scaling model for lean liver volume.

$$LLV_i = \theta_{LLV} \times \left(\frac{Size_i}{Size_{std}}\right)^{\theta_{size}} \times \left[1 + \theta_{cov}\left(\frac{Cov_i - Cov_{std}}{Cov_{std}}\right)\right]$$

Eq 6.10 Linear model for lean liver volume.

$$LLV_{i,obs} = LLV_i + \epsilon_i \quad [\text{where } \epsilon_i \sim N(0, \sigma^2)]$$

Eq 6.11 Error model for lean liver volume

6.2.3. Model evaluation

Goodness-of-fit (GoF) plots were used for preliminary evaluation of the models. A marginal visual predictive check (VPC) plot was created to assess the predictive performance of the final model. The model estimated fixed effects and the distribution of the residual error were used to (parametrically) generate 1000 simulated *LLV* values for each subject in the dataset that was used for modelling. The 5th, 50th, and 95th prediction percentiles along with their 95% confidence intervals (CI) from the simulated *LLV* data were plotted with the observed data (5th, 50th, and 95th percentiles) superimposed.

In addition, non-parametric bootstrap analysis of the final model was performed with 1000 replicates from the dataset and the mean of the parameter

estimates along with the boundaries of their interquartile range (IQR) and relative standard error (RSE) were reported.

6.3. Results

FFM data predicted by Janmahasatian's model (FFM_{Jan}) demonstrated deviation from the FFM data that was predicted by Kulkarni's model (FFM_{Kul}) [194], (see Figure 4.2 of Chapter 4:). Overall, FFM_{Jan} estimates were higher than the FFM_{Kul} estimates, particularly in males, and the mean difference [95%CI] was -1.9 [(-2.6) – (-1.2)] kg with a standard deviation of 3 kg (see Table 4.2 of Chapter 4:).

All size descriptors (i.e. WT, BSA, and FFM) were found to be statistically significant covariates of LLV irrespective of whether scaled linearly (i.e. fixed exponent 1) or *allometrically* (i.e. exponent is estimated) (Table 6.2: M2 to M11 performed better than M1). The *allometric* models (M3, M6, M9) performed better than their linear counterparts (M2, M5, M8), in terms of AIC reduction, although this improvement was marginal for $FFM + sex$. Notably, the BSA model (M6) was most preferred (statistically) among the *allometric* models tested. However, including sex in the FFM model (M10) significantly further decreased the AIC value from 1220 to 1205 units, which left the FFM model being preferred to all models based on WT, but not to the allometrically scaled BSA model (M6). Both WT and the BSA models were insensitive to sex (i.e. M4 and M7). Therefore, the final model was selected from the two candidates allometrically scaled BSA (M6) and FFM + sex (M10). We note that allometric scaling of FFM + sex provided no benefit, since the estimated *allometric* exponent of the FFM + sex model (M10) was 1.05 indicating essentially linear scaling and this was subsequently fixed to 1 (i.e. M11). It is now seen that M11 has a marginally lower AIC value than M6 (allometrically scaled BSA). Also when interpreting an exponent on BSA we note that BSA is proportional to $WT^{2}/_{3}$ (i.e. $WT^{0.67}$), and thus scaling BSA raised to a power of 1.58, i.e.

$(WT^{0.67})^{1.58}$ would yield a model that is approximately a linear scaling on WT ($\approx WT^1$) and hence this scaling on BSA appears to have no biological plausibility.

Table 6.2 Summary of model selection from various size descriptors

Model No.	Covariate(s)	Model	Exponent (θ_{size}) [a]	AIC
M1	NA	Base	NA	1275
M2	WT	Linear	1 (fixed)	1211
M3	WT	Allometric	0.79	1207
M4	$WT + Sex$	Allometric	0.79	1208
M5	BSA	Linear	1 (fixed)	1215
M6	BSA	Allometric	1.58	1204
M7	$BSA + Sex$	Allometric	1.65	1204
M8	FFM	Linear	1 (fixed)	1222
M9	FFM	Allometric	0.82	1220
M10	$FFM + Sex$	Allometric	1.05	1205
M11	$FFM + Sex$	Linear	1 (fixed)	1203

NA not applicable, WT total body weight, BSA body surface area, FFM fat-free mass, AIC Akaike Information Criteria, [a] Estimated unless mentioned as 'fixed'

All of the tested clinical chemistry markers were found to be not significant during the successive modelling steps and thus were not included in the model. The structure of the final models for females and males are shown in the Eq 6.12 and Eq 6.13 respectively, along with their parameter estimates in Table 6.3. The plots of GoF and VPC are shown in Figure 6.1 and Figure 6.2 respectively.

$$LLV_{i\ (female)} = \theta_{LLV\ (female)} \times \left(\frac{FFM_i}{40}\right)$$

Eq 6.12 Final model structure of lean liver volume for females.

$$LLV_{i\ (male)} = \theta_{LLV\ (male)} \times \left(\frac{FFM_i}{55}\right)$$

Eq 6.13 Final model structure of lean liver volume for males.

Table 6.3 Parameter estimates along with their bootstrap results of the final model

Parameter	Estimates		Bootstrap Results			
			Mean (IQR)		RSE (%)	
	Female	Male	Female	Male	Female	Male
θ_{LLV} (mL)	1250	1420	1255 (1226 – 1281)	1422 (1402–1442)	3	2
σ (mL)	241.5		238 (227 - 250)		14	

θ_{LLV} population standard lean liver volume, σ standard deviation of the residual error, IQR boundaries of inter-quartile range of the estimates, RSE relative standard error

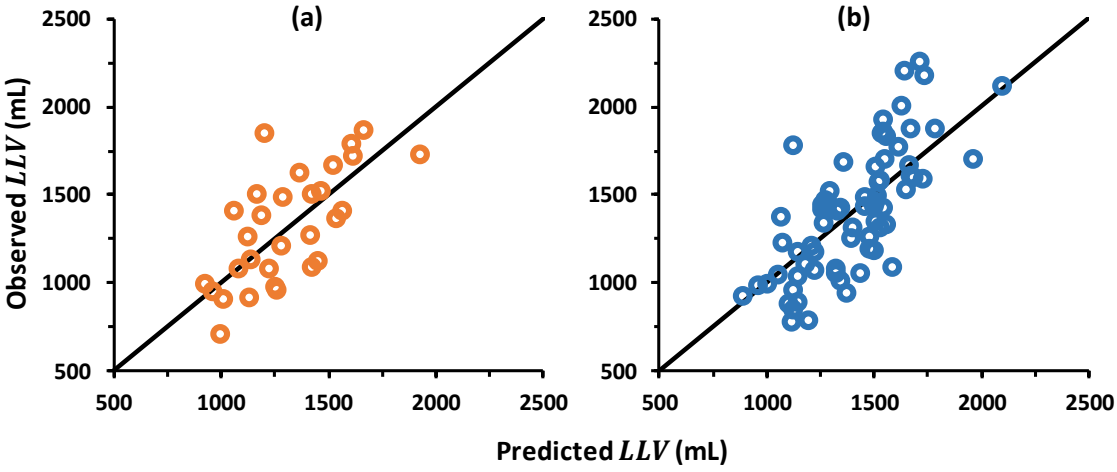

Figure 6.1 Goodness-of-fit plots of lean liver volume (*LLV*) for females (a) and males (b) of the final model

The solid black line represents the line of unity.

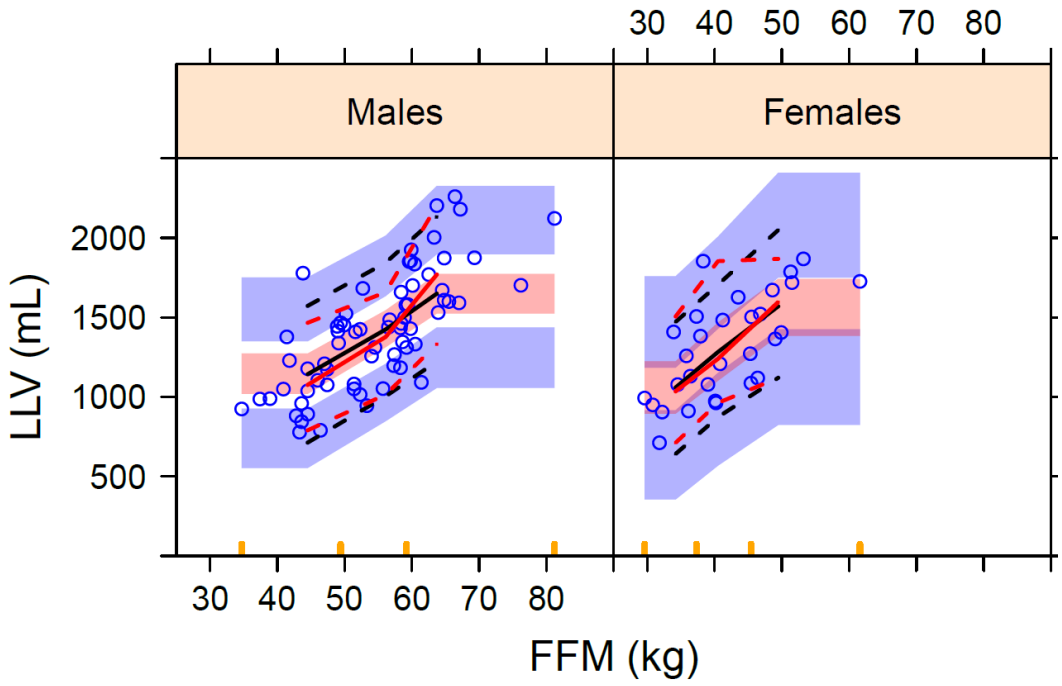

Figure 6.2 Visual predictive check (VPC) plots of the final model.

Fat-free mass (FFM) is calculated using Kulkarni's model. The red and the black lines represent the percentiles of the observed and simulated data respectively. The solid lines represent the 50th percentile (median) while the dotted lines represent the 5th and 95th percentiles respectively. The shaded area represents the 95$^{\%}$ confidence interval of the model predicted percentiles.

6.4. Discussion

In this work, we have investigated the most relevant size descriptor of lean liver volume (*LLV*), which provides a measure of 'functional' *Liver Size*. This finding would provide the theoretical basis of the *CL vs. FFM* relationship, and can help rationalise maintenance dose scaling in obese patients.

Physiological properties such as liver size and function are known to vary with body size [220]. By convention, total liver volume (*LV*) has been used to describe the liver size, and the available predictive models of *LV* had considered *BSA* as the body size descriptor [221]. There are currently no models to predict *LLV* and its relation to body size which is a more relevant descriptor of 'functional' *Liver Size*, especially in the obese. In this work, we showed that *FFM*, in conjunction with sex, described the size related variation in *LLV* better

than the traditional descriptor BSA (Table 6.2). This supports the observation that $FFM + sex$ is the best descriptor of basal metabolic rate (BMR) in human, which was reported to describe 63% of the inter-individual variability of BMR [222, 223]. It is also known that BMR of the whole body is majorly defined by the metabolic activities of the 'functional' cell mass of various organs, which depends on their size [224]. As discussed, for the liver, LLV is a more accurate descriptor of the 'organ size' that is metabolically active, irrespective of body size and composition. Therefore in theory, $FFM + sex$ should be the descriptor of LLV. Hence, choice of FFM was finally made based on biological plausibility, apart from the statistical preference over BSA. Further stepwise covariate modelling with available clinical chemistry measures including liver function markers did not result in any additional covariates in the final model. Hence, the final model retained FFM and sex as the covariates.

Selection of the FFM model was important because Janmahasatian's model (FFM_{Jan}) largely deviated (i.e. over-predicted) from the Kulkarni's model predictions (FFM_{Kul}) (see Table 4.2 and Figure 4.2 of Chapter 4:). In the absence of measured FFM data, there was no direct evidence which supports the selection of one FFM model over the other in this work. However, Srigiripura et al. [105] had reported that FFM_{Jan} substantially over-predicted the observed FFM data in Indian males, measured by bio-impedance analysis (BIA), whereas Kulkarni's model best predicted the observed data among the four different FFM models tested, including FFM_{Jan}. They reported that the mean error [95%CI] of the prediction by the Janmahasatian's model ($FFM_{BIA} - FFM_{Jan}$) and the Kulkarni's model ($FFM_{BIA} - FFM_{Kul}$) were -3.76 [(-7.96) – (0.44)] kg and 0.33 [(-4.26) – (4.91)] kg respectively. This could be due to the fact that Kulkarni's model was developed in a large cohort of Indian population, while the Janmahasatian's model was developed in a population of mainly a European ancestry. Therefore, FFM_{Kul} predictions were used during modelling throughout this work based on the assumption that FFM_{Kul} reasonably approximates the true FFM in Indian subjects.

The estimate (95% CI) of the exponent, i.e. θ_{size} in M10 was 1.05 (0.86 – 1.24), which implies that LLV scales linearly with FFM, and hence it was fixed to 1 in the final model (M11). This in turn, would support the linear scaling of CL by FFM as per Eq 6.1 to Eq 6.3. This might appear contradictory to the average relationship derived by McLeay et al. [60], i.e. $CL \propto FFM^{2/3}$, since the 95% CI of the estimate did not include $2/3$. However, their meta-analysis involved pooling drugs from a range of mechanisms (i.e. renal, hepatic, and mixed) and extents (i.e. low and high liver extraction ratios) of elimination. It is possible that elimination that is dependent on perfusion (as in high extraction ratio drugs) may have different limiting anatomical conditions than liver volume.

It is noted that liver intrinsic clearance (CL_{int,u_H}) is believed to be proportional to $Liver\ Size$ (i.e. Eq 6.1) on the assumption that *in vitro* intrinsic clearance ($CL_{int,u}$) and other physiological scaling factors as shown in Eq 6.14 are constant across the human FFM range (i.e. not affected by obesity) [66]. These physiological scaling factors include CYP abundanc ($[CYP]$, microsomal protein per gram of liver ($MPPGL$), etc., however, wide variability across individuals has been reported and the cause is poorly understood [225-227]. Particularly, the influence of obesity on expression and function of CYP enzymes (that might affect $CL_{int,u}$, $[CYP]$ and $MPPGL$) have remained mostly inconclusive [11]. In addition, the true CL (total) vs. FFM relationship can be masked in reality, if protein binding variation is large across normal and obese individuals. Therefore, in the absence of the predictability of these additional variance components, it might be acceptable to assume that the linear relationship between LLV and FFM translates to CL (thus dose) vs. FFM relationship, particularly for low-clearance drugs. Notably, this would require sex to be also considered while scaling CL by FFM as per the final model M11 in Table 6.2. On the contrary, allometric scaling by WT does not have the additional covariate sex, as inclusion of sex (M3 vs. M4 in Table 6.2) did not improve the model fit. Also, the estimated exponent for WT was close

to its theoretical value of 0.75 [94]. Therefore, the conventional allometric scaling of CL by WT may still appear a plausible scaling method based on the results. However, the objective of this work was not to recommend the right size scaler for CL (and dose), rather to investigate the theoretical relationship between CL and FFM, if exists. The choice of dose scaler should be guided by biological and clinical relevance. At least for FFM (among others), a biological plausibility exists, as FFM relates to BMR.

$$CL_{int,u_H} = CL_{int,u} \times [CYP] \times MPPGL \times \ Liver\ Size$$

Eq 6.14 Equation for hepatic intrinsic clearance.

The estimates (IQR) of population standard LLV measure, i.e. θ_{LLV} were 1250 mL (1226 – 1281) and 1420 mL (1402 – 1442) for females and males respectively (Table 6.3), which were similar to the median LV measures reported by Yu et al. [228] and Vauthey et al. [229] in Korean and Western populations respectively. Since, these median LV measures were reported for patients without liver abnormality (e.g. steatosis) they were expected to closely approximate the median LLV in the respective populations and hence, indirectly support the θ_{LLV} estimates in this work. Considering separate exponents for males and females (i.e. sex as a covariate on the exponent) did not additionally improve the model fit over a fixed exponent of 1. Further, the standard FFM values, i.e. 40 kg and 55 kg used in the model (corresponding to the median values in the data) well represented the population FFM as evident from a large population survey conducted by NHANES [230]. This implies that the θ_{LLV} estimates in this study well represent a larger population, and not limited to Indians. The final model is shown in here in Eq 6.15 and Eq 6.16.

$$LLV_{i\,(female)} = 1250 \times \left(\frac{FFM_i}{40}\right)$$

Eq 6.15 Final model of lean liver volume in females.

$$LLV_{i\,(male)} = 1420 \times \left(\frac{FFM_i}{55}\right)$$

Eq 6.16 Final model of lean liver volume in males

The final model performed well according to the bootstrap results (Table 6.3) and VPC plots (Figure 6.2). According to the final model, population *LLV* estimate per kg of *FFM* was higher in females (i.e. 31 mL) than in males (i.e. 26 mL), which is also apparent in the data (Figure 6.3). This observation is partly supported by the findings of Kwo et al. [231] where a higher (~ 36%) *LV* per kg of *FFM* was reported in females than in males, both without any liver disease. A possible explanation of the higher ratio in females could be that *LLV* per kg of *WT* is similar between females and males while *FFM* per kg of *WT* is lower in females than males.

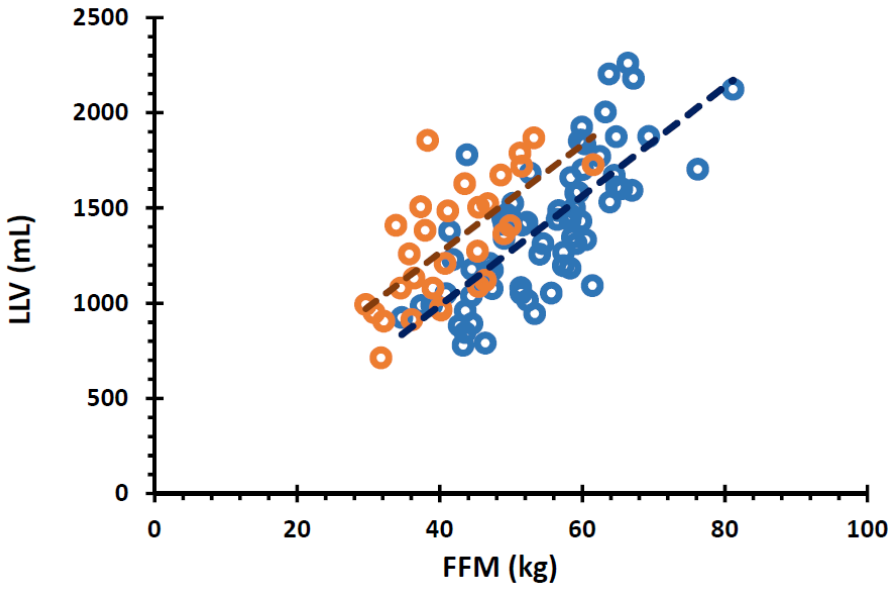

Figure 6.3 Plots of observed lean liver volume (*LLV*) data against fat-free mass (*FFM*), stratified by sex.

The orange and the blue circles represent female and male respectively. The brown and dark blue lines represent the regression lines for females and males respectively.

In addition, a potential application of LLV model could be *in vitro-in vivo* extrapolation of CL (IVIVE) in obese. Use of IVIVE, as a 'bottom up' approach has been recommended for predicting the initial dose in clinical pharmacology studies that include obese patients, in the absence of prior information of CL in this special population [112, 114, 232]. One motivating example is drug development in non-alcoholic fatty liver disease (NAFLD) that includes non-alcoholic steatohepatitis (NASH), where nearly 20 investigational drugs are under clinical development pipeline [76, 233]. For non-flow dependent drugs (i.e. low-extraction), the key step in IVIVE is to scale the intrinsic clearance of the liver (CL_{int,u_H}) from the *in vitro* intrinsic clearance data ($CL_{int,u}$). This needs scaling for $Liver\ Size$ with respect to body size. By convention, total liver volume (LV) is commonly considered for $Liver\ Size$ and scaled with a BSA based equation [221]. This might lead to substantial over-estimation of CL and dose in most (~90%) obese patients due to presence of steatosis and hence LLV would be a better descriptor of $Liver\ Size$ in IVIVE, at least for the low-extracted compounds, in order to predict the right dose in obese. On the other hand, no conclusion can be drawn from this study whether LLV can be considered as a potential dose scaler in standard 'top down' approach. In top-down approach, it is common to test all available scalers like WT, BSA, FFM etc. where LLV can be additionally tested. Although measurement of LLV needs CT scan it can be predicted by the model. This would need demonstration of improved scaling of CL by LLV as compared to the standard size descriptor like WT, FFM. At least, in the case of comparison with FFM, LLV is least likely to perform better given its proportional relationship with FFM. However, validation studies are required for a conclusive remark.

6.5. Conclusion

A model to predict lean liver volume (LLV) from readily available patient variables was developed and evaluated. Fat-free mass (FFM) and sex were found to be the best body size descriptor to scale LLV . LLV is likely an appropriate representation of the functional size of the liver, particularly in the obese, and correlates with FFM. FFM has recently emerged as an alternative body size scalar for drug clearance (CL) in obese patients. Whether FFM and drug CL scale linearly is currently under debate. The utility of the LLV model in scaling drug CL and dose requirements of hepatically cleared drugs, particularly in the obese, will need further exploration.

Chapter 7: Lean liver volume as a potential scaler for *in vitro-in vivo* extrapolation of drug clearance in obesity

7.1. Introduction

Obesity is known to influence drug clearance (CL) due to changes in body size and composition, with obese patients often requiring a different dose than standard adults [183, 214, 215]. Prior information about body size and composition driven changes in CL can help identify an initial dose for designing clinical pharmacology studies involving obese patients. Such studies are typically not performed during drug development and hence are often limited to post-marketing clinical studies [24]. In some exceptional situations, obese patients are studied during the drug development phases in order to meet the requirement(s) of the specific therapeutic areas, such as non-alcoholic steatohepatitis (NASH) [81, 234].

Recently, an *in vitro-in vivo* extrapolation (IVIVE) based approach has been proposed for predicting CL change in the obese population [112, 114, 235]. IVIVE of CL refers to the scaling of *in vitro* (unbound) intrinsic clearance ($CL_{int,u}$) data to hepatic intrinsic clearance (CL_{int,u_H}) as shown in Eq 7.1 of this chapter and in Eq 6.14 of Chapter 6: [66]. This involves scaling of the relevant physiological variables such as CYP abundance ($[CYP], as\ pmol/mg\ of\ microsomal\ protein$), microsomal protein per gram of liver ($MPPGL$), and $Liver\ Size$ by body size. Here, $Liver\ Size$ represents the *functional* size of the liver that describes the volume of liver where drug elimination occurs. While the influence of body size and composition on the variation of $Liver\ Size$ has been well quantified [221], their influence on other variables i.e. $[CYP]$ and $MPPGL$ has not been determined [225, 226]. Therefore the accuracy of CL_{int,u_H}scaling would largely depend on the accuracy in scaling of $Liver\ Size$ at an individual level. Theoretically, scaling of intrinsic clearance is particularly important for low-extraction drugs (e.g. warfarin) since *in vivo* CL is approximated by CL_{int,u_H} when corrected for relevant factors, e.g. free fraction in blood ($f_{u,b}$) as per the 'well-stirred' model (Eq 7.2, Eq 7.3). Thus, CL prediction of low-extraction drugs in a differently sized population (i.e. obese)

would largely depend on accurate prediction of individual (functional) $Liver\ Size$.

$$CL_{int,u_H} = CL_{int,u} \times [CYP] \times MPPGL \times Liver\ Size$$

Eq 7.1 Scaling of hepatic intrinsic clearance by liver size (same as Eq 6.14 Chapter 6:)

$$CL_H = \frac{Q_H \times f_{u,b} \times CL_{int,u_H}}{Q_H + f_{u,b} \times CL_{int,u_H}}$$

Eq 7.2 Well-Stirred Liver model for hepatic clearance

$$\text{If, } \left[f_{u,b} \times CL_{int,u_H}\right] \ll Q_H \text{ then } CL \approx f_{u,b} \times CL_{int,u_H}$$

Eq 7.3 Approximation of hepatic clearance for low-extraction drugs

Antipyrine can be considered as a classic example for phase-1 metabolism. It is completely metabolised by multiple CYP enzymes in the liver and freely distributes in total body water by passive diffusion [236]. Antipyrine has a systemic CL that approximately equals its CL_{int,u_H} satisfying Eq 7.3 [237] because its unbound intrinsic clearance (CL_{int,u_H}) is less than 5% of liver blood flow (Q_H) [238] and its free fraction in blood ($f_{u,b}$) is almost equal to 1 [6] due to negligible plasma protein binding and blood cell partitioning [239]. In addition, antipyrine is ~100% absorbed after oral administration without evidence of pre-systemic elimination [240]. Hence, variability in antipyrine CL is expected to be largely driven by the variation in $Liver\ Size$ and enzymatic content and/or activity.

Traditionally, total liver volume (LV) is used to describe functional $Liver\ Size$ and is scaled to the individual using body surface area (BSA) [221]. However, it is unclear if LV accurately describes functional $Liver\ Size$ in the obese population. From a biological point of view, LV represents the

summation of the lean liver volume (LLV) and liver fat ($LFAT$) as shown in Eq 7.4 (also shown in Eq 6.4 of Chapter 6:). The lean portion of the liver primarily consists of hepatocytes that contribute to drug elimination where as the metabolic activity of $LFAT$ is considered minimal [60]. In healthy livers, the presence of $LFAT$ is negligible (<2% of LV) [216, 217] and thus LV is a sufficient approximation of the $Liver\ Size$. However, nearly 90% of obese patients have some degree of steatosis [110, 111] a condition where liver fat is > 5% of LV and reported to be as high as ~ 50% of LV [79, 115, 218]. In this group of patients, LV would be an over-approximation of functional $Liver\ Size$, and hence scaling of CL_{int,u_H} by LV would potentially over-estimate CL. Therefore, we hypothesise that LLV is a closer approximation of the functional $Liver\ Size$ universally that can be particularly useful in scaling CL_{int,u_H} in the obese.

$$LV = LLV + LFAT$$

Eq 7.4 Components of total liver volume (same as Eq 6.4 of Chapter 6:

The objective of this work is to assess the application of LLV in CL extrapolation in overweight and obese patients (BMI >25 kgm^2).

7.2. Materials and Methods

Antipyrine was chosen as a model drug to test the LLV hypothesis since $Liver\ Size$ is expected to describe the inter-individual variation of antipyrine CL to a reasonable extent. Published individual CL data of antipyrine along with measured LV and other patient characteristics were identified from a previous publication, extracted, and summarised in Table 7.1 [64]. Patients (N=21) had no evidence of liver, kidney, or heart disease and had not received any chemotherapy/radiation/medication for the previous six months. Each patient was administered a single oral dose of 1200 mg antipyrine and CL was determined from their salivary concentrations.

Patient characteristics including sex, total body weight (WT), body surface area (BSA), and fat-free mass (FFM) were available. FFM was measured by using dual energy X-ray absorptiometry (DXA) and body fat ($BFAT$) percentage values were calculated from the corresponding FFM and WT. In this analysis, participants were grouped into normal weight ($BMI \leq 25$ kg/m^2) and overweight ($BMI > 25$ kg/m^2) categories. The overweight group includes obese patients as per the classical definition of obesity, i.e. $BMI >$ 30kg/m^2. The reported Individual LV values were measured by CT scan. The LLV values were then predicted by the LLV model (Eq 7.5, Eq 7.6) that was developed in the previous chapter (see Eq 6.15 and Eq 6.16 of Chapter 6:) [241], which incorporates FFM and sex. The individual LV values (observed) were plotted against the corresponding LLV values (predicted) in Figure 7.1. The individual CL values were plotted against their LV and LLV values in Figure 7.2 and their coefficients of determinations (R^2) were compared. A higher R^2 value would be indicative of a higher degree of correlation, and hence assumed to be a more appropriate scaler of $Liver\ Size$.

$$LLV_{(female)}\ in\ mL = 1250 \times \left(\frac{FFM\ in\ kg}{40}\right)$$

Eq 7.5 Lean liver volume model for females (same as Eq 6.15 of Chapter 6:

$$LLV_{(male)}\ in\ mL = 1420 \times \left(\frac{FFM\ in\ kg}{55}\right)$$

Eq 7.6 Lean liver volume model for males (same as Eq 6.16 of Chapter 6:

7.3. Results

The mean (range) of the calculated LLV values were 1245.9 (1027.2 – 1527.4) mL and 1226.6 (1024.0 – 1594.3) mL in normal and overweight groups respectively. The calculated mean $LFAT$ (range) values were 8.2% (0 – 14.9%) and 29.3% (2 – 70.8%) in the normal and overweight groups (Table 7.1).

Table 7.1 Summary of patient characteristics reported by Nawaratne et al. [64].

Characteristics	**Median (range)**	
Sub-group	**Normal weight**	**Overweight**
Sample Size (N)	8 (Male = 5, Female = 3)	13 (Male = 9, Female = 4)
BMI (kg/m^2)	23.6 (21.1–24.9)	28.7 (25.2 – 35.8)
BSA (m^2)	1.75 (1.51 – 1.95)	1.88 (1.65 – 2.15)
FFM (kg) [a]	48.5 (32.1 – 59.4)	47.7 (32.0 – 62.0)
$BFAT$ (%)	28.7 (19.7 – 41.6)	43.4 (24.4 – 55.9)
LV (mL) [b]	1316.0 (1090.0 – 1610.0)	1535.0 (1225.0 – 1989.0)
LLV (mL) [c]	1245.9 (1027.2 – 1527.4)	1226.6 (1024.0 – 1594.3)
$LFAT$ (%)	8.2 (0 – 14.9)	29.3 (2.0 – 70.8)
CL (L/h)	1.2 (0.7 – 3.3) [d]	1.5 (0.9 – 2.3) [e]

BMI body mass index, BSA body surface area, FFM fat-free mass, LV total liver volume, LLV lean liver volume, $BFAT$ body fat, $LFAT$ liver fat (as percentage of LLV), CL clearance, [a] Measured by dual energy X-ray absorptiometry, [b] measured by computerised tomography, [c] predicted by Eq 7.5 and Eq 7.6, [d, e] clearance was reported for 6 and 11 patients respectively, The clearance (CL) was calculated after single oral dose of 1200 mg antipyrine.

In the normal weight groups, the values of *LV* and *LLV* are scattered around the line of unity (Figure 7.1a) indicating that *LV* is a reasonable approximation of *LLV*. Where as in overweight groups, *LV* values are scattered above the line of unity (Figure 7.1b) indicating that *LV* overestimates *LLV* which suggests that in these patients *LV* would overestimate functional capacity. In the scatter plots of antipyrine *CL* values of the normal weight group (Figure 7.2a, Figure 7.2b), R^2 values were 0.43 and 0.58 against *LV* and *LLV* respectively. In the overweight group (Figure 7.2c, Figure 7.2d), the values of R^2 are 0.17 and 0.36 against *LV* and *LLV* respectively.

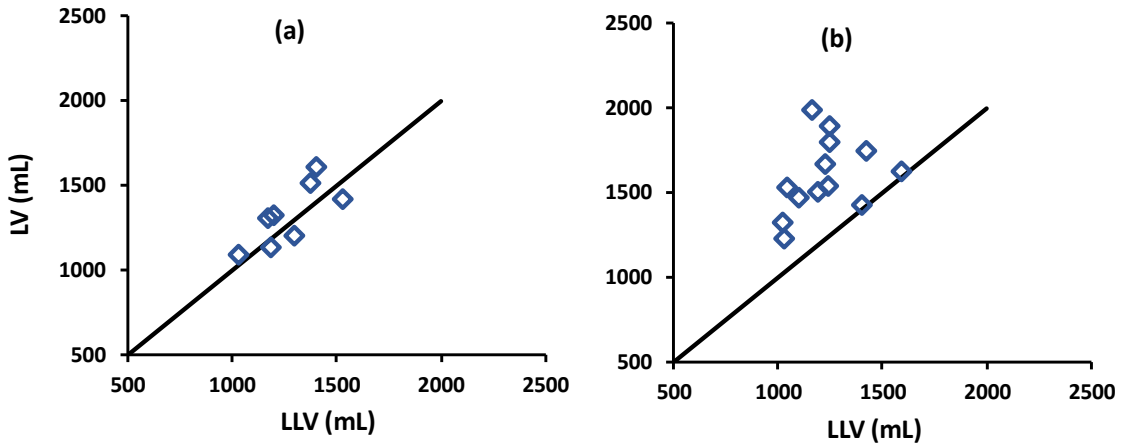

Figure 7.1 Individual measured total liver volume (*LV*) vs. predicted lean liver volume (*LLV*) in (a) normal weight (*BMI* <25 kgm2, n=8) and (b) overweight (*BMI* >25 kgm2, n=13) patients as reported by Nawaratne et al. [64]

The solid line represents the line of unity.

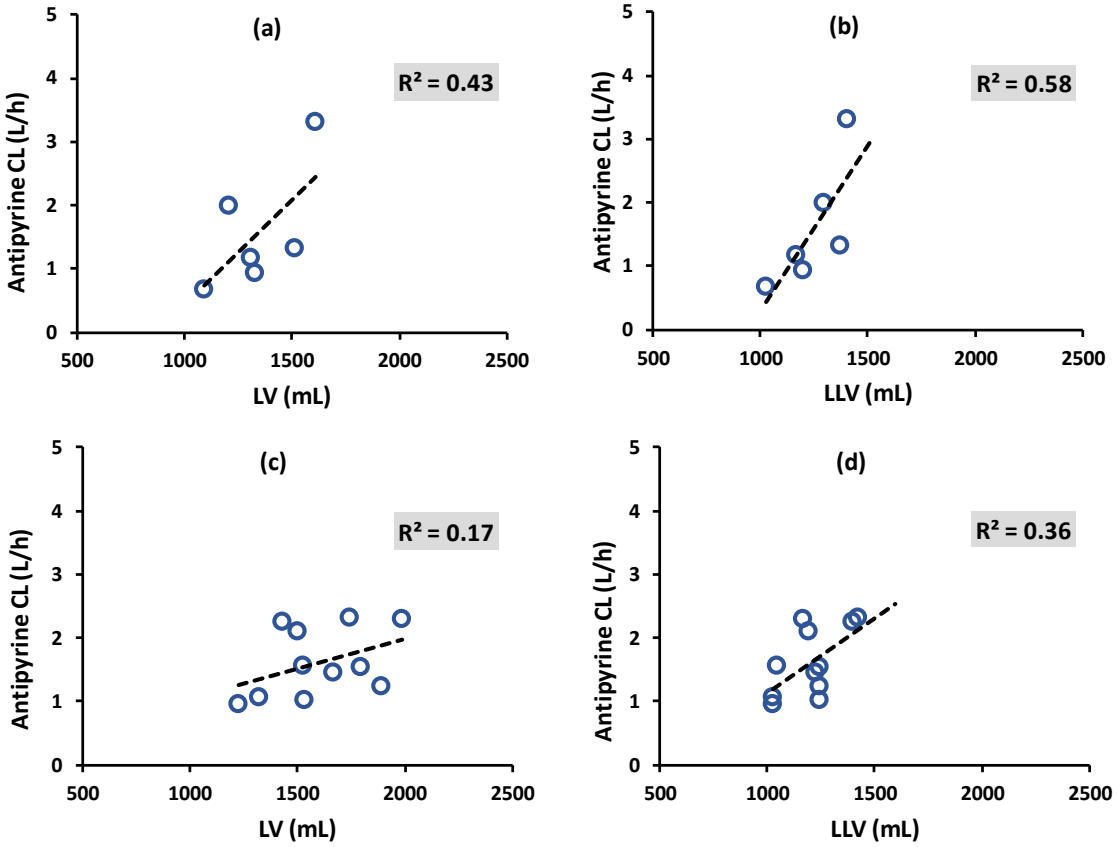

Figure 7.2 Antipyrine clearance (*CL*) vs. total liver volume (*LV*) and lean liver volume (*LLV*) plots of the study population reported by Nawaratne et al. [64].

The upper row (a, b) and lower row (c, d) represent the normal weight (BMI <25 kgm^2, n=8) and overweight (BMI >25 kgm^2, n=13) subgroups respectively. The broken line represents the regression line, and the R^2 represents the coefficient of determination.

7.4. Discussion

In this work, *Liver Size* is used to represent the 'functional' size of liver where drug elimination occurs. The results of this work suggest that total liver volume (*LV*) over-estimates the 'functional' *Liver Size* for overweight and obese individuals.

The mean *LV* value was 1535.0 (1225.0 – 1989.0) in the overweight group which was higher than the mean *LV* value of 1316.0 (1090.0 – 1610.0) mL in the normal weight group (Table 7.1). However, the mean (range) *LLV* values were not very different between these two groups, i.e. 1226.6 (1024.0 – 1594.3) mL and 1245.9 (1027.2 – 1527.4) mL in the overweight and the normal weight

groups, respectively. This implies the presence of substantial amounts of liver fat ($LFAT$) in the over-weight group which adds extra volume to the liver while the functional liver volume is only minimally affected. The calculated mean (range) $LFAT$ in the over-weight group was 29.3% (2.0 – 70.8) which was much higher than 8.2% (0 – 14.9%) $LFAT$ in the normal weight group. This indicates that the difference between these two descriptors of liver size (i.e. LV and LLV) is expected to be significantly larger in the over-weight individuals than their normal weight counterparts (see Figure 7.1 and Table 7.1). In this dataset, the median difference ($LV - LLV$) was 25% and 6% in the over-weight and the normal weight groups respectively.

Overall, LLV described about 36% of the variance of antipyrine CL in overweight patients which was about 2-fold higher than 17% variation that was described by LV (Figure 7.2c, Figure 7.2d) . In normal weight patients, both LV and LLV described the variance of CL to a similar extent as evidenced from 1.3 fold improvement in the R^2 value from 0.43 (against LV) to 0.58 (against LLV) (Figure 7.2a, Figure 7.2b). This implies that LV is less likely to represent 'functional' size of the liver particularly in overweight individuals (that includes obese) because of steatosis, and hence conventional approaches of scaling the hepatic intrinsic clearance by LV needs to be revisited with the proposed adoption of LLV as the predictor. Interestingly, approximately half of the variability in antipyrine CL in the normal weight group was described by fat-free mass (as the covariate of LLV) which is similar to other influential covariates (e.g. creatinine clearance for renally cleared drugs [242]. Importantly we see that the predictive performance of LLV as a covariate for CL was poorer in the overweight group than normal weight group which indicates that additional processes occur in the overweight group that are not described by $liver\ size$, which might potentially link back to changes in metabolic activity of oxidative enzymes.

Future IVIVE studies which include a range of drugs and a variety of populations (e.g. different ethnicities) are needed to validate the wide use of LLV in IVIVE studies.

PART V

DISCUSSION AND CONCLUSION

Chapter 8: Discussion and conclusions

8.1. Discussion

In this thesis, pharmacokinetic (PK) scaling methods using body size and composition were assessed. Total body weight (WT) is a widely-used measure of body size but fat-free mass (FFM) is increasingly used for PK scaling as it describes both body size and composition.

The traditional 'one size fits all' scheme of drug dosing has been consistently questioned in the literature [243-246] due to its implications on drug safety and effectiveness, and the scope of dose scaling has been well recognised in this regard [247, 248]. In this thesis, dose scaling refers to dose extrapolation from standard adults to differently sized groups of patients (i.e. children and the obese) based on differences in body size and/or composition. Dose scaling is most relevant for drugs that have a narrow therapeutic window, e.g. aminoglycosides [248, 249].

Dose scaling is aimed to achieve a target PK exposure, e.g. average steady state concentration ($C_{p,ss,avg}$) that has been proven to be efficacious in the standard population. The attainment of target PK exposure is a common strategy to scale the initial dose, which might be subjected to further adjustments based on other factors such as pharmacodynamics (PD) response(s) in the patient. Therefore, scaling of the initial dose is based on the underlying assumption that a similar exposure-effect relationship exists across the populations. Under this assumption, dose scaling (in this thesis) actually simplifies to scaling of pharmacokinetics (PK). This work has particularly focussed on maintenance dose scaling that is needed for chronic drug therapy. Hence, this work has particularly assessed the standard scaling methods of drug clearance (CL) using WT and FFM.

The first aim of the thesis was to assess the empirical ways of choosing the allometric exponent. Conventionally, allometric scaling refers to a less than proportional scaling of CL by WT, where use of an exponent of $3/4$ commonly used [61, 69]. On the other hand, the traditional 'mg/kg' dosing that is mostly practised in the clinic assumes a proportional scaling (i.e. exponent 1) of CL. Due to lack of

consensus over the right value of the exponent, it is empirically determined with the data either by choosing from the set of *a priori* values mentioned above or by estimating it. In either way, the accuracy of the empirically determined value of the exponent is limited by the study design. Therefore, choice of the allometric exponent should be supported by appropriate study design which has been addressed in Chapter 2.

Typical to the first approach, the exponent is chosen by comparing the model fits (e.g. AIC) of covariate models carrying possible *a priori* values (i.e. 0.67, 0.75, 1) and selecting the one that gives the lowest AIC value. However, this method risks choosing the wrong exponent. The fundamental flaw is that this method inherently assumes that the true exponent belongs to the tested set of *a priori* values, which may not be true as Calvier et al. [97] have indicated that the allometric exponent can range between 0.5 to 1.2. Even if such an assumption is made, it is still impossible to choose the true value in regular clinical pharmacology studies (less than 200 adults excluding children) that are often inadequately (<80%) powered. Under regular circumstances (with 40-60% BSV in CL), more than 250 adult participants are required to choose the correct exponent given the options of theory-based *allometric* scaling (0.75) and linear scaling (1) exponents. Furthermore, identification of the correct exponent from choices of theory-based *allometry* (0.75) and body surface area (BSA)-based scaling (0.67) is practically impossible with any sort of regular study design as it requires >1000 adult participants.

The second approach that empirically estimates the exponent has the advantage of not depending upon any *a priori* assumption. However, this method always carries the risk of over-estimating the exponent, particularly if the studies are under-powered. This is known as selection bias which was described for linear models by Ribbing et al. [56]. In this work, the bias in the estimated exponent is found to be directly (inversely) related to study power. The higher the study power the lower is the estimate bias, which means the higher is the chance of estimating the true exponent. Based on the simulation-estimation based analysis, a cut-off point of 80% power has been identified beyond which the bias in the estimate of exponent

becomes minimal. In this work, it is also shown that study power is positively related with the study design variables sample size, study population (i.e. covariate range) and BSV of CL. Therefore, further assessment was done to determine the minimal study design requirements that can ensure an optimal power of ≥80%.

Under regular circumstances (with 40% BSV in CL), it is possible to achieve the required power with about 100 adult participants without the need of including children in the study. The sample size requirement can be drastically cut down if children (>2 years of age) and adolescents are included in the study along with adults, and all age groups are stratified in equal proportions. As per the analysis, 10-20 participants under stratified design can minimise the bias below 10%. However, it has been also noted that such a low sample size may lead to imprecise estimate of the exponent. A sample size of about 50 participants including children and adolescents (stratified) appeared optimal for estimating the allometric exponent accurately and precisely. Notably, such a study design resemble regular clinical studies that include minors. Hence estimation of the *allometric* exponent appeared to be a reasonable approach to determine the scaling relationship between CL and WT.

Similar power requirement needs to be considered in case of empirical allometric scaling of CL by FFM. This is important since there is no consensus on the FFM exponent as well and it is often estimated empirically [250]. However, the exact study design requirement may be slightly different than WT based scaling to achieve the optimal power. While extrapolating the findings, the range of covariate needs to be considered in this case. In the WT based analysis it has been shown that the range of covariate values (i.e. WT) has a positive influence on the power. This explains the benefit of including children in the study cohort and a size of 50 participants were adequate to estimate the exponent. Since the range of FFM values would always be narrower than WT in the population the sample size requirement would be higher. This needs to be assessed in a separate analysis in the future.

Overall, the findings of Chapter 2 indicates that empirical estimation can be a good choice to determine the allometric exponent for body size and composition given the study design is optimal to achieve at least 80% power. In drug

development, the early phase (first in human to proof of concept) clinical trials typically recruit standard adult population (excluding children) and may not reach the required sample size of 100. Such studies are likely to be under-powered to estimate the exponent of body size and hence to estimate clearance. A biased estimate of the exponent can lead to biased prediction of CL if extrapolated to other sub-groups of population such as children and the obese that are studied at the post-approval stage. Therefore, estimation of the *allometric* exponent is not recommended in under-powered studies. For under-powered studies, it would be wise to use mechanistic approaches like IVIVE (as shown in Chapter 7) if data are available.

Although a theoretical value has been proposed for WT it is currently lacking for scaling by FFM. There is an expectation that CL scales with FFM linearly (i.e. exponent 1) since drug elimination almost exclusively occurs in the fat-free portion of body [25]. Some researchers believe that CL should be scaled in the obese by $FFM^{3/4}$ since it is equivalent to the theoretical allometric scaling with an additional correction for body composition [126, 199]. This is perhaps because *allometric* scaling conclusions were made on normal physiological considerations which does not include obesity. For example, the observed inter-species scaling of BMR was based on animals having normal body composition, since obese animals are outliers in nature. Noteworthy to mention that use of the 3/4 exponent in pharmacology was built on two phenomena: (1) inter-species scaling of basal metabolic rate (BMR) and (2) the theory of "quarter power law" proposed by West et al. [94]. However, there is limited evidence or support that can validate the universality of these phenomena (discussed below).

First, the exponent 3/4 was originally adopted from the observed inter-species scaling of BMR by using a 3/4 power to body weight [251], with the underlying assumption that drug clearance (CL) is proportional to BMR. However, there is no empirical evidence to support this assumption. BMR is a measure of the overall rate of endogenous metabolic processes (measured as oxygen consumption from samples of expired air [252]) that are active within the entire cellular mass of a human body at basal condition [253, 254]. On the other hand, CL is indicative of body's capacity of

eliminating xenobiotics by metabolism and/or excretion that are limited to the clearing organ(s) and further to a specific set of hepatocellular enzymes. Unlike BMR, CL does not merely represent the metabolic rate, and can be rate limited by a range of physiological variables such as liver blood flow (e.g. propanolol, lidocaine [62]), plasma protein binding (e.g. warfarin [255]), and active hepatocellular transport (e.g. atorvastatin [256, 257]). Therefore, proportionality between BMR and CL may not exist universally.

Secondly, the "quarter power" law was derived on an excellent theoretical framework that describes the rate of mass transfer across the branching vasculature (from aorta to capillary level) of mammalian cardio-vascular system. Notably, the key assumption of West's model was that the metabolic rate ("B") is proportional to volumetric flow rate ("Q"). Therefore, they actually determined the relationship between "Q" and body size ("M") to be scaled by 3/4 power (i.e. $Q = M^{3/4}$), and thus claimed that metabolic rate ("B") scales with $M^{3/4}$. The key assumption of $B \propto Q$ perhaps is suitable for describing the metabolism of endogenous substrates where the metabolic processes might be rate limited by the supply of fresh oxygenated blood. However, clearance of xenobiotics need not to be necessarily rate limited by their supply to the metabolically active cells of the clearing organ (e.g. liver), but can also be rate limited by clearing organ's intrinsic capacity (known as intrinsic clearance). In the case of xenobiotic metabolism, mid to high extraction drugs are likely to follow the former assumption, where as the low-extraction drugs are most likely to follow the latter assumption. Hence, whether the quarter power theory by West et al. is a universal approximation for drug CL is unclear. Even for high extraction drugs, the validity of theory based allometry in the obese is debatable. This is because the fractal analysis (by West et al.) for mammalian cardio-vascular system did not consider obese physiology, where pathological alterations in cardiac output [258] and peripheral blood flow (especially to the clearing organs [62, 259]) has been well documented.

Overall, there is a paucity in the knowledge of correct value of the exponent for scaling CL. In this context, the second aim was to find out a theoretical value of the allometric exponent for scaling CL by FFM. The findings of Chapter 6 suggests that the theoretical value should be 1 which indicates proportional scaling of CL by FFM. This relationship is particularly applicable for low-clearance drugs (hepatically cleared) where systemic CL approximates to hepatic intrinsic clearance (CL_{int,u_H}). This is of great importance because achieving low-extraction is one of the primary goals of drug discovery projects, in order to ensure less dose and dosing frequency in the clinic [108, 109]. Since functional liver size is a key determinant of the predictable part of the variation in CL_{int,u_H}, its relationship with FFM is expected to translate to CL vs. FFM relationship. Functional liver size should be best described by lean liver volume (LLV) as it excludes all liver fat that is present in substantial amount in most obese patients [79, 110, 111, 115]. The results suggest that LLV scales linearly with FFM.

Whether such linear scaling of CL by FFM would be applicable to moderate to high clearance drugs was not assessed in this thesis. Theoretically, CL of high clearance drugs approximates to hepatic blood flow which is assumed to be certain percentage (~25%) of cardiac output under regular circumstances [66]. Cardiac output is believed to scale with BSA, and thus BSA is conventionally used to scale liver blood flow [66]. Whether liver blood flow scales with FFM better than BSA is unknown. Likewise, how liver blood flow scales to FFM (i.e. the exponent) is also not known. Such mechanistic understanding might help better describe the scaling exponent of high clearance drugs by FFM.

However, scaling of CL of high clearance drugs may not be needed for the obese as has been shown in the literature. Studies of various high extraction drugs such as propanolol, verapamil, lidocaine, sufentanil, and paclitaxel did not show any statistical differences in CL between obese and non-obese individuals [62]. Since CL of these drugs approximates to liver blood flow, results of these studies indicate that hepatic blood flow remains unaltered in obesity. Obesity, with an otherwise normal heart function, increases cardiac output due to increased stroke volume and heart rate that causes increased perfusion to the tissues [112]. Obesity driven fatty

infiltration (steatosis) in the liver, at the same time, causes sinusoidal narrowing and decrease liver perfusion thereby. It has been postulated that as a results of these two opposing influences of obesity on liver, the hepatic blood flow remains unaltered [62] in obese.

The third aim of this thesis was to explore whether the expected proportional relationship between CL and FFM appears is evident empirically. This has been assessed by a model-based meta-analysis (MBMA) and described in Chapter 5. The MBMA only considered drugs that are preferentially cleared by liver and fall into the low-clearance category (<30 L/hr). The result suggests an estimated average exponent of 0.68 which is near to the BSA based scaling exponent 2/3. However, there was 45% variation in the exponent between drugs. This may be due to the variation in other factors (mostly unpredictable) such as protein binding and enzyme abundance which are poorly understood. Although the estimated value of 0.68 well aligns with the estimated average value of FFM exponent by McLeay et al. [60] there is limited evidence to support the similarity from theoretical perspective. This is because their analysis was based on a pooled dataset including different categories of drugs, e.g. low- and high clearance and hepatic and renal clearance, whereas we only considered low-clearance hepatically-cleared drugs.

In the classic 'top-down' approach, the accuracy of scaling CL by body size is very much dependent on the accuracy of choosing the allometric exponent. This thesis assessed how this traditional approach is limited by study design. An alternative approach that has been recently recommended involves the scaling of CL of the target population by *in vitro-in vivo* extrapolation (IVIVE) [112, 114, 232]. The utility of this approach has been particularly shown for selecting the initial dose for obese patients in clinical studies that are typically done at the post-approval stage. This involves the use of total liver volume (LV) as a scaler. However, this approach may result in the over-estimation of drug CL in obese individuals as LV may potentially over-represent functional liver size.

In this context, the fourth aim of this thesis was to assess the current standard of IVIVE for predicting CL in obese individuals. In particular, the potential of LLV was assessed in Chapter 7 in comparison to LV which is the current scaler for liver size. In IVIVE, accuracy of CL prediction largely depends on the accuracy of functional liver size prediction. Functional liver size represents the size of the liver that actively contributes to drug elimination, which excludes liver fat. More than 90% of obese patients have non-alcoholic fatty liver disease (NAFLD) [110, 111], where LV over-estimates the functional size due to the presence of substantial liver fat (steatosis). The analysis of the antipyrine dataset in Chapter 7 suggests that LLV is a better descriptor of functional liver size in the obese. This implies that LV over-estimated the functional liver size (i.e. LLV) by as much as 70% in the dataset (corresponding to the maximum %liver fat in Table 7.1 of Chapter 7:). The finding of high liver fat content is well aligned with several literature reports [79, 115, 218], where liver fat was measured in obese population by magnetic resonance imaging (MRI). Because of the better description of the functional liver size, LLV improved the correlation with antipyrine CL in the obese as compared to LV. However, further validation studies with larger datasets are required to adopt LLV in IVIVE based dose prediction in obese patients.

In practice, predictive models are preferred to avoid experimental methods of FFM measurement which are too resource intensive for regular use. These methods were described in Chapter 3: . The model developed by Janmahasatian et al. [102] is used extensively in clinical pharmacology because of its semi-mechanistic nature. However, a recent validation study reported by Srigiripura et al. [105] has shown that Janmahasatian's model over-predicts FFM in Indian population. This is expected since Jamahasatian's model was largely based on data that arose from individuals of European descent who potentially have different body composition from other populations, e.g. Indians [196]. In this context, the fifth aim of the thesis was to develop an extension of Janmahasatian's FFM model that accounts for the inter-ethnic difference in body composition wherever applicable. Another objective was to utilise the general extended model structure to develop an extended FFM model in individuals of Indian descent.

The structure of the extended FFM model was developed by incorporating a set of ethnicity specific parameters (Ψ) into the existing Janmahasatian model by relaxing the key assumption of the original model. The assumptions and model development have been described in detail in Chapter 4. The extended model was further used to estimate the Ψ parameters for Indians using a dataset of 100 adult Indian patients. The extended model needs further validation in Indian population, preferably covering a wide range of BMI. Since FFM is measure of body composition, mechanistic models are expected to account for all possible causal factors that are known to influence body composition. The extended FFM model, in this regard, gives the flexibility to account for the causal factors between relevant ethnicities, in terms of incorporating estimable correction parameters (Ψ) into the existing Janmahasatian's model. By this way, the extension of Janmahasatian's model potentially extends its applicability to other patient populations.

8.2. Limitations and future implications

The results of the simulation-estimation based work in Chapter 2 was based on a 'true' exponent 0.75. There was no intension to support or oppose the use of the theory based exponent (i.e. 0.75) in this work; the value was used just for the sake of simulation where any value could have been used.

In reality, however, the true exponent might vary, as pointed out by Calvier et al.[260]. A smaller value than 0.75 would indicate a smaller effect size than the current simulation scenarios. The smaller the effect size the larger would be the required sample size to achieve the required power (80%) of identifying WT as a statistically significant covariate. This is because the magnitude of the difference between the null (i.e. base model) and the alternative hypothesis (i.e. true exponent) would be smaller (than the current analysis) for a true value less than 0.75. On the other hand, a larger true value of the exponent would require a smaller sample size (than100 adults) to accurately estimate the exponent in regular clinical pharmacology studies. Therefore, additional analysis needs to be done using at least the minimum and the maximum possible values of allometric exponent (i.e. 0.5 and 1.20, as hypothesised by Calvier et al) as the 'true' values for simulation.

A simple one compartment unit model with IV bolus input was considered in the simulation-estimation analysis where only one parameter (i.e. CL) has a single covariate (i.e. WT). More complex situations might be expected in reality. For example, WT is often found as a covariate of volume of distribution (V) as well and CL can have multiple covariates in addition to WT (e.g. age). Moreover, in practice, multiple body size descriptors (e.g. WT, FFM, BSA) are tested during covariate model building and often provide reasonable model fit and this can potentially impact the power to select the best covariate and accurately estimate the exponent. Such considerations can further have influence on the minimum sample size requirements which are currently unknown based on this analysis. Therefore, such additional scenarios need to be tested in the future to more closely mimic clinical

studies. Further considerations such as oral dosing and correlation between parameters should also be incorporated.

The meta-analysis in Chapter 5 revealed disconnect between the theoretical (i.e. 1) and empirical (i.e. ~0.67) values of the exponent for scaling CL by FFM. However, the current meta-analysis may not be fully conclusive due to the lack of adequate power to estimate the exponent. This happened because a few studies in the literature have reported individual data of CL and FFM for low-clearance drugs. A more comprehensive analysis including more low-clearance drugs with a range of hepatic elimination mechanisms is needed to confirm the true exponent. Additional pooling of high-clearance drugs might be performed as well to check for its potential confounding effect on the empirical value of the exponent; this would also improve the study power to estimate the exponent.

The extended Janmahasatian model developed in Chapter 4 needs to be validated with an external FFM dataset in Indian population, preferably with a wide range of BMI. This should also be accompanied with a comparison of the predictions from the original Janmahasatian's model and the Kulkarni's model which was developed in Indians. Such comparative validation would help confirm the applicability of the extended FFM model. Model extension can also be considered for other ethnicities as well (e.g. pacific islanders), where significant alteration in body composition has been documented [104, 196].

The potential application of LLV model in IVIVE of CL in the obese has been briefly examined in Chapter 7. This work is limited by the small dataset which includes one model drug, antipyrine. Future efforts should be made in validating the LLV's application by using *in vitro* and *in vivo* data of drugs that cover a range of mechanisms of hepatic elimination, e.g. different CYP isoforms.

Further to it, applicability of LLV may be restricted to obese patients who are at the early stages of fatty liver disease (NAFLD). The current study population (in Chapter 6) most likely represent the early stage NAFLD patients, since there was no evidence of structural and functional abnormality in their livers as demonstrated by

their normal ultra-sonography scan and normal liver function test results. In advanced fibro-inflammatory stages of NAFLD (i.e. Non-alcoholic steatohepatitis to cirrhosis), substantial hepatocellular loss occurs due to tissue necrosis which is replaced by scar tissue (i.e. collagen). These scar tissues are not metabolically active. Therefore, in advanced NAFLD patients, LLV may not represent the true functional liver size and may potentially over-estimate hepatic CL if used for IVIVE.

Overall, the choice of exponent of body size should be made based on the targeted population (Figure 8.1). If dose scaling is meant for patients within standard body size range, the traditional 'mg/kg' dosing that underpins linear scaling of CL by WT appears to be no different than allometric scaling that assumes a non-linear scaling of CL (see Figure 2.6 and Figure 2.7). Apart from the exponent, the choice of scaler itself (i.e. WT vs. FFM) would hardly influence the predictions in this population, since scaling by FFM would be equivalent to a less than proportional scaling (i.e. non-linear) by WT. Hence, considering the complexity of mathematical calculations associated with allometric scaling and/or FFM prediction, the traditional 'mg/kg' dosing appears an acceptable method of dose scaling in the standard population.

On the other hand, choice of scaling method becomes critical when dose scaling is intended for a differently sized population such as obese or children. When CL is extrapolated outside the standard body size range, a wrong choice of exponent of WT can cause deviation in CL (from true value) as high as 2-fold and 4-fold in obese and children (≥3 years of age) respectively (see Figure 1.6). Since there is no consensus on the true value of the exponent, a reasonable approach would be to estimate the value from an adequately powered (at least 80%) study. Studies with a minimum of 100-200 adult participants within standard body size range appears to be sufficiently powered to accurately estimate the exponent. Such design typically resembles phase 2b to phase 3 studies under standard drug development regime. However, most of the post-approval clinical pharmacology studies might be limited by sample size (hence power). For those studies, inclusion of children and adolescents can help achieve the required power with sample size as low as 10-50;

otherwise, pooling of studies might be another alternative. The empirical approach should also be considered when FFM is used as the scaler in order to account for body composition. This is because a linear scaling by FFM (as per the expectation) has been confounded by the empirical values of the exponent that suggest a less than proportional scaling. Since, within the standard population, FFM varies similar fold to that of WT, a similar sample size requirement of 100-200 would also be required to estimate the exponent of FFM. Hence, this general study design requirement (to achieve power) applies to both the chosen size scalers and needs to be considered irrespective of the mechanism of elimination of the drug.

For under-powered studies (that do not meet the above design criteria), an alternative 'bottom-up' approach can be considered at least for hepatically eliminated drugs, where CL is scaled by IVIVE. Particularly, for non-flow dependent drugs, the accuracy of IVIVE scaled CL in differently sized population would largely depend on the accuracy of scaling the 'functional' liver size in the target population. At least for obese, it has been shown that LLV is potentially a better descriptor of the 'functional' liver size than LV, which needs further evaluation. However, scaling of 'functional' liver size in children was not subject to assessment in this thesis. For flow dependent drugs, the key would be to understand the scaling of liver blood flow with body size, which was not assessed in this work. At least for obese, a general hypothesis is that liver blood flow remains unaltered (in spite of increased cardiac output) due to sinusoidal narrowing and/or increased peripheral resistance, which renders CL of flow-dependent drugs unaffected [62]. If IVIVE cannot be readily applied (e.g. renally cleared drugs, lack of data), an alternative approach could be to scale CL using a fixed exponent that appropriately supports the biology. For example, if there is evidence that GFR is proportional to renal blood flow, and blood flow scales to $WT^{3/4}$ (as shown for cardiac output by West et al. [94]), then an exponent of 0.75 can be a possible choice. Alternatively, if there is evidence that GFR scales to FFM linearly [65], then linear scaling of CL by FFM can be a choice. Similar scaling relationship of (hepatic) blood flow and WT can also be considered for choosing the fixed exponent for high extraction drugs, if presence of any confounding physiological effects (e.g. sinusoidal narrowing) are least expected in

the target population. Therefore, if a fixed exponent needs to be used, the choice of its value should be justified by *a priori* knowledge of the biology, which was not subject to assessment in this thesis.

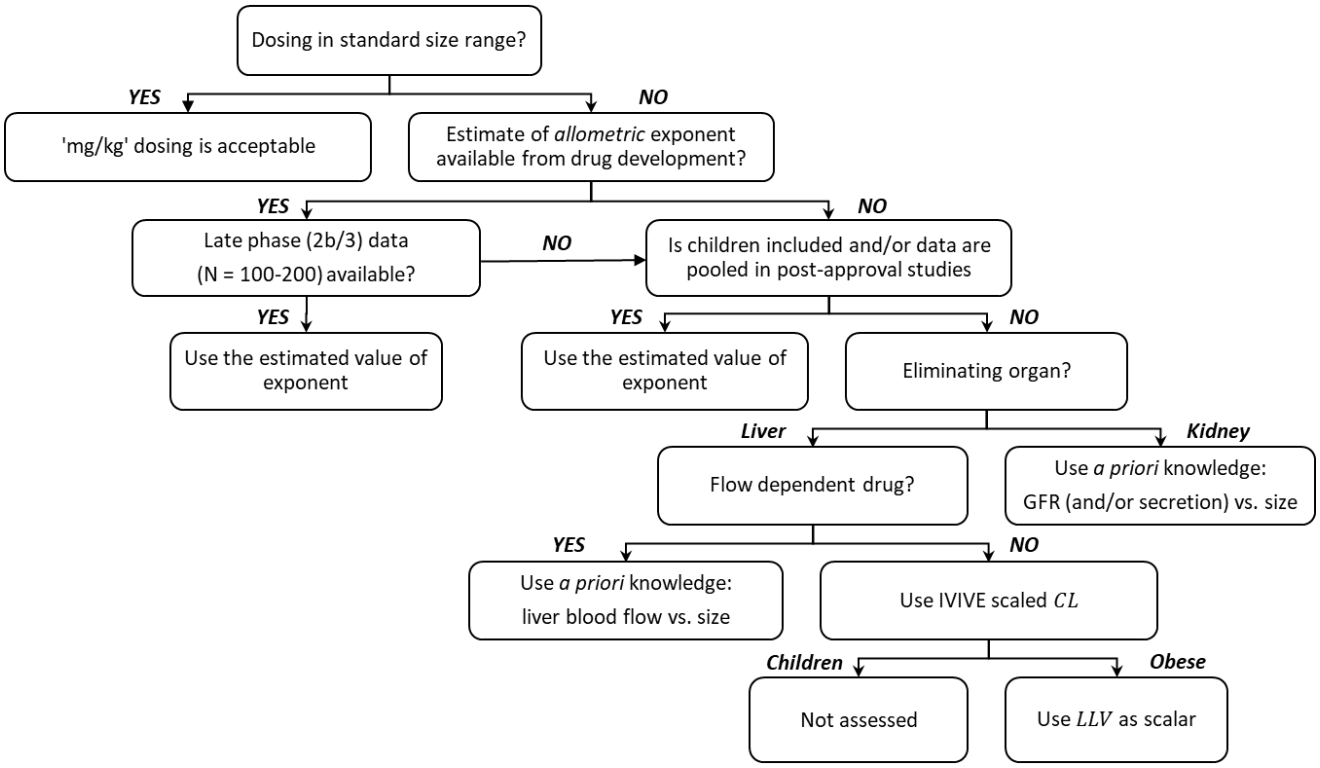

Figure 8.1 Flow chart for guiding the selection of dose scaling method in clinical practice

8.3. Conclusions

In this thesis, methods of scaling drug clearance (CL) using body size (i.e. WT) and composition (i.e. FFM) were assessed. When scaling CL by WT in typical clinical pharmacology studies, the selection of the allometric exponent from a set of plausible *a priori* values (e.g. $2/3$, $3/4$) can potentially lead to biased prediction of CL. Alternatively, accurate estimation of the exponent is possible provided that the study is adequately (>80%) powered. Studies consisting of only adults or studies that additionally include children and adolescents can accurately estimate the allometric exponent with a minimum of 100 or 10 participants respectively.

For studies that do not meet the required design (i.e. inadequately powered), fixing the exponent to a biologically plausible value would be appropriate. This also applies to the use of FFM. For scaling CL by FFM, the theoretical value is found to be 1 in this thesis, which has been determined via modelling the relationship between lean liver volume (LLV) and FFM. However, a meta-analysis of published individual data has estimated this exponent to be $2/3$, which is equivalent to body surface area (BSA) based scaling.

The theoretical value of the allometric exponent for FFM based scaling remains inconclusive. Therefore, a 'bottom-up' approach using *in vitro-in vivo* extrapolation (IVIVE) of CL might be a reasonable alternative for initial dose scaling. For dose scaling particularly in obese patients, the accuracy of IVIVE scaled CL would depend on the accuracy of the descriptor of 'functional' liver size. This work has shown that LLV is a more accurate descriptor of 'functional' liver size than total liver volume (LV) particularly in the obese. Therefore, LLV has a potential use in IVIVE based scaling of CL and can help the selection of the initial dose for studies that include obese patients.

Finally, an extended FFM model based on the commonly used Janmahasatian's model was developed and shown to predict FFM in patients of Indian descent. The

general structure of the extended FFM model can be used to develop ethnicity-specific FFM models in other populations as well, in the future.

APPENDICES

ADDITIONAL MATERIALS OF THE CHAPTERS

Appendix 1: Additional material for Chapter 2

A1.1. Results of Objective 1 and Objective 2 with additional populations

The results under objective 1 and 2 including two additional populations i.e. A_{all} and B_{all} along with the population A and B of the main text have been shown in Table A1.1 and Table A1.2 (i.e. extension to the Table 2.5 and Table 2.6 respectively of the main text). Population A_{all} and B_{all} represent adults including obese (i.e. all-comer adults) and unstratified cohorts of population B. Looking at tables, it is evident that stratification of study cohort based on age groups of the population B did not improve the power as compared to its all-comer counterpart (B_{all}). Although inclusion of obese patients in the study (A_{all}) theoretically improves the power compared to the population A (excluding obese) the results of the obese population may not be valid in reality. The use of 0.75 and 0.67 in scaling of clearance (CL) originated on the grounds that basal metabolic rates across normal-weighted species can be scaled by $(WT)^{3/4}$ [93, 94, 116-118] or by $(WT)^{2/3}$ [92, 123, 124]. Notably, the concept of allometry was developed to scale for physiologically mature normal body size (on the basis that obese animals in nature are uncommon) and not for body composition. Hence, the use of allometric scaling in obese is not fundamentally supported [126]. The use of linear scaling in obese is also not supported biologically since CL is not anticipated to correlate linearly with the additional WT gained due to excess adiposity which contributes little to the CL. Hence, there is no evidence for the existence of a general scaling factor in obesity based on WT that is biologically plausible. The results of this work are not anticipated to be applicable if obese participants are included in the study and a different size metric (e.g. fat-free mass [25, 60, 91, 103, 106, 107, 137]) that appears biologically more plausible should be considered.

Table A1.1 The N_{80} values at all scenarios calculated by linear interpolation

True	Population	False								
		20% BSV			40% BSV			60% BSV		
		0.67	0.75	1	0.67	0.75	1	0.67	0.75	1
0.67	A	NA	760	50	NA	>1000	170	NA	>1000	390
	A_{all}		470	30		>1000	100		>1000	220
	B		70	10		200	20		500	40
	B_{all}		80	<10		230	20		560	40
0.75	A	750	NA	80	>1000	NA	310	>1000	NA	660
	A_{all}	390		50	990		170	>1000		400
	B	90		10	370		30	830		60
	B_{all}	90		10	360		30	820		60
1	A	40	70	NA	150	260	NA	360	680	NA
	A_{all}	30	50		90	160		200	360	
	B	10	10		20	40		50	80	
	B_{all}	<10	10		20	40		50	70	

N_{80} values were rounded off to nearest 10's multiple, NA not applicable

Table A1.2 Summary of power (%) and estimate bias (%) in all scenarios

Population	N	20% BSV		40% BSV		60% BSV	
		Power (%)	Bias (%)	Power (%)	Bias (%)	Power (%)	Bias (%)
A	10	46	39	21	115	15	193
	20	73	14	31	75	18	145
	50	98	2	63	26	35	65
	100	100	0	87	5	55	27
	200	100	1	99	1	85	7
	500	100	0	100	0	100	0
	1000	100	0	100	0	100	0
A_{all}	10	62	22	27	91	18	165
	20	87	5	44	43	25	92
	50	100	-1	78	8	46	37
	100	100	1	98	2	78	11
	200	100	0	100	0	97	1
	500	100	1	100	1	100	1
	1000	100	1	100	1	100	1
B	10	100	0	81	8	53	27
	20	100	0	97	0	79	9
	50	100	-1	100	-1	99	-2
	100	100	-1	100	-1	100	-2
	200	100	0	100	-1	100	-1
	500	100	0	100	0	100	0
	1000	100	0	100	-1	100	-1
B_{all}	10	96	0	76	10	51	29
	20	100	-1	96	-1	77	8
	50	100	0	100	0	99	0
	100	100	-1	100	-1	100	-1
	200	100	0	100	-1	100	-1
	500	100	0	100	0	100	0
	1000	100	0	100	-1	100	-1

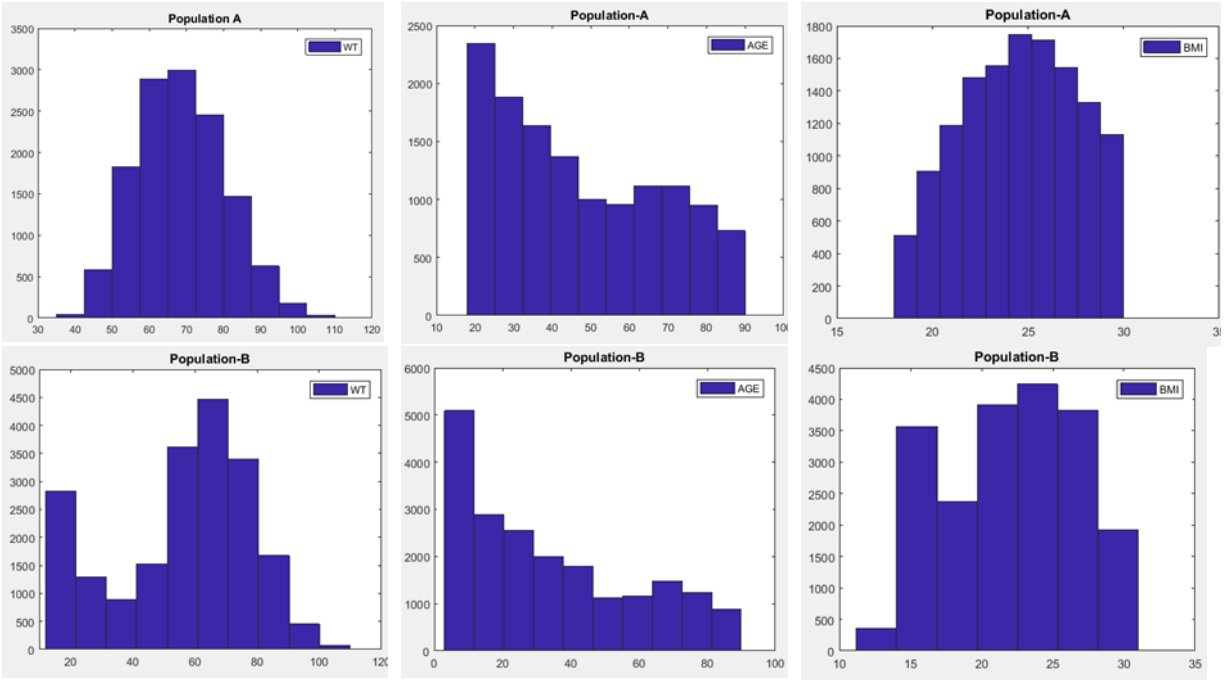

Figure A1.1 Distributions of the covariates in the populations used in the simulation

A1.2. MATLAB simulation-estimation code for Objective 1:

Sim-Est code 1:

Consider changing the details of following BLOCKS as required before run

```
BLCOK-1: Change the simulation setting as per the specific scenario
BLCOK-3: Change the database name and column#
BLOCK-8: Change the path of NONMEM .bat file and .ctl file name.
Importantly, change the exponent values within the .ctl files
according
to the simulation scenarios below:
if EXP = 0.67, then false1 = 0.75 and false2 = 1
if EXP = 0.75, then false1 = 0.0.67 and false2 = 1
if EXP = 1, then false1 = 0.75 and false2 = 0.67
BLOCK-9 & 11: Change the path of .smy files
```

Set up environment

```
clear all
clc
tic
```

BLOCK-1: Simulation setting

```
NSUB = 100;         % sample size
EXP = 0.75;         % true exponent
SD_ETA = 0.4;       % SD of ETA (log-normal)
```

BLOCK-2: Default setting

```
NREP = 1000;                                % number of replicates
V  = 1;                                     % standard volume
CL = 0.693;                                 % standard clearance
dose = 1 ;                                  % unit dose
trange = [0; 0.25; 0.5; 1; 3; 5];           % sampling schedule
AUC= dose/CL;                               % standard AUC
C_ave = AUC/max(trange);                    % average concentration
SD_EPS1 = 0.1;                              % SD of EPS1 (exponential
error)
SD_EPS2 = 0.1*C_ave;                        % SD of EPS2 (additive
error),i.e. 10% of average concentration
```

BLOCK-3: Reads covariate database (e.g. population A or B)

```
[NUM,TXT,RAW] = xlsread('population-A.xls');  % reads NHANES data
weight = NUM(:,4);                           % define the column#
of WT (here 4th column)
```

BLOCK-4: Defines vectors

```
count_all1 = [];                            % data vector-1 for all
success records
count_all2 = [];                            % data vector-2 for all
success records
```

BLOCK-5: Loop for sim-est of NREP=1000 replicates

```
for j=1:NREP
    rng(j);                                 % sets the seed
```

BLOCK-6: Below loop repeats the sim-est steps if any NONMEM estimation is aborted (i.e. no objective function value is obtained)

```
    for m = 1:1000
```

BLOCK-7: Generates NONMEM input file (.csv)

```
  %Below loop generates dataset for NONMEM input and stores in "data_rep"

   WT = datasample(weight,NSUB);            % random covariate
```

```
sampling
   ETA = 0+ SD_ETA.*randn(NSUB,2);            % ETA vectors for CL and V
   data_rep = [];                             % vector for NONMEM input

for i = 1:NSUB
   CLi = CL *(WT(i,1)/70)^EXP * exp(ETA(i,1));   % ith subject's CL
   Vi = V * exp(ETA(i,2));                    % ith subject's V
   Ci = [];                                   % vector for ith subject's conc.

 for t = 1:length(trange)                     % loop for every time point
   Ct = (dose/Vi)*exp((-CLi/Vi)*trange(t,1));    % conc. at each time point
   Ci = [Ci; Ct];
 end

   DV =[];                                    % DV vector for ith subject

   % Below loop adds residual error to ith subject's conc. and stores in DV

 for t = 1:length(trange)                     % loop for every time point
   EPS1 = 0+ SD_EPS1.*randn(1,1);             % generate EPS1
   EPS2 = 0+ SD_EPS2.*randn(1,1);             % generate EPS2

   if t==1
      C_obs= 0;                               % observed conc.
   else C_obs = Ci(t,1)*exp(EPS1)+ EPS2;
   end

   DV =[DV;C_obs];

 end

  AMT = [dose; zeros(length(trange)-1,1)];      % generate dose column
  MDV = [1;zeros(length(trange)-1,1)];          % generate MVD
```

```
column

   % Below functions creates ith individual's dataset and adds into
"data_rep"

   data_ind =
[repmat(i,length(trange),1),trange,DV,AMT,MDV,repmat(WT(i,1),length(
trange),1)];
   data_rep =[data_rep; data_ind];

end
    csvwrite('input.csv',data_rep);     % creates NONMEM input file
in .csv format
```

BLOCK-8: Estimation

```
    %Below functions call NONMEM .ctl files sequentially saved in
the same folder to estimate using 'input.csv'
    %For example, .ctl files for true, false1 and false2 models are
saved as
    %"est_true.ctl", "est_false1.ctl" and "est_false2.ctl"

    !C:\NONMEM_7.2.0_For_Desktop\nm720\nm7\bin\wfn.bat gf reg & nmgo
est_true.ctl;
    !C:\NONMEM_7.2.0_For_Desktop\nm720\nm7\bin\wfn.bat gf reg & nmgo
est_false1.ctl;
    !C:\NONMEM_7.2.0_For_Desktop\nm720\nm7\bin\wfn.bat gf reg & nmgo
est_false2.ctl;
```

BLOCK-9: Picks up Objective function values

```
% Below functions pick up the respective OFVs from .smy files of NONMEM outputs

NM_output = fopen('D:\Projects\AllomScaling\est_true.reg\est_true.smy');
A = textscan(NM_output,'%s','delimiter','');
B = str2mat(A{1,1}(2,1));
C = sscanf(B,'%f');
if prod(size(C))== 1
OFV_true = 'NaN';
else OFV_true =C(2,1);
```

```
end
    fclose(NM_output);

    NM_output =
fopen('D:\Projects\AllomScaling\est_false1.reg\est_false1.smy');
    A = textscan(NM_output,'%s','delimiter','');
    B = str2mat(A{1,1}(2,1));
    C = sscanf(B,'%f');
    if prod(size(C))== 1
    OFV_false1 = 'NaN';
    else OFV_false1 =C(2,1);
    end
    fclose(NM_output);

    NM_output =
fopen('D:\Projects\AllomScaling\est_false2.reg\est_false2.smy');
    A = textscan(NM_output,'%s','delimiter','');
    B = str2mat(A{1,1}(2,1));
    C = sscanf(B,'%f');
    if prod(size(C))== 1
    OFV_false2 = 'NaN';
    else OFV_false2 =C(2,1);
    end
    fclose(NM_output);
```

BLOCK-10: Ensures avoiding aborted NONMEM runs

```
    % Below 'if-else' statements ensure to repeat the simulaion-
estimation
    % steps if any NONMEM run is aborted

 if OFV_true== 'NaN';
    continue
elseif OFV_false1== 'NaN';
    continue
elseif OFV_false2== 'NaN';
    continue
else
    break
 end

    end
```

BLOCK-11: Post-estimation analysis

```
    count1 = OFV_true<OFV_false1;
    count2 = OFV_true<OFV_false2;
    count_all1 = [count_all1;count1];
    count_all2 = [count_all2;count2];

end
```

BLOCK-12: Calculates power out of 1000 replicates

```
    power1 = sum(count_all1)*100/NREP;
    power2 = sum(count_all2)*100/NREP;
    result = [power1,power2];
    csvwrite('result.csv',result);        % result is generated in
.csv file

    toc
```

Published with MATLAB® R2017a

A1.3. MATLAB simulation-estimation code for Objective 2:

Sim-Est code 2:

Consider changing the details of following BLOCKS as required before run

```
BLCOK-1: Change the simulation setting as per the specific scenario
BLCOK-3: Change the database name and column #
BLOCK-8: Change the path of NONMEM .bat file and .ctl file name
BLOCK-9 & 11: Change the path of .smy and .smr files
```

Set up environment

```
clear all
clc
tic
```

BLOCK-1: Simulation setting

```
NSUB = 100;          % sample size
EXP = 0.75;          % true exponent
SD_ETA = 0.4;        % SD of ETA (log-normal)
```

BLOCK-2: Default setting

```
NREP = 1000;                % number of replicates
V  = 1;                  % standard volume
CL = 0.693;                 % standard clearance
```

```
dose = 1 ;                                  % unit dose
trange = [0; 0.25; 0.5; 1; 3; 5];           % sampling schedule
AUC= dose/CL;                               % standard AUC
C_ave = AUC/max(trange);                    % average concentration
SD_EPS1 = 0.1;                              % SD of EPS1 (exponential
error)
SD_EPS2 = 0.1*C_ave;                        % SD of EPS2 (additive
error),i.e. 10% of average concentration
```

BLOCK-3: Reads covariate database (e.g. population A or B)

```
[NUM,TXT,RAW] = xlsread('population-A.xls');  % reads NHANES data
weight = NUM(:,4);                            % define the column#
of WT (here 4th column)
```

BLOCK-4: Defines vectors

```
count_all = [];                             % data vector
EXP_est_all = [];                           % data vector
EXP_est_all_discard = [];                   % data vector
```

BLOCK-5: Loop for sim-est of NREP=1000 replicates

```
for j=1:NREP
    rng(j);                                 % sets the seed
```

BLOCK-6: Below loop repeats the sim-est steps if any NONMEM estimation is aborted (i.e. no objective function value is obtained)

```
    for m = 1:1000
```

BLOCK-7: Generates NONMEM input file (.csv)

```
  %Below loop generates dataset for NONMEM input and stores in "data_rep"

  WT = datasample(weight,NSUB);      % random covariate sampling
  ETA = 0+ SD_ETA.*randn(NSUB,2);    % ETA vectors for CL and V
  data_rep = [];                % vector for NONMEM input
```

```
for i = 1:NSUB
   CLi = CL *(WT(i,1)/70)^EXP * exp(ETA(i,1));   % ith subject's CL
   Vi = V * exp(ETA(i,2));                    % ith subject's V
   Ci = [];                              % vector for ith subject's conc.

 for t = 1:length(trange)                  % loop for every time point
   Ct = (dose/Vi)*exp((-CLi/Vi)*trange(t,1));    % conc. at each time point
   Ci = [Ci; Ct];
 end

   DV =[];                               % DV vector for ith subject

   % Below loop adds residual error to ith subject's conc. and stores in DV

 for t = 1:length(trange)                  % loop for every time point
   EPS1 = 0+ SD_EPS1.*randn(1,1);            % generate EPS1
   EPS2 = 0+ SD_EPS2.*randn(1,1);            % generate EPS2

   if t==1
      C_obs= 0;                          % observed conc.
   else C_obs = Ci(t,1)*exp(EPS1)+ EPS2;
   end

   DV =[DV;C_obs];

 end

  AMT = [dose; zeros(length(trange)-1,1)];      % generate dose column
  MDV = [1;zeros(length(trange)-1,1)];         % generate MVD column

  % Below functions creates ith individual's dataset and adds into "data_rep"

  data_ind =
```

```
[repmat(i,length(trange),1),trange,DV,AMT,MDV,repmat(WT(i,1),length(
trange),1)];
   data_rep =[data_rep; data_ind];

end
    csvwrite('input.csv',data_rep);     % creates NONMEM input file
in .csv format
```

BLOCK-8: Estimation

```
    %Below functions call NONMEM .ctl files sequentially saved in
the same folder to estimate using 'input.csv'
    %For example, .ctl files for base and covariate models are saved
as
    %"est_base.ctl" and "est_cov.ctl"

    !C:\NONMEM_7.2.0_For_Desktop\nm720\nm7\bin\wfn.bat gf reg & nmgo
est_base.ctl;
    !C:\NONMEM_7.2.0_For_Desktop\nm720\nm7\bin\wfn.bat gf reg & nmgo
est_cov.ctl;
```

BLOCK-9: Picks up Objective function values

```
% Below functions pick up the respective OFVs from .smy files of NONMEM outputs

NM_output = fopen('D:\Projects\AllomScaling\est_base.reg\est_base.smy');
A = textscan(NM_output,'%s','delimiter','');
B = str2mat(A{1,1}(2,1));
C = sscanf(B,'%f');
if prod(size(C))== 1
OFV_base = 'NaN';
else OFV_base =C(2,1);
end
fclose(NM_output);

NM_output = fopen('D:\Projects\AllomScaling\est_cov.reg\est_cov.smy');
A = textscan(NM_output,'%s','delimiter','');
B = str2mat(A{1,1}(2,1));
C = sscanf(B,'%f');
```

```
if prod(size(C))== 1
    OFV_base = 'NaN';
    else OFV_cov =C(2,1);
    end
    fclose(NM_output);
```

BLOCK-10: Ensures avoiding aborted NONMEM runs

```
    % Below if else statements ensure to repeat the simulaion-
estimation
    % steps if any NONMEM run is aborted

 if OFV_base== 'NaN';
    continue
elseif OFV_cov== 'NaN';
    continue
else
    break
 end
```

```
    end
```

BLOCK-11: Post-estimation analysis

Below function picks up the estimate of EXP from .smr file

```
NM_output = fopen('D:\Projects\AllomScaling\est_cov.reg\est_cov.smr');
A = textscan(NM_output,'%s','delimiter','');
B = str2mat(A{1,1}(5,1));
D = B(1,12:35);
E = sscanf(D,'%f');
EXP_est = E(2,1);
fclose(NM_output);

 % Below function does log-likelyhood ratio test

LLR = OFV_base - OFV_cov;
count = LLR > 3.84;
count_all = [count_all;count];

 % Below functions ensure that only the significantly different exponent estimates(LLR > 3.84)are
considered for bias calculation
```

```
if count == 1
        EXP_est_all = [EXP_est_all; EXP_est];
    else
        EXP_est_all_discard = [EXP_est_all_discard; EXP_est];
    end
end
```

BLOCK-12: Calculates power & bias and percentiles of exponent estimates out of 1000 replicates

```
    power = sum(count_all)*100/NREP;
    bias = (median(EXP_est_all)- EXP)*100/EXP;
    result = [power,bias, quantile(EXP_est_all,[0.025 .50 0.975])];
    csvwrite('result.csv',result);           % result is generated
in .csv file

    toc
```

Published with MATLAB® R2017a

A1.4. NONMEM codes for Objective 1:

A1.4.1. Code for 'est_true.ctl' file (called from Sim-Est code-1 of MATLAB)

```
; To fit the Matlab simulated data (input.csv) using true covariate model

$PROB Allom Scaling-Objective 1
$INPUT ID TIME DV AMT MDV WT
$DATA ..\input.csv IGNORE=#
$SUBR ADVAN1 TRANS2

$PK
  TVCL=THETA(1)*(WT/70)**0.75     ;covariate model
  TVV=THETA(2)
  CL=TVCL*EXP(ETA(1))             ;BSV model
  V=TVV*EXP(ETA(2))               ;BSV model
  S1=V                            ;scale conc.

$ERROR
  Y=F*EXP(EPS(1))+EPS(2)          ; combined error

$THETA
  (0.1,0.693)                     ; CL
  (0.01,1)                        ; V

$OMEGA
  0.1                             ; PPVCL
  0.1                             ; PPVV

$SIGMA
  0.01                            ; RUVPROP
  0.01                            ; RUVADD

$EST MAX=9990 SIG=5 PRINT=1 METHOD=1 INTERACTION NOABORT
```

A1.4.2. Code for 'est_false1.ctl' file (called from Sim-Est code-1 of MATLAB)

```
; To fit the Matlab simulated data (input.csv) using false1 covariate model

$PROB Allom Scaling-Objective 1
$INPUT ID TIME DV AMT MDV WT
$DATA ..\input.csv IGNORE=#
$SUBR ADVAN1 TRANS2

$PK
  TVCL=THETA(1)*(WT/70)**0.67     ;covariate model
  TVV=THETA(2)
  CL=TVCL*EXP(ETA(1))             ;BSV model
  V=TVV*EXP(ETA(2))               ;BSV model
  S1=V                            ;scale conc.

$ERROR
  Y=F*EXP(EPS(1))+EPS(2)          ;combined error

$THETA
  (0.1,0.693)                     ; CL
  (0.01,1)                        ; V

$OMEGA
  0.1                             ; PPVCL
  0.1                             ; PPVV

$SIGMA
  0.01                            ; RUVPROP
  0.01                            ; RUVADD

$EST MAX=9990 SIG=5 PRINT=1 METHOD=1 INTERACTION NOABORT
```

A1.4.3. Code for 'est_false2.ctl' file (called from Sim-Est code-1 of MATLAB)

```
;To fit the Matlab simulated data (input.csv) using false2 covariate model
$PROB Allom Scaling-Objective 1
$INPUT ID TIME DV AMT MDV WT
$DATA ..\input.csv IGNORE=#
$SUBR ADVAN1 TRANS2

$PK
  TVCL=THETA(1)*(WT/70)          ;covariate model
  TVV=THETA(2)
  CL=TVCL*EXP(ETA(1))            ;BSV model
  V=TVV*EXP(ETA(2))              ;BSV model
  S1=V                           ;scale conc.

$ERROR
  Y=F*EXP(EPS(1))+EPS(2)         ;combined error

$THETA
  (0.1,0.693)                    ; CL
  (0.01,1)                       ; V

$OMEGA
  0.1                            ; PPVCL
  0.1                            ; PPVV

$SIGMA
  0.01                           ; RUVPROP
  0.01                           ; RUVADD

$EST MAX=9990 SIG=5 PRINT=1 METHOD=1 INTERACTION NOABORT
```

A1.5. NONMEM codes for Objective 2:

A1.5.1. Code for 'est_base.ctl' file (called from Sim-Est code-2 of MATLAB)

```
;To fit the Matlab simulated data (input.csv) using base model
$PROB Allom Scaling-Objective 2
$INPUT ID TIME DV AMT MDV WT
$DATA ..\input.csv IGNORE=#
$SUBR ADVAN1 TRANS2

$PK
  TVCL=THETA(1)
  TVV=THETA(2)
  CL=TVCL*EXP(ETA(1))          ;BSV model
  V=TVV*EXP(ETA(2))            ;BSV model
  S1=V                         ;scale conc.

$ERROR
  Y=F*EXP(EPS(1))+EPS(2)       ;combined error

$THETA
  (0.1,0.693)                  ; CL
  (0.01,1)                     ; V

$OMEGA
  0.1                          ; PPVCL
  0.1                          ; PPVV

$SIGMA
  0.01                         ; RUVPROP
  0.01                         ; RUVADD

$EST MAX=9990 SIG=5 PRINT=1 METHOD=1 INTERACTION NOABORT
```

A1.5.2. Code for 'est_cov.ctl' file (Sim-Est code-2 of MATLAB)

```
;To fit the Matlab simulated data (input.csv) using covariate model to estimate exponent
$PROB Allom Scaling-Objective 2
$INPUT ID TIME DV AMT MDV WT
$DATA ..\input.csv IGNORE=#
$SUBR ADVAN1 TRANS2

$PK
  TVCL=THETA(1)*(WT/70)**THETA(2)          ;covariate model
  TVV=THETA(3)
  CL=TVCL*EXP(ETA(1))                      ;BSV model
  V=TVV*EXP(ETA(2))                        ;BSV model
  S1=V                                     ;scale conc.

$ERROR
  Y=F*EXP(EPS(1))+EPS(2)                   ;combined error

$THETA
  (0.1,0.693)                              ; CL
  (0.01,1)                                 ; EXP
  (0.01,1)                                 ; V

$OMEGA
  0.1                                      ; PPVCL
  0.1                                      ; PPVV

$SIGMA
  0.01                                     ; RUVPROP
  0.01                                     ; RUVADD

$EST MAX=9990 SIG=5 PRINT=1 METHOD=1 INTERACTION NOABORT
```

Appendix 2: Additional material for Chapter 3

A2.1. Derivation of Eq 3.6 in the main text

$$\frac{BM}{\rho_{BM}} = \frac{BM \times f_{FM}}{\rho_{FM}} + \frac{BM \times f_{FFM}}{\rho_{FFM}}$$

$$\frac{1}{\rho_{\mathrm{BM}}} = \frac{f_{\mathrm{FM}}}{\rho_{\mathrm{FM}}} + \frac{f_{\mathrm{FFM}}}{\rho_{\mathrm{FFM}}}$$

$$\frac{1}{\rho_{\mathrm{BM}}} = \frac{f_{\mathrm{FM}}}{\rho_{\mathrm{FM}}} + \frac{1 - f_{\mathrm{FM}}}{\rho_{\mathrm{FFM}}}$$

$$\frac{1}{\rho_{\mathrm{BM}}} = \frac{f_{\mathrm{FM}} \times \rho_{\mathrm{FFM}} + \rho_{\mathrm{FM}} \times (1 - f_{\mathrm{FM}})}{\rho_{\mathrm{FM}} \times \rho_{\mathrm{FFM}}}$$

$$\frac{1}{\rho_{\mathrm{BM}}} = \frac{f_{\mathrm{FM}} \times \rho_{\mathrm{FFM}} + \rho_{\mathrm{FM}} - \rho_{\mathrm{FM}} \times f_{\mathrm{FM}}}{\rho_{\mathrm{FM}} \times \rho_{\mathrm{FFM}}}$$

$$\frac{1}{\rho_{\mathrm{BM}}} = \frac{f_{\mathrm{FM}} \times (\rho_{\mathrm{FFM}} - \rho_{\mathrm{FM}}) + \rho_{\mathrm{FM}}}{\rho_{\mathrm{FM}} \times \rho_{\mathrm{FFM}}}$$

$$\frac{\rho_{\mathrm{FM}} \times \rho_{\mathrm{FFM}}}{\rho_{\mathrm{BM}}} = f_{\mathrm{FM}} \times (\rho_{\mathrm{FFM}} - \rho_{\mathrm{FM}}) + \rho_{\mathrm{FM}}$$

$$f_{\mathrm{FM}} \times (\rho_{\mathrm{FFM}} - \rho_{\mathrm{FM}}) = \frac{\rho_{\mathrm{FM}} \times \rho_{\mathrm{FFM}}}{\rho_{\mathrm{BM}}} - \rho_{\mathrm{FM}}$$

$$f_{\mathrm{FM}} = \frac{1}{(\rho_{\mathrm{FFM}} - \rho_{\mathrm{FM}})} \times \left(\frac{\rho_{\mathrm{FM}} \times \rho_{\mathrm{FFM}}}{\rho_{\mathrm{BM}}} - \rho_{\mathrm{FM}}\right)$$

Putting the values of $\rho_{\mathrm{FM}} = 0.90$ and $\rho_{\mathrm{FFM}} = 1.10$ in Eq 3.6 of main text (as per human cadaver analysis in the following section), it becomes the popularly known Siri's equation.

$$f_{\mathrm{FM}} = \left(\frac{4.95}{\rho_{\mathrm{BM}}} - 4.5\right)$$ Siri's Equation

A2.2. Derivation of body composition constants from human cadaver analysis

Various methods of determining body composition in human largely depends on a universal value of some constants e.g. $\rho_{\mathrm{FM}}, \rho_{\mathrm{FFM}}, R_{\mathrm{water/FFM}}$ which is a key assumption of these methods. Therefore, it is very essential to understand how these body composition constants were derived. A thorough literature survey was carried out for this purpose and described here.

A2.2.1. $\boldsymbol{\rho_{\mathrm{FM}}}$ (0.90 g/mL):

Fidanza et al. (1953) collected samples of subcutaneous and internal fat during surgery from human subjects. Upon ether extraction of the fat samples, they measured the densities at 37°C and reported. As evident from the results, the inter-individual variability of body fat density is quite negligible across the sexes and various physical status. It is also noted that the difference in fat densities from different parts of the body is trivial.

Table A2.1 Body fat densities (mean ± SEM) in human subjects

Subject	Sex	Age (Years)	Physical State	D_s (g/mL)	D_i (g/mL)
1	F	76	Moderate thin	0.8998	0.8998
2	F	56	Well nourished	0.8992	0.9002
3	M	38	Well nourished	-	0.8998
4	M	54	Well nourished	0.9009	0.9004
5	M	53	Obese	0.9006	0.8999
			Mean	0.9001 ± 0.0004	0.9000 ± 0.0001

D_s and D_i are the densities of subcutaneous and internal fat respectively, refer to Fidanza et al. [144] for detail calculations

A2.2.2. $\boldsymbol{R_{\mathrm{water/FFM}}}$ (0.73):

Schoeller compiled all the FFM water content data published in the literature till date which were determined by complete analysis of water, protein, fat and mineral of human cadavers. Water content was calculated as the percentage of FFM from the chemical analysis results.

$$Water\ (\%FFM) = \frac{Weight\ of\ Water\ (kg)}{TBW(kg) - Fat\ Weight(kg)}$$

Table A2.2 Water content (%) of FFM (mean ± SEM) in individual human cadavers

Cadaver#	Sex	Age (Years)	Weight (kg)	Reason of death	Water (%FFM)	Source [160, 261-264]
1	F	42	45.1	Suicide by drowning	73.30	Forbes et al. (1953) Mitchell et al. (1945) Widdowson et al. (1951)
2	M	25	71.8	Uraemia	72.62	
3	M	46	53.8	Cerebral injury	68.36	
4	M	35	70.6	Prolonged heart disease	77.60	
5	M	63	58.6	Oesophageal cancer	72.70	Knight et al., 1986
6	F	59	25.9	Cervical cancer	73.00	
7	F	67	43.4	Metastatic carcinoma	73.70	Moore et al., 1968
				Mean	73.0 ± 1.02	

In addition, water/FFM ratio has been widely studied in many mammalian species (mouse, rat, rabbit, dog, seal, monkey) and found to be consistent with human (73%).

A2.2.3. ρ_{FFM} (1.10 g/mL):

The density of FFM was calculated from the chemical analysis data of three male cadavers mentioned above in the Table A2.2 (cadaver # 2, 3, 4) by Brozek et al. (1963) and the calculation is shown in Table A2.3 below. The FFM weight (WT_{FFM}) of the individual cadavers were calculated by adding the weights of the water (WT_{water}), protein ($WT_{protein}$) and body mineral ($WT_{mineral}$). Protein weight was determined by multiplying the nitrogen content with 6.25 and body mineral weight was determined by multiplying the ash value with 1.0354. These scaling factors represent the 16% average nitrogen content in protein and 96.58% the ash content in the whole body [145]. Volume of water, protein and mineral components were

calculated by dividing their weights by their corresponding reported densities at 36°C, i.e. 0.994, 1.34 and 3.038 g/mL for water, protein and mineral respectively.

$$\rho_{FFM} = \frac{WT_{FFM}}{V_{FFM}} = \frac{WT_{water} + WT_{protein} + WT_{mineral}}{V_{water} + V_{protein} + V_{mineral}}$$

Table A2.3 Density of FFM (mean ± SEM) in individual human cadavers [145]

Cadaver #	WT_{water} (g/kg)	$WT_{protein}$ (g/kg)	$WT_{mineral}$ (g/kg)	V_{water} (mL/kg)	$V_{protein}$ (mL/kg)	$V_{mineral}$ (mL/kg)	ρ_{FFM} g/mL
2	618.0	166.0	77.7	621.9	123.9	25.6	1.12
3	551.0	186.0	55.9	554.5	138.8	18.4	1.11
4	679.0	144.0	49.7	683.3	107.5	16.4	1.08
						Mean	1.10 ± 0.01

Refer to Brozek et al. [145]

A2.2.4. $R_{TBK/FFM}$ (68.1 mmol/kg FFM):

Summary of the calculations is presented in Table A2.4. Forbes et al. (1956), did chemical analysis of two human cadavers (# 9,10 in Table A2.4) and collected data from two preveously reported cadaver analysis data (#1, 8 in Table A2.4), where cadavers were appearantly free from any serious disease.

Table A2.4 TBK content in FFM (mean ± SEM) in human cadavers

Cadaver#	Sex	Age (Years)	Weight (kg)	Reason of death	TBK (mEq/kg FFM)	Source
1[a]	F	42	45.1	Suicide by drowning	72.6	Forbes et al. [265]
8	NR[b]	NR[b]	70.0	NR[b]	66.8	
9[c]	M	46	53.8	Fractured skull	66.5	
10[d]	M	60		Found dead in hotel room	66.6	
				Mean	68.1 ± 2.99	

[a] From Table A2.2, not reported whether incident happened in fresh or salt water; [b] not reported; [c] Post-mortem findings: Tissues appeared in a normal state of hydration with no abnormality; [d] Post-mortem findings: Tissues appeared in a normal state of hydration but severe abnormalities were observed: arteriosclerosis of abdominal aorta and coronary arteries, hemorrhages in edges of mitral and tricuspid valves but no definite endocarditis, moderate cardiac enlargement moderate fatty degeneration of myocardium and liver and marked passive congestion of both lungs.

A2.3. Derivation of DXA equations (Eq 3.30, Eq 3.31 and Eq 3.32 of main text)

Figure 3.2 in the main text represents a schematic of a pixel which corresponds to an infinite depth of tissue with infinite set of composition (of lean, fat and bone mineral) through which X-ray beams travel and the cross sectional area represents the pixel area. As the X-ray beams traverse through a pixel area, physical interactions take place with the tissue components that reduce beam intensity, referred to as attenuation and is recorded by the DXA scanner. The attenuation holds an inverse relationship with the incident beam energy, therefore attenuation of higher energy (A_H) is lower than that of lower energy (A_L) beam.

$$A_L = ln\frac{(I)_L}{(I_0)_L} \text{ and } A_H = ln\frac{(I)_H}{(I_0)_H}$$

For a particular energy, attenuation also depends on the fractional composition and density (mass/unit volume of pixel) of each component (lean, fat and bone mineral) of that particular pixel. For example, a soft tissue pixel ([fat] or [lean] or [fat + lean]) attenuates less than a bone mineral containing pixel (it could be either [bone + lean] or [bone + lean + fat], since bone is directly attached to skeletal muscle)

because of difference in individual fractional masses of each component. Also, a bone mineral containing pixel of an osteoporosis patient will attenuate less than that of a healthy subject because of less bone mineral mass/unit volume of pixel.

In DXA, attenuation is expressed as the ratio of A_L to A_H ('r') as below.

$$r = \frac{A_L}{A_H} = \frac{ln\frac{(I)_L}{(I_0)_L}}{ln\frac{(I)_H}{(I_0)_H}}$$

Therefore, the 'r' value of i^{th} pixel containing all the three components can be expressed as below.

$$r_i = f_{fat_i} \times r_{fat} + f_{lean_i} \times r_{lean} + f_{bone_i} \times r_{bone}$$

where, f_{fat_i}, f_{lean_i} and f_{bone_i} are the fractional masses of fat, lean and bone mineral in i^{th} pixel and r_{fat}, r_{lean} and r_{bone} values are known from previous work by Pietrobelli et al. [172] or can be determined experimentally with animal tissues. Therefore, whole body DXA records the 'r_i' values of all pixels generated, and then solves the fractional masses.

Derivation of lean fraction of soft tissue: Since more than two unknown fractions in the previous equation cannot be solved, it is therefore necessary to conduct this in a two stage process. In the first stage, pixels related to bone mass are separated from the non-bone pixels of a whole body scan. This is performed based on a threshold value of 'r', below which non-bone (soft) tissue pixels appear and the bone containing pixels appear above it. This then simplifies the system and the non-bone (soft) pixels are now considered to be a standard two component system of lean and fat tissue and thus 'r' of i^{th} soft tissue pixels (r_{ST_i}) can be defined the following equation.

$$r_{ST_i} = f_{fat_i} \times r_{fat} + f_{lean_i} \times r_{lean}$$

Pietrobelli et al. [172] calculated the theoretical values of r_{fat} =1.21 based on elemental composition of human triglycerides, r_{lean} =1.36 based on elemental

composition of lean tissue obtained from a reference man (theoretical elemental composition of a man having standard body composition) and from eleven healthy volunteer men studied using neutron activation analysis-whole body counting. They further, validated these values to be $r_{fat} = 1.20$ and $r_{lean} = 1.40$ experimentally by using animal fat and lean tissues. Therefore, r_{fat} and r_{lean} values can be experimentally determined prior to the whole body DXA scan. Given, r_{fat} and r_{lean} are known *a priori*, solution for f_{lean_i} in the previous equation can be obtained by rearranging as below, since $\left(f_{fat_i} + f_{lean_i}\right) = 1$.

$$r_{\mathrm{ST}_i} = (1 - f_{lean_i}) \times r_{fat} + f_{lean_i} \times r_{lean}$$

$$r_{\mathrm{ST}_i} = r_{fat} - f_{lean_i} \times r_{fat} + f_{lean_i} \times r_{lean}$$

$$r_{\mathrm{ST}_i} - r_{fat} = f_{lean_i}(r_{lean} - r_{fat})$$

$$f_{lean_i} = \frac{r_{\mathrm{ST}_i} - r_{fat}}{r_{lean} - r_{fat}} \qquad \text{(Eq 3.30 in the main text)}$$

Further, the average fraction of lean tissue in the whole body's soft tissue mass, i.e. $f_{lean\,(ST)}$ can be determined by dividing the summation of all f_{lean_i} values by total number (N_{ST}) of soft tissue pixels.

$$f_{lean\,(ST)} = \frac{\sum_{i=1}^{N_{ST}} f_{lean_i}}{N_{ST}} \qquad \text{(Eq 3.31 in the main text)}$$

Derivation of bone mineral content (BMC): In the next step, the bone mineral areal densities (g/cm²), i.e. M_{BM_i} are computed from all the bone pixels using the following equation [266, 267], where $\left[\mu_{\mathrm{m_{BM}}}\right]_{\mathrm{L\ or\ H}}$ are respective mass attenuation coefficients of bone mineral at both energy levels.

$$M_{\mathrm{BM}_i}(\mathrm{g/cm^2}) = \frac{r_{\mathrm{ST}} \times \mathrm{A_H} - \mathrm{A_L}}{\left[\mu_{\mathrm{m_{BM}}}\right]_{\mathrm{L}} - \left[\mu_{\mathrm{m_{BM}}}\right]_{\mathrm{H}} \times r_{\mathrm{ST}}}$$

Attenuations (A_L, A_H) are directly measured by the DXA instrument, the attenuation coefficients ($[\mu_{m_{BM}}]_L$, $[\mu_{m_{BM}}]_H$) can be fixed to their theoretical values 0.9039 and 0.3159 (from standard elemental composition of bone mineral), respectively as derived by Pietrobelli et al. [172] or can be experimentally determined. In this case, r_{ST} is representative of all non-bone (i.e. soft) tissues which can vary widely depending upon the composition in the particular pixel. Several approximations have been used to impute the value of r_{ST} including the average over all soft tissues and a uniform soft tissue composition surrounding the bones across the whole body. This approximation is known as the uniform distribution model [268], and is restricted to the spinal bones only, as most of the bones deviate from this assumption. Other, and more recent, approximations are being used which account for a weighted average of r_{ST} in the bone containing pixels and calculates the M_{BM_i}. This approach is known as weighted linear distribution model [268]. Total BMC thus, can be estimated by multiplying each M_{BM_i} with their pixel area and summing them up, where N_{BM} represents total number of bone mineral pixels.

$$BMC\ (g)\ = \sum_{i=1}^{N_{BM}} M_{BM_i}(g/cm^2) \times Pixel\ Area_i\ (cm^2) \qquad \text{(Eq 3.32 in the main text)}$$

A2.4. Limitation of Assumptions

The typical values used for these parameters are $\rho_{FM} = 0.90$ g/mL, $\rho_{FFM} = 1.10$ g/mL, $R_{water/FFM} = 0.73$, $R_{TBK/FFM} = 68.1$ mmol/kg FFM, $[K^+]_i = 150$ mmol/L, $f_{AT} = 0.8$, $\rho_{AT} = 0.95$ g/mL. These deviations are largely due to biological variation caused by various factors such as age, disease, pregnancy etc, apart from natural inter-individual variation in healthy adult population. ρ_{FM} remains fairly constant because of negligible variation occurs in animal fat composition. On the other hand, ρ_{FFM} is expected to vary widely because of the biological variation in its composition i.e. water, protein, carbohydrate, minerals. Disease states [188] can alter ρ_{FFM} and also, it is known that children (1.068 to 1.096 g/mL) [186] and body builders (1.091 ± 0.012 g/mL) have lower values [269] of ρ_{FFM}. However, the universality of ρ_{FFM} was reported across sex, race and range of adiposity [270]. Similarly, FFM calculation from

TBW entirely depends on the assumed constant $R_{\mathrm{water/FFM}}$ which is very susceptible to (patho)physiological changes caused by disease, age etc. For example, higher $R_{\mathrm{water/FFM}}$ (~0.80) ratio was reported in children at one month [187]) of age, which gradually normalises to adult value. Similar to TBW, TBK measurement entirely depends on the assumed constant $R_{\mathrm{TBK/FFM}}$ which is very susceptible to (patho)physiological changes caused by disease, age etc. For example, lower $R_{\mathrm{TBK/FFM}}$ (54-62 mmol/kg FFM [154]) ratio was reported in children. Moreover, deficit in TBK does not necessarily decrease the FFM proportionately in certain pathological conditions such as in solid tumours [189]. This is primarily because K+ is restricted to the intracellular space or the body cell mass which constitutes only 50-60% of FFM. Further to this, water migration from intracellular to extracellular compartment during TBK deficit can lower the $R_{\mathrm{TBK/FFM}}$ ratio. Also, the assumed value of $[\mathrm{K}^+]_i = 150$ mmol/L is not constant and is reported to vary during diseases causing acid-base imbalance [159] or due to therapeutic intervention (e.g. β-blockers) [190, 191]. For CT/MRI, measurements are dependent on assumed values of f_{AT} and ρ_{AT}. Although 80% fat content ($f_{\mathrm{AT}} = 0.8$) is commonly used in literature [99, 176, 177] it should be noted that it is not universal. A range of 54% – 85% fat content [271] and an even a higher range of 62% – 91% [177] have been reported by other researchers based on human cadaver analysis. Moreover, f_{AT} is positively correlated with adiposity (% fat $= 0.327 + 0.0124 \times$ % adiposity) [271]. But, the influence of gender, ethnicity, pathological status on this parameter is not well understood. In addition, ρ_{AT} also varied between 0.925 – 0.970 gm/mL among the cadavers studied. However, variation in f_{AT} and ρ_{AT} is not important to consider for densitometry based methods that also derive FM as the first step to drive FFM. Therefore, universal use of these constants can lead to erroneous result in FFM determination and thus, is not advisable under such circumstances

A2.5. Operational limitations

First of all, the total number of whole body counters installed across the world is very few and those are mostly attached to nuclear plants for routine safety evaluation of the workers. Therefore, the use of whole body counting in regular

body composition studies can be ruled out. Also, hydrometry based on Br^- or Cl^- dilution space is not a feasible option to determine FFM since it requires ICW to be measured in parallel by whole body counting. Most of the remaining methods require access to an in house set up and thus are not suitable for field studies. Hydrostatic weighing requires access to in house pool, hydrometry requires access to LC-MS or scintillation counters installed in a laboratory, BOD POD, DXA, CT and MRI instruments are also not portable. Therefore, bioimpedance analysis and anthropometry are the only options available for field studies. For in house studies, hydrostatic weighing is not a preferred method of choice since it requires the subject to submerge under the water with maximal exhalation. On the other hand, CT is not recommended for the purpose of body composition analysis due to its high radiation exposure and MRI, in spite of being free from ionising radiation is very costly and has limited access. Among the remaining methods, isotope dilution is practically limited by its long waiting time for equilibration, limited access to analytical instruments, i.e. LC-MS (^2H_2O, $H_2{}^{18}O$), scintillation detector (^3H_2O) and particularly, the tritium dilution (^3H_2O) is not advisable for use in children and child bearing women due to radiation exposure. Therefore, BOD POD, anthropometry, bioimpedance analysis and DXA appear to be reasonably feasible options for FFM measurement from operational point of view. Due to less practical constraints, these four methods are mostly fit for clinical use. A detailed list of advantages and disadvantages of all the methods are shown in Table A2.7.

Table A2.5 Examples of FFM calculation for a standard 70 kg man using standard values of parameters

Method based on		Measurement	Primary Outcome	Model Used to Calculate Primary Outcome	Standard Values	FFM Model	Assumed Constants	FFM (Kg)
Body Density	Hydrostatic Weighing	WT_{air}, WT_{water}	ρ_{BM}	$\rho_{BM} = \frac{WT_{air}}{\Delta WT} \times 0.9957$	ρ_{BM} = 1.064 g/mL[a]	$f_{\mathrm{FM}} = \frac{1}{(\rho_{\mathrm{FFM}} - \rho_{\mathrm{FM}})} \times \left(\frac{\rho_{\mathrm{FM}} \times \rho_{\mathrm{FFM}}}{\rho_{\mathrm{BM}}} - \rho_{\mathrm{FM}}\right)$ $FFM = WT \times (1 - f_{FM})$	ρ_{FM} = 0.90 g/mL ρ_{FFM} = 1.10 g/mL	59.3
	BOD POD®	WT, V_B, V_L, BSA		$\rho_{BM} = \frac{WT}{V_B + 0.40 \times V_L - \delta \times BSA}$				
	Anthropo-metry	$(X_1), (X_2), (X_3), (X_4)$		$\rho_{BM} = C_1 - m_1 \times X_1 + m_2 \times (X_1)^2 - m_3 \times X_2 - m_4 \times X_3 + m_5 \times X_4$				
Hydrometry	Isotope Dilution	Post-equilibrium concentration	TBW	$TBW = \frac{Dose\ ^b}{Concentration}$	TBW = 40 kg[a]	$FFM = \frac{TBW}{R_{water/FFM}}$	$R_{water/FFM}$= 0.73	54.8
Bioimpedance	BIA	Z or $R, Ht, WT,$ Age, Sex (M=1, F=0)		$TBW = \theta_1 \times \left[\frac{HT^2}{R\ or\ Z}\right] + \theta_2 \times [Sex] + \theta_3 \times [WT] + \theta_4 \times [Age] + \theta_5$				
WBC	WBC	^{40}K content	TBK	$TBK = \frac{Radioactive\ K\ content}{0.000118 \times 39.102}$	TBK = 3581 mmol[a]	$FFM = \frac{TBK}{R_{TBK\ /\ FFM}}$	$R_{TBK\ /\ FFM}$ = 68.1 mmol/kg	52.6

Method based on		Measurement	Primary Outcome	Model Used to Calculate Primary Outcome	Standard Values	FFM Model	Assumed Constants	FFM (Kg)
X-Ray Attenuation	DXA	r_{ST_i} $A_L,\ A_H$	$f_{lean\ (ST)}$ BMC	$f_{lean_i} = \frac{r_{\mathrm{ST}_i} - r_{fat}}{r_{lean} - r_{fat}}$ $f_{lean\ (ST)} = \frac{\sum_{i=1}^{N_{ST}} f_{lean_i}}{N_{ST}}$ $BMC = \sum_{i=1}^{N_{BM}} M_{BM_i} \times Pixel\ Area_i$	$(f_{\mathrm{lean}})_{\mathrm{ST}} = 0.8375$ [c] $BMC = 3$ kg [d]	$FFM = WT_{ST} \times f_{lean\ (ST)} + BMC$	$r_{fat} = 1.21$ $r_{lean} = 1.36$	59.1
Medical Imaging	CT/MRI	CT numbers on every slice	Adipose tissue volume	$V_{AT} = \sum_{i=1}^{N_s} l \times \frac{(Area_i + Area_{i+1})}{2}$	$V_{AT} = 14.74$ kg [e]	$FFM = WT - V_{AT} \times \rho_{AT} \times f_{AT}$	$\rho_{\mathrm{AT}} = 0.95$ gm/mL $f_{\mathrm{AT}} = 0.80$	58.8

[a] for a standard 70 kg man [147]; [b] dose corrected with urine, [c] calculated from total soft tissue r_{ST} value of 1.334 of a reference man [172]; [d] average value of several male subjects (unpublished data from Taylor et al. [272]), [e] mean adipose tissue volume of six cadavers studied [271]

WT total body weight, ΔWT difference between WT in air (WT_{air}) and WT in water (WT_{water}), ρ_{BM} total body density, FM fat mass, FFM fat-free mass, ρ_{FM} density of FM, ρ_{FFM} density of FFM, f_{FM} fraction of FM in WT, V_B total body volume, V_L lung volume, BSA body surface area, δ instrument specific constant, X_1 sum of seven skin folds, X_2 age, X_1 waist circumference, X_4 fore arm circumference, $m_1 = 4.115 \times 10^{-4}$, $m_2 = 0.0069 \times 10^{-4}$, $m_3 = 2.2631 \times 10^{-4}$, $m_4 = 59.239 \times 10^{-4}$, $m_5 = 190.632 \times 10^{-4}$, $C_1 = 11010 \times 10^{-4}$, $C_2 = 11470 \times 10^{-4}$, TBW total body water, Z impedance, R resistance, Ht height, $R_{\mathrm{water/FFM}}$ ratio of TBW to FFM, WBC whole body counting, TBK total body potassium, $R_{\mathrm{TBK\,/\,FFM}}$ ratio of TBK to FFM, A_L, A_H attenuation of low and high energy beams respectively, BMC bone mineral content, r_{ST_i} attenuation ratio of i^{th} soft tissue pixel, $f_{lean\ (ST)}$ average fraction of lean in soft tissue, f_{lean_i} fraction of lean in i^{th} pixel, r_{fat} attenuation ratio of fat, r_{lean} attenuation ratio of lean, N_{ST} total number of soft tissue pixels, CT computerised tomography, MRI magnetic resonance imaging, V_{AT} volume of adipose tissue, l inter-slice distance, N_s number of slices, ρ_{AT} density of adipose tissue, f_{AT} fractional fat content in adipose

Table A2.6 Various models published in literature for predicting body composition

SL #	Model	Author	Description	Population used for model development
1	$FFM = P1 \times WT + P2 \times Ht - P3$	Hume [178]	$P1$= 0.32810 (male), 0.29569 (female), $P2$= 0.33929 (male), 0.41813 (female), $P3$= 29.5336 (male), 43.2933 (female). Ht in cm;	N = 29 (male) + 27 (female); Weight range: 42.9-132.8 kg (male) and 44.7-115.5 kg (female); Age range: 40-77 years (male) and 37-80 years (female)
2	$FFM = P4 \times WT - P5 \times \left(\frac{WT}{Ht}\right)^2$	James [101, 183]	$P4$ = 1.1 (men), 1.07 (women), $P5$ = 128 (men), 148 (women). Ht in cm.	N = 89 (male) + 94 (female); weight range: 32.3-121.8 kg; age range: 16-84 years
3	$FFM = P6 \times WT + P7 \times Ht^2$	Garrow and Webster [180]	$P6$= 0.285 (male), 0.287 (female), $P7$= 12.1 (male), 9.74 (female), Ht in metre	N = 24 (male) + 105 (female); weight range: 43.5-126 kg; range of BMI: 16.7 - 50.1 kg/m²; range of height: 1.57-1.86 m
4	$FM = P8 \times BMI + P9 \times WT + P10 \times Age - P11$	Heitmann [181]	$P8$= 0.988 (male), 0.988 (female), $P9$= 0.242 (male), 0.344 (female), $P10$= 0.094 (male), 0.094 (female), $P11$= 30.180 (male), 30.180 (female)	N = 72 (male) + 67 (female); Range of body fat: 7.2 - 42.3 kg; Age range: 35-65 years
5	$\%FM = P12 \times BMI + P13 \times Age - P14 \times Sex - P15$	Deurenberg [182]	$P12$= 1.2 (adult), 1.51 (children), $P13$= 0.23 (adult), 0.70 (children), $P14$= 10.8 (adult), 3.6 (children), $P15$= 5.4 (adult), 1.4 (children); sex =1 (male) or 0 (female)	N = 521 (males) + 728 (females) including older men and children ; Age range: 7 - 83 years; BMI range: 13.9 - 40.9 kg/m²

6	$FFM = \frac{9.27 \times 10^3 \times WT}{P16 + P17 \times BMI}$	Janmahasatian [102]	$P16 = 6.68 \times 10^3$ (male), 8.78×10^3 (female); $P17$= 216 (male), 244 (female)	N= 168 (male) + 205 (female); weight range: 40.7-216.5 kg; BMI range: 17.1-69.9 kg/m²; age range: 18-82 years
7	$FFM_{\text{obesefemale}} = -11.41 + 0.354 \times WT + 11.06 \times Ht$	Bucaloiu [184]	Ht in metre	N= 70 (Morbidly obese females); BMI: 48.3 ± 4.8 kg/m²; weight: 128.1 ± 13.8 kg; Age: 43 ± 11 years
8	$FFM_{children} = \left(P18 + \frac{P19}{\left[1 + \left(\frac{Age}{P20}\right)^{-P21}\right]} \right) \times \frac{9.27 \times 10^3 \times WT}{P16 + P17 \times BMI}$	Al-Sallami [185]	$P18$= 0.88 (male), 1.11 (female); $P19$= 0.12 (male), 0.11 (female); $P20$= 13.4 (male), 7.1 (female), $P21$= −12.7 (male), −1.1 (female)	N= 515 (male) + 496 (female); BMI range: 12 - 44.9 kg/m²; age range: 3 - 29 years

FFM fat-free mass in kg, FM fat mass in kg, WT total body weight in kg, BMI body mass index in kg/m² Ht height, Age in year

Table A2.7 Operational advantages, disadvantages and reliability of currently used *FFM* methods

Method		Operational advantages	Operational disadvantages	Reliability of measurement
Densitometry [a]	Hydrostatic Weighing	- Ionising radiation free - Non-invasive - No body size limitation	- Experimentally challenging: not suitable for unfit subjects, e.g. children, frails - Subjects needs to be trained well - Not suitable for field studies	Precision/Variability of ρ_{BM}: - Reported SD of ρ_{BM} measured in multiple subjects at multiple occasions was 0.008 g/mL, given both the subject and investigator were well trained
	BOD-POD®	- Ionising radiation free - Non-invasive - Suitable for all including children - No body size limitation	- Not suitable for field studies	Precision of V_B: - Reported CV value was < 0.1% for an inanimate object having comparable volume to an adult human and measured in multiple occasions
	Anthropometry	- High patient compliance: no experimental procedure; fast, safe and inexpensive - Suitable for all including children - Suitable for field studies	- Identifying the waistline in severely obese subjects is often difficult	Precision of skinfold thickness (X_1): variable - subject to anthropometrist's skill - variability can be limited within 5% if properly trained

Hydrometry	Isotope dilution (for TBW) and ion space/dilution (for ECW, ICW)	- Ionising radiation free (except $^{3}H_20$) - No age limitation - No body size limitation	- Low patient compliance: invasive procedure, long waiting time before sampling - Ionising radiation exposure with $^{3}H_20$: not recommended in children and child bearing women - Expensive: specialised analysis (LC-MS) needed for $^{2}H_2O$, $H_2{}^{18}O$ - ICW by TBK is not recommended if altered $[K^+]_i$ is suspected - Not suitable for FFM estimation in abnormally hydrated subjects	Precision of TBW: - Depends on the analytical technique used - CV of 1-2% noted with LC-MS - But 2-4% for other analytical methods Precision of ECW, ICW: - Not well characterised as with isotope dilution - TBW measurement by adding ECW and ICW is likely to lack precision, as errors with both variable will be added up Accuracy of TBW: - Isotope dilution slightly overestimates TBW by about 1% due to non-aqueous exchange Accuracy of ECW, ICW: - Unknown due to lack of direct chemical analysis method

Bioimpedance	BIA	- Ionising radiation free - Fast and non-invasive procedure - No age limitation - No body size limitation - Suitable for field studies	- Not suitable for FFM extrapolation in abnormally hydrated subjects	Precision/Variability of Z: - CV of within day and between day measurements was shown to be 0.3-0.8% and 0.9-1.7% respectively Accuracy of FFM: - Subject to population specific regression equation
Whole body counting	TBK	- Ionising radiation free - Non-invasive - Suitable for all including children	- Limited access: very few laboratory across the world have whole body counters	Precision/Variability of TBK: - 2-5% precision in adults for a typical whole body counting - Worse in infants, about 8-12% Accuracy of TBK: unknown - Unknown due to the lack of whole body counting data in human cadaver
X-ray Attenuation	DXA	- Safe: very low ionising radiation exposure comparable to that of natural background radiation/day received by us - Non-invasive - Suitable for all including children	- Variable estimates between various hardware and software systems	Precision/Variability of $\%FM$: - CV of 1.89% was reported for 20 subjects over four consecutive days Accuracy of $\%FM$: - DXA can have 1-3% error in $\%FM$ if compared with results of multi-compartmental analysis of body composition

Medical Imaging	CT/MRI	- MRI is safe (no ionising radiation) - Both are non-invasive - MRI is suitable for all including children - Newer MRI scanners have larger gantry size: fit severely obese subjects	- CT involves ionising radiation, not suitable for repeated use - MRI is not suitable for patients having pacemaker - Old scanners face difficulty in accommodating severely obese subjects - Both are not cost effective	Precision of V_{AT}: - An average CV of 0.6% and 0.7% were reported for intra and inter-observer error in V_{AT} measurement from the same scan Accuracy of V_{AT}: -Unknown, because comparison between imaging derived V_{AT} and direct chemical analysis data of cadaver has not been reported - Only the quality of tissue has been compared between imaging and biopsy results in human. For example, liver fat index determined by MRI strongly correlates with biopsy data from the same subjects

[a] for all the three densitometry based methods, accuracy is measured in terms of error in $\%FM$, which is highly variable and can be attributed primarily to the biological variation in ρ_{FFM}; ρ_{BM} total body density, V_B total body volume, TBW total body water, ECW extracellular water, ICW intracellular water, Z impedance, FFM fat-free mass, FM fat mass, TBK total body potassium, V_{AT} volume of adipose;

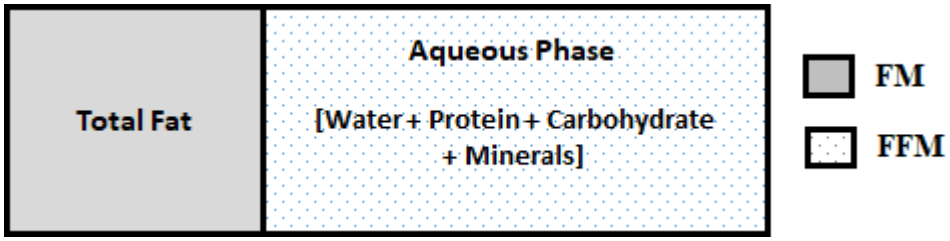

Figure A2.1 Schematic representation of two-component model of human body composition

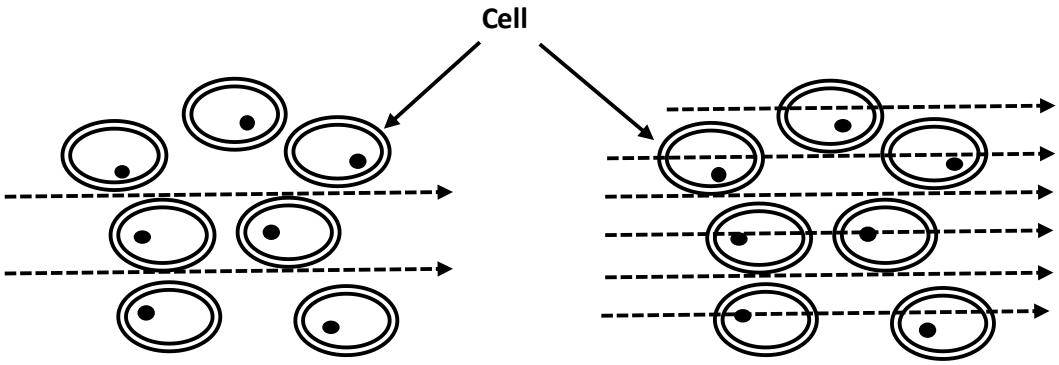

$$Z = \sqrt{R^2 + X_c^{\,2}} \qquad Z \approx R$$

Figure A2.2 Schematic representation of AC current flow through body water

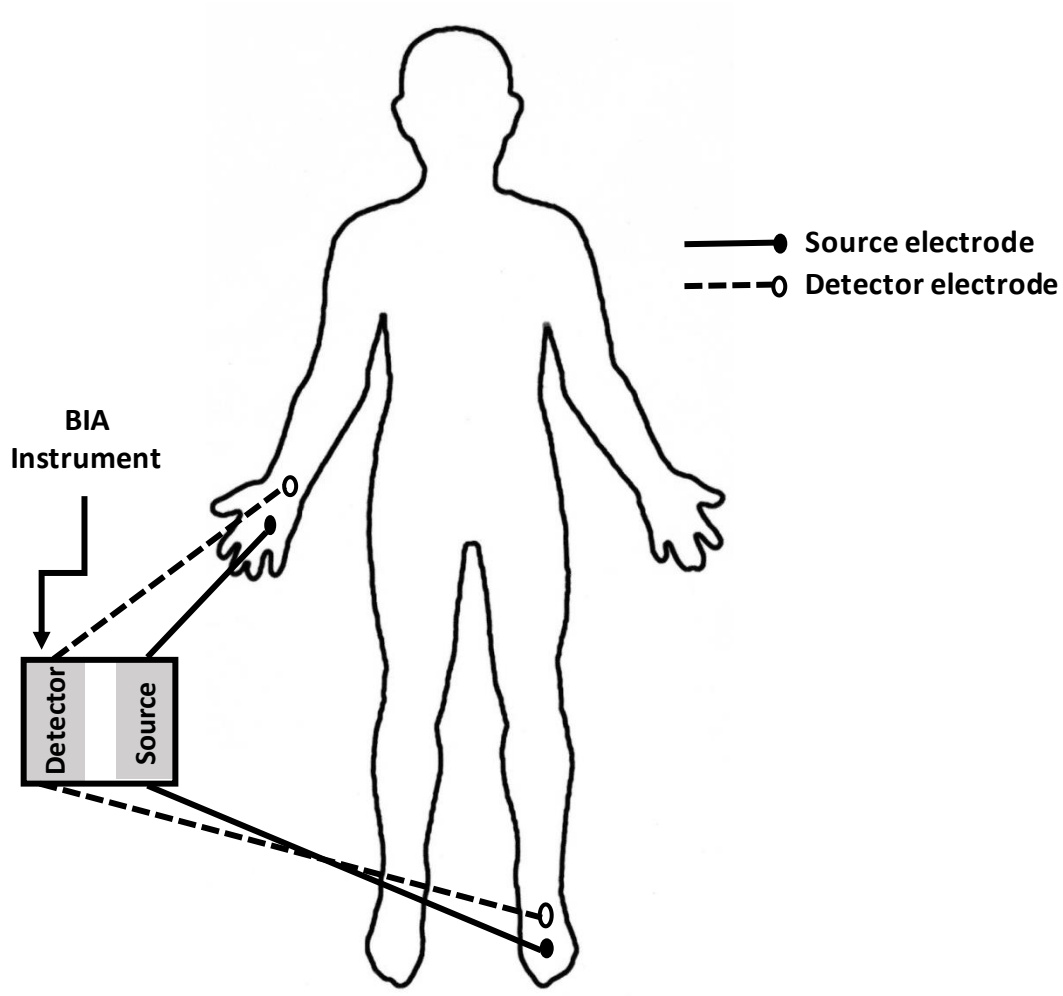

Figure A2.3 Schematic representation of tetra-polar foot-to-hand BIA experimental arrangement

Appendix 3: Additional material for Chapter 5

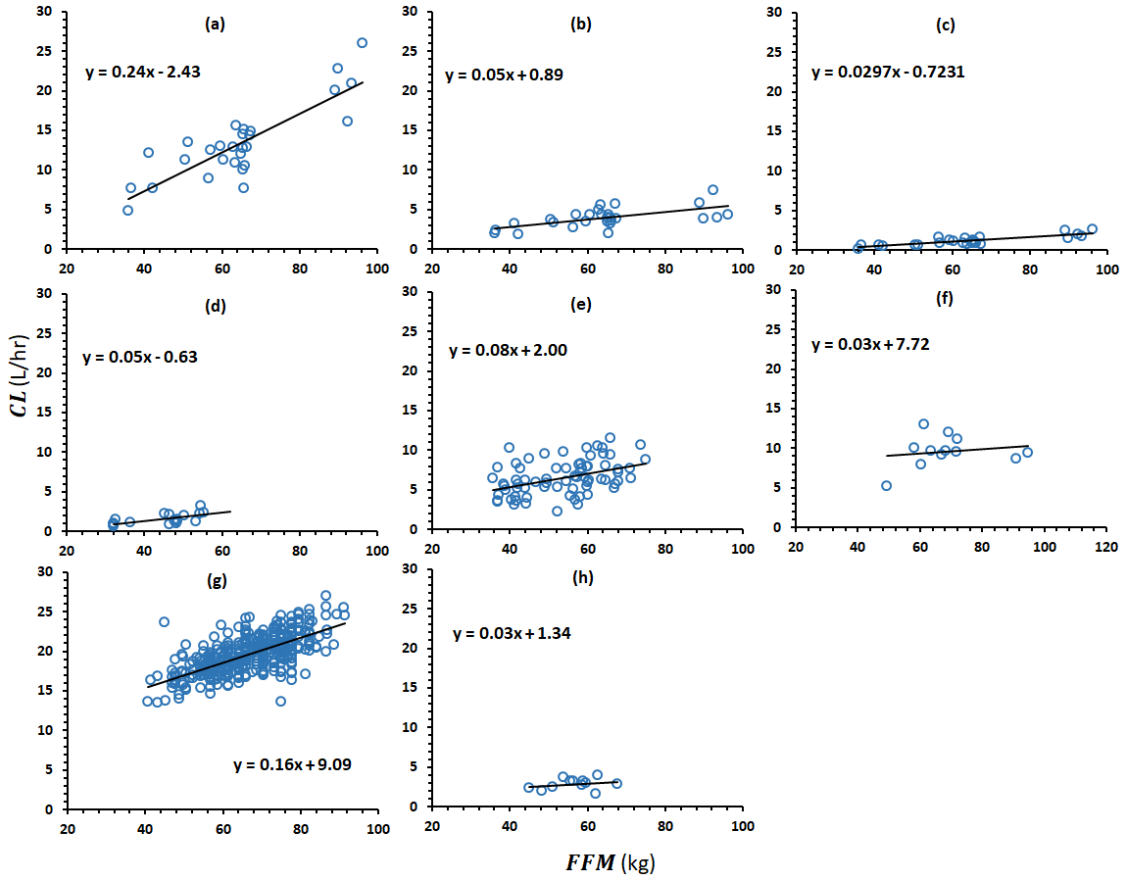

Figure A3.1 Observed individual *CL* vs. *FFM* plots

Plots are for acetaminophen glucuronidation (a), acetaminophen sulfation (b), acetaminophen oxidation (c), antipyrine (d), efavirenz (e), moxifloxacin (f), ribavirin (g) and theophylline (h). The solid black line represent the regression line with the fitted regression equation in MS excel.

References

1. Rowland M, Tozer TN. Clinical pharmacokinetics/pharmacodynamics: Lippincott Williams and Wilkins Philadelphia:; 2005.

2. Meibohm B, Derendorf H. Basic concepts of pharmacokinetic/pharmacodynamic (PK/PD) modelling. International journal of clinical pharmacology and therapeutics. 1997;35(10):401-13.

3. Holford NH, Sheiner LB. Kinetics of pharmacologic response. Pharmacology & therapeutics. 1982;16(2):143-66.

4. Sheiner L, Steimer J-L. Pharmacokinetic/pharmacodynamic modeling in drug development. Annual review of pharmacology and toxicology. 2000;40(1):67-95.

5. Huang S-M, Lertora JJ, Markey SP, Atkinson Jr AJ. Principles of clinical pharmacology: Academic Press; 2012.

6. Soberman R, Brodie BB, Levy BB, Axelrod J, Hollander V, Steele JM. The use of antipyrine in the measurement of total body water in man. Journal of Biological Chemistry. 1949;179:31-2.

7. Odeh YK, Wang Z, Ruo TI, Wang T, Frederiksen MC, Pospisil PA, et al. Simultaneous analysis of inulin and 15N2-urea kinetics in humans. Clinical Pharmacology & Therapeutics. 1993;53(4):419-25.

8. Estes JW, Poulin PF. Pharmacokinetics of heparin. Thrombosis and Haemostasis. 1975;33(01):026-37.

9. Gustafsson L, Walker O, Alvan G, Beermann B, Estevez F, Gleisner L, et al. Disposition of chloroquine in man after single intravenous and oral doses. British journal of clinical pharmacology. 1983;15(4):471-9.

10. Abernethy DR, Greenblatt DJ. Phenytoin disposition in obesity: determination of loading dose. Archives of neurology. 1985;42(5):468.

11. Knibbe CA, Brill MJ, van Rongen A, Diepstraten J, van der Graaf PH, Danhof M. Drug disposition in obesity: toward evidence-based dosing. Annual review of pharmacology and toxicology. 2015;55:149-67.

12. Jain R, Chung S, Jain L, Khurana M, Lau S, Lee J, et al. Implications of obesity for drug therapy: limitations and challenges. Clinical Pharmacology & Therapeutics. 2011;90(1):77-89.

13. Van Kralingen S, Diepstraten J, Peeters MY, Deneer VH, Van Ramshorst B, Wiezer RJ, et al. Population pharmacokinetics and pharmacodynamics of propofol in morbidly obese patients. Clinical pharmacokinetics. 2011;50(11):739-50.

14. Triginer C, Izquierdo I, Fernandez R, Rello J, Torrent J, Benito S, et al. Gentamicin volume of distribution in critically ill septic patients. Intensive care medicine. 1990;16(5):303-6.

15. Gonzalez D, J Conrado D, Theuretzbacher U, Derendorf H. The effect of critical illness on drug distribution. Current pharmaceutical biotechnology. 2011;12(12):2030-6.

16. Teorell T. Kinetics of distribution of substances administered to the body, II: the intravascular modes of administration. Archives internationales de pharmacodynamie et de therapie. 1937;57:226-40.

17. Black JW, Leff P. Operational models of pharmacological agonism. Proceedings of the Royal society of London Series B Biological sciences. 1983;220(1219):141-62.

18. Levy G. Relationship between rate of elimination of tubocurarine and rate of decline of its pharmacological activity. BJA: British Journal of Anaesthesia. 1964;36(11):694-5.

19. Levy G. Kinetics of pharmacologic effects. Clinical Pharmacology & Therapeutics. 1966;7(3):362-72.

20. Sheiner LB, Stanski DR, Vozeh S, Miller RD, Ham J. Simultaneous modeling of pharmacokinetics and pharmacodynamics: application to d-tubocurarine. Clinical Pharmacology & Therapeutics. 1979;25(3):358-71.

21. Holford NH, Sheiner LB. Understanding the dose-effect relationship. Clinical pharmacokinetics. 1981;6(6):429-53.

22. Wright DF, Winter HR, Duffull SB. Understanding the time course of pharmacological effect: a PKPD approach. British journal of clinical pharmacology. 2011;71(6):815-23.

23. Dayneka NL, Garg V, Jusko WJ. Comparison of four basic models of indirect pharmacodynamic responses. Journal of pharmacokinetics and biopharmaceutics. 1993;21(4):457-78.

24. Leykin Y, Miotto L, Pellis T. Pharmacokinetic considerations in the obese. Best practice & research Clinical anaesthesiology. 2011;25(1):27-36.

25. Han P, Duffull S, Kirkpatrick C, Green B. Dosing in obesity: a simple solution to a big problem. Clinical Pharmacology & Therapeutics. 2007;82(5):505-8.

26. Cella M, Knibbe C, Danhof M, Della Pasqua O. What is the right dose for children? British journal of clinical pharmacology. 2010;70(4):597-603.

27. Lagishetty C. Covariates in Pharmacometrics: University of Otago; Retrieved from http://hdl.handle.net/10523/4520.

28. Ette EI, Williams PJ. Population pharmacokinetics I: background, concepts, and models. Annals of Pharmacotherapy. 2004;38(10):1702-6.

29. Ette EI, Williams PJ. Population pharmacokinetics II: estimation methods. Annals of Pharmacotherapy. 2004;38(11):1907-15.

30. Ette EI, Williams PJ, Lane JR. Population pharmacokinetics III: design, analysis, and application of population pharmacokinetic studies. Annals of Pharmacotherapy. 2004;38(12):2136-44.

31. Sheiner LB, Beal SL. Evaluation of methods for estimating population pharmacokinetic parameters II. Biexponential model and experimental pharmacokinetic data. Journal of pharmacokinetics and biopharmaceutics. 1981;9(5):635-51.

32. Sheiner LB, Beal SL. Evaluation of methods for estimating population pharmacokinetic parameters. I. Michaelis-Menten model: routine clinical pharmacokinetic data. Journal of pharmacokinetics and biopharmaceutics. 1980;8(6):553-71.

33. Lagishetty CV, Vajjah P, Duffull SB. A reduction in between subject variability is not mandatory for selecting a new covariate. Journal of pharmacokinetics and pharmacodynamics. 2012;39(4):383-92.

34. Duffull SB, Kirkpatrick CMJ, Green B, Holford NHG. ANALYSIS OF POPULATION PHARMACOKINETIC DATA USING NONMEM AND WinBUGS. Journal of Biopharmaceutical Statistics. 2004;15(1):53-73.

35. Owen JS, Fiedler-Kelly J. Introduction to population pharmacokinetic/pharmacodynamic analysis with nonlinear mixed effects models: John Wiley & Sons; 2014.

36. Sheiner L, Ludden T. Population pharmacokinetics/dynamics. Annual review of pharmacology and toxicology. 1992;32(1):185-209.

37. Sheiner LB, Rosenberg B, Melmon KL. Modelling of individual pharmacokinetics for computer-aided drug dosage. Computers and Biomedical Research. 1972;5(5):441-59.

38. Proost JH. Combined proportional and additive residual error models in population pharmacokinetic modelling. European Journal of Pharmaceutical Sciences. 2017;109:S78-S82.

39. Davidian M, Giltinan DM. Nonlinear Models for Repeated Measurement Data. 1995.

40. Beal S, Sheiner L, Boeckmann A, Bauer R. NONMEM Users Guides. 1989-2011. Icon Development Solutions, Ellicott City, Maryland, USA. 2011;1(1):1.

41. Aarons L. Software for population pharmacokinetics and pharmacodynamics. Clinical pharmacokinetics. 1999;36(4):255-64.

42. Kim M-G, Yim D-S, Bae K-S. R-based reproduction of the estimation process hidden behind NONMEM® Part 1: first-order approximation method. Translational and Clinical Pharmacology. 2015;23(1).

43. Bae K-S, Yim D-S. R-based reproduction of the estimation process hidden behind NONMEM® Part 2: First-order conditional estimation. Translational and Clinical Pharmacology. 2016;24(4).

44. Schoemaker RC, Cohen AF. Estimating impossible curves using NONMEM. British journal of clinical pharmacology. 1996;42(3):283-90.

45. Mould DR, Upton RN. Basic Concepts in Population Modeling, Simulation, and Model-Based Drug Development—Part 2: Introduction to Pharmacokinetic Modeling Methods. CPT: Pharmacometrics & Systems Pharmacology. 2013;2(4):e38.

46. Maitre P, Bührer M, Thomson D, Stanski D. A three-step approach combining Bayesian regression and NONMEM population analysis: application to midazolam. Journal of pharmacokinetics and biopharmaceutics. 1991;19(4):377-84.

47. Mandema JW, Verotta D, Sheiner LB. Building population pharmacokineticpharmacodynamic models. I. Models for covariate effects. Journal of pharmacokinetics and biopharmaceutics. 1992;20(5):511-28.

48. Jonsson EN, Karlsson MO. Automated covariate model building within NONMEM. Pharmaceutical research. 1998;15(9):1463-8.

49. Savic RM, Karlsson MO. Importance of shrinkage in empirical bayes estimates for diagnostics: problems and solutions. The AAPS journal. 2009;11(3):558-69.

50. Xu XS, Yuan M, Yang H, Feng Y, Xu J, Pinheiro J. Further Evaluation of Covariate Analysis using Empirical Bayes Estimates in Population Pharmacokinetics:

the Perception of Shrinkage and Likelihood Ratio Test. The AAPS Journal. 2017;19(1):264-73.

51. Bonate PL, Steimer J-L. Pharmacokinetic-pharmacodynamic modeling and simulation: Springer; 2011.

52. Duffull SB, Wright DF, Winter HR. Interpreting population pharmacokinetic-pharmacodynamic analyses–a clinical viewpoint. British journal of clinical pharmacology. 2011;71(6):807-14.

53. Nguyen T, Mouksassi MS, Holford N, Al-Huniti N, Freedman I, Hooker AC, et al. Model evaluation of continuous data pharmacometric models: metrics and graphics. CPT: pharmacometrics & systems pharmacology. 2017;6(2):87-109.

54. Karlsson M, Savic R. Diagnosing model diagnostics. Clinical Pharmacology & Therapeutics. 2007;82(1):17-20.

55. Akaike H. A new look at the statistical model identification. IEEE transactions on automatic control. 1974;19(6):716-23.

56. Ribbing J, Jonsson EN. Power, selection bias and predictive performance of the Population Pharmacokinetic Covariate Model. Journal of pharmacokinetics and pharmacodynamics. 2004;31(2):109-34.

57. Han PY, Kirkpatrick CM, Green B. Informative study designs to identify true parameter–covariate relationships. Journal of pharmacokinetics and pharmacodynamics. 2009;36(2):147-63.

58. La Caze A, Duffull S. Estimating risk from underpowered, but statistically significant, studies: was APPROVe on TARGET? Journal of clinical pharmacy and therapeutics. 2011;36(6):637-41.

59. Lagishetty CV, Coulter CV, Duffull SB. Design of pharmacokinetic studies for latent covariates. Journal of pharmacokinetics and pharmacodynamics. 2012;39(1):87-97.

60. McLeay SC, Morrish GA, Kirkpatrick CM, Green B. The relationship between drug clearance and body size. Clinical pharmacokinetics. 2012;51(5):319-30.

61. Anderson BJ, Holford NH. Mechanistic basis of using body size and maturation to predict clearance in humans. Drug metabolism and pharmacokinetics. 2009;24(1):25-36.

62. Brill MJ, Diepstraten J, van Rongen A, Van Kralingen S, van den Anker JN, Knibbe CA. Impact of obesity on drug metabolism and elimination in adults and children. Clinical pharmacokinetics. 2012;51(5):277-304.

63. Tunblad K, Lindbom L, McFadyen L, Jonsson EN, Marshall S, Karlsson MO. The use of clinical irrelevance criteria in covariate model building with application to dofetilide pharmacokinetic data. Journal of pharmacokinetics and pharmacodynamics. 2008;35(5):503-26.

64. Nawaratne S, Brien JaE, Seeman E, Fabiny R, Zalcberg J, Cosolo W, et al. Relationships among liver and kidney volumes, lean body mass and drug clearance. British journal of clinical pharmacology. 1998;46(5):447-52.

65. Janmahasatian S, Duffull SB, Chagnac A, Kirkpatrick CM, Green B. Lean body mass normalizes the effect of obesity on renal function. Br J Clin Pharmacol. 2008;65(6):964-5.

66. Howgate EM, Rowland Yeo K, Proctor NJ, Tucker GT, Rostami-Hodjegan A. Prediction of in vivo drug clearance from in vitro data. I: Impact of inter-individual variability. Xenobiotica. 2006;36(6):473-97.

67. Alcorn J, McNamara PJ. Ontogeny of hepatic and renal systemic clearance pathways in infants part I. Clinical pharmacokinetics. 2002;41(12):959-98.

68. Alcorn J, McNamara PJ. Ontogeny of hepatic and renal systemic clearance pathways in infants: part II. Clinical pharmacokinetics. 2002;41(13):1077-94.

69. Anderson B, Holford N. Mechanism-based concepts of size and maturity in pharmacokinetics. Annu Rev Pharmacol Toxicol. 2008;48:303-32.

70. Wang YC, McPherson K, Marsh T, Gortmaker SL, Brown M. Health and economic burden of the projected obesity trends in the USA and the UK. The Lancet. 2011;378(9793):815-25.

71. James PT. Obesity: the worldwide epidemic. Clinics in dermatology. 2004;22(4):276-80.

72. James WPT. WHO recognition of the global obesity epidemic. International journal of obesity. 2009;32(S7):S120.

73. Schelbert KB. Comorbidities of obesity. Primary Care: Clinics in Office Practice. 2009;36(2):271-85.

74. Halford JC. Clinical pharmacotherapy for obesity: current drugs and those in advanced development. Current Drug Targets. 2004;5(7):637-46.

75. Brautbar A, Ballantyne CM. Pharmacological strategies for lowering LDL cholesterol: statins and beyond. Nature Reviews Cardiology. 2011;8(5):253.

76. Cassidy S, Syed BA. Nonalcoholic steatohepatitis (NASH) drugs market. Nature reviews Drug discovery. 2016;15(11):745-6.

77. Lewis JR, Mohanty SR. Nonalcoholic fatty liver disease: a review and update. Digestive diseases and sciences. 2010;55(3):560-78.

78. Diehl AM, Day C. Cause, Pathogenesis, and Treatment of Nonalcoholic Steatohepatitis. N Engl J Med. 2017;377(21):2063-72.

79. Idilman IS, Keskin O, Celik A, Savas B, Halil Elhan A, Idilman R, et al. A comparison of liver fat content as determined by magnetic resonance imaging-proton density fat fraction and MRS versus liver histology in non-alcoholic fatty liver disease. Acta Radiologica. 2016;57(3):271-8.

80. Reeder SB, Cruite I, Hamilton G, Sirlin CB. Quantitative assessment of liver fat with magnetic resonance imaging and spectroscopy. Journal of magnetic resonance imaging : JMRI. 2011;34(4):729.

81. FDA guidance for industry-Noncirrhotic Nonalcoholic Steatohepatitis With Liver Fibrosis: Developing Drugs for Treatment.

[Available from: http://www.webcitation.org/767YxhRGf (archived on 12 February 2019).

82. Gazarian M. Why are children still therapeutic orphans? Australian Prescriber. 2003;26(6):122-3.

83. Pandolfini C, Bonati M. A literature review on off-label drug use in children. European journal of pediatrics. 2005;164(9):552-8.

84. Choonara I, Rieder MJ. Drug toxicity and adverse drug reactions in children-A brief historical review. Paediatric and Perinatal Drug Therapy. 2001;5:12-8.

85. World Health Organization (WHO): Promoting safety of medicines for children, 2007 (https://books.google.co.nz/books?hl=en&lr=&id=mee9jZVxRLUC&oi=fnd&pg=PA7&dq=World+Health+Organization+(WHO):+Promoting+safety+of+medicines+for+children,+2007&ots=stlbG5JAKh&sig=6aa_heWCKcVaJnp-5BBMmyXzW38#v=onepage&q=World%20Health%20Organization%20(WHO)%3A%20Promoting%20safety%20of%20medicines%20for%20children%2C%202007&f=false).

86. FDA Guidance for Industry: General Clinical Pharmacology Considerations for Pediatric Studies for Drugs and Biological Products, 2014 (http://www.fda.gov/downloads/drugs/guidancecomplianceregulatoryinformation/guidances/ucm425885.pdf).

87. Zajicek A. The national institutes of health and the best pharmaceuticals for children act. Pediatric Drugs. 2009;11(1):45-7.

88. US Food and Drug Administration: New Pediatric Labeling Information Database.

89. Wharton GT, Murphy MD, Avant D, Goldsmith JV, Chai G, Rodriguez WJ, et al. Impact of pediatric exclusivity on drug labeling and demonstrations of efficacy. Pediatrics. 2014;134(2):e512-e8.

90. Mahmood I. Prediction of drug clearance in children: a review of different methodologies. Expert opinion on drug metabolism & toxicology. 2015;11(4):573-87.

91. Green B, Duffull SB. What is the best size descriptor to use for pharmacokinetic studies in the obese? British Journal of Clinical Pharmacology. 2004;58(2):119-33.

92. Rubner M. Ueber den einfluss der korpergrosse auf stoffund kaftwechsel. Zeitschrift fur Biologie. 1883;19:535-62.

93. West GB, Woodruff WH, Brown JH. Allometric scaling of metabolic rate from molecules and mitochondria to cells and mammals. Proceedings of the National Academy of Sciences. 2002;99(suppl 1):2473-8.

94. West GB, Brown JH, Enquist BJ. A general model for the origin of allometric scaling laws in biology. Science. 1997;276(5309):122-6.

95. Fisher DM, Shafer SL. Allometry, Shallometry! Anesthesia & Analgesia. 2016;Volume 122(5):1234–8.

96. Hu T-M, Hayton WL. Allometric scaling of xenobiotic clearance: uncertainty versus universality. The AAPS Journal. 2001;3(4):30-43.

97. Calvier EA, Krekels EH, Välitalo PA, Rostami-Hodjegan A, Tibboel D, Danhof M, et al. Allometric Scaling of Clearance in Paediatric Patients: When Does the Magic of 0.75 Fade? Clinical pharmacokinetics. 2017;56(3):273-85.

98. Siri WE. Body composition from fluid spaces and density: analysis of methods. In: Josef Brozek AH, editor. Techniques for measuring body composition. Washington, D.C.: National Academy of Sciences-National Research Council; 1961. p. 223-44.

99. Snyder WS, Cook MJ, Karhausen LR, Nasset ES, Howells GP, Tipton IH. Report of the Task Group on Reference Man. The International Commission on

Radiological Protection [Online Document]. Pergamon Press; 1974 [Available from: http://journals.sagepub.com/doi/pdf/10.1016/S0074-2740(75)80015-8.

100. B. Heymsfield S, Wang Z, Baumgartner RN, Ross R. Human body composition: advances in models and methods. Annual review of nutrition. 1997;17(1):527-58.

101. James WPT, Waterlow JC. Research on obesity: a report of the DHSS/MRC Group. London: HMSO [Her Majesty's Stationery Office]: UK Department of Health and Social Security/Medical Research Council Group on Obesity Research.; 1976.

102. Janmahasatian S, Duffull SB, Ash S, Ward LC, Byrne NM, Green B. Quantification of lean bodyweight. Clin Pharmacokinet. 2005;44(10):1051-65.

103. La Colla L, Albertin A, La Colla G, Porta A, Aldegheri G, Di Candia D, et al. Predictive performance of the 'Minto'remifentanil pharmacokinetic parameter set in morbidly obese patients ensuing from a new method for calculating lean body mass. Clinical pharmacokinetics. 2010;49(2):131-9.

104. Rush EC, Freitas I, Plank LD. Body size, body composition and fat distribution: comparative analysis of European, Maori, Pacific Island and Asian Indian adults. British Journal of Nutrition. 2009;102(4):632-41.

105. Chandan Vinay S, Urooj A, Chaya Sindaghatta K, Mahesh P. Validation of fat-free mass estimation using prediction equations in male patients with chronic obstructive pulmonary disease. International Journal of Nutrition, Pharmacology, Neurological Diseases. 2017;7(4):94-100.

106. Ingrande J, Brodsky JB, Lemmens HJ. Lean body weight scalar for the anesthetic induction dose of propofol in morbidly obese subjects. Anesthesia & Analgesia. 2011;113(1):57-62.

107. Cortinez LI, Anderson BJ, Holford NH, Puga V, de la Fuente N, Auad H, et al. Dexmedetomidine pharmacokinetics in the obese. Eur J Clin Pharmacol. 2015;71(12):1501-8.

108. Di L, Obach RS. Addressing the Challenges of Low Clearance in Drug Research. The AAPS Journal. 2015;17(2):352-7.

109. Rowland M, Pang KS. Commentary on "The Universally Unrecognized Assumption in Predicting Drug Clearance and Organ Extraction Ratio". Clinical Pharmacology & Therapeutics. 2018;103(3):386-8.

110. Marceau P, Biron S, Hould F-S, Marceau S, Simard S, Thung S, et al. Liver pathology and the metabolic syndrome X in severe obesity. The Journal of Clinical Endocrinology & Metabolism. 1999;84(5):1513-7.

111. Merrell MD, Cherrington NJ. Drug metabolism alterations in nonalcoholic fatty liver disease. Drug metabolism reviews. 2011;43(3):317-34.

112. Ghobadi C, Johnson TN, Aarabi M, Almond LM, Allabi AC, Rowland-Yeo K, et al. Application of a Systems Approach to the Bottom-Up Assessment of Pharmacokinetics in Obese Patients. Clinical Pharmacokinetics. 2011;50(12):809-22.

113. HM J, Y C, C G, T H, N P, SA P, et al. Physiologically based pharmacokinetic modeling in drug discovery and development: A pharmaceutical industry perspective. Clinical Pharmacology & Therapeutics. 2015;97(3):247-62.

114. Marsousi N, Desmeules JA, Rudaz S, Daali Y. Usefulness of PBPK Modeling in Incorporation of Clinical Conditions in Personalized Medicine. Journal of Pharmaceutical Sciences. 2017;106(9):2380-91.

115. Szczepaniak LS, Nurenberg P, Leonard D, Browning JD, Reingold JS, Grundy S, et al. Magnetic resonance spectroscopy to measure hepatic triglyceride content: prevalence of hepatic steatosis in the general population. American Journal of Physiology-Endocrinology and Metabolism. 2005;288(2):E462-E8.

116. Kleiber M. Body size and metabolism. Hilgardia. 1932;6(11):315-53.

117. Brody S. Bioenergetics and growth; with special reference to the efficiency complex in domestic animals. New York: Reinhold Publishing Corp.; 1945.

118. West GB, Brown JH, Enquist BJ. The fourth dimension of life: fractal geometry and allometric scaling of organisms. science. 1999;284(5420):1677-9.

119. Mahmood I, Balian J. Interspecies scaling: predicting clearance of drugs in humans. Three different approaches. Xenobiotica. 1996;26(9):887-95.

120. Mahmood I, Green MD, Fisher JE. Selection of the first-time dose in humans: Comparison of different approaches based on interspecies scaling of clearance. The Journal of Clinical Pharmacology. 2003;43(7):692-7.

121. Mahmood I. Interspecies scaling of protein drugs: prediction of clearance from animals to humans. Journal of pharmaceutical sciences. 2004;93(1):177-85.

122. Ling J, Zhou H, Jiao Q, Davis HM. Interspecies scaling of therapeutic monoclonal antibodies: initial look. The Journal of Clinical Pharmacology. 2009;49(12):1382-402.

123. Dodds PS, Rothman DH, Weitz JS. Re-examination of the "3/4-law" of metabolism. Journal of Theoretical Biology. 2001;209(1):9-27.

124. White CR, Seymour RS. Mammalian basal metabolic rate is proportional to body mass2/3. Proceedings of the National Academy of Sciences. 2003;100(7):4046-9.

125. He J-H, Zhang J. Fifth dimension of life and the 4/5 allometric scaling law for human brain. Cell biology international. 2004;28(11):809-15.

126. Eleveld DJ, Proost JH, Absalom AR, Struys MM. Obesity and allometric scaling of pharmacokinetics. Clinical pharmacokinetics. 2011;50(11):751-3.

127. Al-Sallami HS, Cheah SL, Han SY, Liew J, Lim J, Ng MA, et al. Between-subject variability: should high be the new normal? European journal of clinical pharmacology. 2014;70(11):1403.

128. Third National Health and Nutrition Examination Survey (NHANES III), 1988-94 [Internet]. [cited 15 July, 2017]. Available from: https://wwwn.cdc.gov/nchs/nhanes/nhanes3/datafiles.aspx.

129. CDC Growth Chart [Internet]. [cited 15 July, 2017]. Available from: https://www.cdc.gov/growthcharts/html_charts/wtage.htm.

130. European Medicines Agency Guideline on pharmaceutical development of medicines for paediatric use, 2014 (http://www.ema.europa.eu/docs/en_GB/document_library/Scientific_guideline/2013/07/WC500147002.pdf).

131. Nguyen L, Leger F, Lennon S, Puozzo C. Intravenous busulfan in adults prior to haematopoietic stem cell transplantation: a population pharmacokinetic study. Cancer chemotherapy and pharmacology. 2006;57(2):191-8.

132. Peloquin CA, Hadad DJ, Molino LPD, Palaci M, Boom WH, Dietze R, et al. Population pharmacokinetics of levofloxacin, gatifloxacin, and moxifloxacin in adults with pulmonary tuberculosis. Antimicrobial agents and chemotherapy. 2008;52(3):852-7.

133. Petain A, Kattygnarath D, Azard J, Chatelut E, Delbaldo C, Geoerger B, et al. Population pharmacokinetics and pharmacogenetics of imatinib in children and adults. Clinical Cancer Research. 2008;14(21):7102-9.

134. Wang DD, Zhang S, Zhao H, Men AY, Parivar K. Fixed dosing versus body size—based dosing of monoclonal antibodies in adult clinical trials. The Journal of Clinical Pharmacology. 2009;49(9):1012-24.

135. Friberg LE, Ravva P, Karlsson MO, Liu P. Integrated population pharmacokinetic analysis of voriconazole in children, adolescents and adults. Antimicrobial agents and chemotherapy. 2012:AAC. 05761-11.

136. Morgan DJ, Bray KM. Lean body mass as a predictor of drug dosage. Clinical pharmacokinetics. 1994;26(4):292-307.

137. De Baerdemaeker LE, Mortier EP, Struys MM. Pharmacokinetics in obese patients. Continuing Education in Anaesthesia, Critical Care & Pain. 2004;4(5):152-5.

138. De Baerdemaeker LEC, Van Limmen JGM, Van Nieuwenhove Y. How should obesity be measured and how should anesthetic drug dosage be calculated? In: Leykin Y, Brodsky JB, editors. Controversies in the Anesthetic Management of the Obese Surgical Patient. Milan: Springer-Verlag Italia; 2013. p. 15-30.

139. Lukaski HC. Methods for the assessment of human body composition: traditional and new. The American journal of clinical nutrition. 1987;46(4):537-56.

140. Mattsson S, Thomas BJ. Development of methods for body composition studies. Physics in medicine and biology. 2006;51(13):R203.

141. Ellis KJ. Human body composition: in vivo methods. Physiological reviews. 2000;80(2):649-80.

142. Lee SY, Gallagher D. Assessment methods in human body composition. Current opinion in clinical nutrition and metabolic care. 2008;11(5):566.

143. Wells J, Fewtrell M. Measuring body composition. Archives of disease in childhood. 2006;91(7):612-7.

144. Fidanza F, Keys A, Anderson JT. Density of body fat in man and other mammals. Journal of Applied Physiology. 1953;6:252-6.

145. Brožek J, Grande F, Anderson JT, Keys A. Densitometric analysis of body composition: revision of some quantitative assumptions*. Annals of the New York Academy of Sciences. 1963;110(1):113-40.

146. Siri W. E. The gross composition of the body. In: Lawrence JH, editor. Advances in Biological and Medical Physics. 4. New York: Academic Press; 1956. p. 239-80.

147. Going SB. Hydrodensitometry and Air Displacement Plethysmography. In: Heymsfield SB, Lohman TG, Wang Z, Going SB, editors. Human Body Composition. 2nd ed: Human Kinetics, Champaign, IL; 2005. p. 17-33.

148. COSMED. Air Displacement Plethysmography (ADP) Body Composition Rome2011 [Product News]. Available from: http://www.cosmed.com/hires/marketing_literature/product_news/Product_News_Air_Displacement_EN_print.pdf.

149. Dempster P, Aitkens S. A new air displacement method for the determination of human body composition. Medicine and science in sports and exercise. 1995;27(12):1692-7.

150. Ruppel GL. Manual of pulmonary function testing. 9th ed. St Louis: Mosby Elsevier; 2009.

151. Du Bois D, Du Bois E. A formula to estimate the approximate surface area if height and weight be known. 1916. Nutrition (Burbank, Los Angeles County, Calif). 1989;5(5):303.

152. Jackson AS, Pollock ML. Generalized equations for predicting body density of men. British journal of nutrition. 1978;40(03):497-504.

153. Jackson AS, Pollock ML, Ward A. Generalized equations for predicting body density of women. Medicine and science in sports and exercise. 1979;12(3):175-81.

154. Schoeller DA. Hydrometry. In: Heymsfield SB, Lohman TG, Wang Z, Going SB, editors. Human Body Composition. 2nd ed: Human Kinetics; 2005. p. 35-49.

155. Vaisman N, Pencharz PB, Koren G, Johnson JK. Comparison of oral and intravenous administration of sodium bromide for extracellular water measurements. The American journal of clinical nutrition. 1987;46(1):1-4.

156. Bell E, Ziegler E, Forbes G. Corrected bromide space. Pediatric research. 1984;18(4):392-3.

157. Miller ME, Cosgriff J, Forbes GB. Bromide space determination using anion-exchange chromatography for measurement of bromide. The American journal of clinical nutrition. 1989;50(1):168-71.

158. Brodie BB, Brand E, Leshin S. The use of bromide as a measure of extracellular fluid. Journal of Biological Chemistry. 1939;130(2):555-63.

159. Kim J, Wang Z, Gallagher D, Kotler DP, Ma K, Heymsfield SB. Extracellular water: sodium bromide dilution estimates compared with other markers in patients with acquired immunodeficiency syndrome. Journal of Parenteral and Enteral Nutrition. 1999;23(2):61-6.

160. Moore FD, Lister J, Boyden CM, Ball MR, Sullivan N, Dagher FJ. THE SKELETON AS A FEATURE OF BODY COMPOSITION: Values Predicted by Isotope Dilution and Observed by Cadaver Dissection in an Adult Human Female. Human biology. 1968;40(2):135-88.

161. Barnes BA, Gordon EB, Cope O. Skeletal muscle analyses in health and in certain metabolic disorders. I. The method of analysis and the values in normal muscle. Journal of Clinical Investigation. 1957;36(8):1239.

162. Maffy R. The body fluids: volume, composition, and physical chemistry. In: Brenner BM, C RF, editors. The kidney. 1. Philadelphia: WB Saunders,; 1976. p. 65-103.

163. Kushner RF. Bioelectrical impedance analysis: a review of principles and applications. J Am Coll Nutr. 1992;11(2):199-209.

164. Aroom KR, Harting MT, Cox CS, Radharkrishnan RS, Smith C, Gill BS. Bioimpedance analysis: a guide to simple design and implementation. Journal of Surgical Research. 2009;153(1):23-30.

165. LUKASKI H, BOLONCHUK W. Estimation of body fluid volumes using tetrapolar bioelectrical impedance measurements. Aviation, space, and environmental medicine. 1988;59(12):1163-9.

166. Lukaski HC, Johnson PE, Bolonchuk W, Lykken G. Assessment of fat-free mass using bioelectrical impedance measurements of the human body. The American journal of clinical nutrition. 1985;41(4):810-7.

167. Kyle UG, Bosaeus I, De Lorenzo AD, Deurenberg P, Elia M, Gómez JM, et al. Bioelectrical impedance analysis—part I: review of principles and methods. Clinical nutrition. 2004;23(5):1226-43.

168. Wu C-S, Chen Y-Y, Chuang C-L, Chiang L-M, Dwyer GB, Hsu Y-L, et al. Predicting body composition using foot-to-foot bioelectrical impedance analysis in healthy Asian individuals. Nutrition journal. 2015;14(1):1.

169. Ellis KJ. Whole-Body Counting and Neutron Activation Analysis. In: Heymsfield SB, Lohman TG, Wang Z, Going SB, editors. Human Body Composition. 2nd ed: Human Kinetics; 2005. p. 51-62.

170. Damilakis J, Adams JE, Guglielmi G, Link TM. Radiation exposure in X-ray-based imaging techniques used in osteoporosis. European radiology. 2010;20(11):2707-14.

171. IAEA. Dual energy X ray absorptiometry for bone mineral density and body

composition assessment Vienna2010 [Available from: http://www-pub.iaea.org/MTCD/publications/PDF/Pub1479_web.pdf.

172. Pietrobelli A, Formica C, Wang Z, Heymsfield SB. Dual-energy X-ray absorptiometry body composition model: review of physical concepts. American Journal of Physiology-Endocrinology And Metabolism. 1996;271(6):E941-E51.

173. Lohman TG, Chen Z. Dual-Energy X-Ray Absorptiometry. In: Heymsfield SB, Lohman TG, Wang Z, Going SB, editors. Human Body Composition. 2nd ed: Human Kinetics; 2005. p. 63-77.

174. Ross R, Janssen I. Computed Tomography and Magnetic Resonance Imaging. In: Heymsfield SB, Lohman TG, Wang Z, Going SB, editors. Human Body Composition. 2nd ed: Human Kinetics; 2005. p. 89-108.

175. Kvist H, Chowdhury B, Grangård U, Tylen U, Sjöström L. Total and visceral adipose-tissue volumes derived from measurements with computed tomography in adult men and women: predictive equations. The American journal of clinical nutrition. 1988;48(6):1351-61.

176. Kim CG, Kim WH, Kim MH, Kim D-W. Direct determination of lean body mass by CT in F-18 FDG PET/CT studies: comparison with estimates using predictive equations. Nuclear medicine and molecular imaging. 2013;47(2):98-103.

177. Snijder M, Visser M, Dekker J, Seidell J, Fuerst T, Tylavsky F, et al. The prediction of visceral fat by dual-energy X-ray absorptiometry in the elderly: a

comparison with computed tomography and anthropometry. International journal of obesity. 2002;26(7):984.

178. Hume R. Prediction of lean body mass from height and weight. Journal of clinical pathology. 1966;19(4):389-91.

179. Boer P. Estimated lean body mass as an index for normalization of body fluid volumes in humans. American Journal of Physiology-Renal Physiology. 1984;247(4):F632-F6.

180. Garrow JS, Webster J. Quetelet's index (W/H2) as a measure of fatness. International journal of obesity. 1984;9(2):147-53.

181. Heitmann BL. Evaluation of body fat estimated from body mass index, skinfolds and impedance. A comparative study. European journal of clinical nutrition. 1990;44(11):831-7.

182. Deurenberg P, Weststrate JA, Seidell JC. Body mass index as a measure of body fatness: age-and sex-specific prediction formulas. British journal of nutrition. 1991;65(02):105-14.

183. Cheymol G. Effects of obesity on pharmacokinetics. Clinical pharmacokinetics. 2000;39(3):215-31.

184. Bucaloiu ID, Wood GC, Norfolk ER, Still CD, Hartle JE, Perkins RM. Fat-free weight prediction in morbidly obese females. International journal of nephrology and renovascular disease. 2011;4:149.

185. Al-Sallami HS, Goulding A, Grant A, Taylor R, Holford N, Duffull SB. Prediction of Fat-Free Mass in Children. Clinical pharmacokinetics. 2015;54(11):1169-78.

186. Lohman TG. Assessment of body composition in children. Pediatr Exerc Sci. 1989;1(1):19-30.

187. Fomon SJ, Haschke F, Ziegler EE, Nelson SE. Body composition of reference children from birth to age 10 years. The American Journal of Clinical Nutrition. 1982;35(5):1169-75.

188. Werdein EJ, Kyle LH. Estimation of the constancy of density of the fat-free body. Journal of Clinical Investigation. 1960;39(4):626.

189. Cohn S, Vartsky D, Yasumura S, Vaswani A, Ellis K. Indexes of body cell mass: nitrogen versus potassium. American Journal of Physiology-Endocrinology And Metabolism. 1983;244(3):E305-10.

190. Cleroux J, Van Nguyen P, Taylor A, Leenen F. Effects of beta 1-vs. beta 1+ beta 2-blockade on exercise endurance and muscle metabolism in humans. Journal of Applied Physiology. 1989;66(2):548-54.

191. Sica DA. Antihypertensive therapy and its effects on potassium homeostasis. The Journal of Clinical Hypertension. 2006;8(1):67-73.

192. Collaboration NRF. Trends in adult body-mass index in 200 countries from 1975 to 2014: a pooled analysis of 1698 population-based measurement studies with 19·2 million participants. The Lancet. 2016;387(10026):1377-96.

193. Bhavnani SM, Rubino CM, Ambrose PG, Drusano GL. Daptomycin exposure and the probability of elevations in the creatine phosphokinase level: data from a

randomized trial of patients with bacteremia and endocarditis. Clinical Infectious Diseases. 2010;50(12):1568-74.

194. Kulkarni B, Kuper H, Taylor A, Wells JC, Radhakrishna KV, Kinra S, et al. Development and validation of anthropometric prediction equations for estimation of lean body mass and appendicular lean soft tissue in Indian men and women. Journal of Applied Physiology. 2013;115(8):1156-62.

195. McLeay S, Morrish G, Ponnuswamy T, Devanand B, Ramanathan M, Venkatakrishnan L, et al. Noninvasive Quantification of Hepatic Steatosis: Relationship Between Obesity Status and Liver Fat Content. Open Obesity Journal. 2014;6(1):16-24.

196. Rush E, Plank L, Chandu V, Laulu M, Simmons D, Swinburn B, et al. Body size, body composition, and fat distribution: a comparison of young New Zealand men of European, Pacific Island, and Asian Indian ethnicities. The New Zealand Medical Journal. 2004;117.

197. Rush EC, Plank LD, Laulu MS, Robinson SM. Prediction of percentage body fat from anthropometric measurements: comparison of New Zealand European and Polynesian young women. The American journal of clinical nutrition. 1997;66(1):2-7.

198. Deurenberg P, Deurenberg-Yap M, Guricci S. Asians are different from Caucasians and from each other in their body mass index/body fat per cent relationship. Obesity reviews. 2002;3(3):141-6.

199. Odore E, Lokiec F, Cvitkovic E, Bekradda M, Herait P, Bourdel F, et al. Phase I Population Pharmacokinetic Assessment of the Oral Bromodomain Inhibitor OTX015 in Patients with Haematologic Malignancies. Clinical Pharmacokinetics. 2016;55(3):397-405.

200. van Rongen A, Välitalo PA, Peeters MY, Boerma D, Huisman FW, van Ramshorst B, et al. Morbidly obese patients exhibit increased CYP2E1-mediated oxidation of acetaminophen. Clinical pharmacokinetics. 2016;55(7):833-47.

201. Robarge JD, Metzger IF, Lu J, Thong N, Skaar TC, Desta Z, et al. Population pharmacokinetic modeling to estimate the contributions of genetic and nongenetic factors to efavirenz disposition. Antimicrobial agents and chemotherapy. 2017;61(1):e01813-16.

202. Krauss M, Tappe K, Schuppert A, Kuepfer L, Goerlitz L. Bayesian population physiologically-based pharmacokinetic (PBPK) approach for a physiologically realistic characterization of interindividual variability in clinically relevant populations. PloS one. 2015;10(10):e0139423.

203. Wade JR, Snoeck E, Duff F, Lamb M, Jorga K. Pharmacokinetics of ribavirin in patients with hepatitis C virus. British journal of clinical pharmacology. 2006;62(6):710-4.

204. Kees MG, Weber S, Kees F, Horbach T. Pharmacokinetics of moxifloxacin in plasma and tissue of morbidly obese patients. Journal of antimicrobial chemotherapy. 2011;66(10):2330-5.

205. Ahn JE, French JL. Longitudinal aggregate data model-based meta-analysis with NONMEM: approaches to handling within treatment arm correlation. Journal of pharmacokinetics and pharmacodynamics. 2010;37(2):179-201.

206. Piedbois P, Buyse M. Meta-analyses based on abstracted data: a step in the right direction, but only a first step. American Society of Clinical Oncology; 2004.

207. Laporte-Simitsidis S, Girard P, Mismetti P, Chabaud S, Decousus H, Boissel JP. Inter-study variability in population pharmacokinetic meta-analysis: when and how to estimate it? Journal of pharmaceutical sciences. 2000;89(2):155-67.

208. Barrett J, Joshi A, Chai M, Ludden T, Fiske W, Pieniaszek JH. Population pharmacokinetic meta-analysis with efavirenz. 2002.

209. Bruno R, Vivier N, Vergniol JC, De Phillips SL, Montay G, Sheiner LB. A population pharmacokinetic model for docetaxel (taxotere®): Model building and validation. Journal of pharmacokinetics and biopharmaceutics. 1996;24(2):153-72.

210. Ocampo-Pelland AS, Gastonguay MR, French JF, Riggs MM. Model-based meta-analysis for development of a population-pharmacokinetic (PPK) model for Vitamin D3 and its 25OHD3 metabolite using both individual and arm-level data. Journal of pharmacokinetics and pharmacodynamics. 2016;43(2):191-206.

211. Davda JP, Dodds MG, Gibbs MA, Wisdom W, Gibbs JP, editors. A model-based meta-analysis of monoclonal antibody pharmacokinetics to guide optimal first-in-human study design. MAbs; 2014: Taylor & Francis.

212. Sinha J, Al-Sallami HS, Duffull SB. Choosing the Allometric Exponent in Covariate Model Building. Clinical Pharmacokinetics. 2018.

213. Prospective Studies C. Body-mass index and cause-specific mortality in 900 000 adults: collaborative analyses of 57 prospective studies. The Lancet. 2009;373(9669):1083-96.

214. Blouin RA, Warren GW. Pharmacokinetic considerations in obesity. Journal of pharmaceutical sciences. 1999;88(1):1-7.

215. Hanley MJ, Abernethy DR, Greenblatt DJ. Effect of obesity on the pharmacokinetics of drugs in humans. Clinical pharmacokinetics. 2010;49(2):71-87.

216. Riede U, Spycher M, Gitzelmann R. Glycogenosis type I (glucose 6-phosphatase deficiency): I. Ultrastructural morphometric analysis of juvenile liver cells. Pathology-Research and Practice. 1980;167(1):136-50.

217. Rohr H, Lüthy J, Gudat F, Oberholzer M, Gysin C, Bianchi L. Stereology of liver biopsies from healthy volunteers. Virchows Archiv. 1976;371(3):251-63.

218. Mazen N, Jessica L, R. PM, Michael M, Gavin H, Thuy-Anh L, et al. Utility of magnetic resonance imaging versus histology for quantifying changes in liver fat in nonalcoholic fatty liver disease trials. Hepatology (Baltimore, Md). 2013;58(6):1930-40.

219. Du Bois D. A formula to estimate the approximate surface area if height and weight be known. Nutrition. 1989;5:303-13.

220. Holliday MA, Potter D, Jarrah A, Bearg S. The Relation of Metabolic Rate to Body Weight and Organ Size. Pediatric Research. 1967;1:185.

221. Johnson TN, Tucker GT, Tanner MS, Rostami-Hodjegan A. Changes in liver volume from birth to adulthood: A meta-analysis. Liver Transplantation. 2005;11(12):1481-93.

222. Johnstone AM, Murison SD, Duncan JS, Rance KA, Speakman JR. Factors influencing variation in basal metabolic rate include fat-free mass, fat mass, age, and

circulating thyroxine but not sex, circulating leptin, or triiodothyronine. The American journal of clinical nutrition. 2005;82(5):941-8.

223. Weinsier RL, Schutz Y, Bracco D. Reexamination of the relationship of resting metabolic rate to fat-free mass and to the metabolically active components of fat-free mass in humans. The American journal of clinical nutrition. 1992;55(4):790-4.

224. Holliday MA. Body Composition and Energy Needs during Growth. In: Falkner F, Tanner JM, editors. Postnatal Growth Neurobiology. Boston, MA: Springer US; 1986. p. 101-17.

225. Wilson ZE, Rostami-Hodjegan A, Burn JL, Tooley A, Boyle J, Ellis SW, et al. Inter-individual variability in levels of human microsomal protein and hepatocellularity per gram of liver. British Journal of Clinical Pharmacology. 2003;56(4):433-40.

226. Zhang H, Gao N, Tian X, Liu T, Fang Y, Zhou J, et al. Content and activity of human liver microsomal protein and prediction of individual hepatic clearance in vivo. Scientific reports. 2015;5:17671.

227. Achour B, Barber J, Rostami-Hodjegan A. Expression of Hepatic Drug-Metabolizing Cytochrome P450 Enzymes and Their Intercorrelations: A Meta-Analysis. Drug Metabolism and Disposition. 2014;42(8):1349-56.

228. Chul YH, Heecheon Y, Ho L, Zhe-Wu J, Il MJ, Hwan CB. Estimation of standard liver volume for liver transplantation in the Korean population. Liver Transplantation. 2004;10(6):779-83.

229. Vauthey JN, Abdalla EK, Doherty DA, Gertsch P, Fenstermacher MJ, Loyer EM, et al. Body surface area and body weight predict total liver volume in Western adults. Liver transplantation. 2002;8(3):233-40.

230. Lee DH, Keum N, Hu FB, Orav EJ, Rimm EB, Sun Q, et al. Development and validation of anthropometric prediction equations for lean body mass, fat mass and percent fat in adults using the National Health and Nutrition Examination Survey (NHANES) 1999–2006. British Journal of Nutrition. 2017;118(10):858-66.

231. Kwo PY, Ramchandani VA, O'Connor S, Amann D, Carr LG, Sandrasegaran K, et al. Gender differences in alcohol metabolism: Relationship to liver volume and effect of adjusting for body mass. Gastroenterology. 1998;115(6):1552-7.

232. Jones HM, Rowland-Yeo K. Basic Concepts in Physiologically Based Pharmacokinetic Modeling in Drug Discovery and Development. CPT: Pharmacometrics & Systems Pharmacology. 2013;2(8):e63.

233. Konerman MA, Jones JC, Harrison SA. Pharmacotherapy for NASH: Current and emerging. Journal of Hepatology. 2018;68(2):362-75.

234. NASH: Key consideratons for drug development [Available from: http://www.webcitation.org/767YMv1hn (archived on 12 February 2019).

235. Jones H, Rowland-Yeo K. Basic concepts in physiologically based pharmacokinetic modeling in drug discovery and development. CPT: pharmacometrics & systems pharmacology. 2013;2(8):1-12.

236. Mahmoud M, Abdel-Kader R, Hassanein M, Saleh S, Botros S. Antipyrine clearance in comparison to conventional liver function tests in hepatitis C virus patients. European journal of pharmacology. 2007;569(3):222-7.

237. Branch R, Shand D. Propranolol disposition in chronic liver disease: a physiological approach. Clinical pharmacokinetics. 1976;1(4):264-79.

238. Hallifax D, Foster JA, Houston JB. Prediction of human metabolic clearance from in vitro systems: retrospective analysis and prospective view. Pharmaceutical research. 2010;27(10):2150-61.

239. Vesell ES, Passananti GT, Glenwright PA, Dvorchik BH. Studies on the disposition of antipyrine, aminopyrine, and phenacetin using plasma, saliva, and urine. Clinical Pharmacology & Therapeutics. 1975;18(3):259-72.

240. Boobis A, Brodie M, Kahn G, Toverud E-L, Blair I, Murray S, et al. Comparison of the in vivo and in vitro rates of formation of the three main oxidative metabolites of antipyrine in man. British journal of clinical pharmacology. 1981;12(6):771-7.

241. Sinha J, Duffull SB, Green B, Ponnuswamy T, Devanand B, Ramanathan M, et al. Abstracts for the Ninth American Conference on Pharmacometrics (ACoP9): Abstract No. T-014. Journal of Pharmacokinetics and Pharmacodynamics. 2018;45(1):3-134.

242. Begg EJ, Chin PK. A unified pharmacokinetic approach to individualized drug dosing. Br J Clin Pharmacol. 2012;73(3):335-9.

243. Norris DC. One-size-fits-all dosing in oncology wastes money, innovation and lives. Drug Discovery Today. 2018;23(1):4-6.

244. Geli P, Laxminarayan R, Dunne M, Smith DL. "One-size-fits-all"? Optimizing treatment duration for bacterial infections. PloS one. 2012;7(1):e29838.

245. Kuchuk I, Clemons M, Addison C. Time to put an end to the "one size fits all" approach to bisphosphonate use in patients with metastatic breast cancer? Current Oncology. 2012;19(5):e303.

246. Woodcock J. The prospects for "personalized medicine" in drug development and drug therapy. Clinical Pharmacology & Therapeutics. 2007;81(2):164-9.

247. Bouillon T, Shafer SL. Does size matter? Anesthesiology: The Journal of the American Society of Anesthesiologists. 1998;89(3):557-60.

248. Falagas ME, Karageorgopoulos DE. Adjustment of dosing of antimicrobial agents for bodyweight in adults. The Lancet. 2010;375(9710):248-51.

249. Traynor AM, Nafziger AN, Bertino J. Aminoglycoside dosing weight correction factors for patients of various body sizes. Antimicrobial agents and chemotherapy. 1995;39(2):545-8.

250. Mehrotra S, Gopalakrishnan M, Gobburu J, Greer JM, Piekarz R, Karp JE, et al. Population pharmacokinetics and site of action exposures of veliparib with topotecan plus carboplatin in patients with haematological malignancies. Br J Clin Pharmacol. 2017;83(8):1688-700.

251. West GB, Brown JH. The origin of allometric scaling laws in biology from genomes to ecosystems: towards a quantitative unifying theory of biological structure and organization. Journal of experimental biology. 2005;208(9):1575-92.

252. Henry C. Basal metabolic rate studies in humans: measurement and development of new equations. Public health nutrition. 2005;8(7a):1133-52.

253. Pelley JW. 19 - Nutrition. In: Pelley JW, editor. Elsevier's Integrated Review Biochemistry (Second Edition). Philadelphia: W.B. Saunders; 2012. p. 171-9.

254. Marcus JB. Chapter 10 - Weight Management: Finding the Healthy Balance: Practical Applications for Nutrition, Food Science and Culinary Professionals. In: Marcus JB, editor. Culinary Nutrition. San Diego: Academic Press; 2013. p. 431-73.

255. Vacobi A, Udall JA, Levy G. Serum protein binding as a determinant of warfarin body clearance and anticoagulant effect. Clinical Pharmacology & Therapeutics. 1976;19(5part1):552-8.

256. Li R, Barton HA, Varma MV. Prediction of pharmacokinetics and drug–drug interactions when hepatic transporters are involved. Clinical pharmacokinetics. 2014;53(8):659-78.

257. Patilea-Vrana G, Unadkat J. Transport vs. Metabolism: What Determines the Pharmacokinetics and Pharmacodynamics of Drugs? Insights From the Extended Clearance Model. Clinical Pharmacology & Therapeutics. 2016;100(5):413-8.

258. Abel ED, Litwin SE, Sweeney G. Cardiac remodeling in obesity. Physiological reviews. 2008;88(2):389-419.

259. Mohammadi A, Ghasemi-rad M, Zahedi H, Toldi G, Alinia T. Effect of severity of steatosis as assessed ultrasonographically on hepatic vascular indices in non-alcoholic fatty liver disease. Medical ultrasonography. 2011;13(3):200-6.

260. Calvier EA, Krekels EH, Välitalo PA, Rostami-Hodjegan A, Tibboel D, Danhof M, et al. Allometric Scaling of Clearance in Paediatric Patients: When Does the Magic of 0.75 Fade? Clinical pharmacokinetics. 2016:1-13.

261. Forbes R, Cooper A, Mitchell H. The composition of the adult human body as determined by chemical analysis. Journal of Biological Chemistry. 1953;203:359-66.

262. Knight G, Beddoe A, Streat S, Hill G. Body composition of two human cadavers by neutron activation and chemical analysis. American Journal of Physiology-Endocrinology And Metabolism. 1986;250(2):E179-E85.

263. Mitchell H, Hamilton T, Steggerda F, Bean H. The chemical composition of the adult human body and its bearing on the biochemistry of growth. Journal of Biological Chemistry. 1945;168:625-37.

264. Widdowson EM, McCance E, Spray CM. The chemical composition of the human body. Clinical Science. 1951;10:113-25.

265. Forbes GB, Lewis AM. Total sodium, potassium and chloride in adult man. Journal of Clinical Investigation. 1956;35(6):596-600.

266. Heymsfield SB, Wang J, Heshka S, Kehayias JJ, Pierson RN. Dual-photon absorptiometry: comparison of bone mineral and soft tissue mass measurements in vivo with established methods. The American journal of clinical nutrition. 1989;49(6):1283-9.

267. Peppler WW, Mazess RB. Total body bone mineral and lean body mass by dual-photon absorptiometry. Calcified tissue international. 1981;33(1):353-9.

268. Nord R, Payne R. Body composition by dual-energy X-ray absorptiometry: a review of the technology. Asia Pac J Clin Nutr. 1995;4:167-71.

269. Millard-Stafford ML, Collins MA, Modlesky CM, Snow TK, Rosskopf LB. Effect of race and resistance training status on the density of fat-free mass and percent fat estimates. Journal of Applied Physiology. 2001;91(3):1259-68.

270. Visser M, Gallagher D, Deurenberg P, Wang J, Pierson R, Heymsfield S. Density of fat-free body mass: relationship with race, age, and level of body fatness. American Journal of Physiology-Endocrinology And Metabolism. 1997;272(5):E781-E7.

271. Martin A, Daniel M, Drinkwater D, Clarys J. Adipose tissue density, estimated adipose lipid fraction and whole body adiposity in male cadavers. International journal of obesity and related metabolic disorders: journal of the International Association for the Study of Obesity. 1994;18(2):79-83.

272. Taylor RW, Grant AM, Williams SM, Goulding A. Sex Differences in Regional Body Fat Distribution From Pre-to Postpuberty. Obesity. 2010;18(7):1410-6.